A STUDY OF CLIMATE SENSITIVITY

USING ENERGY BALANCE CRYOSPHERIC MODELS

by

TAMARA ANN SHAPIRO LEDLEY

B.S. University of Maryland, College Park
(1976)

Submitted to the Department of
Meteorology and Physical Oceanography
in Partial Fulfillment of the
Requirements for the Degree of

DOCTOR OF PHILOSOPHY

at the

MASSACHUSETTS INSTITUTE OF TECHNOLOGY

April 1983

Signature of Author.......................................
        Department of Meteorology and Physical Oceanography
                                           April 29, 1983

Certified by..
                                          Thesis Supervisor

Accepted by...
        Chairperson, Departmental Committee on Graduate Students

A STUDY OF CLIMATE SENSITIVITY

USING ENERGY BALANCE CRYOSPHERIC MODELS

by

TAMARA ANN SHAPIRO LEDLEY

Submitted to the Department of Meteorology and Physical Oceanography on April 29, 1983 in partial fulfillment of the requirements for the Degree of Doctor of Philosophy

ABSTRACT

An examination of the response of the cryosphere to some of the specified and parameterized atmospheric variables that can vary over the ice age time scales is made. This is done through the use of a zonally averaged continental ice sheet model and a thermodynamic sea ice model which were constructed to be applicable on long climatic time scales, and employ an energy balance parameterization of the net budget of accumulation and ablation.

Sea ice results indicate that Milankovitch insolation variations alone are not sufficient to cause changes in sea ice, but that air temperature variations have a major effect. In addition, results indicate that the energy exchange between the atmosphere and the ocean is greatly affected by the period that open ocean exists. The tendency is for the net upward heat flux to initially decrease when the period of open ocean increases due to a large increase in the absorbed solar radiation; however, the latent heat flux increases due to the increased exposure of the warm ocean. This implies that ocean temperatures could remain relatively warm, keeping the ocean ice free, and the increased latent heat flux could provide a moisture source for snowfall on land areas which could contribute to the growth of ice sheets.

Continental ice sheet results indicate that the initialization of an ice sheet occurs by crossing the threshold of maintaining snow through the summer season, and that reaching this threshold requires not only a large decrease in temperature , but a substantial increase in surface albedo. In addition, it was found that with the present zonally averaged energy balance calculation a northern hemisphere ice sheet once formed fluctuates little in latitudinal extent.

Thesis Supervisor: Reginald E. Newell

Title: Professor of Meteorology

ACKNOWLEDGMENTS

To my husband
Fred David Ledley
and to my parents
Murray and Ina Shapiro

TABLE OF CONTENTS

Chapter I. Introduction

The purpose of this thesis is to attempt to understand the sensitivity of the cryospheric components of the climate system, sea ice and continental ice, to some of the specified and parameterized atmospheric variables that can vary over the ice age time scales (10^4 to 10^5 years).

Over the past 15 years large quantities of data have been gathered and analysed by geologists to produce a climate record which stretches back over the last million years. While the details of this record are still under discussion there seems to be a consensus concerning its major features. These features include a dominant 100k periodicity (k indicates a multiple of 1000 years) which is characterized by a slow build up of ice on the continents over approximately a 90k period, followed by a rapid deglaciation over a 10k period; a 41k periodicity which is most evident in the polar regions; and a 23k periodicity which is strongest in the tropical and subtropical regions.

The question that remains is what are the physical processes which are responsible for these large changes in climate? Various climate models and ice sheet models have been used as tools in attempts to answer this question. The results of these models indicate that the shorter periodicities of 41k and 23k can be attributed to solar insolation variations which are due to orbital variations that occur on those time scales. However, the dominant 100k periodicity still remains the subject of controversy. Some

scientists have attributed this periodicity to
nonlinearities within the climate system; however, it is
still not clear what these nonlinearities are or whether
they result from external forcing or are due to nonlinear
interactions between components of the climate system.

One of the major problems in deciphering the mechanisms
which are important in the long term ice age cycles is that
climate and ice sheet model results are sensitive to the
choice of modeling parameters. Since the enormous complexity
of both the cryospheric and atmospheric systems, and
computer time restrictions make it necessary to use simple
models in the study of long term climate, it is also
necessary to understand how they respond to various choices
of parameters and forcings. This requires extensive
sensitivity studies with both cryospheric and atmospheric
climate models before they can be coupled, and before any
meaningful conclusions can be drawn from the results they
may produce.

In this thesis sensitivity studies along these lines
are made with a dynamic zonally averaged continental ice
sheet model, which encompasses an energy balanced net
accumulation at the surface, vertically averaged horizontal
velocity within the ice, and a time lagged bedrock
depression beneath the ice load; and a thermodynamic sea ice
model which includes leads (cracks in the ice) and is
coupled to a simple mixed layer ocean. In the remaining
section of this chapter a review is made of the previous

work on these topics. Then in chapter II a detailed
description is made of the physics included and the
numerical formulations of the cryospheric models mentioned
above. Chapter III presents the results of the model
simulations of the present day climate, and discusses some
of the problems associated with these simulations. Chapters
IV and V present the models sensitivity to some of the
factors that are both internal and external to the
cryospheric system, and discuss the possible reasons for
those sensitivities. In chapter VI the conclusions that can
be drawn from the results are discussed and suggestions for
future work are made.

The physical mechanisms responsible for the large scale
climate fluctuations of the Pleistocene have puzzled
scientists since the middle of the nineteenth century. In
attempting to explain this phenomenon some theories invoke
processes external to the climate system and include changes
in solar radiation due to 1) changes in solar constant, 2)
variations in the earth's orbital geometry, 3) variations in
the concentration of volcanic dust in the atmosphere, and 4)
variations in the earth's magnetic field (Wollin, Ericson,
and Ryan, 1971). Others propose factors internal to the
climate system which have long response times such as 1) the
growth and decay of ice sheets, 2) the distribution of
carbon dioxide between the atmosphere and the ocean, 3) the

ice cover of the Arctic basin, and 4) deep ocean circulation. A third set of theories speculate that the earth's climate is an almost transitive system which alternates between glacial and interglacial states without any specific internal or external stimulus. (Hays et.al., 1976) It now seems, as will become evident in the following discussion, that many processes, both internal and external to the climate system, contribute to the large scale climate fluctuations of the Pleistocene. However, none of the proposed theories had been formulated in such a way as to submit to verification until 1941 when Milutin Milankovitch published his astronomical theory of the ice ages.

Milankovitch found that there were three orbital elements important in determining the earth's insolation, and that they had definite periodicities. These elements were eccentricity (~100000 year period), obliquity (~41000 year period), and the longitude of perihelion (~23000 year period) (see Figures 1.1 and 1.2). Using these orbital elements he computed the insolation received by the earth as a function of latitude and found that the annual averaged insolation, affected only by eccentricity variations, changed very little; however, the latitudinal and seasonal distribution of the solar radiation varied significantly with the periodicities of the obliquity and longitude of perihelion. Thus, Milankovitch's theory predicted that climate variations could occur with periodicities on the order of 41k and 23k.
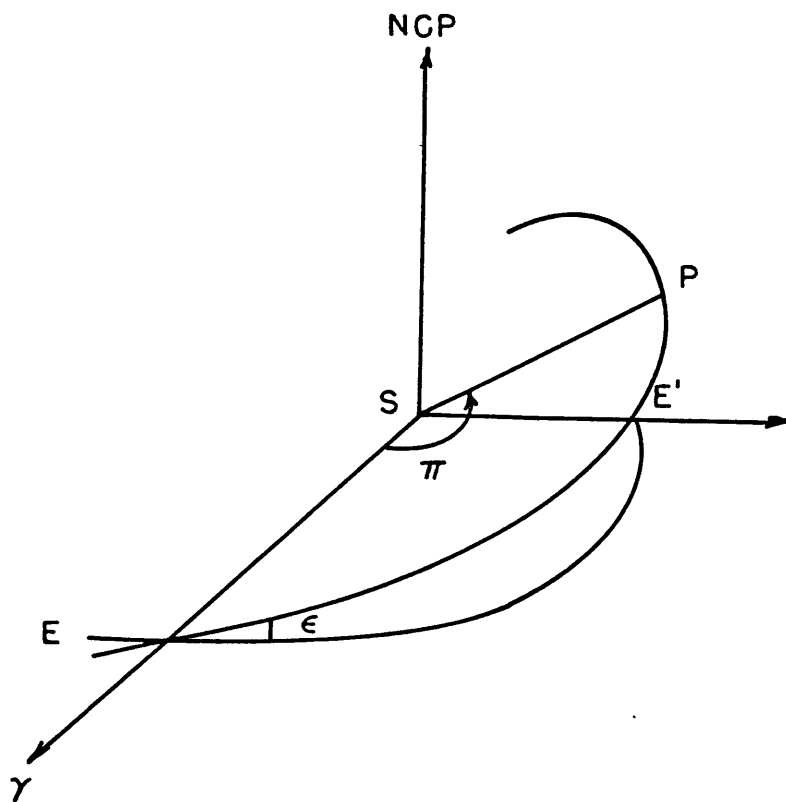
Figure 1.1 The Orbital Elements: S = sun; Y = vernal
        equinox, NCP = north celestial pole;
          ∈ = obliquity; EE' = celestial equator; P = point
        of perihelion; π = longitude of perihelion.
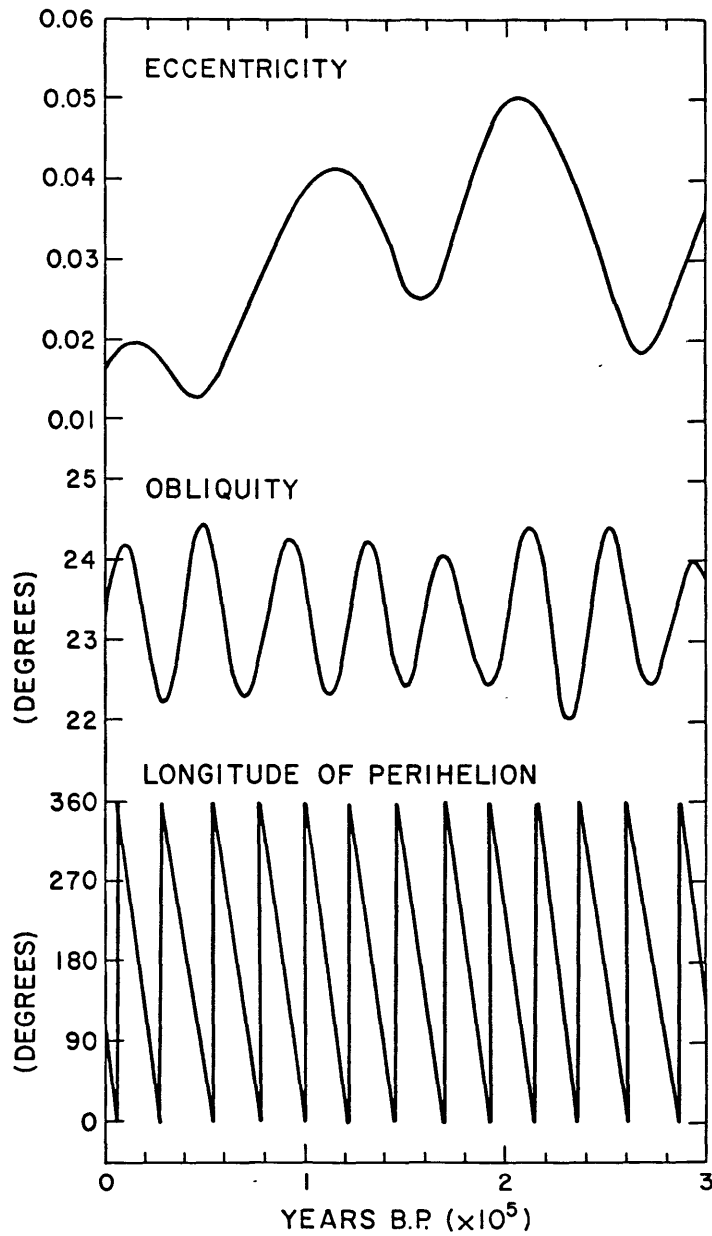
Figure 1.2 Variation of Orbital Elements Over the Past 300k
Years

There are two fields of study which have been pursued
in parallel that have attempted to verify this theory and
understand the physical mechanisms responsible for the
Pleistocene climate fluctuations. These fields are geology
and climatology (or more specifically climate modeling).

Over the past 15 years geologists have gathered a large
quantity of proxy data from deep sea ice cores which they
have analyzed in order to produce a time series of climate
fluctuations on the time scales of the Milankovitch
insolation fluctuations (10^4 to 10^5 years). Some of the
earliest of these records were published by Broecker and van
Donk in 1970. They showed that the main glacial cycle was
sawtoothed in character, with slow build ups of ice over 90k
years, followed by rapid deglaciations in less than one
tenth that time. In addition, there was a secondary cycle of
20k years modulating the sawtoothed pattern. This lent some
support to the astronomical theory; however, the dominant
sawtooth character was unexplained.

A more extensive analysis of the proxy data was done by
Hays, Imbrie, and Shackleton (1976). Their work involved
extracting the time series of three independent climate
parameters from the deep sea cores, performing a spectral
analysis on this data, and comparing the results to a
spectral analysis of the time series of solar insolation
obtained from Berger (1976,1978).

The spectral analysis of the climate parameters showed
a dominant peak at 100k and other significant peaks at 41k

and 23k. These were significant periods in the variation of
the orbital parameters, however, the insolation data showed
spectral peaks at only the 41k and 23k periods corresponding
to the variations in the obliquity and the longitude of
perihelion. These results led Hays et.al. (1976) to conclude
that changes in the earth's orbital geometry were
fundamental in the variations in climate. They did not
suggest the physical mechanisms through which this
astronomical forcing was effective other than that explained
by Milankovitch. Therefore, they could not explain the
presence of the dominant 100k glacial-interglacial cycle in
the geologic record other than to suggest that this cycle
was the result of nonlinear mechanisms within the climate
system not taken into account by their linear theory.

Hays et.al's results indicated that present climate
theories were not adequate to explain long term
glacial-interglacial cycles. Since then many climate studies
have tried to include various nonlinear processes in models
of global climate in attempts to explain those cycles. These
studies have evolved into two schools of thought concerning
the nature of these glacial-interglacial transitions. The
first holds that long term cycles in climate on the order of
10^4 to 10^5 years result from nonlinear interactions internal
to the system and do not need external influences. The
second holds that large scale changes in climate such as
that represented by glacial-interglacial cycles, are forced
or triggered by external factors. Such factors are thought

to be amplified or modified by the climate system through
physical mechanisms, which are as yet unknown, to produce
climate change.

The work of Saltzman (1977,1978), Sergin (1979,1980),
Kallen, Crafoord, and Ghil (1979), Ghil and LeTreut (1981),
and LeTreut and Ghil (1981) follow that of the first school.
They described and built internal oscillator models of the
climate system which produce long term glacial-interglacial
cycles. However, by adjusting the many prescribed constants
and tunable parameters within these models various climates
and climate cycles can be obtained. These range from cycles
with periods and amplitudes similar to those found in the
geologic record, to non cyclic behavior in a variety of
regimes.

Saltzman (1977,1978) developed a set of global water
mass and energy balance equations that were applicable to
the complete atmosphere-hydroshpere-lithosphere-cryosphere
system. An analysis of these equations was made by making a
series of assumptions about the relative magnitudes of the
various terms, and assuming that the atmosphere maintains a
quasi-equilibrium with the ice coverage and the ocean
surface temperature, and that an approximate radiative
equilibrium always prevails. This analysis suggested that
the mean ocean temperature varies in phase with ice volume,
with ocean temperature reaching its maximum value at the
same time as the ice reaches its maximum extent by absorbing
the latent heat released during ice formation; and that

radiative flux (including both long and short wave
radiation) is downward during periods of glaciation and
upward during interglacials. This result supported an ice
age hypothesis proposed by Newell (1974) which suggested
that mean ocean temperatures would increase during an ice
age. However, a dynamical theory that can be used to test
the reality of the proposed oscillation between the ocean
temperature and ice formation has yet to be developed.

Sergin (1979,1980) developed a model which coupled the
atmosphere, ocean, continental ice and the
lithosphere-asthenosphere, in which each included component
and process had its own characteristic time constant. Long
term climate evolution experiments were made using
"realistic" values of the physical parameters incorporated
in the model. His results showed that it was possible to
obtain internal oscillations in climate on the order of
those found in the geologic record; however, when the values
of the physical parameters were varied the oscillation
changed in both period and amplitude, and in some cases
disappeared entirely.

Kallen, Crafoord, and Ghil (1979) developed a model
which computed globally averaged ocean-atmosphere
temperature and latitudinal ice extent. The globally
averaged ocean-atmosphere temperature was computed from a
radiation balance similar to that used by Budyko (1969), and
Sellers (1969); and the ice sheet extent was computed using
the perfectly plastic[1] ice sheet deveolped by Weertman

(1976). The results showed that the model could produce self induced internal oscillations, however, the existence of those oscillations depended on the values chosen for the model's physical parameters.

Ghil and LeTreut (1981) and LeTreut and Ghil (1981) built on the model of Kallen et. al. by adding a simple parameterization of the interaction between the lithosphere-asthenosphere and the cryosphere, thus including a third degree of freedom. The free oscillations exhibited by this model were slightly modified from those of Kallen et. al.. When forced with the orbital frequencies of 19k and 23k, subharmonic and harmonic oscillations on the order of 100k and 10k years were produced with the high amplitude of the free oscillations. However, the existence of these oscillations depended on the values chosen for the model's physical parameters.

Thus internal oscillator models have produced climatic oscillations similar to those found in the geologic record; however, the models sensitivity to the values of the included physical parameters lessens the confidence with which these results are viewed.

The work of Suarez and Held (1976,1979), Schneider and Thompson (1979), Weertman (1976), Birchfield, Weertman and Lunde (1981), Budd and Smith (1981), Oerlemans (1980), Pollard, Ingersoll, and Lockwood (1980), and Pollard (1978,1982a,1982b) follow that of the second school. They built deterministic models which attempt to include the

interaction between the cryosphere and atmosphere. These
models produce the higher frequency cycles found in the
geologic record, however, they are only beginning to
decipher the physical mechanisms which produce the longer
term glacial-interglacial cycles.

Suarez and Held (1976,1979) constructed a zonally
symmetric energy balance climate model coupled to a zero
capacity land surface, a forty meter mixed ocean layer, and
a sea ice model. The model's equilibrium response to the
pattern of insolation was computed at 5000 year intervals
over the past 150000 years. The results showed high
frequency oscillations on the order of 20k and 40k, however,
the dominant 100k periodicity found in the geologic record
was not reproduced.

Schneider and Thompson (1979) used a zonally averaged
energy balance climate model to investigate the climate's
sensitivity to changes in seasonally and latitudinally
varying albedo, in the hemispheric and latitudinally varying
thermal inertia of the climate system, and in the amplitude
of solar radiation variations. They found that by including
these physical processes the model would produce a small
amplitude 40k periodicity in air temperature. They concluded
that it was not likely that a single physical process would
be the dominant mechanism of glacial-interglacial
transitions on the 100k time scale, but that a number of
processes on both the seasonal and 1000 year time scales
would be needed to improve simulations of

glacial-interglacial transitions.

The results of the deterministic studies discussed above showed a consistent phase error when compared to the geologic record. The authors suggested that one possible reason for this discrepancy was that the time lags involved in the growth and decay of ice sheets were neglected. In the following deterministic studies the dynamic growth and decay of ice sheets were included explicitly in the models. This resulted in improved modeled climatic time series when compared with the geologic record.

One of the earliest of these studies (Weertman, 1976) used a perfectly plastic ice sheet model that was forced through a simple parameterization of the net budget of accumulation and ablation by insolation variations. This model produced 20k and 40k variations in ice volume, however, the results showed no variation at the 100k periodicity and proved to be very sensitive to an empirically specified ratio of the rates of accumulation to ablation.

Pollard (1978) and Pollard, Ingersoll, and Lockwood (1980) coupled a zonally symmetric time dependent one level energy balance climate model, which computed the sea level air temperature as a function of latitude and season, to Weertman's perfectly plastic ice sheet model. Again, the model produced only the 20k and 40k periodicities, and the response was found to be sensitive to model parameters.

Subsequent ice sheet models have incorporated the laws

of ice flow, the dynamic equations of motion, and time lagged bedrock depression beneath the ice load. In addition, modifications have been made in the net budget parameterization.

Birchfield et. al. (1981) modified the net budget parameterization used by Weertman (1976) by making the accumulation a decreasing linear function of the elevation of the ice sheet, and thus included the "desert-elevation"[2] effect. The model results lent support to the hypothesis that the nonlinearity inherent in the ice sheet physics is responsible for the 100k periodicity in the geological record, however, the power spectra of the modeled ice volume showed a muted response at the 100k periodicity when compared to the climate record.

Budd and Smith's (1981) three dimensional model determined accumulation and ablation separately. Accumulation was defined at the present day distribution modified by an exponential "desert-elevation" effect. The ablation parameterization was derived from the present distribution of ablation for existing glaciers. The results of this model, although somewhat sensitive to model parameters, indicated that high topography with high precipitation approaching that of the present was necessary for the initiation of the ice sheets, and that the isostatic bedrock depression response beneath the ice with a phase delay of about 5000 years was necessary to cause major deglaciation.

Another parameterization of net budget was developed by
Oerlemans and Bienfait (1980) which involved the computation
of the daily cycle of temperature and melt of and ice-snow
surface layer. This parameterization was subsequently used
in the ice sheet models of Oerlemans (1980) and Pollard
(1982a,1982b). Both of these models produced 100k
periodicities by initializing ice sheets at high altitudes
and including a time lagged bedrock depression as in the
studies discussed above. However, Pollard's model was more
efficient during ice sheet decay, producing complete
deglaciation, due to the inclusion of a calving mechanism at
the southern edge of the northern hemisphere ice sheet into
proglacial lakes formed when the ice sheet began to melt.

Thus deterministic models of climate and ice have
produced the shorter periodicities found in the geologic
record, however, the physical processes involved in the
dominant 100k glacial-interglacial cycle are still not well
understood.

One of the features of the climate system which has
been either completely neglected or included in only a crude
manner is that of sea ice. Ruddiman and MacIntyre (1981)
have suggested that sea ice had an important effect on the
growth and decay of the ice sheets due to the elimination of
the moisture source for snowfall if ice covers the ocean.
Until now sea ice has been included in climate models in
order to include the ice albedo feedback on air
temperatures. The effect of sea ice on the energy and

moisture exchanges with the atmosphere has been neglected.

Sea ice models have been constructed to study both the physics of ice growth and melt at the ocean surface and the interannual, seasonal, and regional variations in sea ice extent. They have not, until now, been applied to the problem of long term climate fluctuations.

One of the first models that was developed to study the physics of sea ice growth was that of Maykut and Untersteiner (1971). This model employed a 10 cm vertical grid and computed the heat flux within the ice using a heat conduction equation which accounted for both ice temperature and salinity. Snowfall was prescribed at the upper surface and melt at that surface and melt and accumulation at the bottom surface were determined from the surplus or deficit of energy computed from the energy balance requirment at those surfaces. This model was very complex and required a large amount of computer time. Semtner (1976) simplified the model by reducing the vertical resolution and neglecting the salinity variations within the ice. He showed that reasonable agreement with observed sea ice variations at high northern latitudes could be obtained with a three layer model, and that a one layer model, while much more inaccurate, would also produce reasonable results.

One of the major features of sea ice that was neglected in these studies was the formation and variation in the extent of leads, or cracks in the ice which expose open ocean to the atmosphere. Since leads can be a major factor

in determining the energy exchange between the atmosphere and ocean a parameterization was developed to include them in Semtner's model.

Semtner's modified model has been used to study the interannual variations of sea ice extent and thickness in both the Arctic basin and around Antarctica (Washington et.al.,1976; Parkinson, 1978; Parkinson and Washington, 1979). The model results indicate that in the Arctic ice grows from a minimum in September to a maximum in March with a maximum thickness of close to 4 meters. In the Antarctic the modeled sea ice expanded from a minimum in March to a maximum in late August, with a maximum thickness of about 1.4 meters. These results compared reasonably well with ice extent measurments.

In all of these sea ice studies the models were constructed to study sea ice variations on short time scales, on the order of ten years, and as a result took very short time steps, on the order of eight hours. In order to study long term variations in sea ice with these short time steps a large amount of computer time is necessary. Lacking such extensive computer resources the model must be reconstructed to be able to handle longer time steps. The model that was deveolped for this study was constructed so that it would remain numerically stable for time steps up to at least two weeks.

Models of continental ice and sea ice are important for understanding the mechanisms of long term glacial

cycles. Previous studies, emphasizing ice sheet and coupled
ice sheet-climate models with parameterizations of snowfall
and ablation have produced 20k, 40k and, 100k year climatic
variations similar to those seen in the geological record.
However, they have not adaquately explained the physical
processes involved in producing the 100k cycle mainly due to
the model's sensitivity to the values chosen for the
physical parameters, and possibly due their neglecting some
important process.

In this study energy balance models of both sea ice and
ice sheets are used to examine the sensitivity of the
cryosphere to various internal and external processes. The
intent is to gain a better understanding of how these
processes affect the cryosphere, and their relative
importance in long term climate fluctuations.

Chapter II. The Models

Described below are two cryospheric models which were
designed to be used in long term climate studies. These
models are a three layer thermodynamic sea ice model which
includes leads and is coupled to a simple mixed layer ocean,
and a zonally averaged dynamic ice sheet model which
includes a time lagged bedrock depression beneath the ice
load.

In the real climate system the atmosphere and
crysophere influence each other through exchanges of energy
and mass at their interface. In this study a surface energy
balance calculation is included in the models in an attempt
to simulate these exchanges and to study their influence on
the cryosphere. The energy exchanges that are included in
this calculation include short wave radiation absorbed at
the surface, incoming long wave radiation from the
atmosphere, outgoing long wave radiation from the surface,
sensible heat, latent heat, and conduction of heat from
below the surface in the case of sea ice. The mass exchanges
at the ice sheet and sea ice surfaces include the
accumulation and ablation of ice and snow.

In the following sections each of the components of the
climate system that are included in the models -- the input
data that defines the state of the atmosphere, the
parameterizations of the various forcings from the
atmosphere, the parameterization of accumulation, the
physical and numerical formulations of the sea ice model

including the simple mixed ocean layer and the lead
parameterization, the physical and numerical formulations of
the continental ice sheet model including time lagged
bedrock depression, and the determination of surface
temperature and ablation in both the sea ice and continental
ice sheet models through the use of the surface energy
balance calculation -- are discussed. The values of the
constants and the variable names used in this model can be
found in Appendix 1. List of Symbols.

A. Input Data

The calculation of the energy fluxes described below
requires input data fields in the form of surface air
temperature, cloud fraction, relative humidity, wind speed,
precipitation rate, atmospheric pressure each over land and
ocean, and land heights zonally averaged over land areas.

The zonally averaged seasonal cycles of air temperature
over both land and ocean were derived from the tabulated
data of Schutz and Gates (1971,1972,1973,1974). Air
temperatures over land were reduced to sea level using a
lapse rate of 6.5 K km^{-1} and then adjusted to the topography
used in the particular experiment. In most cases the
topography was sea level or that used by Pollard (1982a) in
the northern hemisphere.

The zonally averaged seasonal cycles of cloud fraction
were derived from the tabulated values from the
Environomental Technical Appliciations Center (1971) that

were given in Schutz and Gates (1971-1974) for 90N to 30N, from Murakami (1975) for 20N to 20S, and from van Loon (1972) for 20S to 90S.

The zonally averaged seasonal cycles of relative humidity were derived from the data of London (1957).

The three variables discussed above were derived from the tabulated data, which in some cases included only four seasonal values, using harmonic analysis to generate monthly data for every 10 degrees of latitude (S. Thompson, personnal communication). The data was then linearly interpolated in time and interpolated with area weighting in space to produce the time step size and grid spacing required, generally 48 and 24 time steps per year in the sea ice and ice sheet models respectively, and a 5 and 1 degree latitudinal grid respectively.

The zonally averaged seasonal cycles of wind speed for 80N to 40S were derived from data used in the preparation of the general circulation monograph by Newell et.al (1972,1974), and the wind speeds for 50S to 80S were derived from the data of Jenne et.al. (1971). Both sets of data were manipulated using the time and space interpolation procedure described above.

The seasonal cycle of precipitation over land and sea were taken from monthly maps prepared by Jaegar (1976).

The atmospheric pressure was held constant throughout the year. Its latitudinal distribution was derived from the pressure field given in Sellers (1973) using the area

weighting interpolation procedure.

The zonal land heights and land fractions were derived from data given by Gates and Nelson (1973), (S. Warren and S. Thompson, personnal communication).

B. Forcing from the Atmosphere

1. Incoming Solar Radiation and Albedo

The determination of incoming solar radiation is done in two steps. First, the radiation at the top of the atmosphere as a function of latitude and time is computed, and then the fraction of that reaching the surface after being attenuated and reflected by the atmosphere and surface is determined.

a. Radiation at the Top of the Atmosphere

The short wave radiation at the top of the atmoshere is determined using the following formulae given in Sellers (1965)

$$Q = S * (\bar{r}/r)^2 * (H \sin\varphi \sin\delta + \cos\delta \cos\varphi \sin H) / \pi$$

$$\overline{\cos Z} = (1/2H) * \int_{-H}^{H} (\sin\varphi \sin\delta + (\cos\varphi \cos\delta \sin H)/H) \, dH$$

$$\bar{Z} = \cos^{-1}(\overline{\cos Z})$$

where Q is the insolation in W m^{-2}, S is the solar constant (1360.75 W m^{-2}), r is the earth-sun distance, $\bar{r}$ is the mean earth-sun distance, φ is the latitude, δ is the solar declination, H is the half day length or the hour angle at

sunset, and $\bar{Z}$ is the daily mean zenith angle. In these
equations, S and φ are given and δ, r, $\bar{r}$, and H are computed
(see Appendix 2. The Astronomical Parameters) from the
orbital elements and a time of year. The orbital elements
are computed following Berger (1978).

A more complete description of these calculations is
given in Ledley (1979).

b. Radiative Transfer and Albedo Parameterizations

The short wave radiation reaching the surface is
computed using an adaptation of the planetary albedo
parameterization developed by Thompson (1979) and Thompson
and Barron (1981). The solar radiation at the top of the
atmosphere is first reduced through absorption by ozone. It
is further modified, including a division into diffuse and
direct components through Rayleigh scattering and scattering
and absorption by water vapor and dry aerosols. The direct
and diffuse radiation under clear skies is then determined
from the remaining radiation and the direct and diffuse
surface albedos. These are set depending on surface type,
sea ice, open ocean, land, or continental ice, and may be
modified by zenith angle.

The surface albedo of sea ice is a function of air
temperature and ranges between .88 and .51. This functional
relationship was derived from the seasonal cycle of sea ice
albedo used in the sea ice model developed by Semtner (1976)
and takes the form

$$\alpha = \begin{cases} .88 & T_a < 245 \\ .88 - a * (T_a - 245) & 245 < T_a < 271 \\ .79992 - b * (T_a - 271) & 271 < T_a < 280 \\ .51 & 280 < T_a \end{cases}$$

where a = .00308 and b = .0322.

The surface albedo of open ocean is a function of zenith angle. Reflectivities of open ocean for a given zenith angle were obtained from Pickard (1979), then with the solar zenith angle, computed in conjunction with the solar radiation at the top of the atmosphere, the ocean surface albedo is obtained as a function of latitude and time.

In the ice sheet model the surface albedo is set to .6 on continental ice and .16 on land.

Under cloudy skies the short wave radiation reaching the surface is further modified by the cloud albedo, absorption by the cloud, and absorption and multiple reflections between the cloud base and surface.

The total solar radiation available at the surface is a linear combination of that under clear skies and cloudy skies weighted by the cloud fraction.

2. Long Wave Radiation

The long wave radiation from the atmosphere for clear skies is computed using Brunt's formula taken from Sellers (1965).

$$I_{o\downarrow} = -\epsilon\sigma T_a^4 * (a + b\sqrt{e})$$

where ϵ is the emissivity set to 1, σ is the Stefan-Boltzmann constant set to 5.67×10^{-8} W m^{-2}K^{-4}, T_a is the surface air temperature in K, e is the water vapor pressure of the air in kg m^{-1}s^{-2}, and a and b are constants set to .62 and .005 respectively. $I_{o\downarrow}$ is negative because the flux is downward.

This formula is modified to be applied under cloudy conditions as follows

$$F_{lw} = I_{o\downarrow} * (1. + c*n)$$

where n is the cloud fraction and c is a parameter dependent on cloud type but held constant here at .25.

Long wave radiation from the surface is determined using the equation for black body radiation from a body at the surface temperature and an emissivity of 1.

$$F_{ir} = \epsilon\sigma T_s^4$$

3. Sensible Heat

The sensible heat flux is computed using a standard bulk aerodynamic formula similar to that of Parkinson and Washington (1979). Its form is

$$F_s = \rho * C_p * C_D * V * (T_a - T_s)$$

where ρ is the air density held constant at 1.225 kg m^{-3}, C_p is the specific heat of dry air set to 1.0048 x 10^3 J $kg^{-1}K^{-1}$, C_D is the drag coefficient set to .00175 and .003 in the sea ice and continental ice models respectively, V is the wind speed in m s^{-1}, and T_a and T_s are the air and surface temperature respectively in K.

4. Latent Heat

The latent heat flux is also computed from a standard bulk aerodynamic formula similar to that used by Parkinson and Washington (1979). Its form is

$$F_1 = \rho * L_x * C_D * V * (q_a - q_s)$$

where all variables are as defined for sensible heat, L_x is the latent heat of vaporization/sublimation with values of 2.5 x 10^6 or 2.83 x 10^6 J kg^{-1} for temperatures above or below the freezing point respectively, and q_a and q_s are the specific humidities of the "free" air and the air in contact with the surface respectively. Specific humidity is computed from the formula

$$q = (\mathcal{E} * e_s * r) / (P_s - (1-\mathcal{E}) * e_s * r)$$

where $\mathcal{E} = .622$ is the ratio of the molecular weight of water vapor to that of dry air, e_s is the saturation vapor pressure of water, r is the specified relative humidity, and P_s is the specified surface air pressure. The surface is

assumed to be at saturation so the relative humidity there is 100%.

The saturation vapor pressure is computed in two different ways. In the sea ice model e_s is determined from an empirical formula by Lowe (1977)

$$e_s = a_0 + T (a_1 + T (a_2 + T (a_3 + T (a_4 + T (a_5 + a_6*T)))))$$

where T is in Celsius and a_0 through a_6 are the coefficients found in Lowe that differ if the temperature is above or below the freezing point.

This equation is not suited to the continental ice sheet model because it is an empirical fit to the saturation vapor pressure for temperatures above 223 K. Since temperatures over ice at high elevations, such as the center of Antarctica, can drop to 200 K it is necessary to use the Clausius-Clapeyron equation. Its form is

$$e_s = e_s(T_f) * exp((L_x * (T-T_f))/(R_v * T * T_f))$$

where T_f is the triple point of water, 273.16 K; $e_s(T_f)$ is 611 kg m^{-2}K^{-1}; R_v is the gas constant for water vapor, 460.55 J kg^{-1}K^{-1}; and all other variables are as defined earlier.

5. Snowfall

The snowfall rates are determined from present

precipitation rates modified by the atmospheric lapse rate, the "desert-elevation" effect, and a function of temperature which defines the fraction of precipitation that will fall as snow. The equation takes the form

$$S_n = P_r * r_a * F_y * e_s/e_{si}$$

where P_r is the precipitation rate, r_a is the ratio of the density of water to compacted snow or ice set to 3.03 and 1.1 in the sea ice and continental ice sheet models respectively, F_y is the fraction of the precipitation that will fall as snow, and e_s/e_{si} is the ratio of the saturation vapor pressure at the surface air temperature to the saturation vapor pressure at present temperatures. The form of F_y is as follows

$$F_y = \begin{cases} 1. & T_a < 253 \\ .5 + (272-T_a)/38 & 253 < T_a < 272 \\ (281-T_a)/18 & 272 < T_a < 281 \\ 0. & 281 < T_a \end{cases}$$

The qualitative validity of using such a function is derived from two sources. First, Auer (1974) tried to determine the probability that a forcast of precipitation would produce snow given the air temperature. He found that the probability that the precipitation would fall as snow ranged between one and zero for a temperatures from 273.5 K to 278.5 K respectively.

The second source was a review of a year, 1975, of

monthly data from thirty stations chosen across Canada
(Monthly Record, Meteorological Observations in Canada,
1975). This data included the total precipitation in water
equivalent during each month, the total snowfall, and the
monthly averaged air temperature. Assuming a ten to one
ratio for snow depth to water equivalent, the fraction of
the precipitation that fell as snow was determined and
associated with an air temperature. While there was much
scatter in the results (see Figure 2.1) the fraction of
precipitation that fell as snow ranged from one to zero for
temperatures ranging from 263 K to 281 K.

The difference in the range of temperatures from these
two sources is due to the situations to which they apply.
Auer's result applies to individual storms in which the
temperature plays a direct roll. The result derived from the
Canadian data applies to an entire month during which the
temperatures may be warm (cold) overall with occasional
storms accompanied by cold (warm) temperatures and as a
result snow (rain). In this way it is possible to have warm
(cold) monthly temperatures and less than 100% rain (snow).

The relation between air temperature and the fraction
of precipitation that falls as snow chosen for these models
is piecewise linear with a temperature range of 253 K to
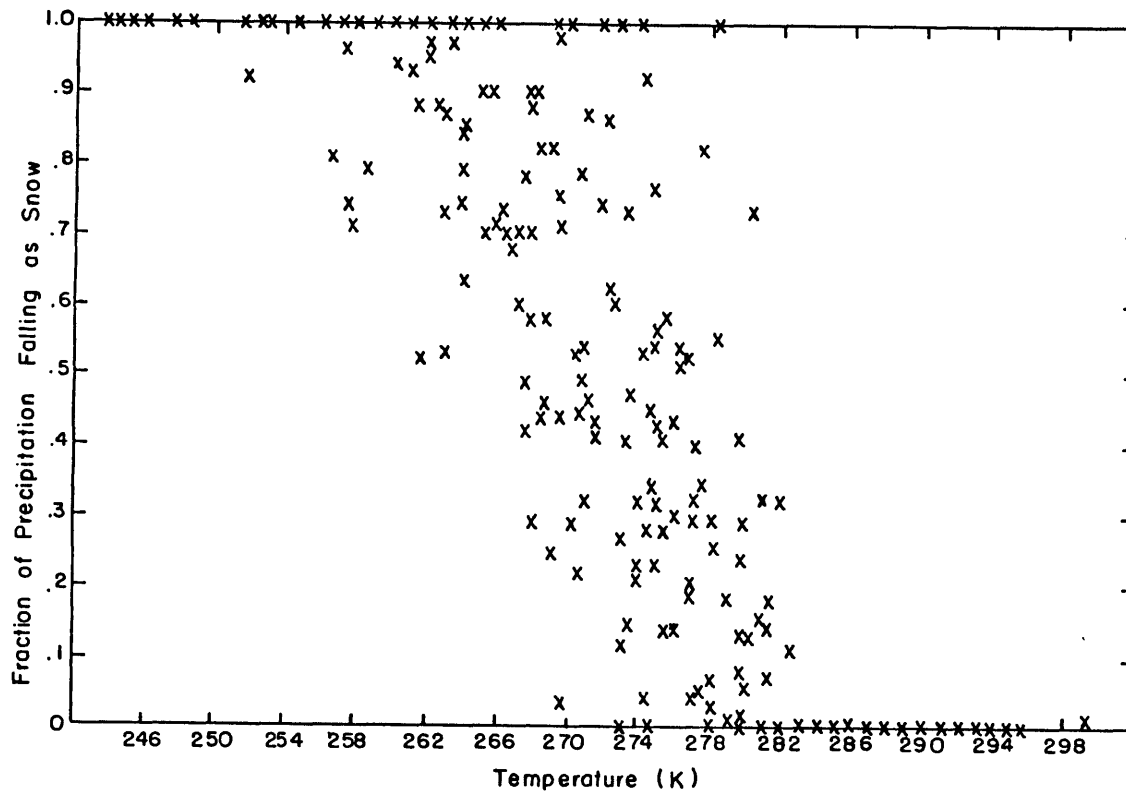
Figure 2.1 Canadian data for 1975 indicating the fraction of monthly precipitation that fell as snow as a function of monthly mean air temperatures.

281 K with F_y = .5 at T_a = 272 K.

The ratio e_s/e_{si} modifies the precipitation in proportion to the amount of water available as defined by the air temperature. Air temperature is changed most dramatically as an ice sheet grows. As the elevation of the surface increases the surface air temperature decreases by a specified lapse rate of 6.5 K km^{-1}, and with it the water available for precipitation decreases exponentially. This is the "desert-elevation" effect.

Air temperature is also different from present values during ice ages and climatic optimums. In the experiments that are performed here the air temperature is varied in different ways in order to simulate these climatic periods, and as a result the snowfall is also varied.

C. The Sea Ice Model

The sea ice model is a modification of that used by Semtner (1976). It is a three layer thermodynamic model which includes conduction within the ice and snow, penetration of solar radiation into ice layers, and surface energy balances. This model is coupled to a very simple mixed layer ocean model which allows the initiation of new ice in open ocean, and the inclusion of a lead parameterization.

1. Model Description

Sea ice is assumed to be a horizontal uniform slab of ice on which snow may accumulate. The temperatures within snow and ice are governed by similar one dimensional heat equations,

$$(\rho c)_s * \partial T / \partial t = k_s * \partial^2 (T) / \partial z^2 \qquad (2.1.a)$$

$$(\rho c)_i * \partial T / \partial t = k_i * \partial^2 (T) / \partial z^2 \qquad (2.1.b)$$

(Maykut and Untersteiner, 1971) where (ρc) is the volumetric specific heat, k is the thermal conductivity, T is temperature in K, t is time in seconds, z is the vertical coordinate in m, s indicates values for snow, and i indicates values for ice.

The values of (ρc) and k are functions of temperature and salinity (Maykut and Untersteiner, 1971). The variations in these paramaters are most significant when the snow and

ice approach the freezing point, a time when conductive fluxes are small. Therefore, I will follow Semtner and hold these parameters constant.

Maykut and Untersteiner (1971) have shown that, when snow free conditions exist, solar radiation penetrating into the interior of ice has an important effect on the thickness and temperature of sea ice. It is therefore important to include this in a simple model. In general, the effect of this penetrating energy is to reduce the energy at the surface available for immediate melting, and to store it for use in the fall to delay cooling of the ice. The net result is that the ice is thicker and warmer than if solar radiation did not penetrate into the interior of the ice.

Maykut and Untersteiner included this effect in their model by adding a heat source term to the conduction equation. This term was represented as a fraction of the non reflected incoming solar radiation which penetrated the ice surface, and exponentally decreased with depth.

Semtner simplified the parameterization for storing and using the penetrating solar energy. During snow free periods the penetrating solar radiation was stored in a heat reservoir which represented internal meltwater, or brine. This heat was used to keep the ice from dropping below the freezing point, simulating refreezing of the brine pockets. Semtner also set a limit on the amount of energy that could be stored in the heat reservoir. The purpose of this was to eliminate the possibility that more energy would be stored

than was needed to melt all the ice. This limit was set at 30% of the energy needed to melt all the ice. If the heat reservoir was full the penetration was set to zero, the heat of fusion at the top surface was dropped by 30%, and the reservoir was used to supply the remaining heat.

In this work Semtner's method has been adopted and somewhat modified. Radiation is stored in a heat reservoir which is restricted to accumulating 30% of the energy needed to melt the ice layer. This energy is used to delay the cooling of the ice at the end of the summer. If the heat reservoir contains energy when there is excess energy from other sources available for melting, the heat reservoir aids in melting in proportion to the amount of ice that can be melted.

The interface of the snow or ice with the atmosphere is considered to be a plane with no heat capacity at which a balance of fluxes is assumed to exist. The balance at the top surface involves fluxes of incoming short wave radiation absorbed at the surface, incoming long wave radiation from the atmosphere, outgoing long wave radiation from the surface, sensible heat, latent heat, and the conduction of heat from below the snow surface (or ice surface in the case of snow free conditions). If this balance requires the surface temperature above the freezing point the surface temperature is held at that point, and the energy excess is balanced by melting ice. The only increase in mass at this surface is the accumulation of snow.

The balance at the bottom surface involves the conductive flux within the ice and the upward flux from the ocean. Any imbalance in these fluxes is offset by the accretion or ablation of ice.

In order to handle the transition from ice free to ice covered ocean an isothermal oceanic mixed layer is assumed to exist below the ice. If ice disappears an energy balance calculation is applied to this layer until the ocean again reaches the freezing point, at which time new ice forms.

Sea ice has a dramatic insulating effect on the transfer of energy between the ocean and atmosphere (Maykut, 1978). This effect is modified by the presence of leads, or cracks, in the ice pack. Leads are generally caused by stresses put on the ice slab by winds and ocean currents. These dynamic mechanisms are not included in this model. However, due to the importance of leads in determining the actual transfer of energy between the ocean and atmosphere a simple parameterization is made to include them in the model.

The lead parameterization assumes a minimum area of open ocean. An energy balance calculation is applied to this open area and any imbalance is offset either by opening the lead wider by melting ice from the edge, or freezing it over with new ice of specified thickness. If new ice forms, its thickness is averaged with that of the old ice, weighted by the relative areas they occupy, to obtain a new ice thickness. Then the minimum lead area is reopened, and the

ice in the lead is assumed to be transported out of the latitude zone. In reality, the formation of leads aids in the transport of ice to different regions and causes compression features away from the lead such as pressure ridges.

2. Numerical Formulation of the Sea Ice Equations
a. Internal Thermodynamic Equations

The sea ice model is a three layer model consisting of one snow layer and two ice layers, or three ice layers in the case of snow free conditions (Figure 2.2) to which equations 2.1.a and 2.1.b are applied. At the beginning of a time step the ice layers are of equal thickness. If during the time step one of the layers grows or melts the resolution of the grid is changed to maintain the number of grid points within the ice.

The form of the heat equations as appled to each of the layers is as follows:

$$\partial T(1)/\partial t = (k_x / (\rho c)_x) * \partial(\partial T/\partial z)/\partial z \qquad (2.2.a)$$

$$\partial T(2)/\partial t = (k_i / (\rho c)_i) * \partial(\partial T/\partial z)/\partial z \qquad (2.2.b)$$

$$\partial T(3)/\partial t = (k_i / (\rho c)_i) * \partial(\partial T/\partial z)/\partial z \qquad (2.2.c)$$

All variables are as defined in the previous section with the subscript x representing snow or ice depending on whether snow is present or not.

These equations are solved numerically using a semi-
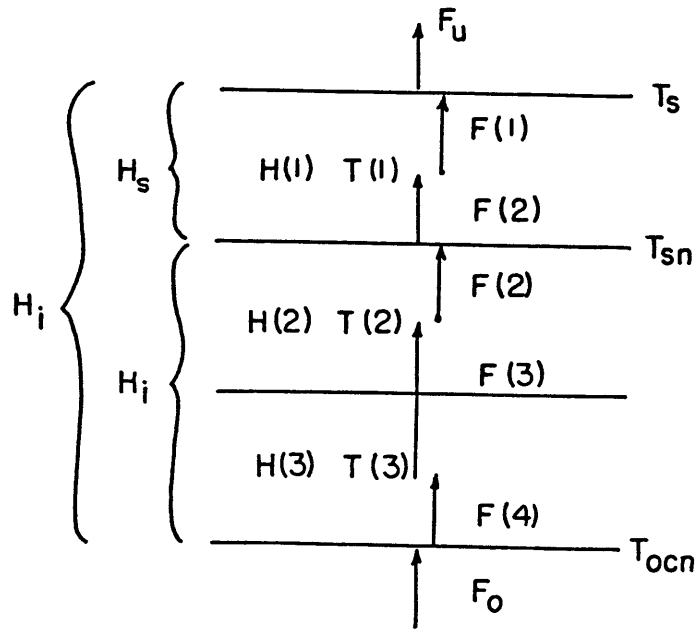
Figure 2.2 Schematic of Sea Ice Model

H_i = total ice thickness

H_s = snow thickness

H = layer thickness

T = layer temperature

T_{ocn} = ocean/ice interface temperature

T_s = the surface temperature

T_{sn} = the temperature between
        layers 1 and 2

F_u = net flux exchange with the atmosphere

F_o = the flux from the ocean

F = internal conductive fluxes

implicit numerical scheme for the time derivative which can
easily be adjusted to be fully explicit or fully
implicit,and centered space differencing for the spatial
derivatives. Most of the experiments in this work utilize
the fully implicit scheme.

The spatial derivatives on the right hand side of
equations 2.2.a, 2.2.b, and 2.2.c represent the vertical
flux convergence. These fluxes, represented by $-k_x(\partial T/\partial z)$,
are determined numerically by assuming a linear temperature
profile between the grid points within the ice, or between
the grid point and the boundary of that layer when a
temperature is defined at that boundary (ie. at the top and
bottom surfaces and the interface of layers 1 and 2,
generally the snow ice interface). The numerical form of
these fluxes, indicated in Figure 2.2, are as follows (here
and in future computations an upward flux is taken to be
positive).

$$F(1) = - k_x * (T_s - T(1)) / (H(1) * .5) \qquad (2.3.a)$$

$$F(2) = - k_i * (T_{sn} - T(2)) / (H(2) * .5) \qquad (2.3.b)$$

$$F(3) = - k_i * (T(2) - T(3)) / (H(3)) \qquad (2.3.c)$$

$$F(4) = - k_i * (T(3) - T_{ocn}) / (H(3) *.5) \qquad (2.3.d)$$

Note that at this point in the calculation H(2) and H(3) are
always equal. Substituting these equations back into
equations 2.2.a, 2.2.b, and 2.2.c and using centered space
differencing results in

$$\partial T(1)/\partial t = - (F(1) - F(2)) / (H(1) * (\rho c)_x) \quad (2.4.a)$$

$$\partial T(2)/\partial t = - (F(2) - F(3)) / (H(2) * (\rho c)_i) \quad (2.4.b)$$

$$\partial T(3)/\partial t = - (F(3) - F(4)) / (H(3) * (\rho c)_i) \quad (2.4.c)$$

The semi implicit time differencing scheme can now be applied. This numerical scheme is semi implicit in that the computation of a new value of the temperature is based on a weighted average of values at the last time step and the new time step. This is a versatile scheme because by changing the weighting parameter it can become explicit, implicit, or in between. Using a weighting parameter (β) of .5, the Crank-Nicolson scheme, numerical oscillations occurred in some experiments in which extreme conditions were specified. Upon changing the weighting parameter to 1. the numerical oscillations disappeared, therefore, experiments were made with this value. When the numerical scheme is applied equation 2.4.a, 2.4.b, and 2.4.c take the form

$$\frac{\partial T(1)}{\partial t} = - \frac{\beta*(F(1,1)-F(2,1))}{(\rho c)_x * H(1,2)} - \frac{(1-\beta)*(F(2,1)-F(2,2))}{(\rho c)_x * H(1,2)} \quad (2.5.a)$$

$$\frac{\partial T(2)}{\partial t} = - \frac{\beta*(F(2,1)-F(3,1))}{(\rho c)_i * H(2,2)} - \frac{(1-\beta)*(F(1,2)-F(2,2))}{(\rho c)_i * H(2,2)} \quad (2.5.b)$$

$$\frac{\partial T(3)}{\partial t} = - \frac{\beta*(F(3,1)-F(4,1))}{(\rho c)_i * H(3,2)} - \frac{(1-\beta)*(F(3,2)-F(4,2))}{(\rho c)_i * H(3,2)} \quad (2.5.c)$$

where β is the weighting parameter which can vary between 0

and 1; and the second subscript represents the time step, 1 being the new time step and 2 being the last time step.

Solving the time differential numerically and substituting in the temperature form of the fluxes, equations 2.3.a-d, equations 2.5.a, 2.5.b, and 2.5.c become

$$\frac{T(1,1)-T(1,2)}{\Delta t} = \frac{-\beta}{(\rho c)_x H(1,2)} \left(\frac{-k_x (T_s(1)-T(1,1))}{H(1,2)*.5} + \frac{k_i (T_{SN}(1)-T(2,1))}{H(2,2)*.5} \right)$$

$$\frac{-(1-\beta)}{(\rho c)_x H(1,2)} \left(\frac{-k_x (T_s(2)-T(1,2))}{H(1,2)*.5} + \frac{k_i (T_{SN}(2)-T(2,2))}{H(2,2)*.5} \right) \qquad (2.6.a)$$

$$\frac{T(2,1)-T(2,2)}{\Delta t} = \frac{-\beta}{(\rho c)_i H(2,2)} \left(\frac{-k_i (T_{SN}(1)-T(2,1))}{H(2,2)*.5} + \frac{k_i (T(2,1)-T(3,1))}{H(3,2)} \right)$$

$$\frac{-(1-\beta)}{(\rho c)_i H(2,2)} \left(\frac{-k_i (T_{SN}(2)-T(2,2)}{H(2,2)*.5} + \frac{k_i (T(2,2)-T(3,2))}{H(3,2)} \right) \qquad (2.6.b)$$

$$\frac{T(3,1)-T(3,2)}{\Delta t} = \frac{-\beta}{(\rho c)_i H(3,2)} \left(\frac{-k (T(2,1)-T(3,1)}{H(3,2)} + \frac{k_i (T(3,1)-T_{OCN}(1))}{H(3,2)*.5} \right)$$

$$\frac{-(1-\beta)}{(\rho c)_i H(3,2)} \left(\frac{-k_i (T(2,2)-T(3,2))}{H(3,2)} + \frac{k_i (T(3,2)-T_{OCN}(2))}{H(3,2)*.5} \right) \qquad (2.6.c)$$

where Δt is the time step. In this model 48 time steps per year are computed making Δt somewhat longer than 1 week.

There are now three equations. In order to solve this system there must be only three unknowns, T(1,1), T(2,1), and T(3,1). All values from previous time steps are known, and all values at the new time step must have a representation in terms of T(1,1), T(2,1), and T(3,1) or

they must be obtained from an earlier computation.

Other unknowns include the new top surface temperature, $T_s(1)$, the new snow-ice interface temperature, $T_{sn}(1)$, and the new ice-ocean interface temperature, $T_{ocn}(1)$. The new values of the top surface temperature are determined from a surface energy balance that is computed immediately prior to the computation of the internal snow and ice temperatures. The ocean-ice interface temperature is always held at the freezing point. The snow-ice interface temperature (the temperature between layers one and two) is the temperature resulting from the requirement that there be a continuity of fluxes across the snow ice interface. If the top two layers are ice this condition automatically holds, and the interface temperature will be the average of the temperatures of the two layers. The representation of the interface temperature in terms of the layer temperatures $T(1,1)$ and $T(2,1)$ is obtained by setting the fluxes on either side of that boundary equal.

$$F(2,1) = \frac{- k_i*(T_{sn}(1)-T(2,1))}{(H(2,2)*.5)} = \frac{- k_x*(T(1,1)-T_{sn}(1))}{(H(1,2)*.5)}$$

Solving for $T_{sn}(1)$ results in

$$T_{sn}(1) = \frac{T(1,1) + T(2,1) * KH)}{(1. + KH)}$$

where $KH = (k_i * H(1,2)) / (k_x * H(2,2))$.

Substituting T_{sn} into equations 2.6.a, 2.6.b, and 2.6.c, and noting that $H(2,2)$ is equal to $H(3,2)$ at this

point in each time step results in the following equations

$$T(1,1) - T(1,2) =$$

$$\frac{-\beta 2\Delta t}{(\rho c)_x H(1,2)} \left(\frac{-k_x(T_s(1) - T(1,1))}{H(1,2)} + \frac{k_i}{H(2,2)} \left(\left(\frac{T(1,1) + T(2,1) * KH}{1 + KH} - T(2,1) \right) \right) \right) \quad (2.7.a)$$

$$\frac{-(1-\beta)2\Delta t}{(\rho c)_x H(1,2)} \left(\frac{-k_x(T_s(2) - T(1,2))}{H(1,2)} + \frac{k_i}{H(2,2)} \left(\left(\frac{T(1,2) + T(2,2) * KH}{1 + KH} - T(2,2) \right) \right) \right)$$

$$T(2,1) - T(2,2) =$$

$$\frac{-\beta \Delta t k_i}{(\rho c)_i H(2,2)^2} \left(-2 \left(\left(\frac{T(1,1) + T(2,1) * KH}{1 + KH} - T(2,1) \right) + (T(2,1) - T(3,1)) \right) \right) \quad (2.7.b)$$

$$\frac{-(1-\beta)\Delta t k_i}{(\rho c)_i H(2,2)^2} \left(-2 \left(\left(\frac{T(1,2) + T(2,2) * KH}{1 + KH} \right) - T(2,2) \right) + (T(2,2) - T(3,2)) \right)$$

$$T(3,1) - T(3,2) =$$

$$\frac{-\beta \Delta t k_i}{(\rho c)_i H(3,2)^2} \left(-(T(2,1) - T(3,1)) + 2 (T(3,1) - T_{OCN}(1)) \right) \quad (2.7.c)$$

$$\frac{-(1-\beta)\Delta t k_i}{(\rho c)_i H(3,2)^2} \left(-(T(2,2) - T(3,2)) + 2 (T(3,2) - T_{OCN}(2)) \right)$$

These equations are now rearranged algebraically to put them in a tridiagonal matrix form. This involves bringing all unknown terms to the left of the equal sign, and all known terms to the right. The resulting tridiagonal matrix equation is

$$(2.8)$$

$$
\begin{vmatrix}
\left(\dfrac{-(\rho c)_x H(1,2)}{2\Delta t} - \dfrac{\beta k_x}{H(1,2)} - \dfrac{\beta k_x k_i}{CK}\right) & \left(\dfrac{-\beta k_i^2 H(1,2)}{H(2,2)\,CK} + \dfrac{\beta k_i}{H(2,2)}\right) & 0 \\[3mm]
\left(\dfrac{2\beta k_x H(2,2)}{CK}\right) & \left(\dfrac{-(\rho c)_i H(2,2)^2}{k_i \Delta t} + \dfrac{2\beta k_i H(1,2)}{CK} - 3\beta\right) & \beta \\[3mm]
0 & \beta & \left(\dfrac{-(\rho c)_i H(3,2)^2}{k_i \Delta t} - 3\beta\right)
\end{vmatrix}
\begin{vmatrix}
T(1,1) \\[3mm]
T(2,1) \\[3mm]
T(3,1)
\end{vmatrix}
$$

$$
=
\begin{vmatrix}
\left(\dfrac{-\beta k_x\, T_s(1)}{H(1,2)} - \dfrac{(1-\beta)k_x\, T_s(2)}{H(1,2)} + \left(\dfrac{-(\rho c)_x H(1,2)}{2\Delta t} + \dfrac{(1-\beta)k_x}{H(1,2)} + \dfrac{(1-\beta)k_x k_i}{CK}\right)T(1,2)\right) \\[4mm]
\left(\dfrac{-2(1-\beta)k_x H(2,2)}{CK}\right)T(1,2) + \left(\dfrac{-(\rho c)_i H(2,2)^2}{k_i \Delta t} - \dfrac{2(1-\beta)k_i H(1,2)}{CK} + 3(1-\beta)\right)T(2,2) - (1-\beta)T(3,2) \\[4mm]
-(1-\beta)T(2,2) + \left(\dfrac{-(\rho c)_i H(3,2)^2}{k_i \Delta t} + 3(1-\beta)\right)T(3,2) - 2\beta\,\overline{T_{ocn}}(1) - 2(1-\beta)\,\overline{T_{ocn}}(2)
\end{vmatrix}
$$

where $\quad CK = k_x\, H(2,2) + k_i\, H(1,2)$

These equations are solved simultaneously for the new layer temperatures using a tridiagonal matrix solver. The only constraint put on the results concerns the possibility that the solution requires any of the layer temperatures to go above the freezing point. In that case the layer temperature is held at the freezing point, and the extra energy is used later toward melting that layer.

b. Brine Storage

As was mentioned in chapter II.C.1., a heat reservoir has been included to store the energy from short wave radiation which has penetrated the ice surface during snow free periods. This stored energy represents brine meltwater pockets within the layer and does not immediately affect the ice thickness. The amount of energy accumulated in any one time step is computed from the following numerical equation

$$F_{st}(1) = -\beta(1-\alpha(1)) * P_e(1) * F_{sw}(1) - (1-\beta) * (1-\alpha(2)) * P_e(2) * F_{sw}(2)$$

where F_{st} is the newly accumulated stored energy, α is the albedo, β is the time step weighting parameter, F_{sw} is short wave radiation, P_e is the percent of nonreflected short wave radiation that penetrates the ice surface, and the subscripts 1 and 2 indicate the time step.

This stored energy is accumulated in the top ice layer and is added to any energy that was previously stored. The stored energy can "migrate" to the lower layers of ice through the process of maintaining layers of equal ice thickness when ice melts away from the lower layer.

The quantity of energy allowed to be stored is restricted to a percentage, set at 30%, of that needed to melt the ice layer. This is to prevent the possiblity that more energy will accumulate in the reservoir than is needed to melt the layer. Once this limit is reached the penetration is set to zero and all short wave radiation is absorbed at the surface. If in one time step part of the penetrating energy fills the heat reservoir the remaining energy is "returned" to the surface energy balance through the addition of an extra term which is non zero only in such a case.

Short wave radiation is allowed to penetrate into the ice layers only when snow free conditions exist. The test for this condition is straight foward for most time steps, however, some care must be taken during no snow-snow and snow-no snow transitions.

In testing for the case of a no snow-snow transition a potential snow thickness is computed at the beginning of each time step. This potential snow consists of new snowfall added to the existing snow at the end of the last time step, zero under no snow conditions. If the potential snow thickness is greater than a minimum value, set to .001 m here, no penetration at that time step is allowed. A discrepancy may occur here if the new snowfall is thin enough for energy from other sources, computed later in the model, to melt it away leaving snow free conditions. However, this probably does not occur often because if there

is snowfall, temperatures in most cases are too cold for there to be any excess energy for melting.

The case of a snow - no snow transition is more complex and speculative because the melting of a snow layer must be anticipated before any computations are made. To anticipate complete snow melt tests of a series of conditions are made. If these conditions are met complete snow melt is assumed, and penetration of solar radiation is allowed. These conditions are 1) the temperature of the snow layer at the last time step must be at the freezing point, 2) the surface temperature at the last time step must be at the freezing point, 3) there is no new snowfall, 4) the snow thickness at the end of the last time step must be less than a specified value, set to .3m, and 5) the new air temperature is above the freezing point by at least some specified amount, set to .2K. The numerical quantities noted above are somewhat arbitrary, having been chosen based on previous experience with the model. However, since these quantities are used only to test for a particular condition their numerical value is not critical. Again a discrepancy can occur if the above conditions are met, but the snow does not melt away. If this does happen then the penetration that occurs goes through the snow and is absorbed in the top ice layer.

c. Surface Energy Balances

The sea ice model is forced through two surface energy balances, one at the snow (ice) - atmosphere interface and

the other at the ice - ocean interface.

The energy equation applied at the snow (ice) - atmosphere interface is a balance of fluxes which include incoming short wave radiation absorbed at the surface, incoming long wave radiation from the atmosphere, outgoing long wave radiation from the surface, sensible heat, latent heat, and the conduction of heat from below the surface. The equation has the form

$$F_1+F_s+(1-\alpha)*(1-P_e)*F_{sw}+F_{sx}+F_{lw}+F_{ir}+F_{cond} = 0 \qquad (2.9)$$

where F_1 is latent heat flux; F_s is sensible heat flux; F_{sw} is short wave radiation; α is albedo; P_e is the fraction of radiation not reflected that penetrates the surface, set to zero if there is a snow surface; F_{lw} is long wave radiation from atmosphere, F_{ir} is long wave radiation from the surface, F_{cond} is conductive flux from below the surface; and F_{sx} is short wave radiation which does not penetrate into the ice layers because the heat reservoir is full (see chapter II.C.2.b. Brine Storage).

The new values of short wave radiation, albedo, and incoming long wave radiation from the atmosphere are known. The other fluxes are functions of the surface temperature and must be determined. They have all been discussed in chapter II.B..

$$F_1 = \rho * L_x * C_D * V * (q_s(T_s+\Delta T_s) - q_a)$$

$$F_s = \rho * C_p * C_D * V * (T_s +\Delta T_s - T_a)$$

$$F_{ir} = \sigma * (T_s +\Delta T_s)^4$$

$$F_{cond} = - k_x * (T(1) - (T_s + \Delta T_s)) / (H(1)*.5)$$

where ρ is the air density, σ is the Stefan-Boltzmann constant, C_D is the drag coefficient, L_x the is latent heat of vaporization/sublimation, T_s is the last value of surface temperature, ΔT_s is the change in surface temperature required to maintain balance, T_a is the new air temperature, V is the new wind speed, C_p is the specific heat, H(1) is the last top layer thickness, T(1) is the new top layer temperature, k_x is the thermal conductivity of the top layer, q_a is the new specific humidity of the air, and $q_s(T_s + T_s)$ is the new specific humidity at the surface.

The latent heat flux and long wave radiation from the surface are nonlinear in ΔT_s. It is therefore necessary to linearize these two terms about the last value of surface temperature, T_s. This is done through the use of a Taylor expansion. The latent heat term becomes

$$F_1 = \rho * L_x * C_D * V * (q_s(T_s) + (\partial q_s / \partial T_s) * \Delta T_s - q_a)$$

$$F_1 = \rho * L_x * C_D * V * (q_s(T_s) - q_a) + \rho * L_x * C_D * V * (\partial q_s / \partial T_s) * \Delta T_s$$

where the value of $\partial q_s / \partial T_s$ is determined from the formula described in chapter II.B.4. The long wave radiation from the surface term becomes

$$F_{ir} = \sigma * (T_s^4 + (\partial T_s^4 / \partial T_s) * \Delta T_s) = \sigma * T_s^4 + 4 * \sigma * T_s^3 * \Delta T_s$$

These terms can now be substituted into equation 2.9 and the equation can be solved for ΔT_s.

$$\Delta T_s \simeq -\left(F_{lw} + (1-\alpha)(1-P_e)F_{sw} + F_{sx} + \rho L_x C_D V (q_s(T_s) - q_a)\right.$$
$$\left. + (\rho C_p C_D V)(T_s - T_a) + \sigma T_s^4 - \frac{k_x (T(1) - T_s)}{H(1) *.5} \right) \qquad (2.10)$$
$$\Big/ \left(\rho L_x C_D V \, \partial q_s / \partial T_s + \rho C_p C_D V + (k_x / (H(1) *.5)) + 4\sigma T_s^3\right)$$

All values on the right side of equation 2.10 are defined at the new time step with the exception of T_s and H, which are defined at the present time step.

The balance of fluxes at the bottom surface involves only the turbulent flux from the ocean, F_o, and the conductive flux within the ice at that surface, F_{cond}. The equation has the form

$$F_o - F_{cond} = 0 \qquad\qquad (2.11)$$

Only the conductive flux is a function of the bottom surface temperature, T_{ocn}, and as in the top surface balance it is a linear function.

$$F_{cond} = k_i * (T_{ocn} + \Delta T_{ocn} - T(3)) / (H(3)*.5)$$

This is substituted into equation 2.11 which can now be solved for ΔT_{ocn}.

$$\Delta T_{ocn} = (F_o - k_i*(T_{ocn} - T(3))/(H(3)*.5))/(k_i/(H(3)*.5)) \qquad (2.12)$$

where F_o and T(3) are defined at the new time step and T_{ocn} and H(3) are defined at the last time step.

Both the top and bottom surface temperatures are constrained by the freezing point. If the balance at either surface would require the temperature to rise above that value or if the balance at the bottom surface would require the temperature to drop, the temperatures are reset to the freezing point and the energy imbalance is computed.

Energy Imbalance at the Top Surface

$$E = -\Delta t * (F_{lw} + (1-\alpha)*(1-P_e)*F_{sw} \quad\quad (2.13.a)$$
$$+ F_{sx} + F_l + F_s + F_{ir} + F_{cond})$$

Energy Imbalance at the Bottom Surface

$$E = -\Delta t * (F_o - F_{cond}) \quad\quad (2.13.b)$$

where Δt is the time step equal to 1/48 of a year.

The resulting surplus of energy at the top and bottom surfaces or deficit of energy at the bottom surface are used to warm and melt the adjacent layers of snow and ice, or grow ice at the bottom surface.

d. Method of Solution of the Snow and Ice Temperature Equations

The surface energy balance equations and internal temperature equations are solved in an interative procedure which includes the computation of brine storage, latent heat flux, and sensible heat flux; and constrains the values of the surface temperatures from exceeding the freezing point and in the case of the bottom surface from dropping below it.

The sequence of steps followed in solving for these temperatures are as follows. At the beginning of a time step the percentage of non reflected short wave radiation permitted to penetrate the surface is set, and any new energy penetrating the surface is computed and added to the heat reservoir.

At this point the iteration loop is entered. The first values to be computed within the loop are the modified forms of the sensible and latent heat fluxes at the surface as defined in equation 2.10. With these fluxes all the terms of equations 2.10 and 2.12 are known and they can be solved for the change in temperature at each of the surfaces.

At this point the new surface temperatures are tested. If the new top surface temperature exceeds the freezing point it is reset to that value, new sensible and latent heat fluxes are computed using this surface temperature, and the excess energy available for warming and melting the snow and ice layers is computed using equation 2.13.a. Note that the free air temperature and the specific humidity of the free air are held fixed.

The bottom surface temperature is not allowed to vary. Therefore, it is automatically reset to the freezing point and the excess or deficit energy available for warming and melting, or growing ice is computed using equation 2.13.b.

With the new surface temperatures the elements of the tridiagonal matrix equation, equation 2.8, are computed, and the system is solved for the new internal layer temperatures.

The calculation of the internal layer temperatures marks the end of the iteration loop. If this is the first pass through the loop the new top surface temperature is saved in a test variable, and another pass is made through the loop. After the second iteration the newly computed top

surface temperature is compared to the test variable. If the surface temperature has converged to within .01K, control is shifted out of the loop, otherwise, the new value of temperature is saved in the test variable and another pass is made through the loop. Experience has shown that the surface temperature generally converges within three to four iterations; however, in order to assure that control eventually leaves the loop the maximum number of iterations has been set to twenty.

Once the internal temperatures have been computed based on conductive fluxes within the ice they may be modified in two ways.

The first involves the refreezing of the brine pockets if the ice layer temperature would otherwise drop more than .1K below the freezing point. At the end of a summer season the ice layers can contain enough energy to warm and melt 30% of the ice. As the ice temperatures begin to drop this energy is used in delaying the drop in ice temperature until the heat reservoir is exhausted. Once this occurs the ice temperatures are allowed to drop further.

- The second modification to internal snow and ice temperatures is made if any of the temperatures is computed to exceed the freezing point. In such a case the temperature is reset to the freezing point and the excess energy available for melting is computed with the formula

$$E = (T(J,1) - T_f) * H(J,2) * (\rho c)_x.$$

With this computation the new temperatures at the surfaces

and within the snow and ice, and the energys available for melting snow and ice and/or growing ice are determined.

e. Determination of Snow and Ice Melt and Growth

Once the temperature and energy computations are complete, the changes in snow and ice thickness can be computed.

The first computation determines the accumulation of new snowfall at the top surface. If snow falls on a bare ice surface it is treated as a temporary new layer at the surface temperature. In the case of an existing snow layer the thickness of the new snow layer is the sum of the old layer thickness and the new snowfall. The temperature of this newly defined layer is the average of the temperature of the old layer weighted by its thickness, and the surface temperature weighted by the thickness of the new snowfall.

The remainder of the sea ice model is devoted to warming and melting snow and ice, and growing ice using the excess and deficit energys computed in chapter II.C.2.d. The method by which this is done is as follows. The energy excess computed at the top surface is combined with that computed for the top layer and will be applied to the top layer, be it snow or ice (if there a newly formed snow layer the energy excess will be applied there first). The energy excess computed for the center layer will be applied there. The energy excess computed for the bottom layer is added to

the energy excess or deficit computed at the bottom surface.
If the quantity is positive it is applied to the bottom
layer for melting. If the net energy is negative the excess
energy applied to melting the bottom layer is set to zero
and the remaining deficit is used later to grow new ice at
the bottom surface.

These quantities of energy are first applied to their
respective layers to warm them. During this process the
energy can be exhausted, in which case the layer will have a
new warmer temperature at or below the freezing point; or
the layer can warm to the freezing point and the remaining
energy used for melting.

If there is any energy left after a layer has been
warmed to the freezing point it is used to melt that layer.
In addition to the remaining excess energy, any heat stored
in the heat reservoir is used to help melt the layer. This
is done in such a way as to make the brine storage a passive
source of heat. It is used only in proportion to the
fraction of the layer melted. This allows more melting to
occur than if there were no stored heat, however, if there
is no excess energy available from the thermodynamic
calculations melting does not occur.

After a layer has entirely melted away, any remaining
energy is redistributed to the remaining layers to warm and
melt. This redistribution continues until the energy is
exhausted or the ice and snow melts away completely (If only
a snow layer remains energy is taken from the ocean to melt

it. If there is still an energy deficit after the energy budget computed for the ocean is complete a new layer of ice is formed). The way this energy is redistributed is stated in Table 2.1.

Table 2.1 Energy Redistribution in Ice Layers

Layer Which Has Melted Away	Layer To Which Remaining Energy Is Redistributed
1	2
1 & 2	3
2	half to 1 & half to 3
2 & 3	1
1 & 3	2
3	2
1, 2 & 3	ocean

Ice growth in general occurs only at the bottom surface. If there is an energy deficit computed at the bottom surface the volume of ice that deficit represents is computed. This new ice represents a new ice layer at the freezing point which is temporarily added to the sea ice grid.

It is also possible for ice to increase at the top surface. This occurs if the net budget of snowfall is positive year after year. At the present time this situation of continually growing snow is not observed over the sea ice on the oceans. However, this situation does occur occasionally over ice on lakes (Weeks and Lee, 1958; Adams and Rogerson, 1968). In these cases the snow layer becomes thick enough to depress the ice below the water level. Water then infiltrates the snow by coming through the ice at leads

and generally freezes there creating "white ice". The effect
is to reduce the snow and increase the ice thickness.

This mechanism is difficult to treat accurately in this
model because it introduces a new material which has a
different specific heat and thermal conductivity into the
system. However, I have introduced a crude method of
representing this process so that the unrealistic situation
of a continually growing snow layer is removed. First the
hydrostatic level of the snow and ice, Figure 2.3, is
computed. If that level would put some of the snow below
the water level, equation 2.14, that snow is simply
transformed into ice and added to the top ice layer (the
temperature of the resulting top ice layer is a weighted
average of the temperature of the original ice layer and the
snow temperature). Solving for x, with H_s - x being the
amount of snow below the water level,

$$x = H_i + H_s - (\rho_s * H_s + \rho_i * H_i)/\rho_w. \qquad (2.14)$$

The major deficiency of this method is that it doesn't
allow for the addition of new mass, the ocean water, into
the system, and results in the converted ice being thinner
than it may be in reality. However, this process has only
been observed in a few locations, and is therefore not well
understood. Further study of this mechanism will allow a
better understanding of its importance in sea ice processes,
and permit more accurate representations of it to be
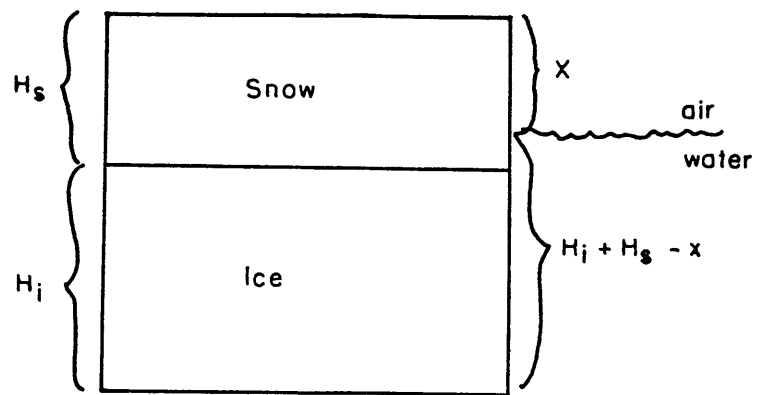
Figure 2.3. Schematic of Depression of Snow Layer Below
Sea Level

$$(\rho_s * H_x + \rho_i * H_i) = \rho_w * (H_i + H_s - x)$$

where: ρ_s = snow density

ρ_i = ice density

ρ_w = water density

H_s = snow thickness

H_i = ice thickness

x = portion of snow and ice
   above water level

included in sea ice models.

f. Method of Maintaining Equal Ice Grid Box Spacing

Once the computations affecting snow and ice thickness are completed it is possible to have ice layers of different thicknesses and the addition of a new snow layer (on bare ice) and a new ice layer at the bottom surface. Before a new time step can begin the assumptions made in constructing the thermodynamic equations concerning the number of layers, 3, and the equal thickness of the ice layers must be restored.

If there is no snow, the ice is divided into three layers. The temperature and the amount of brine stored in these layers is computed by determining the distribution of the old layers in each of the new layers; and then weighting the old values of temperature and brine storage by these distributions. If there is a snow layer the same process is followed except the ice is divided into two layers.

3. Numerical Formulation of the Ocean Model Equations
a. Ocean Layer Energy Balance Equations

The ocean model is a simple isothermal mixed layer to which a layer energy balance is applied. The ocean temperature is free to vary in response to external fluxes of energy if ice free conditions exist. However, if the temperature is required to drop below the freezing point, the ocean temperature is held at that value and new ice is initiated at the surface. A schematic diagram of the ocean
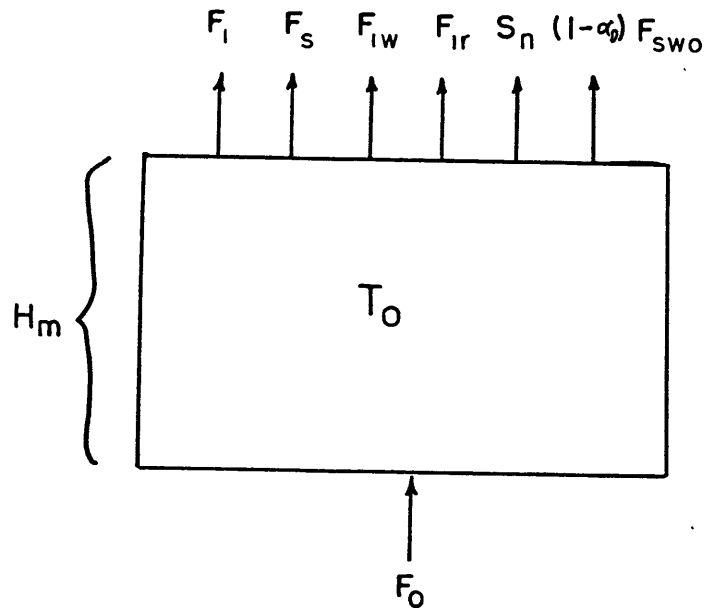
Figure 2.4. Schematic of Ocean Mixed Layer

F_1 = latent heat flux

F_s = sensible heat flux

F_{swo} = short wave radiation over ocean

α_0 = albedo over ocean

F_{lw} = long wave radiation from atmosphere

T_0 = ocean temperature

F_{ir} = long wave flux from ocean

S_n = snowfall melted in ocean

H_m = mixed layer depth

F_0 = net turbulent flux of energy from oceanic sources. In ice covered zone this energy is assumed to be that delivered to the bottom of the ice.

Note: All fluxes are defined as positive upward, therefore F_{sw} and F_{lw}, are always negative quantities.

model is shown in Figure 2.4.

The energy balance equation applied to the ocean layer is similar to that applied to the sea ice surface except that the layer has a heat capacity. The energy equation describing the time rate of change of the ocean layer temperature is as follows

$$(\rho c)_0 * \frac{\partial (H_m * T_0)}{\partial t} = (-F_1 - F_s - F_{lw} - (1-\alpha_0)*F_{swo} - F_{ir} - S_n + F_0) \quad (2.15)$$

where $(\rho c)_0$ is the volumetric specific heat of ocean water. The sensible and latent heats are determined as described for the sea ice model except the ocean layer temperature replaces the snow ice surface temperature. The value of S_n is determined by computing the energy needed to warm the snow from the air temperature (or freezing point if the air temperature is above that value) to the ocean temperature and then to melt it completely. This is a very small term and can probably be neglected.

The numerical scheme applied to equation 2.15 is similar to that applied to the internal ice and snow equations. It is a semi implicit scheme in which there is a weighting of old and new terms which can be varied to make the scheme range from fully explicit to fully implicit. The numerical form of equation 2.15 solved for the new ocean temperature is as follows:

$$
\begin{aligned}
T_o(1) = \Big[&-(F_i(1) + F_s(1)) - \beta(\cdot F_o(1) + F_{lw}(1) + (1 - \alpha_o(1)) F_{swo}(1) \\
&+ \sigma T_o^4(1) + (-T_{sn1} * (\rho c)_s + (vq)_s) A_{hs}(1)) \\
&-(1-\beta)(-F_o(2) + F_{lw}(2) + (1 - \alpha_o(2)) F_{swo}(2) + \sigma T_o^4(2) \\
&+ ((T_o(2) - T_{sn2})(\rho c)_s + (vq)_s) A_{hs}(2)) + (H_m(2)(\rho c)_o /\Delta t) T_o(2) \Big] \\
&/ ((H_m(1)(\rho c)_o /\Delta t) + \beta (\rho c)_s A_{hs}(1))
\end{aligned}
\qquad (2.16)
$$

where $(vq)_s$ is the volumetric heat of fusion of snow, A_{hs} is the snowfall during the time step, T_{sn1} and T_{sn2} are the temperatures of the snow at the new and past time step and are set either to the air temperature or the freezing point whichever is lower, and β is the weighting parameter which ranges from 0 for a fully explicit scheme to 1 for a fully implicit scheme. The new values of the latent heat and sensible heat flux are computed using the weighting parameter, and therefore are not further weighted in equation 2.16.

Equation 2.16 is solved in an iterative procedure. Sensible and latent heat fluxes are first computed with old values of ocean temperature. The new ocean temperature is then computed. This new temperature is used to recompute the sensible and latent heat fluxes. After two iterations are complete a comparison is made between the ocean temperatures computed at the present and last iteration until the ocean temperature has converged to within a specified tolerance, .01K in this model.

Ocean temperature is allowed to change when ice free conditions exist, or until it is required to drop below the freezing point. In either of these cases the ocean

temperature is reset to the freezing point, and the energy
deficit or surplus is computed. An energy deficit will be
used either to initiate new ice if ice free conditions
previously existed, or to freeze new ice in leads. An energy
surplus is used to widen the leads by melting ice from the
edge.

b. Lead Parameterization

Leads, or cracks in the ice pack, are important in
determining the transfer of energy between the atmosphere
and ocean. Therefore, it is important to include them in the
model.

The lead parameterization used here follows, in
general, that described by Semtner (1976) and used by
Washington et. al., 1976.

When ice exists a minimum area of open ocean, leads, on
the order of 1% in the northern hemisphere and 2% in the
southern hemisphere of the total area, is assumed. An energy
balance is applied to the area of open ocean much the same
as that applied to the ocean in ice free conditions. Any
excess energy absorbed in the leads is used to open them
wider by melting laterally. Any net heat loss from the leads
is used to form new ice of specified thickness in the lead.
A new mean ice thickness is obtained through an area
weighted average of the old and new ice thicknesses.

In the case of new ice growth Washington et. al., 1976
open new leads in the ice by essentially distributing the

lead ice mass over the remaining ice area. In this model if new ice is formed in the leads the minimum lead area is reopened, and the ice in that area is assumed to leave the zone. This is a crude simulation of the dynamic transport of ice to other regions, which may be an important mechanism in maintaining a relatively thin ice cover over Arctic regions (Orvig, 1970).

D. The Continental Ice Sheet Model

The continental ice sheet model is essentially made up of two parts which include a two[3] dimensional zonally averaged dynamic model of ice flow, and a surface energy balance that determines the net budget of accumulation at the surface of the ice.

1. Derivation of the Dynamic Equations of Ice Flow

The ice flow model determines the horizontal continental ice velocity and ice thickness as a function of latitude and time. It was derived from the equations of motion, the Generalized Flow Law (Paterson,1969), and Glen's Creep Law (Glen, 1955; Paterson, 1969).

The equations of motion as applied to the ice sheets are

$$\frac{dv}{dt} = f_y - \frac{1}{\rho}\frac{\partial P}{\partial y} + \frac{1}{\rho}\left(\frac{\partial t_{yx}}{\partial x} + \frac{\partial t'_{yy}}{\partial y} + \frac{\partial t_{yz}}{\partial z}\right) \qquad (2.17)$$

$$\frac{dw}{dt} = f_z - \frac{1}{\rho}\frac{\partial P}{\partial z} + \frac{1}{\rho}\left(\frac{\partial t_{zx}}{\partial x} + \frac{\partial t_{zy}}{\partial y} + \frac{\partial t'_{zz}}{\partial z}\right) \qquad (2.18)$$

$$\frac{du}{dt} = f_x - \frac{1}{\rho}\frac{\partial P}{\partial x} + \frac{1}{\rho}\left(\frac{\partial t'_{xx}}{\partial x} + \frac{\partial t_{xy}}{\partial y} + \frac{\partial t_{xz}}{\partial z}\right) \qquad (2.19)$$

where v,w, and u are ice velocities northward, upward, and eastward respectively, f_i are body forces, ρ is the density

of the ice, P is the hydrostatic pressure, τ_{ij} are the shear stresses on a unit volume of ice, and $\tau'_{ii} = \tau_{ii} - P$.

The following assumptions are made:

1) The ice flows under hydrostatic conditions, therefore the normal stresses are zero. ie. $\tau'_{xx} = \tau'_{yy} = \tau'_{zz} = 0$.

2) The ice sheet is zonally averaged, therefore there is no variation in the x direction. ie. $\partial/\partial x = 0$, $\tau_{yx} = 0$, and $\tau_{zx} = 0$.

3) The stress tensor is symmetric, therefore there is no rotation. ie. $\tau_{yx} = \tau_{xy} = 0$, $\tau_{zx} = \tau_{xz} = 0$, and $\tau_{zy} = \tau_{yz}$.

4) A steady state condition is assumed, therefore $\frac{dv}{dt} = \frac{du}{dt} = \frac{dw}{dt} = 0$. Another way to look at this is to say that the velocity field of the ice sheet adjusts much faster to perturbations than the height field.

5) The only body force acting is gravity. ie. $f_x = f_y = 0$, $f_z = -g$.

6) The north-south atmospheric pressure gradient is small compared to that gradient within the ice and is therefore neglected.

7) The north-south gradient of τ_{zy} (the stress on the y plane in the z direction) is small and therefore neglected.

See Figure 2.5 for a schematic diagram of the ice sheet.
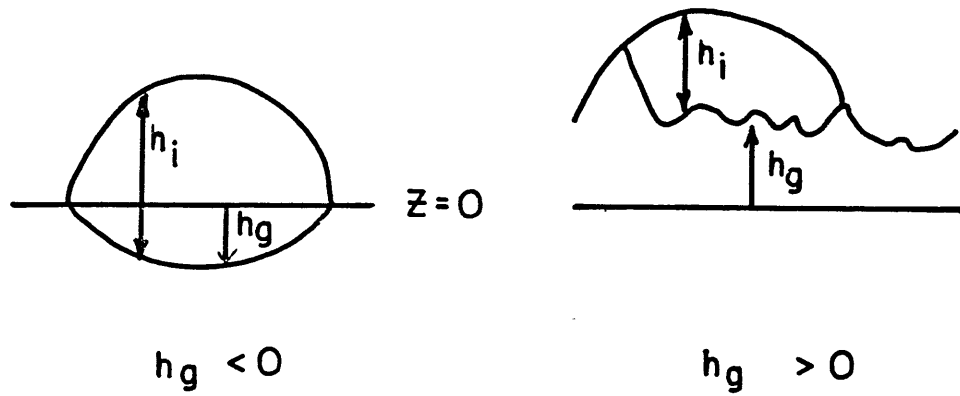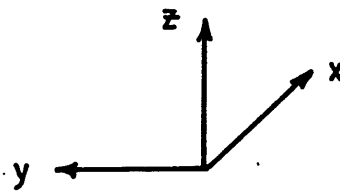
Figure 2.5 Schematic Diagram of Continental Ice Sheet Model

h_i = ice thickness

h_g = bedrock elevation with respect to sea level

x = longitudinal dimension

y = latitudinal dimension

z = vertical dimension

Substituting these into the equation of motion results in the following

$$0 = -\frac{1}{\rho}\frac{\partial}{\partial y}\left(\rho g\left(h_i + h_g - z\right)\right) + \frac{1}{\rho}\frac{\partial t_{yz}}{\partial z} \qquad (2.17')$$

$$0 = -g - \frac{1}{\rho}\frac{\partial P}{\partial z} \qquad (2.18')$$

where h_i is the ice thickness and h_g is the height of the ground above a reference level (taken to be mean sea level). Equation 2.17 can be integrated from the ice sheet surface to some level z within the ice to obtain the shear stress, t_{yz}.

$$t_{yz} = -\rho g * (h_i + h_g - z)\frac{\partial}{\partial y}(h_i + h_g) \qquad (2.20)$$

This is used in conjunction with the Generalized Flow Law and Glen's Creep Law to determine the vertically averaged longitudinal velocity for the ice, $\widetilde{v}$ ($\widetilde{()}$ indicates a vertical average).

The Generalized Flow Law for an isotropic material assumes

$$\dot{\varepsilon}_{yz} = \lambda\, t_{yz} \qquad (2.21)$$

where $\dot{\varepsilon}_{yz}$ and t_{yz} are the component strain rate and shear stress, λ is a parameter that is a function of position. Glen's Creep Law is

$$\dot{\varepsilon} = A \tau^n \qquad (2.22)$$

where $\dot{\varepsilon}$ and τ are the effective strain rate and shear stress, and A and n are constants determined experimentally. Using the following

$$2\tau^2 = \tau'^2_{xx} + \tau'^2_{yy} + \tau'^2_{zz} + 2(\tau^2_{xy} + \tau^2_{yz} + \tau^2_{xz})$$

$$2\dot{\varepsilon}^2 = \dot{\varepsilon}^2_{xx} + \dot{\varepsilon}^2_{yy} + \dot{\varepsilon}^2_{zz} + 2(\dot{\varepsilon}^2_{xy} + \dot{\varepsilon}^2_{yz} + \dot{\varepsilon}^2_{xz})$$

(Paterson, 1969) which relate the effective shear stress and strain rate to the component shear stresses and strain rates, and keeping in mind the assumptions made earlier, equations 2.21 and 2.22 can be combined to give

$$\dot{\varepsilon}_{yz} = A \tau_{yz}^n \qquad (2.23)$$

This strain rate is equal to half the vertical derivative of the longitudinal velocity, ie. $\dot{\varepsilon}_{yz} = .5 * \partial v / \partial z$ (Paterson, 1969). Substituting this into equation 2.23 results in

$$\frac{1}{2} \frac{\partial v}{\partial z} = A \tau_{yz}^n \qquad (2.24)$$

Now, substituting equation 2.20 into equation 2.24, and integrating in the vertical over the thickness of the ice sheet gives an expression for the vertical profile of velocity. This is averaged over the thickness of the ice sheet to determine the vertically averaged northward velocity, $\tilde{v}$.

$$\tilde{V} = \frac{2A(\rho g)^n h_i^{n+1}}{n+2}\left(-\frac{\partial}{\partial y}(h_i+h_g)\right)\left|\left(-\frac{\partial}{\partial y}(h_i+h_g)\right)^{n-1}\right| \qquad (2.25)$$

The value of n is determined experimentally and ranges between 2.5 and 4, with the accepted value being 3. The value of A is a function of temperature (Glen, 1955). Most modeling studies have used n=3; however, the value of A has varied widely. Using a temperature dependent empirical formula of ice flow from Budd (1969) gives a range for A of .03 to .63 $yr^{-1}bar^{-3}$ for a temperature range of -10C to 0C and n=3. Birchfield et. al. (1981), using the laws of ice flow, experimental data and scaling, estimates a range for A of .03 to 2.8 $yr^{-1}bar^{-3}$ with .3 $yr^{-1}bar^{-3}$ being a typical value. Paterson (1969) states that for n=3 the value of A is .03 $yr^{-1}bar^{-3}$ for a temperature of -10C, and .15 $yr^{-1}bar^{-3}$ for a temperature of 0C. Pollard's two dimensional model (1982) uses a value for A of 2.1 $yr^{-1}bar^{-3}$ and n=3. Mahaffy's three dimensional model (1976) experiments with various values which range from .16 to .21 $yr^{-1}bar^{-3}$ for n=3. Budd and Smith's (1979) three dimensional model uses a value of A of .1 $yr^{-1}bar^{-2.5}$ and n=2.5. The values used in this model for most of the experiments are n=3 and A=.15 $yr^{-1}bar^{-3}$.

The thickness of the ice sheet is affected by two processes. The first is the accumulation minus ablation rate, a, which is an exchange with the atmosphere, and the second is the convergence of ice volume due to differential ice flow, $\partial(\tilde{V}*h_i)/\partial y$. The rate of change of ice thickness is

expressed as follows:

$$\frac{\partial h_i}{\partial t} = a - \frac{\partial(\tilde{v} * h_i)}{\partial y} \qquad (2.26)$$

Equations 2.25 and 2.26 are used together to determine the zonally averaged thickness and the zonally and vertically averaged velocity of the ice sheet as a function of latitude and time, given an accumulation minus ablation rate as a function of latitude and an initial ice sheet profile.

Other features that are included in the model are a weighting for the convergence of the longitudes, and isostatic adjustment of the ground beneath the weight of the ice.

Weighting the ice thickness by the area of the latitude band it occupies takes into account the variation with latitude of the horizontal area available for a volume of ice. As a unit volume of ice flows southward in the northern hemisphere it spreads out over a larger area, and therefore thins out. The opposite is true for the ice flowing northward.

The earth's crust floats on a fluid substance called the mantle. When ice sheets form the added weight on the land depresses it deeper into the mantle. This changes the slope of the land surface on which the ice sits, and therefore its flow rate. This feature is incorporated into

the model by determining the time rate of change of the
height of the land surface above the reference level.
Following Weertman (1976), it is assumed that the density of
the crust is three times that of ice. In this case the
amount of ice depressed below the original level of the
ground at equilibrium is half of that above it. The equation
used by Weertman is

$$h_{ge} = h_{go} - h_i/3 \qquad (2.27)$$

where h_{ge} is the equilibrium height of the ground above some
reference level, and h_{go} is the original height of the
ground before ice formed.

Weertman (1976) assumes that the equilibrium value of
h_g is reached instantaneously. Here this assumption is
dropped and hg is allowed to approach its equilibrium value
exponentially. The time rate of change of h_g is

$$\partial h_g/\partial t = - k * (h_g - h_{ge}) \qquad (2.28)$$

where k is the reciprocal of the e-folding time, set to
1/3000 years in this model. Equation 2.27 is used at each
time step to determine h_{ge}. This value of h_{ge} is substituted
into equation 2.28 to determine h_g at the new time step. The
new h_g is then put into equation 2.25 to determine ice
velocities.

With the the inclusion of the features of weighting for

the convergence of the latitudes, and the isostatic adjustment of the land beneath the ice the mathematical derivation of the continental ice sheet model is complete.

2. Numerical Formulation of Dynamic Equations

The model equations derived in chapter II.D.1. include the vertically averaged velocity, equation 2.25, the rate of change of the land height, equations 2.28 and 2.27, and the time rate of change of the ice thickness, equation 2.26.

$$\tilde{V} = \frac{2A(\rho g)^n h_i^{n+1}}{n+2} \left(-\frac{\partial}{\partial y}(h_i + h_g)\right) \left|\left(-\frac{\partial}{\partial y}(h_i + h_g)\right)^{n-1}\right| \qquad (2.25)$$

$$\frac{\partial h_g}{\partial t} = -K * (h_g - h_{ge}) \; ; \quad h_{ge} = h_{go} - h_i/3 \qquad \begin{array}{c}(2.28);\\(2.27)\end{array}$$

$$\frac{\partial h_i}{\partial t} = a - \frac{\partial(\tilde{V} * h_i)}{\partial y} \qquad (2.26)$$

These equations allow the determination of the vertically averaged ice velocity as a function of latitude and the ground height and ice thickness as a function of latitude and time given a value for a.

These equations are applied to a staggered latitudinal grid in which the velocity is defined at one degree latitudinal spacings from 90N and 90S, and the ice thicknesses and land heights are defined at the same grid spacings from 89.5N to 89.5S. Centered space differencing

and previously determined values of ice thickness and land
height are used to diagnostically determine ice velocity and
new land height values. With these the computation of a new
ice thickness can be made.

Equation 2.26 can be divided into two parts, ice
thickness change due to accumulation and ablation at the
surface, and that due to the convergence of ice in a one
degree latitude zone. Thickness change due to net
accumulation is applied at the end of the ice thickness
calculation and will be discussed in chapter II.D.3. The
equation for thickness change due to ice flow,

$$\partial h_i / \partial t = -\partial(\tilde{V} * h_i)/\partial y,$$

is solved using a semi implicit numerical scheme which uses
a weighted average of values from old and new time steps
(when the weighting is equal to .5 the scheme is referred to
as Crank-Nicholson), and centered space differencing which
includes weighting for convergence of the longitudes. Such
an equation is applied to each latitude and the system is
solved simultaneously in a tridiagonal matrix. The numerical
form of these equations is as follows:

$$\tilde{V}(J,2) = \frac{2A(\rho g)^n}{n+2} \left((h_i(J-1,2)+h_i(J,2))/2\right)^{n+1} *$$

$$(-(h_i(J-1,2)+h_g(J-1,2))+(h_i(J,2)+h_g(J,2)))/\Delta y$$

$$* \left|(((h_i(J-1,2)+h_g(J-1,2))-(h_i(J,2)+h_g(J,2)))/\Delta y)^{n-1}\right| \qquad (2.25')$$

$$h_g(J,1) = -\Delta t * K * \left(h_g(J,2) - h_{ge}(J,2) \right) + h_g(J,2) \; ; \qquad \text{(2.28');}$$
$$\text{(2.27')}$$

$$h_{ge}(J,2) = h_{go}(J) - h_i(J,2)/3$$

$$\frac{h_i(J,1) - h_i(J,2)}{\Delta t} = \frac{1}{A_r(J)} * \left((1.-\beta) * \left[\tilde{\tilde{v}}(J,2) * C(J) * ((h_i(J-1,2)+h_i(J,2))/2 \right. \right.$$
$$- \tilde{\tilde{v}}(J+1,2) * C(J+1) * ((h_i(J,2)+h_i(J+1,2))/2 \right] \qquad \text{(2.26')}$$
$$+ \beta * \left[\tilde{\tilde{v}}(J,2) * C(J) * ((h_i(J-1,1)+h_i(J,1))/2 \right.$$
$$\left. \left. - \tilde{\tilde{v}}(J+1,2) * C(J+1) * ((h_i(J,1)+h_i(J+1,1))/2 \right] \right)$$

where the first index, J, indicates spatial grid points and the second index indicates time, 1 for the new time step and 2 for the last time step; $C(J)$ is the length of a latitude circle at the velocity grid points; $A_r(J)$ is the area of a one degree latitude zone centered at the ice thickness grid point; t is the time step, 10 years here, and β is the weighting parameter set to .5. Note that $\tilde{v}(J,2)$ and $h_i(J,2)$ are not evaluated at the same grid point. $\tilde{v}(1,2)$ is located at 90N while $h_i(1,2)$ is located at 89.5N. $\tilde{v}$ and C are defined at the same grid point, and h_i, h_g, and A_r are defined at the staggered grid point.

Equation 2.26' is algebraically rearranged so all values of h_i at the new time step appear on the left hand side with all other terms on the right hand side of the equal sign. In this form the equations for all 180 latitude zones are put into a 180x180 tridiagonal matrix which is

solved using a tridiagonal matrix solver.

Once the change in ice thickness due to ice flow is determined the net accumulation at each latitude is added to obtain the new ice thickness.

3. Surface Energy Balance and Net Budget

The source of a continental ice sheet is the accumulation of snow at its surface. In order to determine the net accumulation of snow it is necessary to compute the total amount of snowfall and the total melt, ablation, over the time step. The amount of snow is a function of present precipitation amounts over land, air temperature and saturation vapor pressure; and is described in more detail in chapter II.B.5. The ablation is determined from a surface energy balance equation, very similar to that described for the top surface of sea ice. The surface energy balance equation is

$$F_1 + F_s + (1-\alpha)*F_{sw} + F_{lw} + F_{ir} = 0 \qquad (2.29)$$

where F_1 is latent heat flux, F_s is sensible heat flux, α is albedo, F_{sw} is incoming short wave radiation, F_{lw} is incoming long wave radiation from the atmosphere, and F_{ir} is the outgoing long wave flux from the surface. There are only two qualitative differences between this and the surface balance equation described in chapter II.C.2.c. for sea ice. First there is no conductive heat flux from below the

surface of the ice; and second, there is no penetration of solar radiation into the ice sheet. The inclusion of these processes would require a thermodynamic calculation and is beyond the scope of this model.

The values of short wave radiation, albedo, and incoming long wave radiaion from the atmosphere are known. The other fluxes are functions of the surface temperature and must be determined. This is done in the same way as described for the sea ice (see chapter II.C.2.c. Surface Energy Balances) and the resulting equation for the change in the surface temperature is

$$\Delta T_s = -\left(F_{lw} + (1-\alpha)F_{sw} + \rho L_x C_D V \left(q_s(T_s) - q_a\right) + \right. \qquad (2.30)$$
$$\left. (\rho C_p C_D V) * (T_s - T_a) + \sigma T_s^4\right) / \left(\rho C_D V \left(L_x \frac{\partial q_s}{\partial T_s} + C_p\right) + 4\sigma T_s^3\right)$$

Equation 2.30 is solved in an iterative procedure which recomputes the temperature at all the latitudes until the slowest to converge gets to within .5K of its value at the last iteration.

The surface temperature is allowed to vary freely if it remains below the freezing point. If a balance would require the surface temperature to rise above the freezing point it is held at that value and the resulting excess energy, 2.31, is computed and used for ablation.

$$E = \left(T_{s1} - T_f\right) * \left(\rho C_D V \frac{\partial q_s}{\partial T_s} + C_p\right) + 4\sigma T_s^3\right) * \Delta t \qquad (2.31)$$

where T_{s1} is the surface temperature computed to maintain energy balance, T_f is the freezing point, and all other variables are evaluated as for sea ice. When the ice melts away completely the surface temperature is allowed to vary freely both below and above the freezing point.

The net budget, a, as required in equation 2.26 is the accumulation minus the ablation which occurs over the time step of integration of the dynamic ice flow equations, 10 years. Since accumulation and ablation vary seasonally, the surface energy balance equation and the snowfall are computed at approximately two week time steps. The net budget computed at each of these time steps is summed over the 10 year period to produce a net budget for the ice sheet time step.

There are only two restraints put on the net budget. The first is put into effect if the ice disappears during the surface integration. The ablation at that time step is then set equal to minus ice and snow present at that point, and any excess energy is allowed to warm the land surface. The second is put into effect if no ice is present at the beginning of the surface integration, and during the last year of integration the newly accumulated snow melts away. In this case the net budget is set to zero. Both of these restraints are implemented in order to prevent the ablation from exceeding the ice and snow available for melting.

In addition to the ablation computed from the surface energy balance equation there is ablation due to calving of

the ice into the oceans at the edges of the continents. As this ice is no longer part of the dynamic flow of ice on the continent it is treated as an ablation and added to the net budget. Regions of calving ablation occur at the southern edge of the Arctic Ocean where it is an abrupt change in the net budget, and at the northern edge of Antarctica where it is a linear change in the net budget over five degrees of latitude that can extend under the edge of the ice sheet..

Once the complete net budget is determined for the ten year ice sheet time step it is used in equation 2.26 to determine the
new ice sheet thickness.

4. Method of Solution of the Ice Sheet Model

At the beginning of an ice sheet computation an initial ice sheet and the atmospheric forcings are specified. The atmospheric forcings are as described in chapter II.B. except for the air temperature which must be modified by the lapse rate to adjust it at each latitude to the elevation of the input ice sheet.

The surface temperatures at each latitude are then initialized as a simple function of the air temperature modified such that the surface is five degrees colder than the air at the poles and five degrees warmer than the air at the equator.

The atmospheric forcings are initially specified at each latitude at which an ice thickness is defined, however,

in order to increase the speed of the model all other
calculations done to determine the atmospheric forcings, the
land energy balance, and the net budget are done every five
degrees of latitude from 87.5N to 87.5S and at the most
poleward latitudes, 89.5N and 89.5S. The atmospheric
forcings at each latitude of the five degree grid is an
average of the forcing at that latitude on the one degree
grid and the two surrounding latitudes. The result of the
net budget on the five degree grid is later interpolated to
the one degree grid required in the dynamic ice sheet
calculations.

Once the net budget is completely determined a new ice
sheet profile is computed, and the first time step
completed.

The next time step begins by adjusting the air
temperature to the new ice sheet elevations and recomputing
any of the atmospheric forcings affected by that change. It
is also possible at this point to vary any of the other
forcings which might vary with time, such as solar radiation
through the Milankovitch mechanism. A new net budget is then
determined and used to compute a new ice sheet profile,
completing another time step.

There are two options involving the computation and use
of the net budget, that have been included in the model in
order to speed up the calculations.

The first of these involves the number of seasonal
cycles computed before the net budget is applied to the ice

sheet. The original form of the net budget required the full ten years of seasonal cycles to be computed. In order to speed up the model an option has been added to decrease the number of time steps to some integral number of years (ie. 24, 48, 72,....240 time steps for 1, 2, 3,....10 seasonal cycles respectively). It has been found that in the context of this model the net budget at the end of one year is equal to that at the end of 10 years; with the difference between corresponding time steps in the first and second years disappearing after the second time step. The reason for this is that all forcing seasonal cycles are specified. The only atmospheric variable which is directly changed is the air temperature and that is due only to the change in the elevation of the ice surface. In one time step the change in ice sheet elevation is small, in general not exceeding a half a meter and usually much less. Even with this "large" a change in elevation the resulting air temperature change is very small, less than .003K. As a result the surface energy balance comes to equilibrium very quickly. To save computer time model experiments are done with only one or two seasonal cycles. However, when the model is eventually coupled to a climate model the magnitude of the change in the net budget resulting from decreasing the number of seasonal cycles computed will have to be reexamined.

The second option included involves the reuse of a computed net budget for a few ice sheet time steps. The original computations required the calculation of a net

budget for each ice sheet time step. In order to speed up
the model further a parameter has been added which specifies
the number of times a net budget is to be used. It has been
found that in this model using the net budget three or five
times before recomputing does not change the equilibrium
situation, only the number of ice sheet time steps it takes
to get there. In the case of a growing ice sheet with no
melt, as in Antarctica, increasing the number of times the
net budget is used decreases the number of time steps needed
to reach equilibrium. This is because as the ice sheet grows
the accumulation decreases, however, if the net budget is
reused the accumulation remains constant as the ice sheet
grows. This in effect adds more snow to the ice sheet
allowing it to grow faster.

In the cases of shrinking ice sheets or for growing ice
sheets which have some melting at the surface the situation
is more complicated due to the competing effects of
accumulation and ablation. However, by reusing the net
budget the rate of change of the ice thickness is either
increased or decreased over the rate of change of ice
thickness resulting from recomputing the net budget for each
ice sheet time step, thus affecting the number of ice sheet
time steps required to reach equilibrium.

In this work this option is used only if equilibrium is
desired. In the sensitivity studies in which the speed at
which the ice sheet varies is of interest, the net budget is
computed for each ice sheet time step.

Chapter III. Simulation

The first experiment that must be done with the sea ice
and continental ice sheet models is to force them with
present day seasonal and latitudinal distributions of air
temperature and solar radiation to see how well they
simulate present cryospheric conditions. In the following
sections the results from such experiments are compared with
results of previous modeling studies and with published and
inferred data of the latitudinal and seasonal distribution
of sea ice and the latitudinal distribution of continental
ice. The methods by which some of the data is inferred, and
the uncertainties in this and the published data are
discussed.

A. Sea Ice - Present Conditions
1. The Base Case for the Original Model

The sea ice model used here is a modification of that
used by Semtner (1976) and Maykut and Untersteiner (1971).
Therefore, the base case will first be chosen by adjusting
the present sea ice model to correspond to these models, by
assuming that there are no leads and specifying albedo, and
then matching the results to those of Semtner's and Maykut
and Untersteiner's models and the results of models from
which they were derived.

The models mentioned above were used to look at sea ice
variations at specific locations. One of the earliest models
of sea ice was developed by Untersteiner (1964) and was used

to simulate the variations in sea ice as recorded by Drift
Station A, located mainly between 83N and 85N, during the
International Geophysical Year 1956/57 (Untersteiner, 1961).
Semtner's (1976) and Maykut and Untersteiner's (1971) models
used seasonal cycles of atmospheric variables to force the
sea ice which are generally typical of the region of 75N to
80N. Since the present model was derived to most closely
resemble Semtner's, the latitude of the base case was chosen
to be 77.5N.

The present sea ice model was forced with zonally
averaged seasonal cycles of the atmospheric variables
representive of 77.5N. This included the air temperature,
solar insolation at the top of the atmosphere, albedo, wind
speed, cloud fraction, relative humidity, and surface air
pressure; and contrasts with the previous models which
specify the fluxes of short wave radiation, long wave
radiation, sensible heat, and latent heat. The only other
variable that needed to be defined was the vertical oceanic
heat flux at the bottom surface of the ice. Since this value
was one of the least well known it was used as the tunable
parameter to adjust the model results to obtain a base case
that was similar the those of the previous studies.

Figure 3.1 shows the equilibrium seasonal cycle of sea
ice thickness for values of oceanic heat flux ranging from 0
to 10 W m^{-2}. Semtner's and Maykut and Untersteiner's results
correspond reasonably well for oceanic heat flux values
ranging from 3 to 4 W m^{-2}, and Untersteiner's (1964)
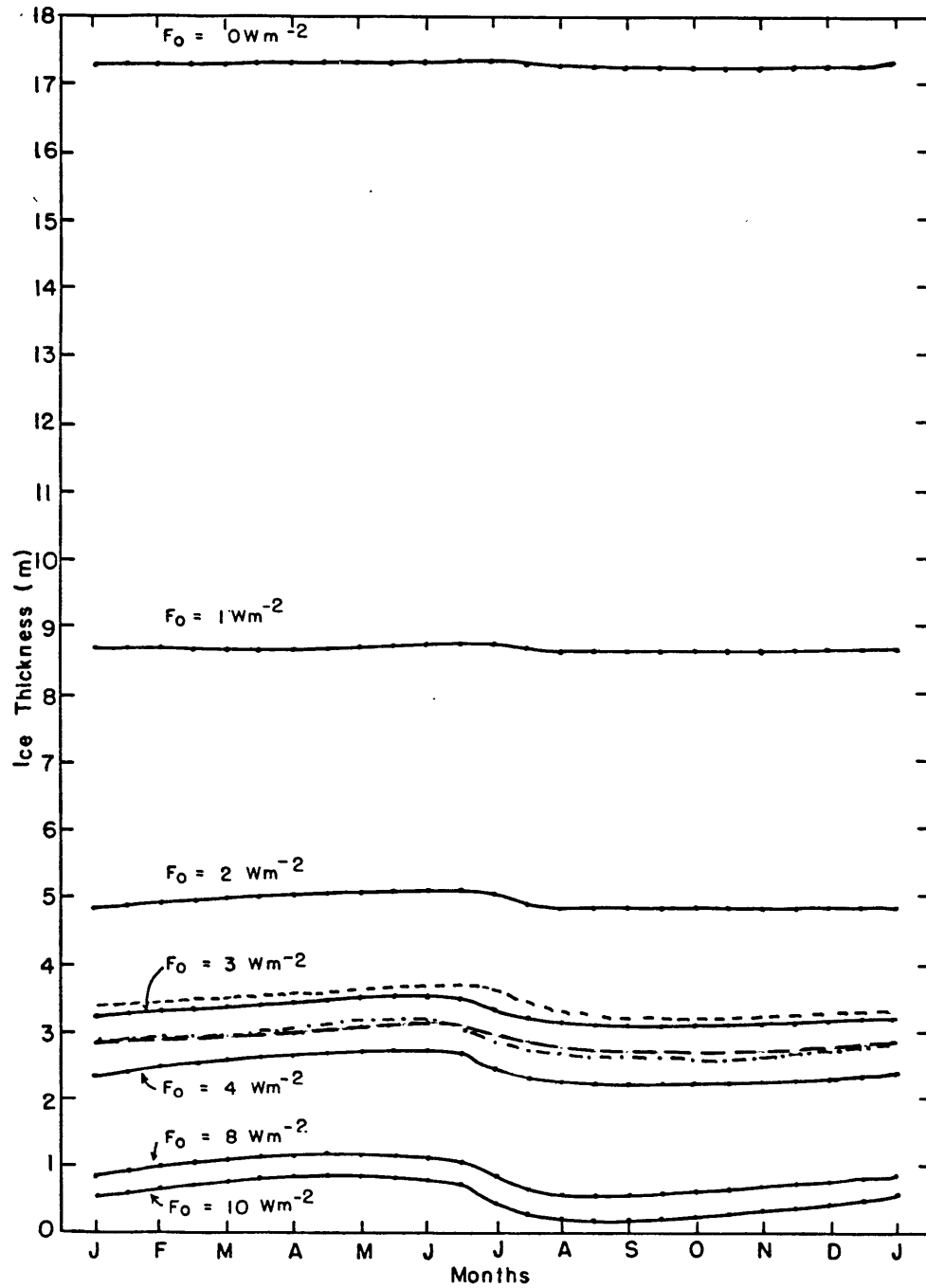
Figure 3.1 Equilibrium seasonal cycle of sea ice thickness
for various values of oceanic heat flux (solid
lines) and the results of Untersteiner 1964
(short dashed line), Maykut and Untersteiner
1971 (long dashed line), and Semtner 1976 (dot
dashed line)

results, applicable to higher latitudes, correspond well with results for an oceanic heat flux of 3 W m^{-2}. However, the value of oceanic heat flux used in these models was 2 W m^{-2}. Table 3.1 shows that for this oceanic heat flux the mean ice thickness computed by the present model was 4.9 m or 1.6 m greater than for an ocean flux of 3 W m^{-2}.

Table 3.1 Variations of Sea Ice Thickness with
Changes in Ocean Flux and for Other Studies

F_o (W m^{-2})	Mean Ice Thickness (m)	Range of Ice Thickness (m)
0.	17.3	.07
1.	8.7	.13
2.	4.9	.28
3.	3.3	.39
4.	2.4	.46
8.	.8	.62
10.	.5	.70
Untersteiner (1964)	3.4	.5
Maykut and Untersteiner (1971)	2.9	.46
Semtner (1976)	2.9	.59

There are a number of possible causes for the differences in ice thickness for comparable values of ocean flux. The first is the difference in the surface energy fluxes as defined in each of the models. Figure 3.2 shows the individual fluxes for both the present model and Semtner's model. Most of the fluxes follow the same general cycle of variation between the two cases. The differences in the magnitude of the fluxes are compensated for by variations in the other fluxes, except for absorbed solar radiation during the ice growing season. During this period,
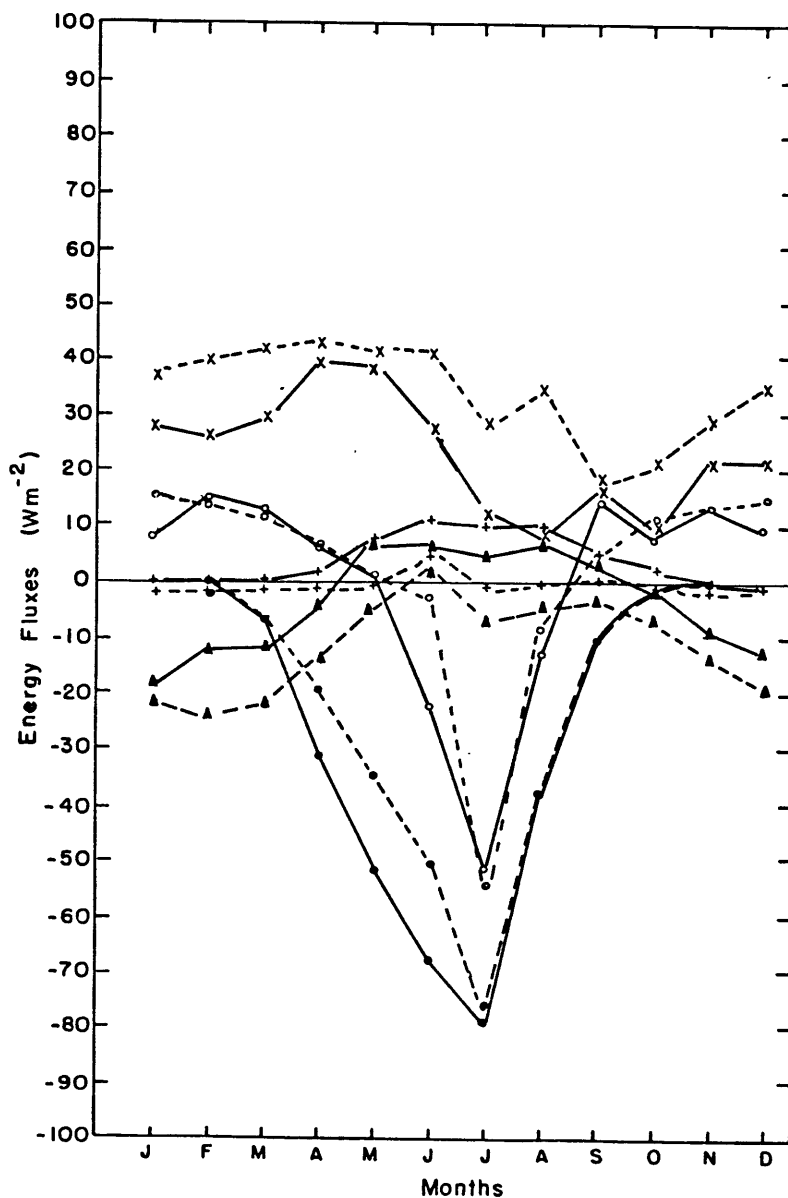
Figure 3.2 Seasonal cycles of the component and net energy
fluxes between the atmosphere and the ice
surface for the original model (dashed lines)
and Semtner 1976 (solid lines). Absorbed short
wave radiation (closed circles), sensible heat
flux (triangles), latent heat flux (plus signs),
net long wave flux (crosses), and net flux (open
circles)

April through June, the present model has lower values of
solar radiation. This is reflected in the net flux in June,
and has the consequence of greater ice growth resulting in
thicker ice.

Another factor which affects the thickness of the ice
is the way in which the freezing point is defined. In
Semtner's model the bottom surface of the ice was held at
271.2 K and new ice was formed at that temperature, while at
the top surface ice was melted at 273.2 K. This was an
attempt to simulate changes in the freezing point with
changes in salinity. However, salinity variations were not
included in Semtner's model. As a consequence freezing point
variations led to energy imbalances. In the present model
the freezing point was kept at a fixed value of 272.9 K in
the experiments under discussion and 271.2 K in the later
experiments. It was found that changing this value did not
greatly affect the seasonal cycle of ice thickness.

The following is an example of how a varying freezing
point can affect the mean thickness of the ice. We start
with a case where ice has just melted away, the ocean water
temperature is 273.2 K and an energy deficit of four units
exists. It takes one deficit unit to cool the water to 271.2
K, and the remaining three units to freeze Y units of ice.
Now we have a surplus of four energy units. One unit is used
to warm the ice to 273.2 K and the remaining three units
melt the ice. The ice thickness is the same as when we
started and the mean ice thickness over the period is Y/2

units.

Now, instead of allowing the freezing point to change we hold it fixed at 272.9 K. Starting with the same condition of ice having just melted away the ocean temperature is 272.9 K, and the energy deficit is four units. No deficit energy is needed to cool the water so the entire four units are used to freeze 4Y/3 units of ice. Now we have a four unit energy surplus. No energy is needed to warm the ice so it is all used to melt it. Again we are back to where we started with no ice. However, the mean ice thickness in this case is 2Y/3, which is larger than the mean ice thickness which results when the freezing point is allowed to vary.

While this example exaggerates the differences in the energy needed for the warming and melting ice it points out how the mean ice thickness can be affected by changes in the freezing point. Since the seasonal cycle of sea ice and net energy fluxes simulated in the models are not symmetrical, as was assumed in the example, the equilibrium ice thickness resulting from a varying and a fixed freezing point can be different.

The amplitude of the seasonal cycle of sea ice thickness is also given in Table 3.1. As oceanic heat flux increases the seasonal range in sea ice thickness also increases. This is due to the fact that less energy is needed to warm and melt the layers of the thinner ice. Since the atmospheric forcings remain unchanged and the

temperatures of the snow and ice layers for the different
ice thicknesses vary very little, except during the period
immediately preceeding melt, the thinner the ice becomes the
easier it is to grow and melt resulting in larger ranges in
the seasonal cycle.

The range of the seasonal cycle of ice thickness in the
present case (ocean flux is 3 W m^{-2}) is only .39 m while the
seasonal cycle for the previous studies ranged from .46 m to
.59 m. It is not clear if this difference is significant,
however, given the difference in the results of previous
studies it seems that the seasonal cycle of the present case
is adequate.

2. Energy Fluxes in the Original Model

In Table 3.2 the seasonal cycles of the various energy
fluxes plotted in Figure 3.2 and the net flux at the
ice-atmosphere boundary are given for the present case,
those specified by Semtner, and those computed by Washington
et.al. (1976) using equations similar to those in the
present model. In comparing these different sources it
should be kept in mind that there exists a wide range of
published values for the various terms in the energy budget.
In addition, most of the published sources refer to specific
locations rather than the zonal representation simulated in
the present case. Therefore, I will not attempt to make a
detailed comparison of the model results with published
data, but will point out some of the major differences which

Table 3.2 Components of the Heat Balance Equation in W m^{-2}
Over Ice for Original Base Case

Flux	Source*	J	F	M	A	M	J	J	A	S	O	N	D	Mean Annual
Absorbed	P	0	0	-6	-21	-34	-50	-76	-37	-10	-2	0	0	-20
F$_{sw}$	S+	0	0	-5	-30	-51	-68	-78	-37	-10	-1	0	0	-23
	W+	0	0	-4	-22	-46	-70	-107	-48	-10	-5	0	0	-26
F$_{lw}$	P	-143	-136	-142	-172	-220	-271	-287	-280	-275	-234	-189	-160	-209
	S	-166	-165	-165	-186	-242	-288	-304	-299	-264	-222	-179	-174	-221
	W	-144	-139	-142	-173	-221	-272	-288	-282	-277	-235	-190	-160	-210
F$_{ir}$	P	181	176	184	215	261	311	315	315	293	255	218	195	243
	S	194	191	194	225	280	316	316	308	280	232	201	196	244
F$_{sh}$	P	-22	-24	-22	-14	-5	2	-7	-5	-3	-7	-14	-19	-12
	S	-19	-12	-12	-5	7	6	5	6	3	-2	-9	-13	-4
	W	-21	-15	-9	-1	13	8	1	0	3	-20	-21	-20	-7
F$_{lh}$	P	-1	-1	-1	-1	0	5	-1	0	1	-1	-2	-1	0
	S	0	0	1	1	7	11	10	11	6	3	0	0	4
	W	0	0	0	0	8	9	1	5	4	-1	0	0	2
Net Flux	P	15	15	12	8	2	-2	-56	-8	5	11	13	15	2.4
	S	9	14	13	6	2	-22	-51	-11	15	10	13	9	.6

* P = Present model simulation at 77.5N for ocean flux of 3 W m^{-2}, equilibrium cycle,
    approximately 21st of month
  S = Semtner (1976) Specified forcing, monthly averages with units conversion
  W = Washington et.al. (1976), computed mid month values with units conversion
+ The absorbed radiation was computed from Washington et.al.'s solar radiation and
    the albedo and percentage penetration specified in the present model

will serve as a guide when the model is extended to include leads and to simulation sea ice in other latitudinal zones.

The simulated values of the absorbed solar radiation correspond relatively well with those of Semtner and Washington et.al. except during the spring and early summer. During this period the simulated absorbed solar radiation is lower than for either of the other studies. This may have led in part to the thicker mean ice thickness in the present case for comparable ocean fluxes.

The simulated values of long wave radiation from the atmosphere compare quite well with those computed by Washington et.al. and in the yearly average are 12 $W\ m^{-2}$ lower than those specified by Semtner. This decrease in the simulated long wave radiation is completely offset by increases in the simulated sensible and latent heat fluxes.

The sensible and latent heat fluxes seem to be the least well simulated. The simulated sensible heat flux is more negative than those specified by Semtner or computed by Washington et.al.. During the summer the simulated sensible heat flux exceeds 0 $W\ m^{-2}$ only during the month of June, while Semtner's and Washington et.al.'s results exhibit positive values up to 13 $W\ m^{-2}$ over a period of five months. This difference in the direction of the flux is a reflection of differences in the temperature gradient between the snow/ice surface and the air. During this period the snow/ice temperature is constant at the melting point, so the air temperatures during this period in the previous

studies must have been lower than in the present case.

In addition to the differences in the summer maximum the simulated sensible heat flux exhibits a broad minimum of upward flux compared to the steady increase in the fluxes specified by Semtner during the period January through March. This broad minimum is seen in the results of Washington et.al., however, it occurs during the period October through January. It is possible that the shifting of this minimum is due to a difference in the seasonal cycle of wind speed, a value which represents a zonal average in the present case and a specific location in the results of Washington et.al..

The simulated latent heat flux has a similar relationship to that in the previous studies as does the sensible heat flux.

The seasonal cycle of the simulated net flux and that specified by Semtner compare quite well. This indicates that the variations in the individual fluxes seem to balance out. The one exception is in June when the lower values of the simulated absorbed solar radiation is directly represented in the net flux.

Despite the many uncertainties the energy fluxes computed in the present model seem to produce reasonable results. The lack of observational data over the oceans and sea ice, and the model simplification preclude stronger statements.

The present case, with an ocean flux of 3 W m^{-2}, will

now serve as the base case, from which the model will be
extended to include leads and to simulate other latitude
zones.

3. The Base Case for the Extended Model - Includes Leads and
Various Latitude Zones.

The sea ice model is now extended to include leads and
is used to examine sea ice variations at various latitude
zones which include 82.5N, 72.5N, 67.5N, 57.5N, 52.5S,
57.5S, 67.5S, 77.5S.

Leads are included in the model by assuming a minimum
area of open ocean, 1% in the northern hemisphere and 2% in
the southern hemisphere, exists at each time step. An energy
balance condition is applied to the layer of open ocean. If
there is a net absorption of energy in the ocean the leads
are opened wider by melting the ice from the edge. If there
is a net deficit of energy in the ocean new ice is formed
with a specified thickness. In the base case the value of
the specified new ice thickness is .4 m. A discussion of how
this values was chosen appears in the next chapter.

The model is used to study sea ice in various latitude
zones by changing the input atmospheric variables to those
representative of the zone of interest, and computing the
energy fluxes as described in chapter II. This differs from
the energy fluxes computed for the base case for the
original model in that surface albedo is now a function of
air temperture and the short wave radiation available at the

surface is computed using the Thompson (1979) parameterization.

The vertical ocean flux of 3 W m^{-2} chosen for the original base case is now used in the northern hemisphere. In the southern hemisphere the ocean flux used for the base case is 12 W m^{-2}. This value is about half of that used in previous modeling studies (Parkinson and Washington used a value of 25 W m^{-2}, 1979). However, results of studies near Mawson, Antarctica indicate that the annual mean oceanic heat flux ranges from 10 to 15 W m^{-2} and that the oceanic heat flux has a very strong seasonality (Allison, 1981; Allison et.al. 1981). A more detailed discussion of this previous work and the effects of varying the means and seasonal cycles of the oceanic heat flux appears in chapter V.

The extended model is now used to determine the base case sea ice variations in the latitudinal zones mentioned above. These results are now compared to available data and other appropriate modeling studies to determine how well sea ice thickness and latitudinal distributions are simulated.

Observational data of sea ice takes two forms, that of ice extent and ice thickness. Sea ice extent is a relatively well known quantity due to the use of satellites, despite large interannual variations. A detailed analysis of sea ice extent and fractions of ocean as a function of latitude was made by Robock (1980) and will serve as observational data here.

Sea ice thickness data are extremely sparse. The studies that have been made apply to drifting stations at which measurements were made over a period of one to two years. One such station was Drifting Stations A during the IGY and was discussed by Untersteiner (1961). A more recent study was made by the Arctic Ice Dynamics Joint Experiment (AIDJEX). In this experiment stations were set up at various locations in the Beaufort Sea between 70N and 80N in 1975. Sea ice thickness measurements ranged from about 1.5 m for young ice to about 4 m for multi year ice (AIDJEX Bulletin no. 32, 1976).

In the southern hemisphere the data is even more sparse. Estimates suggest that the ice thickness reaches a maximum of 1.5 m at the coast of Antarctica (Parkinson, 1978). These estimates are supported by the data used in the study by Allison (1981) which shows ice growth from ice free conditions in the summer to a maximum of about 1.5 m of ice at Mawson, Antarctica.

The ice thicknesses that will be used here to compare with the model results were inferred from tables and maps found in Vowinkel and Orvig (1970). They define three geographical subdivisons of the Arctic Ocean which include the Central Polar Ocean, where less that 10% open ocean occurs in the summer; the Peripheral Seas, where greater than 10% of the ocean is open in the summer and ice covered conditions predominate in the winter; and the Norwegian-Barents Sea, where open water conditions generally

exist. They also have a table which gives the percentage of the Central Polar Ocean that is covered with ice of various ages ranging from one to five years. The distribution of ice ages in the other two seas are then estimated using the region definitions and maps of minimum and maximum ice extent. Then a map which spatially defines the various seas is divided into five degree latitude zones and the percentage of each zone covered by each of the seas is determined. In this way the age distribution of ice in each zone is determined.

Vowinkel and Orvig also have a table which gives the seasonal cycle of sea ice thickness for ice ranging in age from one to greater than five years. Using this table and the age distribution of ice in each zone the seasonal cycle of ice thickness in each zone is determined. This seasonal cycle is applicable only where ice exists and must be averaged with the fraction of open ocean given in Robock (1980) to obtain the zonally averaged sea ice thickness.

Before going further it should be kept in mind that the table of the seasonal cycle of ice thickness for various age ice given in Vowinkel and Orvig (1970) is applicable to ice which is growing. Therefore, sea ice which grows and melts away within one year is not well represented. This probably results in ice thickness estimates which are too large. Despite this caution and given that there are fewer observations of sea ice thickness in the southern hemisphere than in the northern hemisphere, the ocean types, the ice

age distribution within each and the resulting seasonal cycle of ice thickness is applied to the southern hemisphere.

The various latitude zones in the southern hemisphere are assumed to have the ice age distribution of a particular ocean depending on the annual averaged sea ice cover as defined by Robock (1980). If the annual sea ice cover is greater than 90% the distribution is assumed to be that of the Central Polar Ocean; if it is between 50% and 90% the distribution is assumed to be that of the Peripheral Seas; and if it is less than 50% the distribution is assumed to be that of the Norwegian-Barents Seas. Once the ice age distributions for the southern hemisphere latitude zones are known the seasonal cycles of the zonal average ice thicknesses are determined following the same method as used in the northern hemisphere.

Since sea ice thickness in the southern hemisphere is known to be less than that of the northern hemisphere these estimates will most likely be much thicker than measurements around Antarctica than the model results suggest.

Table 3.3 shows the mean annual and range of zonally averaged sea ice thickness for the data inferred above and the base case for each of the latitude zones. At 82.5N the mean annual thickness seems to be well simulated, however, the magnitude of the seasonal cycle does not. Other estimates indicate that the seasonal range of ice thickness in the Arctic Ocean is on the order of one meter (Parkinson

and Washington, 1979). The main reason that this is not reflected in the base case results is that the snow layer is melted away for only a short period of time in the summer. The snow acts as an insulator keeping the ice cold. In reality snow always melts or is blown away so bare ice is exposed to the atmosphere where it is warmed and melted.

Table 3.3 Zonal Mean Sea Ice Thickness and
Range of Variation in meters

Latitude	"Data" (Vowinkel & Orvig, 1970)		Base Case Zonal Average	
	Mean	Range	Mean	Range
82.5N	2.8	.93	2.68	.12
72.5N	1.4	1.8	.65	1.26
67.5N	.8	1.5	.29	.89
57.5N	.2	.59	0.0	0.0
52.5S	0.0	0.0	0.0	0.0
57.5S	.2	.53	.06	.31
67.4S	1.9	2.16	.52	.74
77.5S	2.8	.84	1.02	.25

The simulated mean sea ice thicknesses at 72.5N and 67.5N are are thinner by .75 m and .5 m respectively than those in the estimates. This is due in part to the complete meltaway of ice for 3.5 and 6.5 months respectively in the simulated model (see Figure 3.3). According to Robock (1980) there is at least 25% ice coverage year round at 72.5N and only one month of completely open ocean at 67.5N. Therefore, even if the simulated ice thicknesses matched the estimates when ice exists, the simulated yearly average ice thickness would be much lower than the estimates due to the longer periods of ice free conditions.
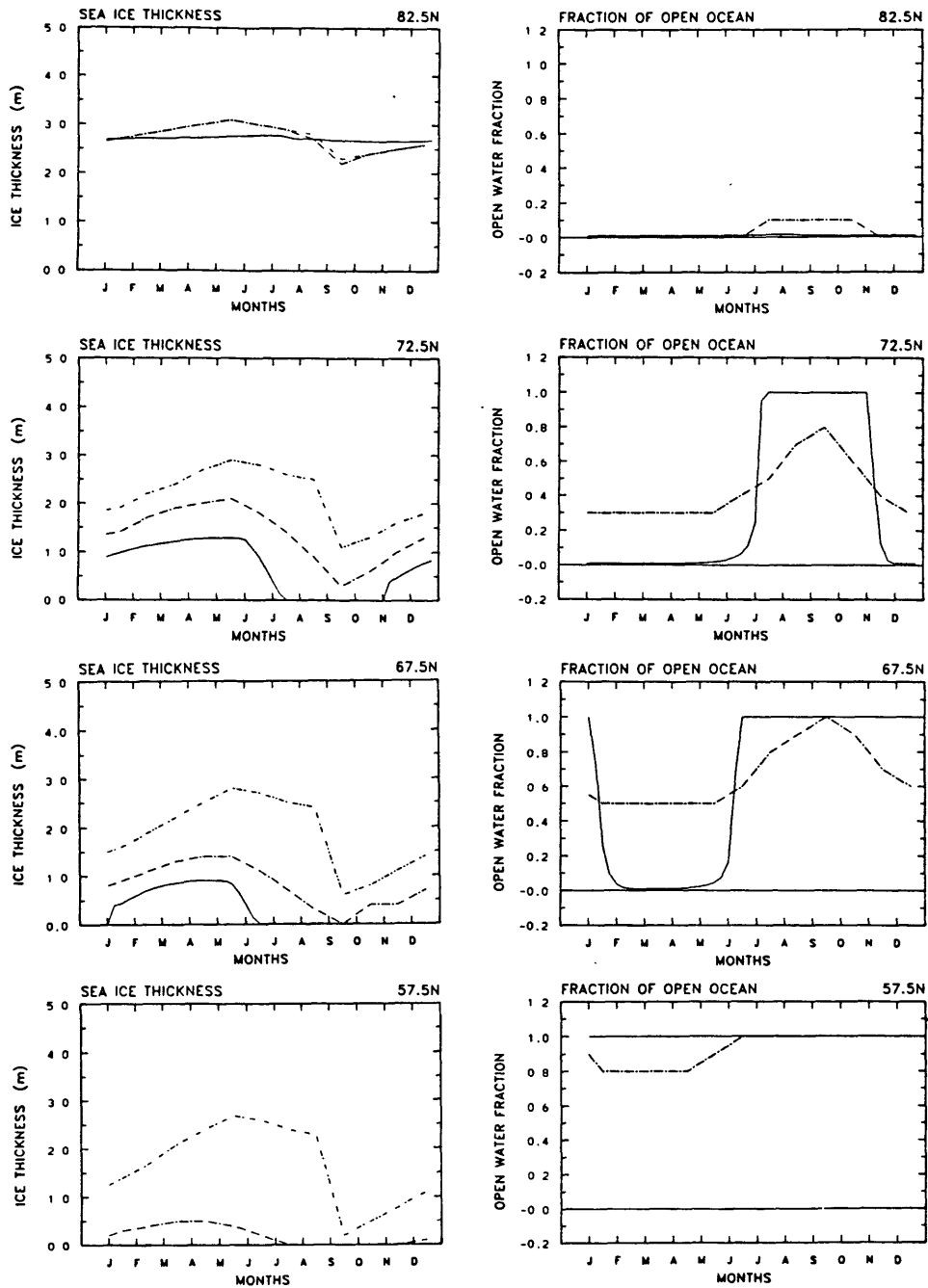
Figure 3.3.a Seasonal cycle of sea ice thickness and the
fraction of open ocean at 82.5N, 72.5N, 67.5N,
and 57.5N simulated by the present sea ice model
(solid line), zonal average data (ice alone)
derived from tables in Vowinkel and Orvig, 1970
(double dot dashed line), and zonal average data
(ice and leads) derived from Vowindel and Orvig,
1970, and Robock, 1980 (single dot dashed line)
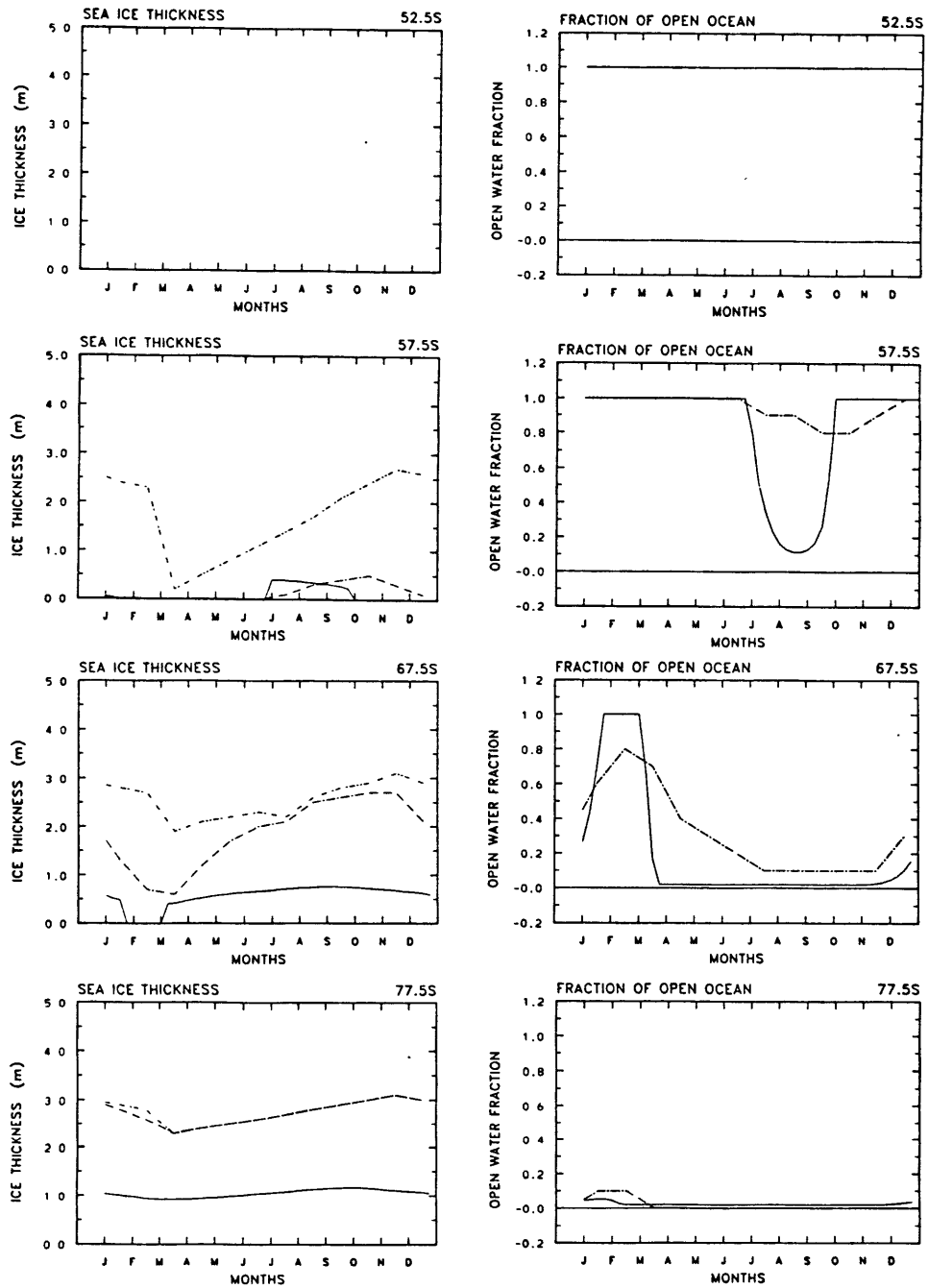
Figure 3.3.b Seasonal cycle of sea ice thickness and the
fraction of open ocean at 52.5S, 57.5S, 67.5S,
and 77.5S simulated by the present sea ice model
(solid line), zonal average data (ice alone)
derived from tables in Vowinkel and Orvig, 1970
(double dot dashed line), and zonal average data
(ice and leads) derived from Vowindel and Orvig,
1970, and Robock, 1980 (single dot dashed line)

Another factor contributing to the larger estimates, as mentioned earlier is the fact that the table of the seasonal cycle of sea ice thickness used to obtain those estimates is applicable to ice that would survive the first year. At 72.5N and 67.5N much of the ice which forms in the winter melts away within the year. In this case and further south the table taken from Vowinkel and Orvig (1970) is not applicable.

The largest discrepancy between simulated and estimated mean sea ice thickness occurs at 57.5N. The present model simulates no ice at any time and an ocean temperature no colder than 278.2 K, while the estimate is .2 m of ice and a seasonal range of about .6 m. Some of this discrepancy is due to the same conditions present at 72.5N and 67.5N. However, it also seems likely that ice does not form in situ at 57.5N, but is brought into that region by the East Greenland and Labrador currents and is maintained by regional rather than zonal conditions. The model is not presently designed to account for ice transport and has been used to study zonal rather than regional variations in sea ice thickness, therefore the comparison that can be made between the simulated and estimated mean sea ice thickness is limited.

In the southern hemisphere the mean sea ice thickness for the simulated and estimated cases agree at only one latitude. Both indicate that there is no sea ice at 52.5S. South of this zone the simulated mean sea ice thickness and

its seasonal range are always smaller than that estimated from the information in Vowinkel and Orvig (1970). This was to be expected since their tables were derived for the Arctic region where thicker ice is prevalent.

However, it is still possible to estimate the quality of the simulated mean sea ice thickensses in the southern hemisphere by comparing them with the model results of Parkinson and Washington (1979). Their results show a seasonal range for sea ice extent from about 65S to 55S and a thickness range from a maximum of 1.2 m at the coast to zero at the edge. Their results also indicated that the seasonal cycle of sea ice thickness at the coast has a small range and that this reduced seasonal range holds for most of the southern hemisphere ice once it is formed. The sea ice simulations made in the southern hemisphere agree very well with these results. Some of the major points of agreement include the lack of ice at 52.5S, the maximum ice thickness of somewhat over one meter, and the relatively small range of the seasonal cycle indicating that, once formed, ice growth is limited.

4. Energy Fluxes in the Extended Model

Tables 3.4.a, 3.4.b, and 3.4.c give the seasonal cycle, of the individual and net energy fluxes at 72.5N and 67.5S. These two latitude zones are representative of the northern and southern hemispheres respectively in that they have characteristics of zones both poleward and equatorward.

Table 3.4.a Components of the Heat Balance Equation in W m^{-2}
Over Ice at 72.5N and 67.5S

Flux	Latitude	J	F	M	A	M	J	J	A	S	O	N	D
F_{sw}	72.5N	-1	-10	-61	-154	-256	-301	-250	--	--	--	--	0
	67.5S	-299	--	--	-36	-7	-1	-3	-19	-70	-162	-267	-329
Absorbed F_{sw}	72.5N	0	-1	-9	-25	-46	-70	-87	--	--	--	--	0
	67.5S	-72	--	--	-6	-1	0	-1	-3	-12	-28	-51	-66
F_{lw}	72.5N	-173	-169	-176	-197	-232	-273	-302	--	--	--	--	-186
	67.5S	-269	--	--	-230	-215	-205	-201	-201	-208	-221	-240	-258
F_{ir}	72.5N	212	205	212	238	281	307	307	--	--	--	--	236
	67.5S	307	--	--	275	260	250	245	246	253	267	285	302
F_{sh}	72.5N	-9	-11	-10	-6	-1	-4	-12	--	--	--	--	-2
	67.5S	-11	--	--	-20	-25	-29	-30	-31	-27	-17	-6	1
F_{lh}	72.5N	-1	-1	-1	-1	1	0	-5	--	--	--	--	0
	67.5S	12	--	--	8	4	2	1	2	3	7	14	21
Net Flux	72.5N	30	23	16	9	3	-40	-99	--	--	--	--	48
	67.5S	-32	--	--	28	23	18	16	13	9	8	2	0

Note: In these three tables the seasonal cycle is made up of every fourth time step but the annual mean is the average of all 48 time steps

Table 3.4.b Components of the Heat Balance Equation in W m^{-2}
Over Ocean at 72.5N and 67.5S

Flux	Latitude	J	F	M	A	M	J	J	A	S	O	N	D	Mean Annual
F_{sw}	72.5N	-1	-8	-50	-125	-201	-239	-207	-133	-64	-18	-2	0	
	67.5S	-226	-157	-80	-28	-5	-1	-2	-15	-54	-123	-200	-245	
Absorbed	72.5N	-1	-7	-44	-113	-184	-220	-189	-122	-58	-16	-2	0	
F_{sw}	67.5S	-208	-142	-72	-24	-5	-1	-2	-13	-48	-112	-182	-226	
F_{lw}	72.5N	-173	-169	-176	-197	-232	-273	-302	-302	-276	-239	-208	-186	
	67.5S	-269	-264	-249	-230	-215	-205	-201	-201	-208	-221	-240	-258	
F_{ir}	72.5N	307	307	307	307	307	307	307	316	320	316	308	307	
	67.5S	307	309	307	307	307	307	307	307	307	307	307	307	
F_{sh}	72.5N	32	33	28	20	9	-4	-12	-7	2	9	17	25	
	67.5S	-11	3	40	99	140	161	173	210	220	179	81	14	
F_{lh}	72.5N	12	12	11	10	7	1	-5	-2	3	7	9	11	
	67.5S	14	25	46	71	82	84	85	102	112	105	64	30	
Net	72.5N	176	175	126	28	-93	-191	-201	-117	-9	77	123	156	22
Flux	67.5S	-166	-71	72	222	309	346	362	406	384	258	31	-134	169

Table 3.4.c Components of the Heat Balance Equation in W m^{-2}
Over Ice and Ocean at 72.5N and 67.5S

Flux	Latitude	J	F	M	A	M	J	J	A	S	O	N	D	Mean Annual
Lead	72.5N	.01	.01	.01	.01	.01	.03	.24	1.0	1.0	1.0	1.0	.01	
Fraction	67.5S	.26	1.0	1.0	.02	.02	.02	.02	.02	.02	.02	.02	.05	
Absorbed	72.5N	0	-1	-9	-26	-47	-75	-111	-121	-58	-16	-2	0	-41
F_{sw}	67.5S	-108	-142	-72	-7	-1	0	-1	-3	-13	-30	-53	-73	-41
F_{lw}	72.5N	-173	-169	-176	-197	-232	-273	-302	-302	-276	-239	-208	-186	-228
	67.5S	-269	-264	-249	-230	-215	-205	-201	-201	-208	-221	-240	-258	-230
F_{ir}	72.5N	213	206	213	239	282	307	307	316	320	316	308	237	272
	67.5S	307	309	307	276	261	251	246	247	254	268	286	302	276
F_{sh}	72.5N	-8	-10	-10	-6	-1	-4	-12	-7	2	9	17	-2	-3
	67.5S	-11	3	40	-17	-22	-25	-26	-26	-22	-14	-4	1	-10
F_{lh}	72.5N	0	-1	-1	-1	1	0	-5	-2	3	7	9	0	1
	67.5S	13	25	46	9	5	4	3	4	5	9	15	21	13
Net	72.5N	31	24	17	10	2	-45	-124	-117	-9	77	123	49	2
Flux	67.5S	-66	-71	72	30	28	24	22	21	18	13	3	-7	8

Some of these characteristics include maximum ice thicknesses similar to those at more poleward latitudes, and periods of ice free conditions similar to those at more equatorward latitudes.

At 72.5N the energy fluxes are somewhat different than those in the original model; however, most of this difference is due to the inclusion of leads in the extended model and the fact that they represent different latitude zones (77.5N in the original model). The short wave radiation shows the result of both of these differences. In the extended model the absorbed short wave radiation at its maximum over ice in July is about 15% larger than that for the original case. When leads are included their effect is small in winter when they make up only about 1% of the total area; however, during the summer when open ocean dominates, the maximum in absorbed solar radiation shifts to August and is about 40% higher than the maximum occurring over ice. Even when ice still exists and occupies 75% of the area, in July, the total absorbed solar radiation is 27% greater than that over ice alone.

The long wave radiation emitted from the surface also shows the effect of including ice free conditions. In the original model the maximum energy flux is constrained by the freezing point since the surface temperature does not exceed that value. In the extended model the ocean temperature is held at the freezing point until ice is completely melted away. At that time the ocean warms and the long wave

radiation emitted from the surface increases.

The turbulent fluxes, sensible and latent heat, over ice in the extended model have a smaller magnitude than that in the original model, and the sensible heat flux in the extended model does not exhibit any positive values in the summer as is suggested in the original model. These differences are due to the effect of looking at different latitudes and to the changing of the definition of the freezing point. In the original model the freezing point was 272.9 K, a value that was a compromise between the melting point of relatively pure ice and the freezing point of the saline ocean. The seasonal variation of air temperature, defined at 77.5N in that model, had summer temperatures that were below the freeezing point of the ice. Therefore, when ice was melting the sensible and latent heat fluxes were directed away from the surface. In the extended model at 72.5N the air temperatures are warmer in the summer than those defined at 77.5N in the original model. In addition, the ice is constrained by a freezing point which is lower than before, 271.2 K (the value used in the previous studies as the freezing point of ocean water). The result is that the air temperature is warmer than the surface during the summer so the sensible and latent heat fluxes are generally directed toward the surface.

The sensible and latent heat fluxes in the extended model also show the effect of including leads. In the original model these fluxes during the period August through

November when the ice is thinnest, are of the same order and sign as those just before maximum thickness, April through May. In the extended model the August through November period is one of relatively warm open water conditions while the atmospheric temperatures are dropping. As a result the direction of the sensible and latent heat fluxes reverses and the magnitude increases.

In this model the incoming long wave radiation from the atmosphere is unaffected by the presence of leads. This is because the air temperatures are specified, and therefore, unaffected by energy exchange between the surface and atmosphere. In previous studies using one air temperature over both ocean and ice was justified by assuming that leads occupied relatively small portions of the total area and that turbulent mixing of the atmosphere smoothed out any horizontal differences that might occur due to surface energy exchanges. While this seems to be a safe assumption at high polar latitudes it may become increasingly inaccurate in regions where the lead area becomes appreciable. In order to handle this situation it may become necessary to define two air temperatures, one over ice and one over open water with a diffusion cofficient which will tend to equalize the temperatures if the lead area becomes small.

There are two other ways to handle the situation of different air temperatures over sea ice and open ocean. The first is appropriate if a distribution of ice thicknesses in

a region is used (Thorndike et.al.,1975; Maykut, 1982). In this case an air temperature could be determined for each of the ice thickness categories based on the fraction of the area that thickness category occupied and the mean air temperature of the region. The other method would be to increase the horizontal resolution to include the longitudinal dimension as done by Parkinson and Washington (1979), and to couple the sea ice model to a climate model with similar resolution. This would allow air temperatures to vary longitudinally as will as latitudinally; however, the subgrid scale variations in the area of open and sea ice would still not be resolved.

A comparison of the net fluxes for the original and extended models show that most of the differences in the individual fluxes cancel each other; however, the effect of the leads in the extended model is dramatic. During the period December through May the net fluxes are generally no more than factor of two different between the two models, but during the period when leads open up completely the net flux can be as much as a factor of 14 greater in the extended model than in the original model.

Overall there are no unexpected differences between the energy fluxes in the extended model and those in the original model, and the major differences that do occur are primarily due to the inclusion of leads in the extended model.

Table 3.5 Components of the Heat Balance Equation in W m^{-2}
from Maykut (1978) and Parkinson (1978)

Flux	Source*	J	F	M	A	M	J	J	A	S	O	N	D
Absorbed F_{sw}+	MO	0	0	-7	-83	-209	-281	--	--	-89	-24	0	0
	M.4	0	0	-4	-46	-114	-153	--	--	-48	-13	0	0
	M3	0	0	-1	-17	-42	-59	--	--	-16	-4	0	0
	PK	0	0	-7	-32	-61	-73	-128	-73	-12	0	0	0
Net F_{lw}	MO	142	147	149	140	98	43	--	--	28	69	114	138
	M.4	45	45	42	51	55	47	--	--	17	19	31	41
	M3	31	29	25	32	38	35	--	--	14	12	18	26
	PK	7	7	16	26	41	42	32	30	20	14	7	7
F_{lw}	PK	-190	-188	-190	-207	-239	-270	-274	-276	-253	-226	-204	-190
F_{ir}	PK	197	195	206	233	280	312	306	306	273	240	211	197
F_{sh}	MO	33	68	259	458	540	543	--	--	575	615	520	276
	M.4	70	77	91	93	82	60	--	--	22	36	62	72
	M3	-17	-16	-12	-9	2	8	--	--	5	0	-6	-11
	PK	8	7	2	12	13	4	-1	0	-2	2	7	10
F_{lh}	MO	145	147	150	144	112	31	--	--	34	108	139	145
	M.4	6	6	5	10	26	44	--	--	19	14	9	6
	M3	0	0	0	0	4	10	--	--	9	4	0	0
	PK	1	1	0	1	8	5	0	-3	4	3	2	1

* M = Maykut (1978) results over open ocean, MO, over ice .4 m thick, M.4, and over ice
   3 m thick
  PK = Parkinson (1978) results for 79N,211E
+ This is absorbed solar radiation for cases M.4, M3, and PK. For MO this is available
   short wave radiation

There is very little observed data with which to compare the simulated energy fluxes at 72.5N, however, there are two sources with which some comparison can be made. These are the results of Parkinson (1978) and Maykut (1978) (see Table 3.5).

Parkinson's results are those simulated for a grid point in the Beaufort Sea at 78.96N and 210.96E. The comparison of the absorbed radiation at this point and that simulated at 72.5N is quite good. There are some differences due to the different latitudes under consideration and the different lead areas resulting when ice begins to melt, however, the variation over the year is the same.

The simulated long wave radiation from the surface also compares well with the results of Parkinson. The only real difference is that the simulated results are about 10% larger than those for Parkinson. This may result from the differences between the air temperatures for a zone and a particular location.

The annual mean of the simulated long wave radiation from the atmosphere and that of Parkinson are almost identical, 228 W m^{-2} compared to 226 W m^{-2} respectively, however, the simulated seasonal amplitude is one and a half times that of Parkinson. This again may be due to the differences in the air temperatures of a zone and a particular region.

The correspondence between the simulated and previously calculated turbulent fluxes is not nearly as good as for the

radiative fluxes. These fluxes are smaller in magnitude than
the radiative fluxes and are therefore more difficult to
determine. Consequently, in Table 3.5 Maykut's 1978 results
have been included showing his computed sensible and latent
heat fluxes over ice which is .4 m and 3 m thick. This table
shows that the simulated sensible heat flux over ice and
that computed by Parkinson fit within the range given by
Maykut. The simulated latent heat flux, however, is negative
where as Maykut's and Parkinson's results indicate positive
values. This discrepancy may be due to the dependence of the
latent heat flux on the difference between the air and
surface temperatures and on the relative humidity. During
the winter the latent heat flux in all cases is small so
that slight differences in air or surface temperature or a
change in atmospheric relative humidity can change the
direction of the latent heat flux. During the summer the
magnitude of the latent heat fluxes are larger; however, the
ice surface temperature is held at a freezing point defined
lower in the simulated case than in those by Maykut or
Parkinson. This causes the saturation vapor pressure of the
air at the surface to be lower than in the previous work
promoting a latent heat flux toward the surface.

Over regions of open ocean the turbulent heat fluxes in
the simulated case are much smaller than in Maykut's results
(see Table 3.4.b and 3.5). This difference is due to two
factors. First, the wind speed, a multiplicative factor in
the determination of the turbulent fluxes, is on the order

of 1 m s^{-1} in the simulated case compared to the values of 5 m s^{-1} used by Maykut. Second, the ocean temperature is held at the freezing point in the simulated case until all ice disappears. This is especially important when leads open up in the spring. In reality the open ocean would warm with the atmosphere maintaining an upward flux of both sensible and latent heat rather than the downward flux simulated with the present model.

Overall the energy fluxes simulated at 72.5N compare reasonably well with available data and previous model results. The largest discrepancies occur in the computation of the turbulent fluxes, however, these are an order of magnitude smaller than the radiative fluxes, and therfore affect the net budget to a lesser degree.

The energy fluxes simulated at 67.5N are similar to those at 72.5N with major differences stemming from the different seasonal cycles of solar radiation, air temperature, and wind speed specified for those regions (see Table 3.4.c). The short wave radiation simulated at 67.5S is somewhat higher than that at 72.5N reflecting the more equatorward latitude zone. The mean annual long wave radiation from the atmosphere is almost the same at 72.5N and 67.5S; however, the annual amplitude at 72.5N (133 W m^{-2}) is about twice that at 67.5S (68 W m^{-2}). This is because the range of the specified seasonal cycle of air temperature at 72.5N (26.4 K) is about twice that at 67.5S (13.6 K) while the annual means are almost identical (263.8

K at 72.5N, 264.6 K at 67.5S). The long wave radiation emitted from the surface at 72.5N and 67.5S also exhibits similar means (272 W m^{-2} at 72.5N and 276 W m^{-2} at 67.5S) with the amplitude of the seasonal cycle at 72.5N (114 W m^{-2}) being almost twice that at 67.5S (63 W m^{-2}). This indicates that the surface temperature mimics the seasonal cycle of the air temperature. This is especially true here where the air temperature is decoupled from surface energy exchanges.

The turbulent fluxes show the most difference between 72.5N and 67.5S. At 72.5N the sensible heat flux has an annual mean of about -3 W m^{-2} with a range of 29 W m^{-2}, while at 67.5S the mean is about -10 W m^{-2} with a range of 66 W m^{-2}. The situation is similar in the latent heat flux. At 72.5N the annual mean is about 1 W m^{-2} with a range of 14 W m^{-2}, while at 67.5S the annual mean is about 13 W m^{-2} with a range of 43 W m^{-2}. The differences in the turbulent fluxes at these two latitudes is mainly due to the difference in the winds specified for the zones. At 72.5N the seasonal cycle of wind ranges from about .5 to 1 m s^{-1}, while those at 67.5S range from 5 to 10 m s^{-1} with the maximum in October. This factor of ten can be directly translated into a factor of ten difference in the turbulent fluxes since wind speed is a simple multiplicative factor in determining those fluxes.

The net energy fluxes at 72.5N and 67.5S follow the same general seasonal cycle. The mean annual net flux is

toward the atmosphere at both latitudes and at 67.5S it is about a factor of four larger than at 72.5N. However, the exchange at 72.5N is much more vigorous with a seasonal range of 247 W m^{-2} compared to 143 W m^{-2} at 67.5S.

There is little data with which the simulated energy fluxes in the southern hemisphere can be compared. One study that does exist is that of Allison et.al. (1981) in which a general summary of the surface energy balance at Mawson, Antarctica (67.4S, 65.6E) is given. This study can be used to estimate the quality of the simulation of energy fluxes in the southern hemisphere.

Allison et.al.'s study indicates that in the autumn (March) the major loss of heat by the open ocean is through turbulent fluxes. This is reflected in the simulated results at 67.5S where the net radiative flux provides a gain of 14 W m^{-2} to the surface while the turbulent fluxes show an 86 W m^{-2} loss by the surface (see Table 3.4.c). Once ice forms both Allison et.al. and the simulated results show a large decrease in the turbulent fluxes. These fluxes change sign as the ice grows thicker and the gain in energy by the surface, according to Allison et.al., is partially balanced by the net radiative flux. In the simulated results the net radiative loss is about twice that of the gain by the turbulent fluxes. In the late spring (November) both Allison et.al.'s results and the simulated fluxes show a net radiative gain by the surface which is balanced by turbulent heat losses. Then, once the ice pack begins to break up, a

large increase in absorbed solar radiation occurs because of the large decrease in surface albedo. By mid summer the ice disappears and the open ocean gains heat both by radiative and sensible heat fluxes before starting another cooling cycle in February.

The above scenario indicates that the general fluctuations in the energy fluxes simulated for 67.5S correspond well with the results of Allison et.al.. However, the correspondence between the simulated results and the few quantitative values given by Allison et.al. vary. In the fall Allison et.al. indicate an upward net radiative flux of about 55 W m^{-2} compared to 39 W m^{-2} simulated for April. They also suggest that the downward net radiative flux in mid summer has a magnitude of 100 W m^{-2} over ice to 200 W m^{-2} over ocean compared to the 97 W m^{-2} simulated in February when ice free conditions exist. There are other discrepancies involving the net turbulent fluxes. Allison et.al. report a maximum upward turbulent flux of 120 W m^{-2} over open water in mid summer, with a value of 40 W m^{-2} over thin ice in the fall, and negative values in the spring. The maximum simulated turbulent flux is 86 W m^{-2} occurring in March and is followed by a rapid drop to negative values as ice forms. These differences may be caused by the differences in the zonal conditions used in the simulation and the local conditions at Mawson, Antarctica. One feature that has been left out of the simulation that may account for some of the descrepancy between the turbulent fluxes in

the two cases is the effect of the katabatic winds that come
off the Antarctic continent. Including these winds may
increase the simulated of the turbulent fluxes to values
more comparable to those of Allison et.al.

Overall the simulated energy fluxes in the southern
hemisphere correspond well with the available data
indicating that the present model produces reasonable
results.

In summary the processes involved in the seasonal
variation of sea ice and its formation include short and
longwave radiative fluxes and turbulent fluxes at the
atmosphere-ice/ocean boundary. In the northern hemisphere
the radiative processes dominate, with the net loss of long
wave radiation from the ocean and the decreasing input of
short wave radiation in the fall contributing to the
formation of sea ice; and the increase in the incoming short
wave radiation in the spring and summer contributing to its
decay. In the southern hemisphere the radiative processes
are still important especially in contributing to the decay
of sea ice in the spring and summer; however, the turbulent
energy losses dominate the surface energy balance in the
fall, especially over open ocean, and are the major cause of
the formation of new sea ice.

The simulated seasonal cycle of sea ice variations
discussed above and presented in Figure 3.3 for 82.5N,
72.5N, 67.5N, 57.5N, 52.5S, 57.5S, 67.5S, and 77.5S will now
be used as the base cases to which the sensitivity

experiments discussed in the following chapters will be
compared.

B. Continental Ice - Present Base Case

1. Northern Hemisphere

The continental ice sheet model is a zonally averaged
model in which it is assumed that there is no strain, ie. no
flow, in the longitudinal direction. Another way of
expressing this is to say that an ice sheet produced by the
model is infinitely wide in the longitudinal direction
forming a ring of ice around the latitudinal zone in which
it exists. Because of this unrealistic feature in the model
it is difficult to define a present day zonally averaged ice
sheet with which to compare the model results.

The present day northern hemisphere continental ice
sheet consists of the Greenland Ice Cap. Figure 3.4 shows
various vays of looking at this ice sheet, from a simple
cross section through some of the highest altitudes to a
zonal average over all land areas, which seems more
appropriate for comparison with the model. All the data
presented in this figure is from Flint (1971) with the
exception of the zonal land heights which come from Gates
and Nelson (1973).

Figure 3.4 Altitude profiles of Greenland
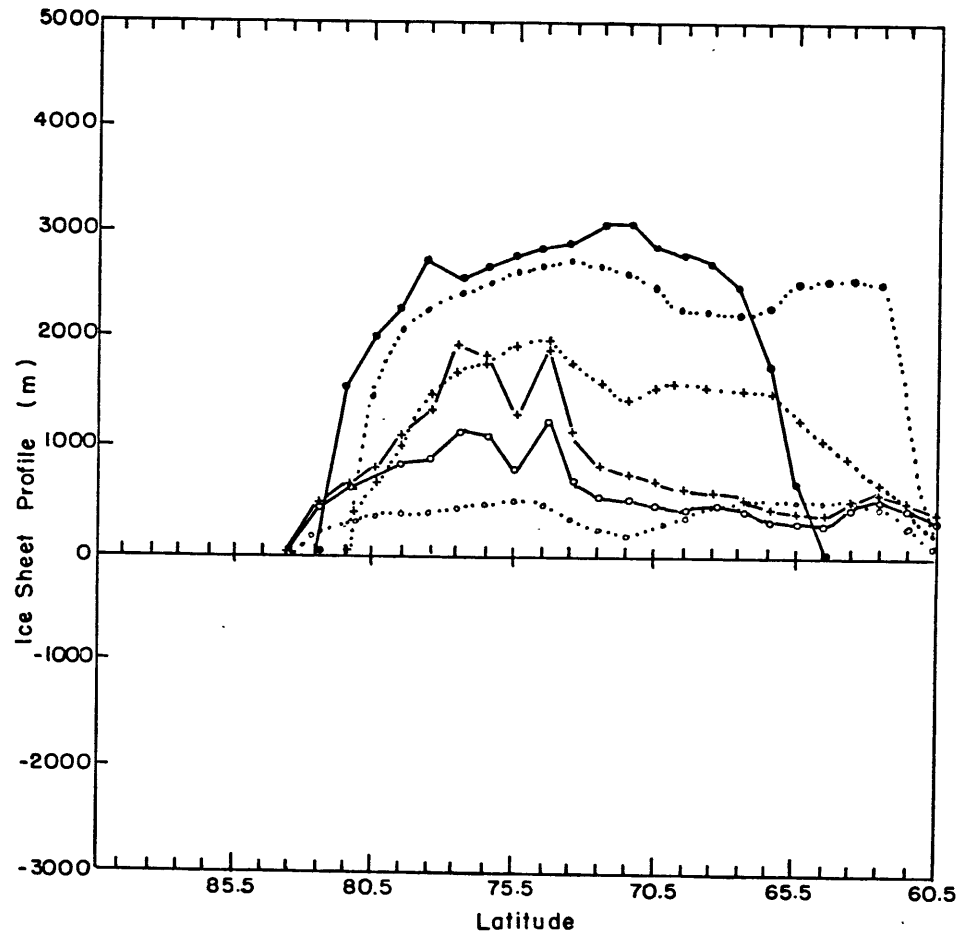———•—•—• Altitude profile along 40W from Flint, 1971
···•···•···• Altitude profile along 45W from Flint, 1971
Zonal average across Greenland from Flint, 1971
Zonal average across all land from Flint, 1971 and Gates and Nelson, 1973

Two of the altitude profiles in Figure 3.4 are simple cross sections through Greenland along 40W and 45W. Along 40W the ice sheet extends from 82.5N to 64.5N and reaches an altitude of over 3000 m. Along 45W the Greenland ice sheet extends from 81.5N to 60.5N and has a maximum altitude of about 2800 m. These two profiles show that the Greenland ice sheet has a large latitudinal and vertical extent. However, its magnitude is reduced somewhat when the ice thicknesses are zonally averaged across Greenland. The latitudinal extent remains the same, but the maximum altitude is reduced to 2000 m. This type of average is still not useful for comparison with the ice sheet model because Greenland accounts for only a small portion of the land area at the latitudes it occupies. The last ice sheet profile in Figure 3.4 shows what zonally averaging over all land areas does to the magnitude of the Greenland ice sheet. Its maximum thickness is about 800 m at 77.5N and drops to less than 150 m (much too low for significant ice flow) south of 70.5N and north of 79.5N. In addition the ice profile sharply mimics the land surface indicating that much of the topography included in this average is ice free. These results indicate that the Greenland Ice Cap is more likely maintained by regional rather than zonal effects, and for present day conditions a zonally symmetric ice sheet does not exist.

The problem of defining a zonally symmetric northern hemisphere ice sheet does not only apply to present conditions. In the following chapters experiments will be

described in which simulations of ice age conditions were attempted. Zonally symmetric ice sheets of various sizes and time evolutions were produced in these experiments, but the fidelity with which they can simulate ice age conditions is questionable.

A zonally symmetric ice sheet is one which covers a latitudinal zone and as a result has a flow which is constrained to the north-south direction. However, during the height of the last ice age (18000 years ago) ice sheets covered the North American continent from about 80N to 40N and from 55W to 135W; Greenland from about 85N to 60N and from 15W to 50W; and Europe and Scandinavia from 65N to 50N and 10W to 35W; and from 85N to 70N and 35E to 115E (CLIMAP Project Members, 1981). In addition, the flow of all of these ice sheets was directed radially from their centers (in the case of the Laurentide ice sheet, over North America, the center was located approximately over Hudson Bay) rather than being constrained to the north-south direction.

These zonally asymmetric features of the northern hemisphere ice sheets during the last glacial cycle point out the difficulty in trying to describe them in a zonally symmetric way.

In the following discussions of the results of the zonally averaged ice sheet model the purpose will be to investigate the sensitivity of continental ice to various changes in the energy balance at the ice surface and to some

of the factors which affect ice flow. It is hoped that the
results of this investigation will be useful in the
development of higher dimensional models of ice flow which
are more applicable for the study of the evolution of ice
sheets through glacial and interglacial periods.

The first experiment attempts to produce from an
initial ice sheet an equilibrium ice sheet with present
atmospheric conditions at the latitudes of Greenland.
Figures 3.5.a and 3.5.b show the results of this experiment
for a zonally symmetric ice sheet, with sea level bedrock
topography, for present atmospheric conditions, and the
southern edge of the Arctic Ocean at 83.5N, the northen edge
of Greenland. The ice sheet extends from 81.5N to 73.5N and
shows a negative net budget on the order of .15 m yr^{-1} at
both to the north and south edge. The ice sheet is
maintained by a positive net accumulation in its center
with a maximum value of about .15 m yr^{-1}.

While this ice sheet seems to be latitudinally situated
reasonably well for comparison with Greenland there are
features which are incongruous. One of these is that the
simulated ice sheet does not reach to the Arctic Ocean. This
is because the energy balance calculation at 81.5N produces
a net ablation of ice and the flow from the ice sheet to the
south is too small to make up the ice deficit.

At first the net ablation of ice to the north of a net
accumulation zone seems strange, however, it indicates that
present zonally averaged air temperatures at sea level are
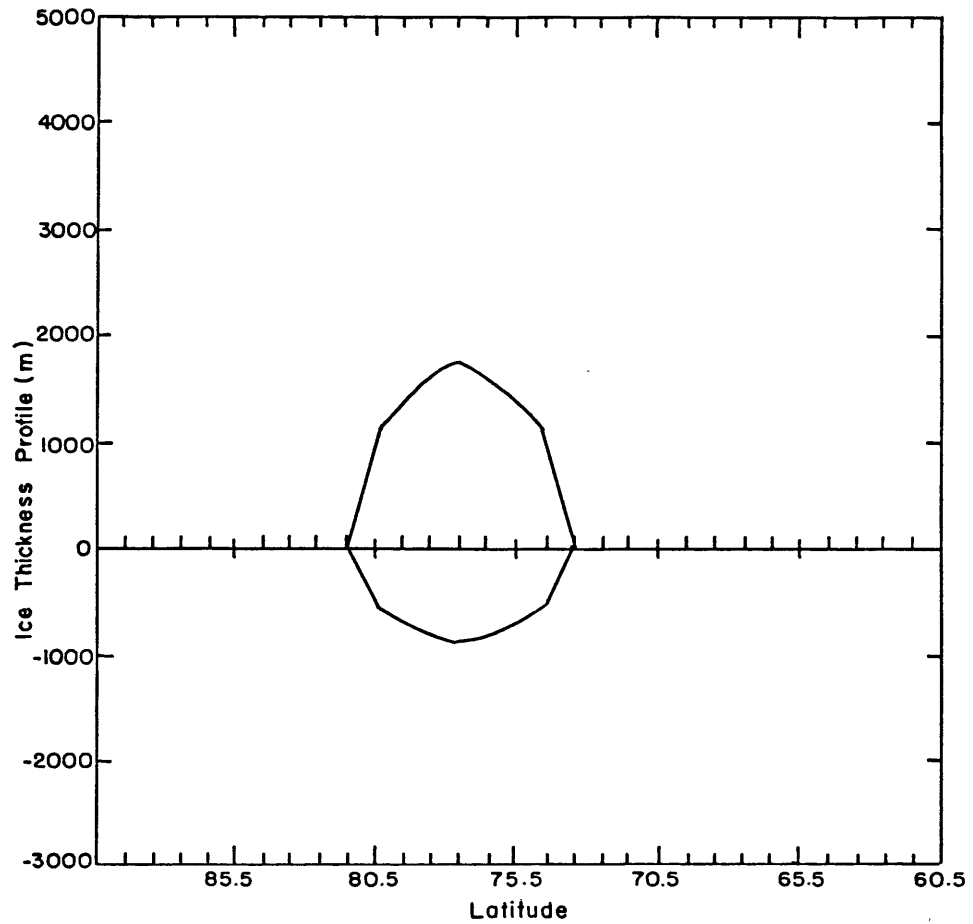
Figure 3.5.a Equilibrium northern hemisphere ice sheet, when the flow parameter A is set to .15 $yr^{-1}bar^{-3}$ and the Arctic Ocean calving line set at 83.5N
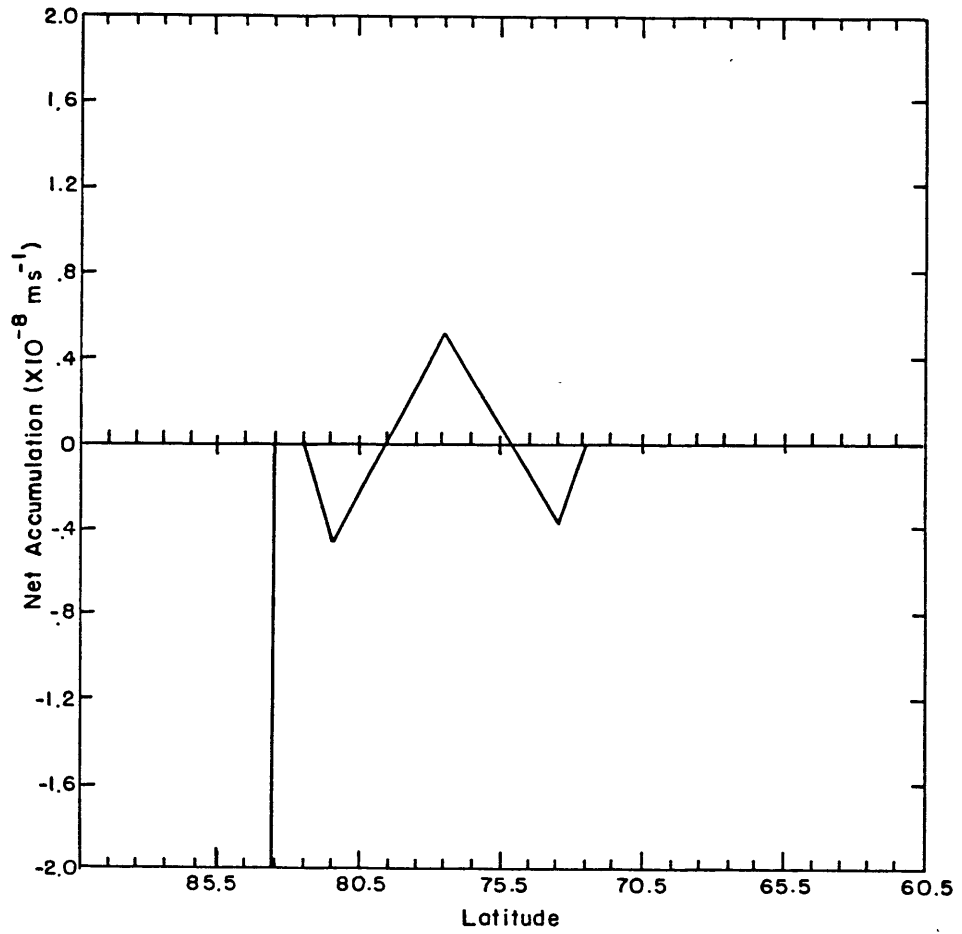
Figure 3.5.b Equilibrium northern hemisphere net budget for
equilibrium ice sheet in Figure 3.5.a

too warm to maintain ice cover during the summer. The net accumulation at 77.5N is the result of the lowering of air temperature at a rate of 6.5 K km^{-1} to the surface of the ice sheet, which in this case lowers it about 11 K. The lower air temperature inhibits ablation in the summer and as a result the net budget of accumulation and ablation is positive so the ice sheet is maintained. This result was possible because the experiment was initialized with an ice sheet of sufficient size to lower the air temperature at its center to the point where the net budget was positive and large enough to offset flow to other regions. If a smaller ice sheet or ice free conditions were used to initialize the experiment, the equilibrium results would have been ice free conditions.

The choice of the latitude of Arctic ice calving in the last experiment was the northern edge of Greenland. This position, however, does not represent the southern edge of the Arctic Ocean because most of the land surrounding the Arctic Ocean is further south. In the next experiment the position of the calving line was placed at 73.5N to be more representative of the southern edge of the Arctic Ocean.

This experiment was initialized with an ice sheet similar to the equilibrium ice sheet in Figure 3.5.a displaced to the south of the new position of the Arctic Ocean calving line. The result of the time integration was that the ice sheet melted away completely. The disappearance of the ice sheet was due to the fact that the air

temperatures at these latitudes were much warmer than at the latitudes where ice was located in the previous experiment. As a result the elevation of the ice sheet could not be maintained against the loss by ice flow to the north and south. Once the center of the ice sheet shrunk below a critical elevation the warm air temperatures put the entire ice sheet into a net ablation zone which accelerated the complete melt away of the ice.

Birchfield et.al. (1982) and Pollard (1982a) suggested that ice sheets initialized and grew from positions on high altitude plateaus. The idea is that at the higher bedrock elevations the air temperatures would be cold enough to maintain the snow cover through the summer, thus permitting ice sheet growth. In order to test if under present conditions an ice sheet could be maintained at higher elevations, topography similar to that of Pollard (1982a) (see Figure 3.6) was introduced under the original ice sheet. Although the higher elevations reduced the rate at which the ice sheet decayed the result was complete melt away.

Once the ice sheet melts away the question is what does it take to reinitialize it? A series of experiments were performed using present atmospheric conditions except for a decrease in mean annual air temperature and initializing the ice sheet with ice free conditions (surface albedo was .16 when there was no snow and .8 when there were winter accumulations of snow). Under these conditions a drop in
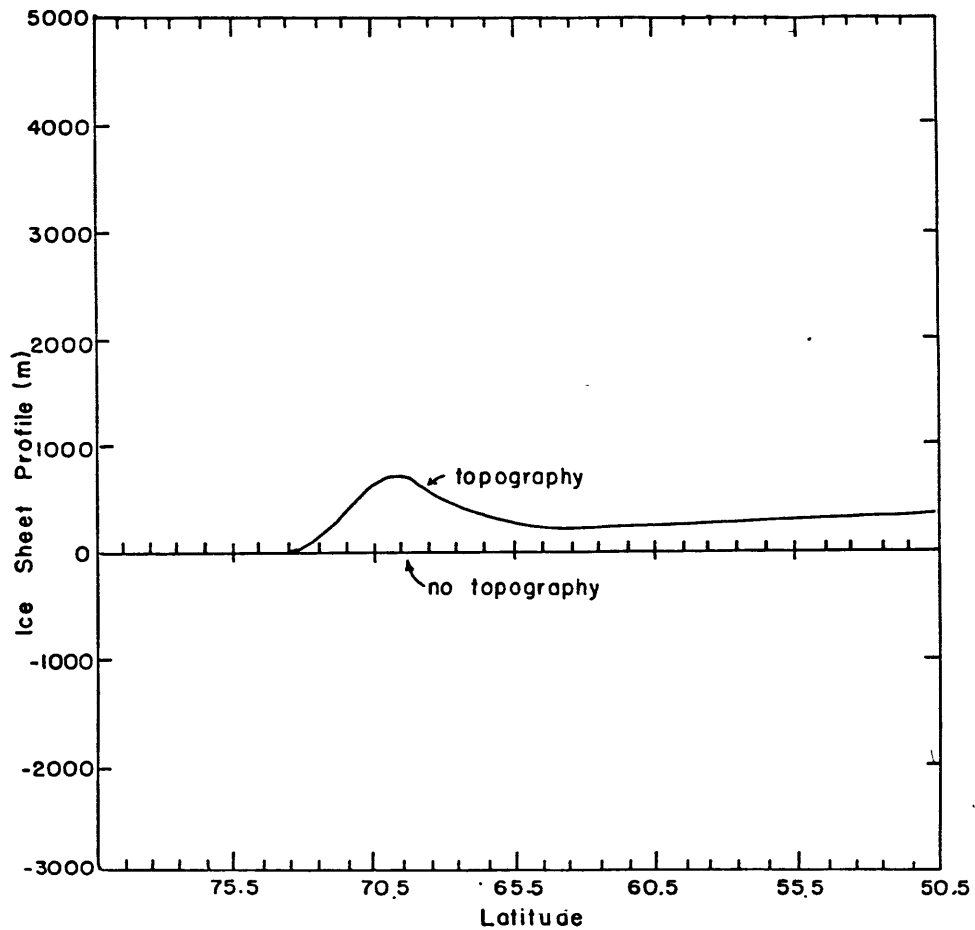
Figure 3.6 Results of northern hemisphere ice sheet
experiments for topography and no topography
cases when Arctic Ocean calving line is moved to
73.5N. All ice melts away.

mean air temperature of 10K was not enough to initialize an ice sheet. This was despite the fact that at the northern most latitude capable of supporting ice accumulation, 72.5N, the maximum summer air temperature was below the freezing point.

Besides colder air temperatures the other major difference between ice free and ice covered conditions is the albedo of the surface during the summer. In the above experiments the low surface albedo occurred only during the summer; during the winter a thin layer of snow, the accumulation of one season, covered the surface. It may be possible that during this short period of low albedo conditions enough solar radiation was absorbed to counter the increased accumulation effects of the lower air temperatures. In order to test this the above experiment was repeated except that it was initialized with a ten meter thick ice field with a surface albedo of .8 rather than the ice free conditions.

It seems that two factors are at work. First, when initializing with a snow field, and therefore high albedo, ice free conditions result only if the air temperatures are high enough to cause an energy surplus at the surface to melt away the exisiting and accumulating snow. The critical change in mean annual air temperatures from present mean temperatures for the melt away to occur seems to lie somewhere between a drop of 2 K to 3 K. However, when initializing with ice free conditions there was no ice

growth despite the fact that the air temparatures were dropped well below those needed to grow an ice sheet with the initial ice field conditions. This points to the second factor which plays a part in ice sheet growth, the surface albedo. When ice free conditions were specified the surface albedo was .16 during periods of zero snowfall and as a result 84% of the solar radiation incident at the surface was absorbed. During the summer this energy surplus aided in raising surface temperatures to the freezing point and melting away accumulating snowfall despite the lower air temperatures. When the initial snowfield was present the albedo was .8 so only 20% of the available solar radiation was absorbed, resulting in lower ice temperatures and less ice ablation.

The low albedo of ice free conditions tends to be a large obstacle to overcome in the initialization of an ice sheet. The range in the long wave radiation emitted from the surface for a drop in air temperature of 2 K to 10 K is about 20 W m^{-2}. Much of this is compensated for by a similar change in the long wave radiation from the atmosphere. However, the change in the surface albedo from .8 to .16 can change the absorbed solar radiation during the height of the summer by as much as 150 W m^{-2}. In order to overcome this large amount of absorbed solar radiation during ice free conditions and initialize an ice sheet, the mean annual air temperature must be dropped more than 10 K, a value which seems very large for zonally averaged conditions. Once a

snow cover can be maintained through the summer modest drops in mean annual air temperature are enough to continue ice growth.

While these results suggest there is great difficulty in making the transition from interglacial to glacial conditions it is possible that the zonally averaged nature of the model exaggerates it. Ice sheets may initialize on high altitude plateaus where small drops in air temperature may be enough the support snow cover during the summer. Ice sheets may also initialize in regions over which storms preferentially move. Modest decreases in air temperature may cause more of the precipitation from these storms to be in the form of snow, making the winter accumulation more likely to survive the summer. These are a few ways that ice sheets may initialize regionally. However, the large restraining effect, indicated in the results of this model, of surface albedo on interglacial-glacial transitions also applies to regional situations and may dominate them. More research is needed into the response of the net budget to variations in both surface albedo and air temperature in order to determine the magnitude of the restraining effect of low surface albedo on ice sheet initialization.

2. Southern Hemisphere

Present day southern hemisphere ice consists of the Antarctic Ice Cap. Figure 3.7 shows three different profiles of Antarctica which indicate the extent to which the ice

sheet is not zonally symmetric. The first altitude profile
is a cross section through East Antarctica from the highest
elevation of 4000 m at approximately 82S, 80E to the edge at
67S, 130E taken from a contour map in Swithinbank and
Zumberge (1965). In order to make the profile more
applicable for comparison with the zonally averaged model it
was recentered on the south pole. From the south pole the
ice sheet gently slopes northward to about 2600 m at 74.5S,
and then drops to zero at 70.5S. The second altitude profile
is an average of east and west cross sections through
Antarctica from Mirny (66S, 93E), through Vostok (78S,
106E), the south pole, the Thiel Mountains (about 85S, 90W),
the Ellsworth Mountains (about 75-80S, 85W), to the
Bellingshausen Sea (about 73S, 75-100W) taken from King
(1979). This profile shows a maximum ice thickness of about
3500 m that covers the latitudinal range from 81.5S to
74.5S, a dip to 3000 m at the south pole, and the northern
edge at 66.5S. In contrast, the third profile shows the
zonally averaged elevations taken from Gates and Nelson
(1973). This profile shows a much more variable terrain
which averages about 2000 m in elevation from 84.5S to
69.5S, a peak elevation of almost 3000 m at the south pole,
and a northern extent to 63.5S.
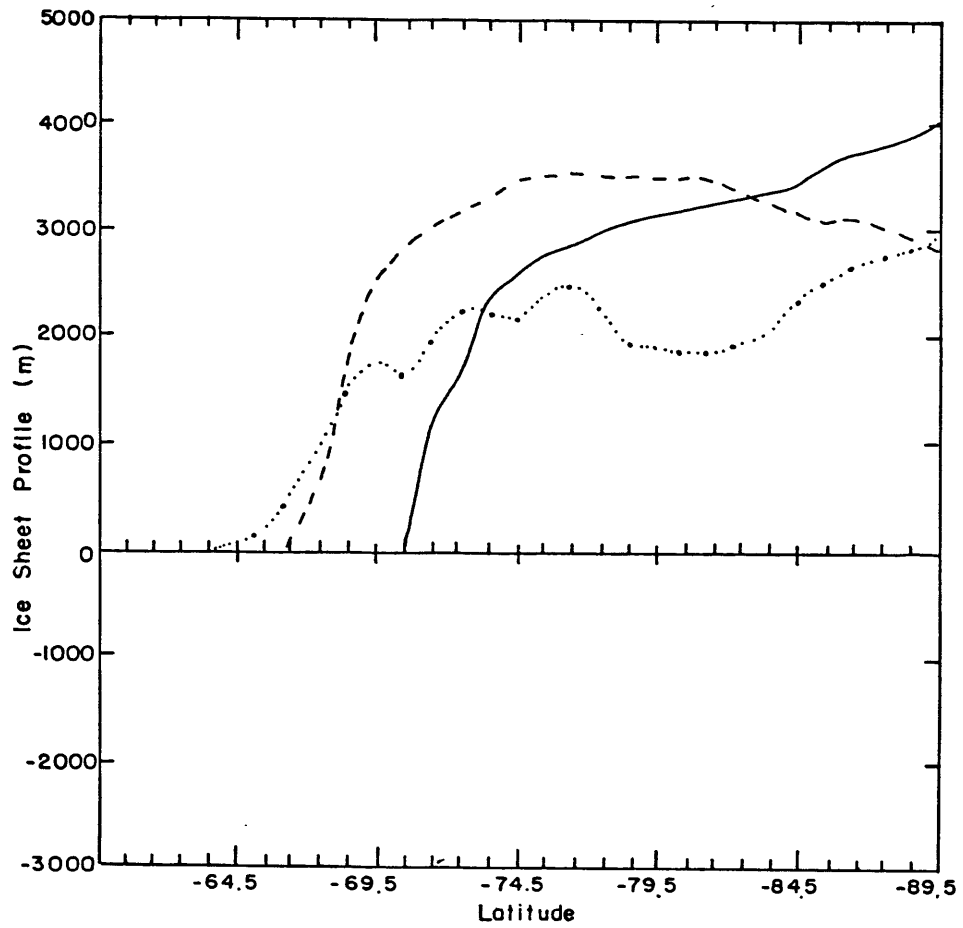
Figure 3.7 Antarctic ice sheet profile
———— Altitude profile through East Antarctica from
        Swinthinbank and Zumberge, 1965
— — — — Average of east-west cross sections through
        Antarctica from King, 1969
·•····· Zonal heights over land from Gates and Nelson,
        1973

These profiles give a general idea of the size and extent of Antarctica with which to compare model results. The ice sheet reaches elevations which range from 2000 m to 4000 m and extends to the general region of 70.5S to 66.5S. The more northerly extent of the zonally averaged elevations represents the Antarctic Penninsula which can not be handled by the model, and will therefore not be considered. In the following experiments the latitudinal position of the calving line was set at 66.5S which is generally representative of the northern extent of East Antarctica.

Figures 3.8.a and 3.8.b show the ice sheet profiles and net budgets for two equilibrium simulations of the Antarctic Ice Cap for present conditions. The first simulation makes the assumuption that the equilibrium ice free bedrock topography is at sea level at all latitudes. The maximum thickness of the equilibrium ice sheet (occurring at the south pole) in this case is 5.4 km and reaches to an elevation of 3.6 km. This compares moderately well with the altitude profiles in Figure 3.7, however, the ice thickness seems to be high compared to estimates of ice thicknesses over Antarctica today and the ice seems to be depressed much deeper (to 1.8 km below sea level) compared to the what is known about the present bedrock topography. Profiles of the Antarctic ice sheet, which are based on data from many traverses up until 1964, show that much of the bedrock is at or above sea level (King, 1969). The cross section from Mirny to the Bellingshausen Sea shows that the bedrock under
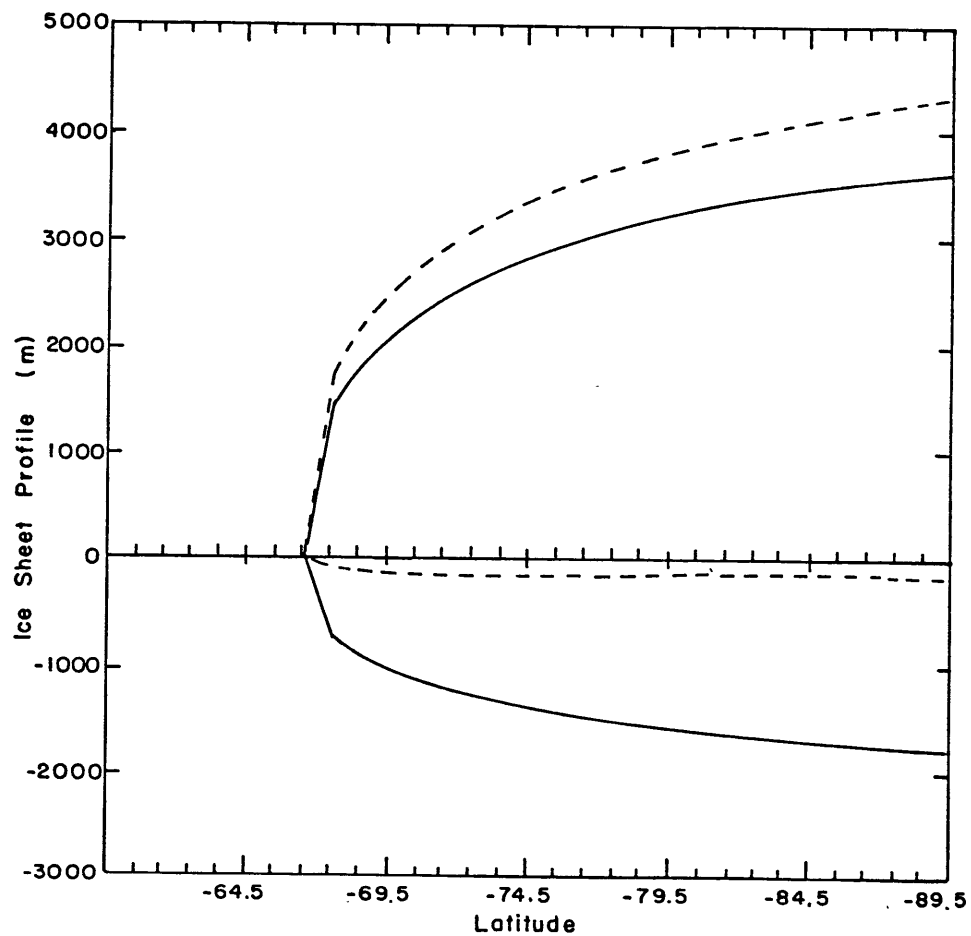
Figure 3.8.a Equilibrium southern hemisphere ice sheet
profile for cases of no topography (solid line)
and topography cases (dashed line).
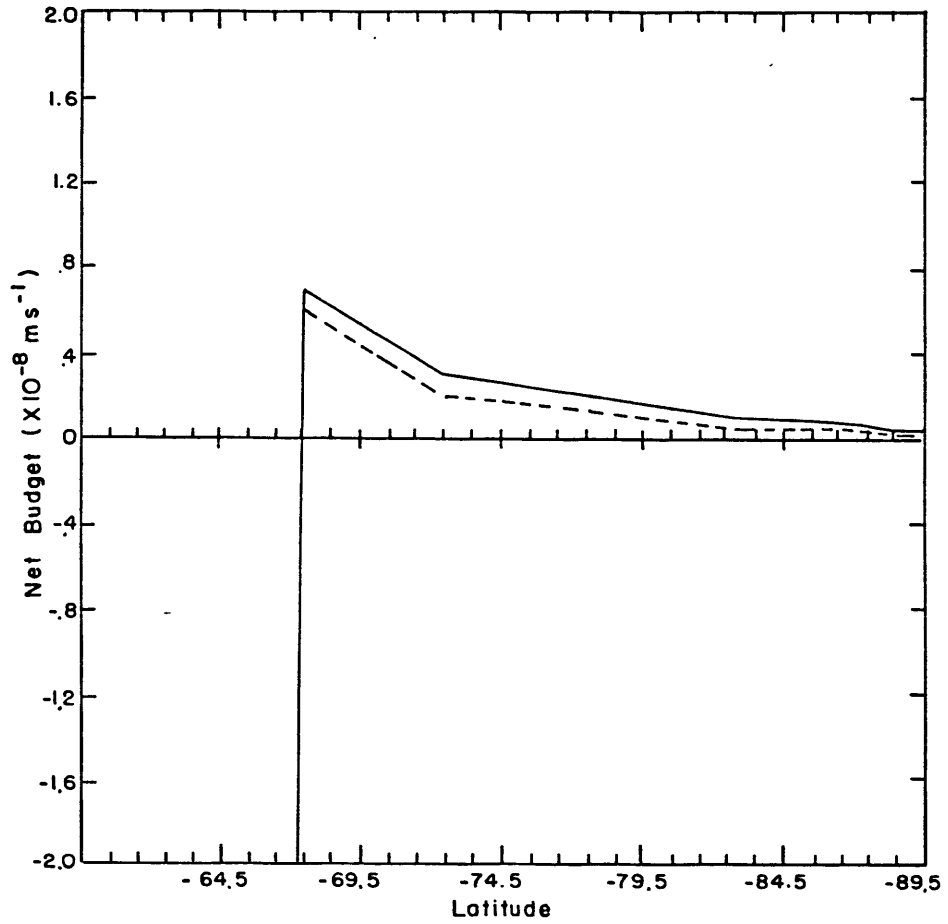
Figure 3.8.b Net budgets for southern hemisphere equilibrium
ice sheet profiles in Figure FIG8a.

the East Antarctic ice sheet, where the ice is thickest, is at sea level except for a region at about 70S which reaches elevations of about 1000 m (the ice elevation there is about 2600 m). The bedrock under West Antarctica in this cross section is much more rugged ranging from 1000 m below sea level to about 2200 m above sea level, with the averge elevation slightly above sea level.

In another cross section from the Weddell Sea to the Ross Ice Shelf the bedrock elevation ranges from about sea level to over 3500 m above sea level. Under the ice the elevation generally range from sea level to over 1000 m. The higher elevations in the cross section are for the most part exposed through the ice.

Oerlemans (1982) gives estimates of ice free equilibrium bedrock topography as a function of latitude and longitude under Antarctica which were derived from the Atlas Antarktiki (1966). The estimates show that the elevations of much of the ice free bedrock in Western Antarctica would range between 1 km below sea level to 2 km above sea level with much of the bedrock at or below sea level. The estimates for an ice free East Antarctica show that almost all the area would be above sea level with the majority above 1 km and some regions reaching to 2 km.

The cross sections from King and the ice free bedrock estimates from the Atlas Antarkitiki indicate that the assumption of sea level ice free topography is not justified and that the ice thicknesses produced with this assumption

are on the order of 1.5 km to high.

The second simulation introduces a simple equilibrium ice free bedrock topography which mirrors the depression below sea level for the sea level equilibrium bedrock case. the equilibrium ice sheet that results in this experiment is about 4.5 km thick, .9 km thinner than that of the previous simulation, but now reaches an elevation of 4.3 km. In addition, the bedrock is depressed only a couple of hundred meters below sea level, which is a much better simulation of the bedrock under the present Antarctic ice sheet.

The mechanisms by which the ice sheet is thinned are as follows. The first is that the slope of the bedrock beneath the ice from the northern edge of the ice sheet to the pole is drastically reduced by introducing topography. This increases the ice surface slope from the pole to the northern edge and thus increases northward ice velocities. The increased northward velocities are accompanied by a decrease in the surface accumulation due to the decrease in air temperature with altitude. These two processes have the effect of draining ice from the more poleward regions to the northern edge of Antarctica until ice thickness is reduced to the point where ice flow once again comes into balance with net accumulation.

Figure 3.8.b shows the net budget of ice over the Antarctic Ice Cap for both of the simulations described above. In the case of no topography (equilibrium ice free bedrock at sea level) the net accumulation ranges from 24 cm

yr^{-1} of water equivalent at the northern edge to 1.1 cm yr^{-1} at the south pole. When topography is introduced the rates are reduced, due to the increased elevation, to 21.2 cm yr^{-1} at the northern edge to .67 cm yr^{-1} at the south pole. Averaged over the ice cap this leads to net accumulation rates of 11.7 cm yr^{-1} and 9.2 cm yr^{-1} for the no topography and topography cases respectively. These values compare reasonably well with, but are somewhat lower than estimates from various sources. Giovinetto (1964) estimates that the mean net accumulation over Antarctica is 16 ± 3 cm yr^{-1} with a range from 8 ± 2 cm yr^{-1} to 58 ± 11 cm yr^{-1}. Rubin (1962) estimates a mean net accumulation of 14.5 cm yr^{-1} with a range from less than 5 cm yr^{-1} to greater than 55 cm yr^{-1} in some regions on the coast. Another estimate (Stephen Warren, personal communication) indicates a mean net accumulation of 17 cm yr^{-1} water equivalent with a maximum of 40 cm yr^{-1} at the coast, and a minimum of 3 cm yr^{-1} in the interior of the continent.

The reason the net accumulation rates are lower in the simulation is that the simulated ice sheet profiles extend to higher elevations, and therefore, have lower mean annual temperatures at every latitude than the zonally averaged topography. The mean annual temperature over the south pole is 224.2 K (Schutz and Gates, 1971-4) compared to means of 220.9 K and 216.5 S in the no topography and topography simulation respectively. Changes in air temperature at these low temperatures make a large difference in the saturation

vapor pressure, and therefore, in the accumulation rate.

The higher elevations in the simulations which lead to the low accumulation rates are probably the result of several simplifying features of the model. The two simulations show the large effect of varying the bedrock topography beneath the ice. The inclusion of a more realistic bedrock topography may improve the simulation of ice sheet thickness and elevation.

Another simplifying feature included in the model is the specification of the flow parameter, A. Ice velocities are directly proportional to A which is an increasing function of ice temperature. The present model holds A fixed, but if it were parametrically varied with latitude to simulate the change in ice temperature the result would be to increase the ice velocities in the northern regions of the ice sheet and thus decrease the simulated ice sheet elevations. Previous modeling studies have held the values of A fixed for all latitudes so the magnitude of the effect of varying it with latitude is not known.

Another possible discrepancy between the simulated equilibrium ice sheet and the present day Antarctic ice sheet is that is not clear whether or not Antarctica is in equilibrium. Estimates of net budget seem to suggest that Antarctica is in equilibrium or is slightly growing (Dolgushin, Yevteyev and Kotliakov, 1962), however, one source admitted that there is not enough evidence to really know (Wexler, 1961). In any case, Antarctica is not changing

very rapidly so comparison with an equilibrium simulation may be a good approximation.

Despite the simplifications and the resulting inaccuracies in the simulations, the zonally averaged ice sheet model does a reasonably good job of simulating the present day Antarctic Ice Cap. The model will now be used to examine the sensitivity of the modeled ice sheet to various changes and perturbations in some of the parameters and variables that are thought to be important in the growth and decay of ice sheets.

IV. Sensitivity of Models

A. Sea Ice

1. Lead Parameterization and Time Step Size

Leads have a large effect on the energy exchange between the atmosphere and ocean, and are therefore important to include in studies of the sensitivity of sea ice to climatic variations and in coupled sea ice-climate model experiments. Previous studies with sea ice models have parameterized leads in a number of ways. Washington et.al (1976) specified a minimum area of open ocean that was assumed to exist due to dynamic stresses placed on the ice by wind and ocean currents. An energy budget equation was applied to the open ocean. Any surplus energy accumulating in the leads opened them wider and any deficit was used to form new thin ice which was averaged with the old ice thickness. Parkinson and Washington (1979) treated leads in a more complex fashion. They maintained two values of ocean water temperature, that under the ice and that in the leads. An energy budget equation was applied to the open ocean area. Any surplus energy was partitioned between warming ocean water and laterally melting ice to open leads further. Any deficit energy was offset by cooling the ocean water to the freezing point and then forming new ice of the same thickness as the existing ice. If the freezing over of leads resulted in ice coverage exceeding 98% in the southern hemisphere or 99.5% in the northern hemisphere, the ice coverage was restricted to those values. The remaining

energy deficit was offset by the cooling of the water under the ice and the formation of new ice at the bottom of the existing ice.

The lead parameterization used in this model is essentially patterned after those mentioned above with two modifications. A minimum lead area is assumed and an energy budget equation is applied to the open water area. An energy surplus is used to open leads wider as in Washington et.al (1976). However, an energy deficit is offset through the formation of new ice of a specified thickness (the first modification). If the extent of the new ice would exceed the lead area the new ice thickness is defined by the lead area. The new ice thickness is then averaged with the existing ice thickness to obtain a single ice thickness. The minimum lead area is then assumed to reopen due to dynamic processes not explicit in the model.

The second modification is that the time step size is on the order of one week (48 time steps per year) rather than the 8 hours used by Washington et.al. (1976) and Parkinson and Washington (1979). This modification was introduced to make the model more adaptable to long term climate studies which require long time integrations and thus large amounts of computer time. However, the change in time step size has major implications when considering the growth of new ice on an ice free ocean or in leads.

When new ice forms on open ocean its initial growth rate is high. This is due to the large turbulent energy

exchanges between the atmosphere and the relatively warm ocean. As the ice grows thicker it acts as an efficient insulator which effectively cuts off the ocean-atmosphere energy exchange and thus dramatically reduces the ice growth rates. An example of how large this effect is can be seen in the ice growth rates in the central Arctic during the winter which range from 13 cm day^{-1} (1.5 x 10^{-6} m s^{-1}) for new ice, to 2 cm day^{-1} (2.3 x 10^{-7} m s^{-1}) for ice .5 m thick, and less than 1 cm day^{-1} (9.2 x 10^{-8} m s^{-1}) for ice 1 m thick (Thorndike et.al., 1975).

When new ice is formed on open ocean or in leads the growth rate computed by the model for the initial ice-free conditions is held fixed and the insulating effect of the growing ice is neglected for the length of the time step. The magnitude of the discrepancy between the ice growth in the central Arctic computed for long and short time steps can be estimated from the graph of ice growth vs thickness given in Thorndike et.al. (1975). New ice is estimated to grow at a rate of 13 cm day^{-1}, which for a one week time step (7 days) gives .91 m of ice. If 8-hour time steps are used instead, as was done in previous modeling studies, and everything else is assumed to remain the same, the growth rate decreases as the ice grows, and at the end of 7 days the ice grows to about .47 m.

The above result indicates that a model which initiates ice on open oceans and includes leads would be sensitive to time step size, especially to those over one day in length.

And indeed, when it was assumed in the present model that
new ice covered the entire ice free area the ice thickness
in essence became defined by the length of the time step
(see Table 4.1). It was also found that if the lead
parameterization was eliminated from the model the
sensitivity to time step size was extremely small.

Table 4.1 Maximum Ice Thickness When New Ice is Assumed
          to Cover the Entire Ice Free Ocean - in meters

Latitude	Number of Time Steps Per Year			
	24	48	72	576
82.5N	3.61	2.40	1.89	.63
72.5N	1.41	1.17	1.07	.55
67.5N	.86	.78	.73	.48
57.5N	0.0	0.0	0.0	0.0
52.5S	0.0	0.0	0.0	0.0
57.5S	.16	.13	.08	.07
67.5S	.80	.71	.65	.28
77.5S	1.43	1.15	.99	.38

One method of reducing the sensitivity to time step
size is to define the new sea ice thickness formed over open
ocean except when the ice of that thickness would more than
cover the available open area. In this way the area of open
ocean becomes ice covered over a few rather than one time
step and the thickness of the ice becomes less sensitive to
the time step size. Table 4.2 shows the maximum ice
thickness at each latitude for cases when the new ice
thickness is specified at .2 m, .4 m, and .8 m.

This table shows that even with the new specified ice
thickness the sea ice model is sensitive to time step size
although the sensitivity is greatly reduced. The reason for

Table 4.2 Maximum Ice Thickness When New Ice Thickness
is Specified - in meters

Latitude[*]	New Ice Thickness	Number of Time Steps Per Year		
		24	48	576
	.2	3.75	2.54	1.64
82.5N	.4	3.84	2.78	2.57
	.8	4.14	3.86	3.86
	.2	1.41	1.20	1.10
72.5N	.4	1.42	1.28	1.25
	.8	1.58	1.56	1.54
	.2	.86	.82	.77
67.5N	.4	.92	.90	.87
	.8	1.18	1.13	1.10
	.2	.25	.2	.2
57.5S	.4	.4	.4	.4
	.8	.8	.8	.8
	.2	.79	.73	.47
67.5S	.4	.83	.76	.64
	.8	.9	.9	.9
	.2	1.44	1.16	.67
77.5S	.4	1.45	1.17	.9
	.8	1.48	1.21	1.20

* At 57.5N and 52.5S no ice was formed at any time step size

the continued sensitivity to time step size is that during
the winter the volume of ice that is formed covers an area
greater than that of the leads at the specified thickness,
and therefore, the thickness of the lead ice is adjusted to
accommodate the available area. The new ice thickness is
greater than the specified value and is sensitive to the
time step size. This is especially true in the southern
hemisphere where the winds, which are an order of magnitude
higher than those in the northern hemisphere, induce
extremely high turbulent energy losses by the ocean and thus

high sea ice growth rates which are extrapolated over the time step. However, this does not cause the extreme sensitivity to time step size as before because during the winter the leads are restricted to 1% and 2% of the total area in the northern and southern hemispheres respectively.

The specified new sea ice thickness chosen for the base case described in chapter III was .4 m. The reason for this choice was based on two factors. First, the value chosen had to show at least a moderate insensitivity to time step size, and second, it could not be too high so that thinner ice and the accompanying higher exchange between the atmosphere and ocean compared to that of thicker ice could still be distinguished.

The value of .4 m works well in the northern hemisphere. It is a moderately thin value of ice thickness whose growth rate according to Thorndike et.al.'s (1975) graph is on the order of 4 cm day^{-1} indicating a moderately high rate of turbulent energy exchange between the atmosphere and ocean. On the other hand it shows only a mild sensitivity to time step size. At 82.5N the highest sensitivity to time step size is seen with a decrease of 28% in maximum ice thickness between 2-week time steps (24 time steps per year) and 1-week time steps (48 time steps per year). However, on reducing the time step size to about .6 days (576 time steps per year) the maximum ice thickness is further reduced by only 8%. The situation is even better at 72.5N where the maximum ice thickness is reduced 10% between

24 and 48 time steps per year and only an additional 2%
between 48 and 576 time steps per year. At 67.5N the overall
sensitivity to time step size is even smaller with only a 5%
decrease in the maximum ice thickness for a change from 24
to 576 time steps per year.

At the smaller value of the specified new sea ice
thickness, .2 m, the maximum sea ice thickness shows a
moderately larger sensitivity to time step size which
becomes worse at the more northerly latitudes. The
sensitivity ranges from a total of a 56% decrease in maximum
sea ice thickness at 82.5N to a 10% decrease at 67.5N for a
change from 24 to 576 time steps per year. The larger value
of the specified new sea ice thickness, .8 m, shows less
sensitivity to time step size than .4 m with a range from 1%
to 7%, however, the larger value is less representative of
new sea ice with a growth rate approaching that of
multi-year ice.

In the southern hemisphere the sea ice thickness is
more sensitive to the time step size. Unlike the northern
hemisphere, the percentage the maximum ice thickness
decreases is greater for the change from 48 to 576 time
steps per year rather than for the initial decrease in time
step size. When .4 m is specified for the thickness of new
ice at 77.5S, the maximum sea ice thickness is reduced 19%
when the time step is changed from 24 to 48 time steps per
year and an additional 23% when the time step is further
decreased to 576 time steps per year. At 67.5S the maximum

sea ice thickness is reduced 8% for the initial change in
time step size and an additional 16% for the remaining
change in time step size. This seemingly increased
sensitivity as the time step size decreases only indicates
that the southern hemisphere is more sensitive than the
northern hemisphere. The larger percentage decrease in ice
thickness between 48 and 576 time steps per year is a result
of the fact that that decrease in time step size is 23 times
greater than the decrease between 24 and 48 time steps per
year.

The increased sensitivity to time step size in the
southern hemisphere is due to the large turbulent energy
exchanges between the atmosphere and ocean that are caused
by wind speeds which are a factor of ten greater than those
in the northern hemisphere. Large turbulent energy losses in
both hemispheres during the winter cause the leads to fill
with ice which is thicker than the specified value of ice
thickness. However, in the southern hemisphere the lead ice
can be a factor of 4 thicker than the .4 m value and covers
2% of the total area, compared to a factor generally less
than 2 which covers 1% of the total area in the northern
hemisphere. These differences between hemispheres leads to a
greater sensitivity to time step size in the southern
hemisphere.

The exception to this result occurs at 57.5S. At that
latitude there seems to be essentially no sensitivity to
time step size with the maximum sea ice thickness being the

initial new ice thickness at the beginning of the winter.
The reason for this is that this region is on the edge of
the northern extent of the Antarctic sea ice. In the late
fall there are large turbulent energy losses from the ocean
which cause its temperature to drop and new ice to form. The
energy losses are not enough to cause the zone to become
completely ice covered; however, the new ice diminishes the
energy loss by the ocean to the extent that ice growth is
immediately reduced to zero. Ablation then occurs at the
bottom surface due to the vertical flux from the ocean until
the ice melts away at the end of the winter. This result
indicates that the method of ice initialization on open
ocean and in leads used here is capable of indicating where
the equatorward limits of sea ice might be but has trouble
representing the seasonal cycle of the sea ice at that
limit.

It may be possible to better represent the seasonal
cycle of sea ice in the more equatorward latitudes and to
reduce the sensitivity of the model to time step size if the
specified new ice thickness is made a function of latitude.
The more polar zones would specify thicker initial ice
thicknesses which would make them less sensitive to time
step size (see 82.5N and 77.5S in Table 4.2). The more
equatorward zones would specify thinner initial ice which
would reduce the ice growth rate more slowly so the sea ice
could go through a more reasonable seasonal cycle. However,
more research is needed to determine how the thickness of

newly formed ice varies with latitude.

The present parameterization of leads seems to be adaquate for the present purpose of sensitivity studies of sea ice to variations in climatic variables. However, before the model can be coupled to a global climate model a method of representing leads and new ice which is less sensitive to the long time step size and can handle the seasonal variation of sea ice at its equatorward limits must be found.

In addition to the suggestion of varying the sea ice thickness with latitude there are two possibilities for changing the lead parameterization. One possibility is to partition the energy deficits (surpluses) in the ocean between cooling (warming) the ocean, rather than holding it at the freezing point unless ice free conditions exist; freezing (melting) ice; and cooling the new ice, rather than holding it at the freezing point. The possible advantage of this method is that the energy will be distributed among some of the various physical processes that are associated with sea ice growth and decay, rather than concentrating it all in that process alone. This will reduce the large computed growth rates of ice on an ice free ocean and thus make the model less sensitive to time step size.

Another possibility is to assume for the purpose of computing the ice growth rates that a thin layer of ice exists in the lead, and then use the sea ice model to compute the growth rates rather than an energy balance

equation applied to the ocean. In this way the ice growth rates in the leads will be lower and thus reduce the model sensitivity to time step size.

2. Oceanic Heat Flux

The seasonal cycle of oceanic heat flux in previous modeling studies was set to a constant value of 2 W m^{-2} in the northern hemisphere and 25 W m^{-2} in the southern hemisphere (Maykut and Untersteiner, 1971; Semtner, 1976; Parkinson and Washington, 1979). The reason for this rather crude parameterization was the general lack of knowledge concerning these fluxes.

The value of 2 W m^{-2} in the northern hemisphere was chosen by Maykut and Untersteiner (1971) because it gave the most satisfactory seasonal cycle of sea ice thickness in their studies of high northern latitudes. In addition, the rather small value seemed justified because the Arctic Ocean is strongly stratified so that vertical mixing is surpressed. Later studies (Semtner, 1976; Parkinson and Washington, 1979) used this value of oceanic heat flux in order to make their results more directly comparable with Maykut and Untersteiner's.

The value of 25 W m^{-2} in the Antarctic Ocean was chosen because it was believed that the less stratified structure there would more readily allow vertical exchange, creating heat fluxes which could reach 25 W m^{-2} (Gordon, 1981). Parkinson (1978) tested several values and found that 25W

m^{-2} gave the most satisfactory results.

The constant seasonal cycle of ocean flux was used in these studies because there was no information concerning what the seasonal cycle might be. However, a recent study done by Allison and Akerman (1980) and Allison (1981) has shown that there is a very strong seasonal cycle in the southern hemisphere vertical oceanic heat flux. Allison's measurments indicate that the maximum oceanic heat flux occurs when the ice is thin and just beginning to grow in the early winter, and that the flux may reach 40 W m^{-2}. The high value of the vertical oceanic heat flux is due to the formation of a high salinity layer just below the ice as a result of salt rejection by the new ice. This high salinity layer is denser than underlying water and sinks, forcing up warmer deeper water, and thus producing the vertical oceanic heat flux. This process slows as the ice gets thicker and the growth rate decreases, and as a result the oceanic heat flux decreases.

A secondary peak in the oceanic heat flux occurs in the spring, and reaches a value of about 20 W m^{-2}. Allison (1981) suggests that this peak may be due to an influx of heat and salt into the region by horizontal oceanic heat transports.

Despite these relatively high peaks in the oceanic heat flux of the southern hemisphere the remainder of the year has relatively low values producing an annual average oceanic heat flux of 10 - 15 W m^{-2}.

In the following sections the sensitivity of the sea ice and the energy exchange between the atmosphere and ice/ocean surface to variations in the oceanic heat flux at 72.5N and 67.5S will be explored. First, the response to variations in the mean of the constant seasonal cycle of oceanic heat flux from the base case of 3 W m^{-2} and 12 W m^{-2} at 72.5N and 67.5S respectively, will be examined. Then as a first attempt to examine sea ice response to a varying seasonal cycle of oceanic heat flux, a sinusoidal varying heat flux will be introduced. Then the response of the sea ice and the energy exchange between the atmosphere and the ice/ocean surface to variations in the amplitude and phase of the sinusoidal oceanic heat flux will be examined.

a. Vary Mean of Constant Seasonal Cycle of Oceanic Heat Flux

Figure 4.1 shows the response of the sea ice to variations in the oceanic heat flux from 2 W m^{-2} to 8 W m^{-2} at 72.5N and from 10 W m^{-2} to 25 W m^{-2} at 67.5S. The response at 72.5N is moderate with a decrease in the maximum ice thickness from 1.33 m to 1.09 m and an increase in the period of ice free conditions from 15 to 18 time steps (from about 4.1 to 4.9 months) for an oceanic heat flux of 2 W m^{-2} and 8 W m^{-2} respectively (see Table 4.3). The response at 67.5S is greater ranging from .80 m to .51 m in ice thickness and 2 to 13 time steps (about .5 to 3.5 months) in the period of ice free ocean for an oceanic heat flux ranging from 10 W m^{-2} to 25 W m^{-2}. The larger response at

67.5S is probably due to the fact that the range over which
the ocean flux is varied here is greater and the ice is
thinner than in the northern hemisphere.

In addition to these individual characteristics the
changes in the oceanic heat flux also affect the seasonal
cycle of sea ice thickness. The effect can be seen in Figure
4.1 at both 72.5N and 67.5S. Here the ice growth rate seems
to be only slightly lower early in the winter season for the
higher values of oceanic heat flux. However, the amount of
ice growth becomes much smaller at the end of the winter and
the ice melt period begins earlier when the oceanic heat
flux is higher. The resulting thinner ice allows the period
of ice free conditions to begin about 2 weeks earlier at
72.5N and 3 to 4 weeks earlier at 67.5S. In addition, at
67.5S the ice thickness for an ocean flux of 25 W m^{-2} is on
the order of half the ice thickness when the oceanic heat
flux is 10 W m^{-2} during most of the winter and early spring.

The effect these changes have on the energy exchange
between the atmosphere and the ice/ocean surface are mostly
due to the change in the period of partially and fully ice
free conditions (see Table 4.4).

The increase in the infrared flux to the atmosphere
when the oceanic heat flux is increased at both latitudes is
due to two factors. First, the longer period of ice free
conditions cause the ocean layer to warm more, providing a
period of higher surface temperatures; and second, the
warmer ocean is exposed longer producing a higher average
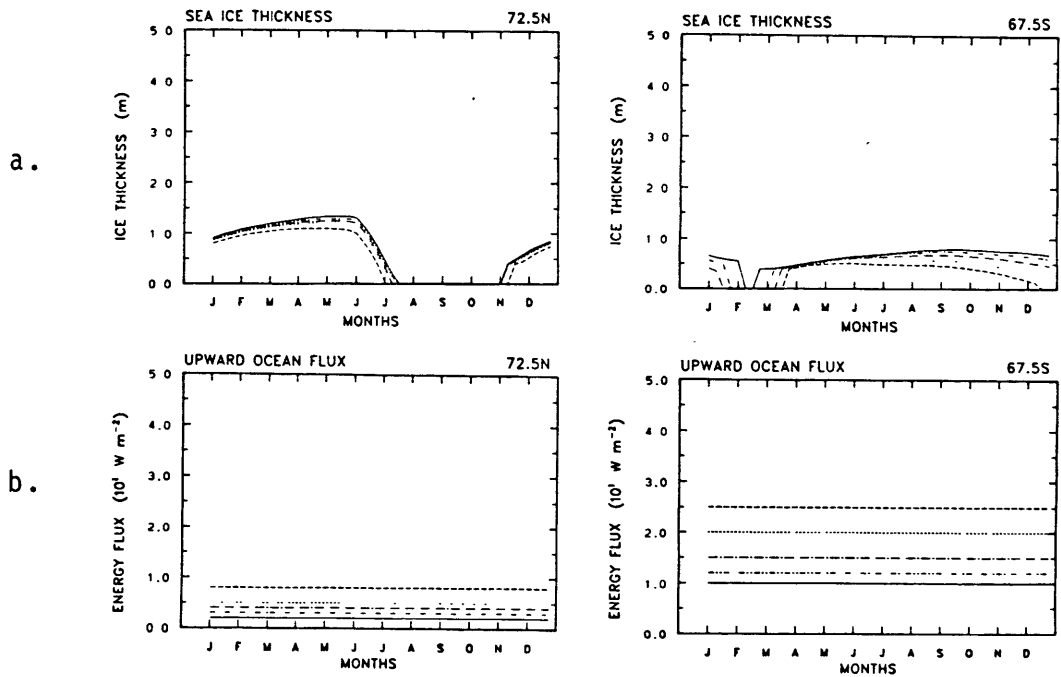
Figure 4.1 a) Seasonal cycle of sea ice thickness for an oceanic heat flux of (72.5N/67.5S) 2/10 (solid line), 3/12 (double dot dashed line), 4/15 (single dot dashed line), 5/20 (dotted line), and 8/25 (dashed line) W m^{-2}. b) Seasonal cycle of oceanic heat flux corresponding to the values indicated in a.

Table 4.3 Maximum Ice Thickness in meters and Period
of Ice Free Conditions for Variations in
the Mean of the Oceanic Heat Flux in W m^{-2}.

Latitude	F_o	Maximum Ice Thickness	Ice Free TS[+]
72.5N	2	1.33	15
	3	1.28	15
	4	1.24	16
	5	1.20	16
	8	1.09	18
67.5S	10	.80	2
	12	.76	6
	15	.68	8
	20	.58	11
	25	.51	13

+ TS used here and in similar tables means time steps

Table 4.4 Annual Mean Components of Heat Balance Equation
Over Ice and Ocean at 72.5N and 67.5S for
Changes in the Mean of Oceanic Heat Flux in W m^{-2}.

Latitude	F_o	F_{ir}	F_{sw}	F_{lh}	F_{sh}	F_{lw}	Net
72.5N	2	272	-40	1	-3	-228	2
	3	272	-41	1	-3	-228	2
	4	272	-41	1	-3	-228	2
	5	273	-41	1	-2	-228	3
	8	276	-43	2	-1	-228	5
67.5S	10	275	-37	12	-13	-230	7
	12	276	-41	13	-10	-230	8
	15	277	-45	15	-7	-230	11
	20	279	-50	18	-2	-230	15
	25	280	-55	20	2	-230	18

Note: F_{sw} is absorbed short wave flux unless otherwise noted

surface temperature. Enhancing this effect is a reduction in

the downward turbulent fluxes in response to the warmer

surface temperatures. Partially offsetting the effects of

the changes in the turbulent and long wave fluxes is the

increase in the absorbed solar radiation which results from

the changes in surface albedo caused by varying the period

of open ocean.

The result of these changes in the individual fluxes at 72.5N is to increase the net flux to the atmosphere from 2 W m^{-2} for an oceanic heat flux of 2 W m^{-2}, 3 W m^{-2}, and 4 W m^{-2} to 5 W m^{-2} for an oceanic heat flux of 8 W m^{-2}. The response at 67.5S of the individual fluxes is greater, especially the turbulent fluxes, therefore creating a greater range for the net flux to the atmosphere from 7 W m^{-2} to 18 W m^{-2} for an oceanic heat flux of 10 W m^{-2} to 25 W m^{-2} respectively.

This result indicates the need for a better understanding of the magnitude of the oceanic heat flux and the processes that cause it. This is especially true in the Antarctic Ocean where the flux is relatively large, exerting more of an effect on sea ice.

b. Vary Amplitude of Sinusoidal Seasonal Cycle of Oceanic Heat Flux

Figure 4.2 shows the response of the seasonal cycle of sea ice thickness and the fraction of open ocean to various amplitudes of a sinusoidal cycle of oceanic heat flux for which the mean is held at 3 W m^{-2} at 72.5N and 12 W m^{-2} at 67.5S.

The response at 72.5N to a cycle of oceanic heat flux with ranges of 0 W m^{-2}, 1 W m^{-2}, 2 W m^{-2}, 3 W m^{-2}, and 6 W m^{-2} is almost negligible. The maximum ice thickness increases slightly from 1.28 m to 1.31 m and the opening of
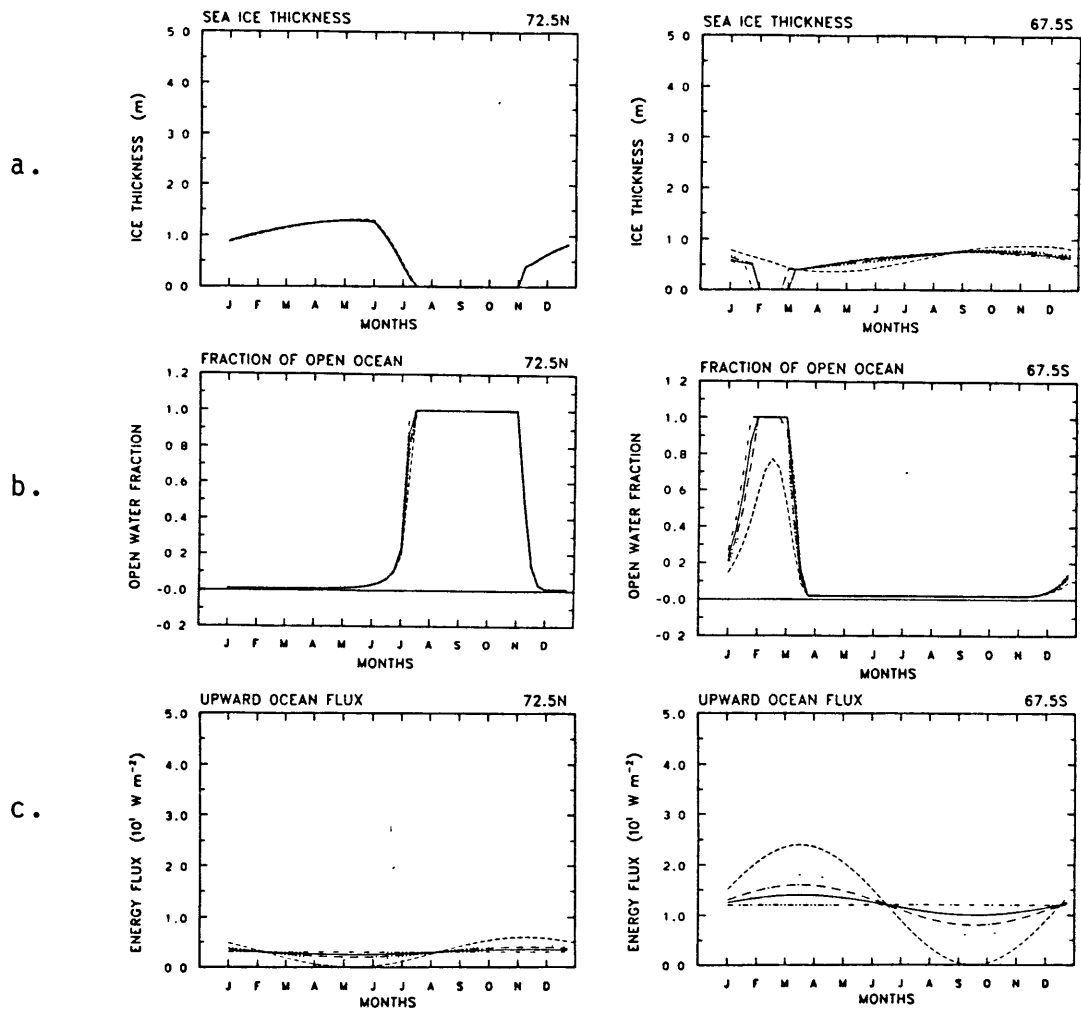
Figure 4.2 a) Seasonal cycle of sea ice thickness for a mean oceanic heat flux of 3 and 12 W m^{-2} at 72.5N and 67.5S respectively and a seasonal range of (72.5N/67.5S) 0/0 (double dot dashed line), 1/4 (solid line), 2/8 (single dot dashed line), 3/12 (dotted line), and 6/24 (dashed line) W m^{-2}. b) Seasonal cycle of fraction of open corresponding to the cases in a. c) Seasonal cycle of oceanic heat flux corresponding to the values indicated in a.

Table 4.5 Maximum Ice Thickness in meters and Period
         of Ice Free Conditions for Variations in
         the Range of the Seasonal Cycle
         of the Oceanic Heat Flux in W m^{-2}.

Latitude	Rng of F_0	Maximum of Ice Thickness	Ice Free TS
72.5N	0	1.28	15
	1	1.29	15
	2	1.29	15
	3	1.30	15
	6	1.31	15
67.5S	0	.76	6
	4	.77	5
	8	.79	4
	12	.81	3
	24	.88	0

the leads is somewhat slower for the higher amplitudes, but
the period of ice free conditions remains at 15 time steps
(about 4.1 months) regardless of the changes in the oceanic
heat flux (see Table 4.5).

The response at 67.5S of the sea ice is larger. The
maximum ice thickness increases from .76 m to .88 m for an
oceanic heat flux seasonal range from 0 W m^{-2} to 24 W m^{-2};
however, Figure 4.2 indicates that the mean ice thickness
remains about the same.

In addition to the changes in ice thickness the period
of ice free conditions drops from 6 to 0 time steps (about
1.6 to 0 months) for the increase in range from 0 W m^{-2} to
24 W $^{-2}$. This drop in the period of ice free conditions
seems very curious because the period of time leads open is
a time of above average heat flux from the ocean. Higher
amplitudes of the oceanic heat flux should therefore produce

higher summer heat fluxes to the bottom of the ice which should make it easier to melt the ice away. However, the higher amplitude oceanic heat fluxes also produce much lower heat fluxes in the winter. This decrease in the energy available in the winter causes more ice to grow in the leads and at the bottom surface of the existing ice layer. This results in thicker ice by the end of the winter than if the amplitude of the heat flux were low. The dominant process in eliminating this sea ice during the summer is melting from the edge, using energy absorbed in leads. The energy needed to open the leads in thicker ice is greater than if the ice were thin, and as a result leads open at a lower rate. The smaller lead areas then restrict the amount of energy that can be absorbed in the ocean, reducing the rate at which the leads open even further. Therefore, despite higher oceanic heat flux rates in the summer, lead areas are reduced as the amplitude of the oceanic heat flux is increased.

The effect that introducing a seasonal cycle of the oceanic heat flux and varying its amplitude has on the annual net energy flux between the atmosphere and ice/ocean surface is small when compared to that when the mean of the oceanic heat flux was varied. Table 4.6 shows the annual averages of the various components of the heat balance equation and the net flux. The net flux at 72.5N varies by at most 1 W m^{-2} over the entire range of amplitude variations with the entire variation resulting from absorbed solar radiation changes occurring during the period that the

leads open up. The range in the variation in the net flux at
67.5S is about the same; however, almost all of the
component fluxes respond to the changes in the amplitude of
oceanic heat flux. This is because the amplitude variations
change the period over which ice free conditions exist. The
variations in the component fluxes, however, almost
completely compensate for each other producing the small
range in the net heat flux.

Table 4.6 Annual Mean Components of Heat Balance Equation
Over Ice and Ocean at 72.5N and 67.5S for
Variations in the Range of the Seasonal
Cycle of Oceanic Heat Flux in $W\ m^{-2}$.

Latitude	Rng of F_o	F_{ir}	F_{sw}	F_{lh}	F_{sh}	F_{lw}	Net
72.5N	0	272	-41	1	-3	-228	2
	1	272	-41	1	-3	-228	2
	2	272	-40	1	-3	-228	2
	3	272	-40	1	-3	-228	2
	6	272	-40	1	-3	-228	3
67.5S	0	276	-41	13	-10	-230	8
	4	276	-40	13	-10	-230	9
	8	276	-39	12	-11	-230	8
	12	276	-38	12	-12	-230	9
	24	275	-34	11	-13	-230	9

c. Vary the Mean of the Sinusoidal Seasonal Cycle of Oceanic
Heat Flux

Figure 4.3 shows the response of the sea ice to
variations of the mean of the seasonal cycle of the oceanic
heat flux for which the range is held at 6 $W\ m^{-2}$ at 72.5N
and 24 $W\ m^{-2}$ at 67.5S. Both latitudes show a response
similar to that when the constant oceanic heat flux was
varied. The maximum ice thickness at 72.5N drops .09 m and

the number of ice free time steps increases by 1 for a change in the mean from 3 W m^{-2} to 5 W m^{-2}. This is not much different from the .08 m change in the ice thickness and the increase of 1 time step in the period of ice free conditions when the mean oceanic heat flux is changed over the same range but the seasonal cycle is a constant (see Table 4.7). The maximum ice thickness at 67.5S drops .37 m and the period of ice free conditions increase 13 time steps (about 3.5 months) when the mean oceanic heat flux is increased from 12 W m^{-2} to 28 W m^{-2}. While this is not directly comparable to the variations made in the constant oceanic heat flux because the same values were not used, the variation in the ice thickness over the year is similar. The ice growth at the beginning of the winter proceeds at comparable rates for each value of the mean oceanic heat flux at both 72.5N and 67.5S. However, as the ice gets thicker the growth rate in the cases of higher oceanic heat flux decrease more rapidly resulting in thinner ice. Then during the summer the thinner ice melts away more rapidly resulting in longer periods of ice free conditions.

The effect that these variations have on the energy exchange between the atmosphere and the ice/ocean surface is also much the same as when the seasonal cycle was constant. Table 4.8 shows that at 72.5N the net flux to the atmosphere is 3 W m^{-2} regardless of the mean of the heat flux, while at 67.5S the net flux increases from 9 W m^{-2} to 23 W m^{-2} for a change in the mean of the oceanic heat flux from 12 W m^{-2} to
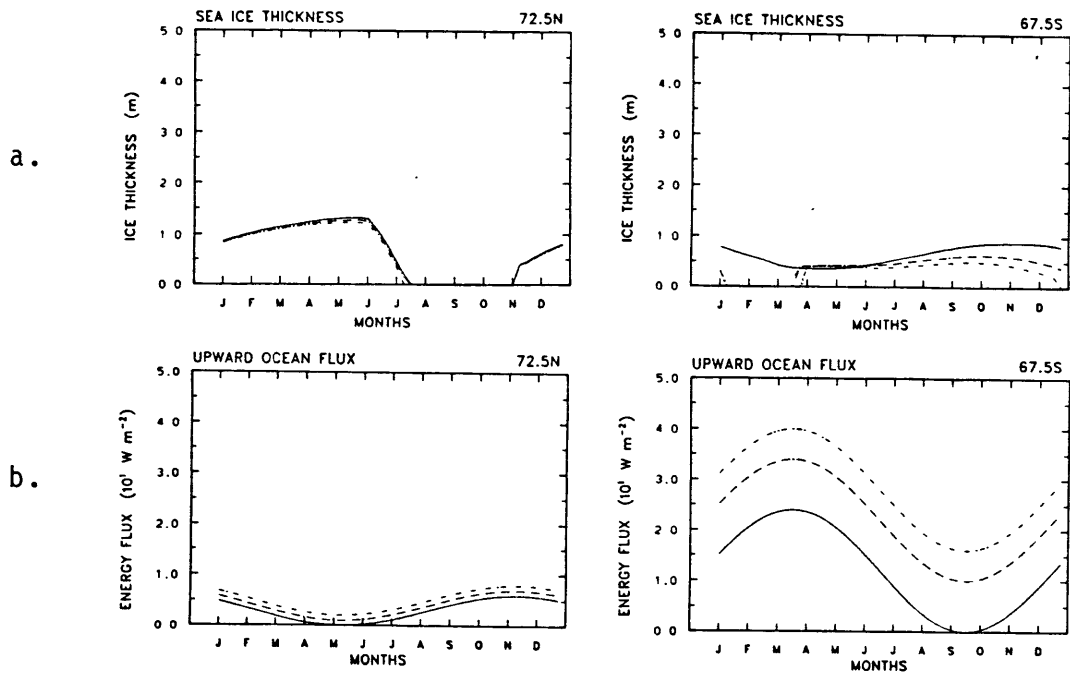
Figure 4.3 a) Seasonal cycle of sea ice thickness for a mean oceanic heat flux of (72.5N/67.5S) 3/12 (solid line), 4/22 (single dot dashed line), 5/28 (double dot dashed line) W m^{-2} with a seasonal range of 6 and 24 W m^{-2} at 72.5N and 67.5S respectively. b) Seasonal cycle of oceanic heat flux corresponding to the values indicated in a.

Table 4.7 Maximum Ice Thickness in meters and Period of Ice Free Conditions for Variations of the Mean of the Oceanic Heat Flux in $W\ m^{-2}$ with a Range Amplitude of 6 and 24 $W\ m^{-2}$ in the Northern and Southern Hemispheres Respectively

Latitude	Mean F_o	Maximum Ice Thickness	Ice Free TS
72.5N	3	1.31	15
	4	1.27	15
	5	1.22	16
67.5S	12	.88	0
	22	.64	10
	28	.51	13

Table 4.8 Annual Mean Components of Heat Balance Equation Over Ice and Ocean at 72.5N and 67.5S for Variations in the Mean of the Oceanic Heat Flux with a Seasonal Range of 6 and 24 $W\ m^{-2}$ in the Northern and Southern Hemispheres Respectively

Latitude	Mean F_o	F_{ir}	F_{sw}	F_{lh}	F_{sh}	F_{lw}	Net
72.5N	3	272	-40	1	-3	-228	3
	4	273	-41	1	-3	-228	3
	5	273	-41	1	-3	-228	3
67.5S	12	275	-34	11	-13	-230	9
	22	278	-46	17	-2	-230	17
	28	280	-51	21	4	-230	23

28 $W\ m^{-2}$. In both cases these variations are due to the variations in the period of partially and completely ice free conditions. There is only a small change at 72.5N resulting in very small variations in the energy exchange; however, at 67.5S the change in the period of ice free conditions is 3.5 months resulting in a large change in the atmosphere - ice/ocean energy exchange.

d. Vary the Phase of the Sinusoidal Seasonal Cycle of
Oceanic Heat Flux

The choice of the phase of the sinusiodal seasonal
cycle of the oceanic heat flux was made based on the
evidence in Allison (1981) that the highest fluxes occur
when new ice begins to form. This suggests that the time
that ice growth begins and its rate determine the phase and
amplitude of the seasonal cycle of the oceanic heat flux.
However, the present formulation of the sea ice model
requires that the oceanic heat flux be specified. Therefore,
the phase of the oceanic heat flux is chosen so the maximum
occurs when the sea ice in the base case is growing fastest,
despite the possibility that the varying oceanic heat flux
may change the growth rates of the sea ice.

In order to determine how critical the choice of the
phase of the sinusoidal heat flux is to the response of the
sea ice, experiments were performed in which the mean of the
heat flux was held at 3 W m^{-2} and 12 W m^{-2} and the seasonal
range was fixed at 6 W m^{-2} and 24 W m^{-2} at 72.5N and 67.5S
respectively. The phase was then shifted plus and minus 2
and 4 time steps (about .5 and 1.1 months) with a positive
shift placing the maximum flux into a period of relatively
ice covered conditions, and a negative shift placing it into
relatively ice free conditions. Figure 4.4 shows the results
of these experiments.

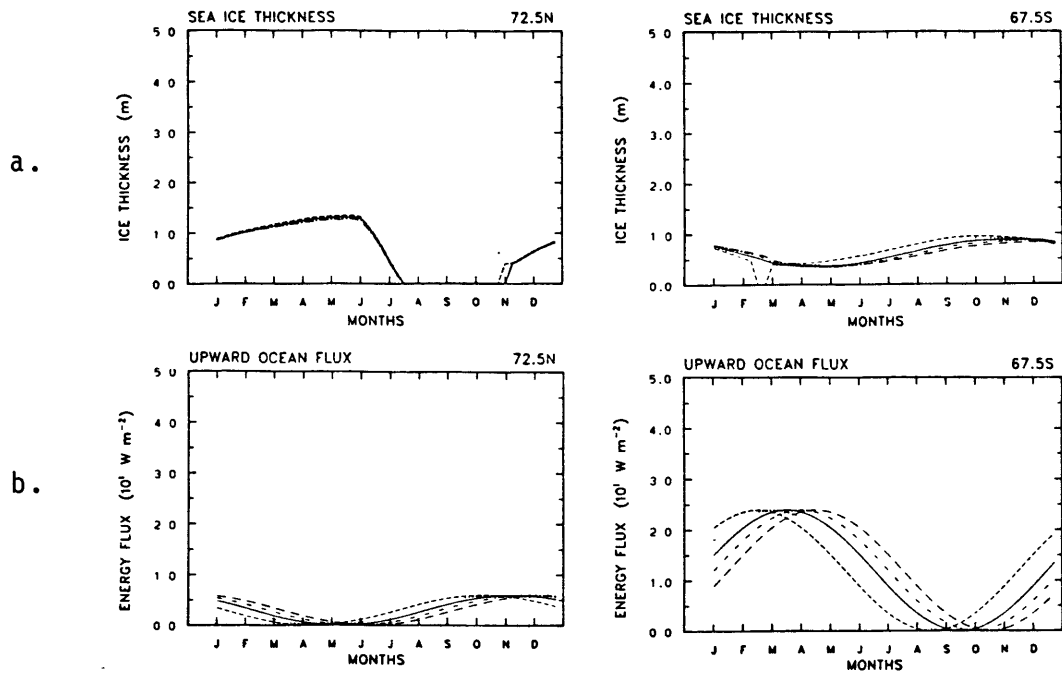Figure 4.4 a) Seasonal cycle of sea ice thickness for a mean oceanic heat flux of 3 and 12 $W\ m^{-2}$ and a seasonal range of 6 and 24 $W\ m^{-2}$ at 72.5N and 67.5S respectively for a change in phase of +4 (single dot dashed line), +2 (double dot dashed line), 0 (solid line), -2 (dotted line), and -4 (dashed line) time steps. b) Seasonal cycle of oceanic heat flux corresponding to the values indicated in a.

The sea ice at 72.5N shows a relatively small response with the maximum sea ice thickness increasing from 1.27 m to 1.35 m and the period of ice free conditions decreasing one time step as the phase is shifted from +4 to -4 time steps (see Table 4.9). The reason for the increase in the ice thickness as maximum oceanic heat flux is shifted into a period of ice free conditions is that the minimum and lower values of the oceanic heat flux are more precisely centered on the period of ice growth. This causes thicker ice to grow by the end of the winter. The period of ice free conditions decrease because at the end of the summer the oceanic heat flux is already beginning to decrease when the phase is shifted -2 and -4 time steps. The decrease in the energy available to the ocean during that time allows the ice to form earlier.

Table 4.9 Maximum Ice Thickness in meters and Period of Ice Free Conditions for Various Phase Shifts in the Seasonal Cycle of Oceanic Heat Flux for a Mean Flux of 3 and 12 $W\,m^{-2}$ and a Seasonal Range of 6 and 24 $W\,m^{-2}$ in the Northern and Southern Hemispheres Respectively

Latitude	Phase Shift[+] in TS	Maximum Ice Thickness	Ice Free TS
72.5N	+4	1.27	15
	+2	1.29	15
	0	1.31	15
	-2	1.33	14
	-4	1.35	14
67.5S	+4	.83	0
	+2	.86	0
	0	.88	0
	-2	.96	0
	-4	.95	2

+ A positive phase shift moves the maximum to a later time.

The sea ice at 67.5S shows a similar response with the maximum sea ice thickness increasing from .83 m to .95 m for a phase shift from +4 to -4 time steps. However, the period of ice free conditions remains at zero except when the phase is shifted -4 time steps, at which time the ocean is ice free for 2 time steps. The reason for this reverse shift in the period of ice free conditions compared to the northern hemsiphere is that the sea ice for most of these cases does not melt away, but shows that during the period January through March the ice thickness differentiates with thinner ice corresponding to the highest ocean flux at that time, ie. the case where the phase shift is -4 time steps. This differentiation in the ice thickness occurs during a period of relatively high solar radiation and air temperatures, and therefore the thinner ice is more readily melted away. This effect also occurs in the other phase shift experiments; however, the larger ice thickness resulting from the shift of the maximum ocean flux to periods of lower solar insolation and air temperatures causes the decay of the sea ice during the summer to be incomplete. When the phase is shifted +4, +2, 0, and -2 time steps the corresponding maximum extent of the lead area is 62%, 67%, 77%, and 92% respectively compared to the complete melting away of the ice when the phase of the oceanic heat flux is shifted -4 time steps.

Table 4.10 shows the effect that the sea ice

variations, caused by shifting the phase of the seasonal cycle of oceanic heat flux, has on the energy exchange between the atmosphere and the ice/ocean surface.

Table 4.10 Annual Mean Components of Heat Balance
Equation Over Ice and Ocean at 72.5N and
67.5S for Variations in the Phase of the
Seasonal Cycle of the Oceanic Heat
Flux for a Mean Flux of 3 and 12 W m^{-2}
and a Seasonal Range of 6 and 24 W m^{-2} in
the Northern and Southern Hemispheres Respectively

Latitude	Phase Shift in TS	F_{ir}	F_{sw}	F_{lh}	F_{sh}	F_{lw}	Net
72.5N	+4	272	-40	1	-3	-228	2
	+2	272	-40	1	-3	-228	3
	0	272	-40	1	-3	-228	3
	-2	271	-40	1	-3	-228	1
	-4	271	-40	1	-3	-228	1
67.5S	+4	275	-33	11	-14	-230	9
	+2	275	-33	11	-14	-230	9
	0	275	-34	11	-13	-230	9
	-2	275	-35	12	-13	-230	9
	-4	276	-37	12	-12	-230	9

When the phase is shifted +2 and +4 time steps at 72.5N there is almost no change in the net flux compared to the original phase of the heat flux. The only change is in the order of less than 1 W m^{-2} and is caused by a change in the absorbed solar radiation. This change results from the different rates at which leads, and thus the surface albedo, varies. When the phase is shifted -2 and -4 time steps the net upward flux drops from 3 W m^{-2} to 1 W m^{-2}. This change is mostly due to a drop in the outgoing long wave radiation from the surface which results from an increase in the insulation of the warm ocean from the atmosphere when the

period of open ocean is reduced.

When the phase of the oceanic heat flux is shifted from +4 to -4 time steps at 67.5S there is almost no change in the net energy exchange between the atmosphere and the ice/ocean surface. This does not mean that the individual fluxes do not change. In fact, the absorbed short wave radiation increases 4 W m^{-2} as the maximum lead area increases; however, this is compensated for by an increase in the upward turbulent fluxes leaving the net flux unchanged.

The results discussed in this section seem to indicate that variations in the mean and amplitude of the seasonal cycle of oceanic heat flux have relatively independent effects on the seasonal cycle of sea ice thickness and the energy exchange between the atmosphere and the ice/ocean surface. They also indicate that variations in the mean oceanic heat flux have a larger impact, especially on the annual net energy flux, than do variations in the amplitude of the seasonal cycle. However, the specified seasonal cycle of oceanic heat flux used here is only a crude first order approximation to that described by Allison (1981) for the southern hemisphere. This seasonal cycle of oceanic heat flux does not accurately reflect the sharp drop in the flux as the new ice growth slows and it neglects completely the spring peak in the flux. In addition, the specified flux

assumes values during the period of ice free conditions, a time which is neglected by Allison completely. Accurately including these features in the seasonal cycle of the oceanic heat flux may increase the small effect that the sinusoidal oceanic heat flux has on sea ice.

More information is needed concerning both the magnitude and the processes which cause the vertical oceanic heat flux under both ice free and ice covered conditions. Until these processes are better understood and quantified it seems from the results discussed here that more complex formulations of the seasonal cycle of oceanic heat flux are not likely to produce more accurate results than that represented by the constant seasonal cycle.

B. Continental Ice

1. Time Step Size

The continental ice sheet model was developed in order to perform experiments which test hypotheses concerning the evolution of the ice ages. Experiments such as these require time integrations on the time scale of the ice ages which is on the order of 10^4 to 10^5 years, and as a result require a large amount of computer time. Since computer time in most cases is limited it is of interest to determine the largest time step size, and thus the fewest number of calculations which will give reasonable results. In most of the previous ice sheet modeling studies the time step taken to determine the dynamic flow of the ice was 2 years, and although

computer dependent, the amount of computer time required to perform ice age experiments was on the order of 30 minutes.

The present model was designed to take longer time steps. Early experiments with the model consisted of introducing arbitrarily chosen parabolic ice sheets as the initial conditions and letting the ice flow with various time step sizes. It was found that in these cases the model remained stable when the time step size was 50 years, but went unstable for 100 year time steps. The 50 year time step was then the upper limit.

The next experiments added the accumulation and ablation of snow and ice at the surface of the ice sheet. The addition of this process made the model less stable. A 50 year time step proved to be stable only if the net budget (accumulation minus ablation) was very smoothly distributed in latitude and there were no sharp slopes on the ice sheet. Other time step sizes that were tried and proved to be stable for the particular cases that were being tested were 25, 20 and 10 years.

In addition to the stability of the model, the sensitivity of the ice sheet thickness to different time step sizes is also of interest. If the model is very sensitive then it is preferable to use small time steps in order to reduce the truncation error. Figures 4.5.a and 4.6.a show an ice sheet in the northern and southern hemispheres respectively at the end of 500 years for a time step size of 10 years. Figures 4.5.b and 4.6.b show the
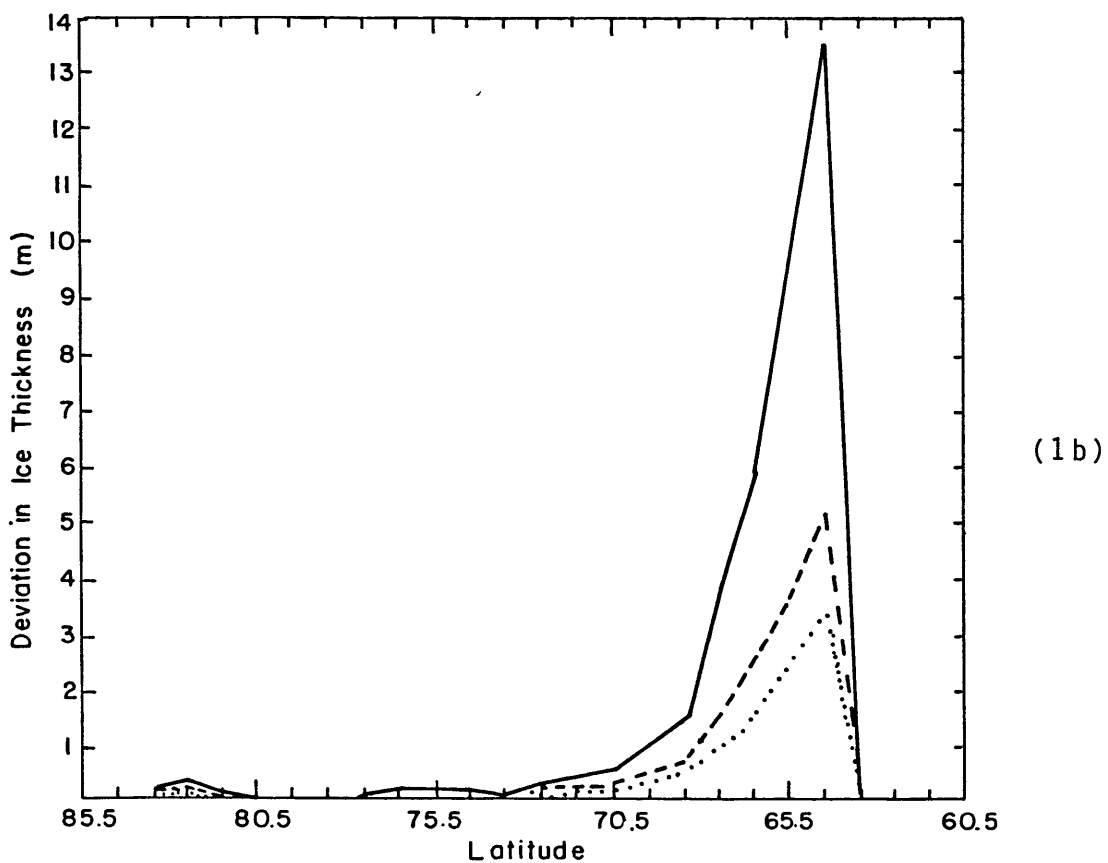
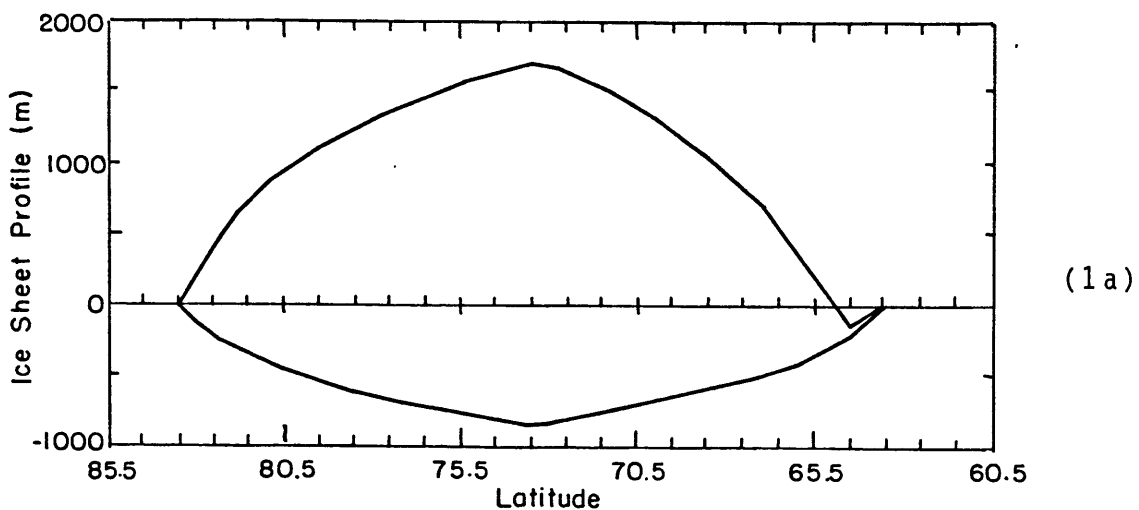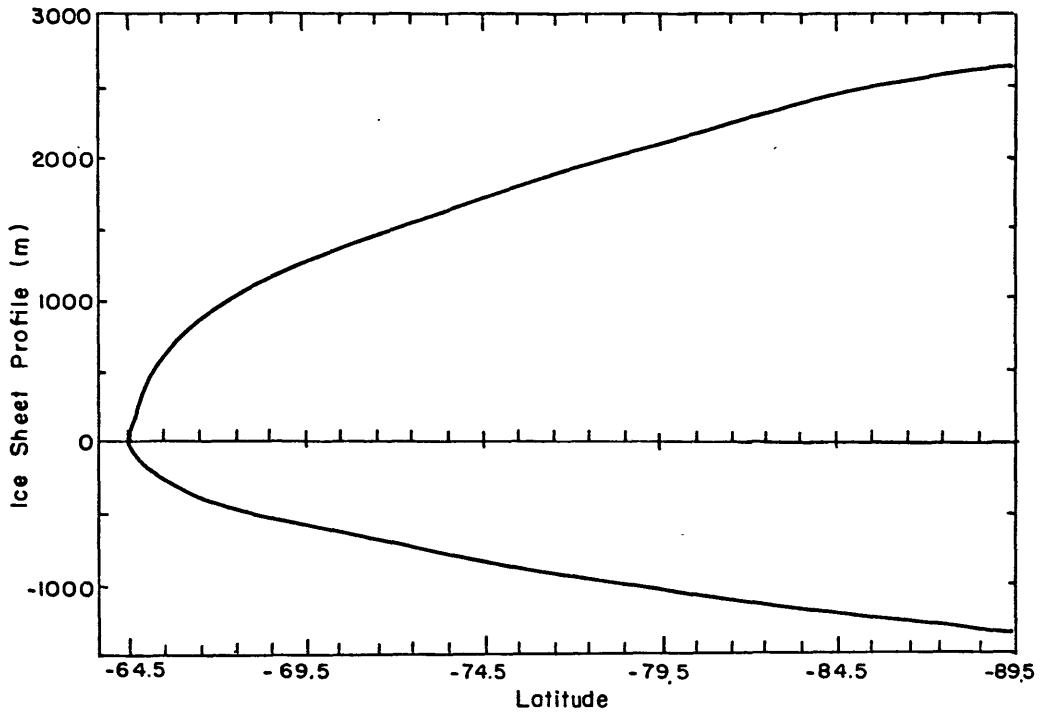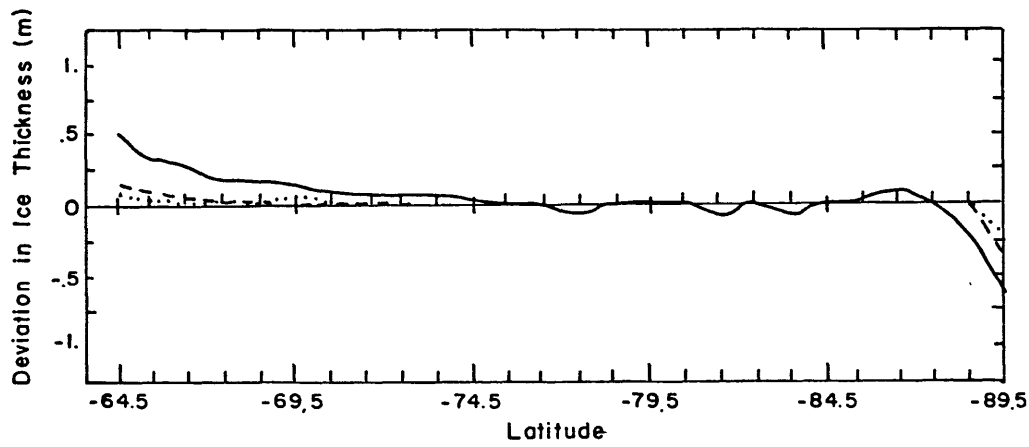Figure 4.5.a) Northern hemisphere ice sheet profile at the
end of 500 years for an ice hseet time step size
of 10 years. b) The deviation of the ice sheet
profile from that in a at the end of 500 years
when the ice sheet time step size is increased
to 50 years (solid line), 25 years (dashed
line), and 20 years (dotted line).

(2a)

(2b)

Figure 4.6 Same as for Figure 4.4.a and 4.5.b for the
southern hemisphere ice sheet.

deviations in the ice sheet thickness between ice sheets
after integrations of 500 years for 50, 25, and 20 year time
steps and that with 10-year time steps.

Figures 4.5 and 4.6 show that the ice sheet thickness
is relatively insensitive to time step size at the center of
the ice sheet where ice surface slopes are small, and at the
edges of the ice sheet where calving ablation occurs.
However, at the southern edge of the northern hemisphere ice
sheet where the ice flows freely there is a difference in
the ice sheet thickness at the end of 500 years which ranges
from a little over 3 m of ice for 20 year time steps to 13.5
m for 50 year time steps. 13.5 m does not seem like much (in
fact it is below the resolution of the graph in Figure
4.5.a) when compared to an ice sheet which is a few thousand
meters thick, and when the uncertainties in knowing the
thickness or extent of a northern hemisphere ice sheet are
considered, but it must be remembered that this was the
result after an integration of only 500 years. The
discrepancy occurring at the end of longer time integrations
is uncertain; however, if the ice sheet depicted in Figure
4.5.a were to flow south of 64.5N the ice at that latitude
would become thicker and the sensitivity to time step size
would be reduced. In addition, if the ice sheet were closer
to equilibrium the changes in ice sheet thickness would be
smaller further reducing the sensitivity to time step size.

These results do not point to an optimum time step
size, but they do indicate that a time step of longer than

10 years may be possible. However, in the interest of assuring numerical stability for a wide variety of ice sheet conditions the continental ice sheet model experiments described in this thesis will use a time step size of 10 years.

2. Asynchronous Coupling with the Atmosphere

The net budget of accumulation and ablation at the surface of the ice sheet was originally computed by summing the accumulation and ablation in approximately 2 week time steps (24 time steps per year) through the ten seasonal cycles that represent the ice sheet time step, and this was repeated for each ice sheet time step. Since the ice sheet model would eventually be used in long time integrations, there would be a tremendous number of calculations that would require a large amount of computer time. In order to make the ice age experiments financially feasible it was necessary to find methods of reducing the number of calculations made in an experiment without significantly changing the results.

In the following two sections the impact of reducing the number of seasonal cycles used to compute the net budget and reusing the computed net budget for multiple ice sheet time steps on the results, and the corresponding financial benefits, are discussed.

a. In Obtaining the Net Budget

One method of reducing the number of calculations required in an ice sheet model experiment is to reduce the number of seasonal cycles used to compute the net budget and extrapolate the computed net budget to the ten year ice sheet time step.

In this method great care must be taken when defining the net budget in regions where the ice is thin and would melt away during the ice sheet time step. In such a case the net budget is minus the thickness of the ice at the beginning of the time step, and that would be the result if the full ten seasonal cycles were used to compute the net budget. However, if the net budget at the end of 3 or 2 seasonal cycles were used the extrapolated net budget would erroneously be 3.3 to 5 times too large. This problem can be overcome by simply testing at each seasonal time step if the ablation is ever enough to entirely melt the ice away, and if so adjusting the extrapolated net budget to a more appropriate value.

The method of reducing the number of seasonal cycles used to compute the new budget was tested with a series of experiments in which initial non-equilibrium ice sheets were introduced in both the northern and southern hemispheres, and integrated for 10000 years. The number of seasonal cycles used to compute the net budget in these experiments was varied from 10 to 3 and 2. The impact on the computer time required was dramatic; this time ranged from 93.4 s

when 10 seasonal cycles were used to 37.5 s and 29.5 s when 3 and 2 seasonal cycles were used respectively.

In addition, the change in the net budget between the three cases was negligible. The reason for the minimal effect on the net budget is that all the atmospheric variables are specified. The only change that occurs is the variation of air temperature with elevation. Since the ice sheet grows so slowly the temperature change is very small (in these experiments the maximum change in ice thickness in 10 years was on the order of .5 m which results in an air temperature change of .0033 K) so the surface energy balance calculation can adjust very quickly to the change. If fact, when comparing the initial seasonal cycles computed in each of the experiments the net budget is exactly the same by the second time step of the first seasonal cycle.

This method of reducing the number of calculations seems to work very well here; however, once the ice sheet model is coupled to a climate model in which many of the atmospheric variables can change the sensitivity of the net budget to the number of seasonal cycles used to compute it must be reexamined.

In the continental ice sheet model experiments that are discussed later 2 seasonal cycles are used to compute the net budget.

b. In Using the Net Budget

Another method of reducing the number of calculations

required in an ice sheet experiment is to reuse the net budget for a few ice sheet time steps.

This method for reducing the number of calculations required by the ice sheet model was tested in a series of experiments in which initial non-equilibrium ice sheets were introduced in the northern and southern hemisphere, 2 seasonal cycles were used to compute the new budget, and the model was integrated for 10000 years. The number of times the net budget was reused was varied from zero to 2 and 5 times. The impact this had on the amount of computer time needed was again dramatic; this time ranged from 31.8 s when the the net budget was computed for every time step to 13 s and 9.1 s when the net budget was reused 2 and 5 times respectively.

Reusing the new budget does have some effect on the resulting ice sheet. It was found that the equilibrium ice sheet was exactly the same reqardless of the number of times the net budget was reused; however, the way it came to equilibrium and the number of time steps it took varied. An example of the reason for this can be see in the case of a growing ice sheet in the southern hemisphere where we will assume there is no ablation. As the ice sheet grows thicker the elevation increases and air temperature decreases. With decreasing air temperatures the amount of moisture in the air decreases and with it the snowfall rate. When the net budget is computed for every ice sheet time step it reflects the decrease in the snowfall; however, if the net budget is

reused the higher snowfall rates computed from the first ice sheet time step are extrapolated over a few ice sheet time steps and the ice sheet grows thicker. In this case the ice sheet would require less time steps to come to equilibrium than if the net budget were computed for every ice sheet time step, but once at equilibrium the net budget would be the same from one time step to the next and therefore the number of times it is reused is irrelevant. In other cases, in which the net budget includes ablation, the situation is more complicated so it is not clear whether the rate of approach to equilibrium would be numerically increased or decreased, however, the increase in computer efficiency seems to be much greater than the possible decrease in the rate of approach to equilibrium.

These results indicate that reusing the net budget is applicable only if the desired end result is an equilibrium ice sheet. If the time series of the variations in the ice sheet or the effect of some change over a finite period is desired the reusing of the net budget would not produce the desired result and should be avoided. In the continental ice sheet model experiments described in the following sections the net budget is not reused except in those cases in which an equilibrium ice sheet is desired.

3. Flow Parameters

The equations of dynamic ice flow were derived in part from the flow law of polycrystaline ice which relates the

final strain rate to the shear stress as follows

$$\dot{\varepsilon}_{yz} = A * \tau_{yz}^{n}$$

where A and n, the flow parameters, are constants.

The value of n has been determined experimentally. The measured values generally range between 1.9 to 4.5 with a mean of about 3 (Paterson, 1969), which is the value used in the majority of the simple ice sheet models and is used here.

The value of A is dependent on the ice temperature. Glen (1955) determined through experimental analysis that this dependency has the form exp(-Q/RT), where T is the absolute temperature, R is the gas constant, and Q is considered an "activation energy" for creep (Paterson, 1969). In most of the simple ice sheet modeling studies the temperature distribution within the ice is unknown so in those cases as in this model a constant value must be chosen.

The choice of the value of A has varied widely from one study to the next. In some studies the value was derived from measurements from Antarctica and Greenland, while in others the value of A was estimated using the laws of ice flow and scale analysis. The values of A used in previous studies generally ranged from .03 $yr^{-1}bar^{-3}$ to .6 $yr^{-1}bar^{-3}$; however, one of the most recent and well known studies of ice age variations (Pollard, 1978,1982a,1982b,1982c) set A equal to 2.1, a factor of 3.5 greater than the top of the range used in most studies and a factor of 14 greater than

the value generally used in this study, .15 $yr^{-1}bar^{-3}$ (see chapter II.D.1).

What is the magnitude of the sensitivity of an equilibrium ice sheet to changes in the value of A? Figures 4.7 and 4.8 show the response of an equilibrium ice sheet when A is equal to .15 $yr^{-1}bar^{-3}$ in the northern and southern hemispheres respectively to a doubling of the value of A to .3 $yr^{-1}bar^{-3}$.

The effect of doubling the value of A was to increase the flow rate of the ice sheet. In the northern hemisphere the increased flow rate was enough to overcome the ablation rate and extend the ice sheet a degree further north at the end of 10000 years. The southern edge of the northern hemisphere ice sheet remained at the same latitude; however, the increased flow rate along with that at the northern edge aided in reducing the elevation of the center of the ice sheet by about 150 m at the end of 10000 years. If the integration were continued the ice sheet might come to a new equilibrium, or it might disappear completely if the central elevation were decreased enough to put the entire ice sheet under ablation.

In the southern hemisphere the increase in ice velocity is enough to initially overcome the calving ablation and extend the ice sheet one degree farther north. This in effect drains ice from the more northerly latitudes which decreases in elevation by about 300 m at the end of 10000 years. With the decrease in elevation the ice velocities are
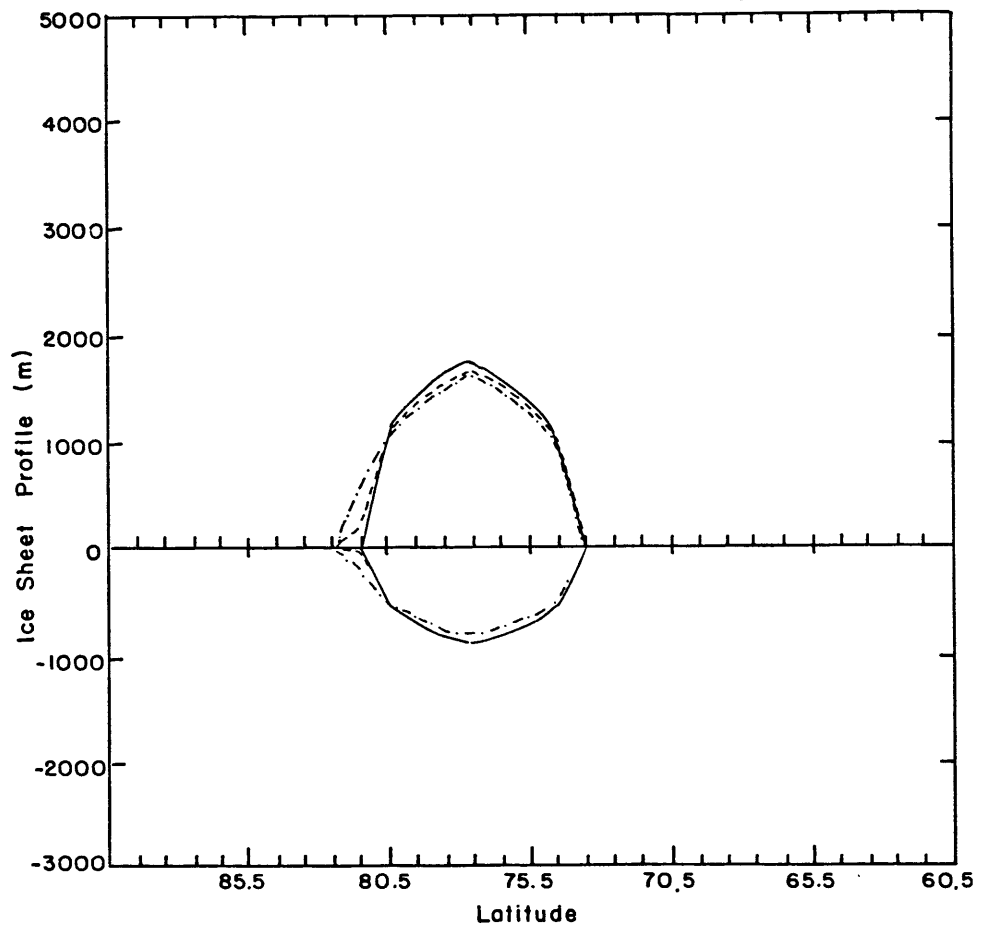
Figure 4.7 Response of northern hemisphere equilibrium ice sheet (solid line) when $A = .15$ $yr^{-1}bar^{-3}$ to a doubling of A to .3 $yr^{-1}bar^{-3}$ at the end of 2000 years (dashed line) and 10000 years (dot dashed line).
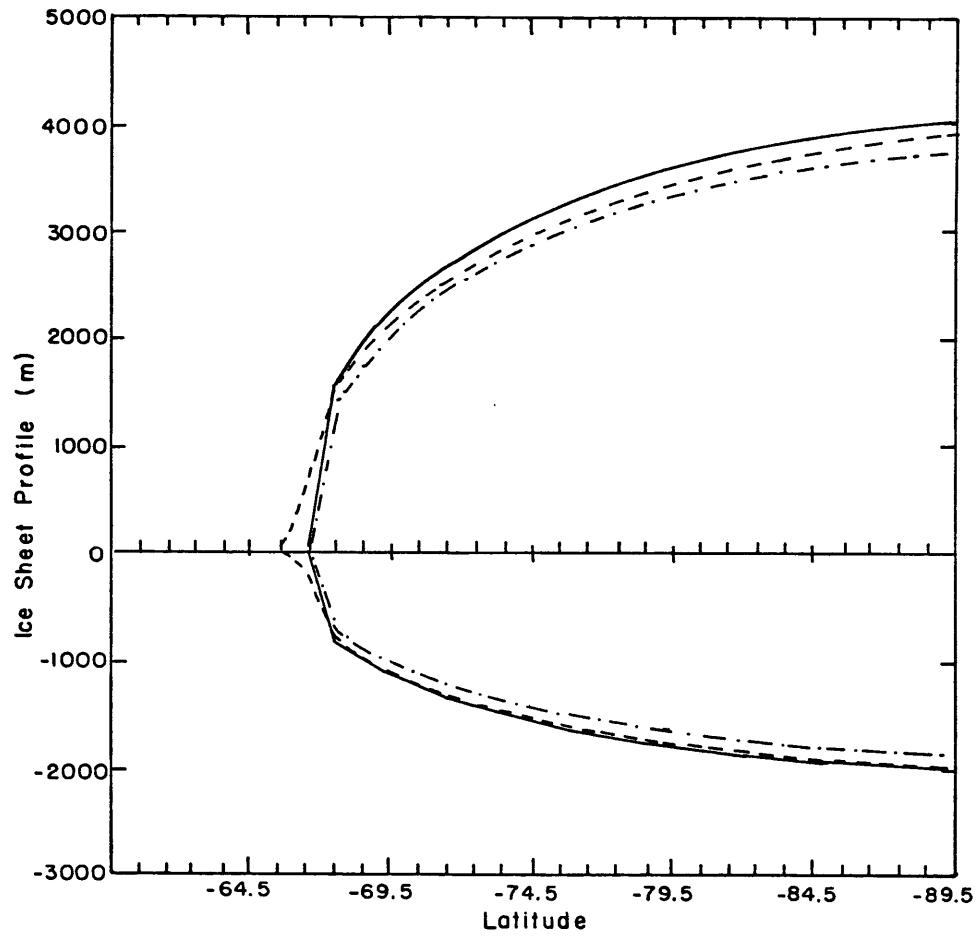
Figure 4.8 Same as for Figure 4.7 for southern hemisphere
ice sheet.

reduced so the calving ablation again dominates the net budget at the northern edge of the ice sheet, shrinking the ice sheet back to its original latitudinal extent. If the integration were continued it seems that the southern hemisphere ice sheet would come to a new equilibrium at a lower elevation. It is not likely that the ice sheet would become dominated by ablation and melt away because of two factors. First, its polar location and high elevations insure cold temperatures and thus a positive net budget. In fact, in all of the experiments done to date the only negative net budget occurring on Antarctica was due to the calving ablation at the northern edge. The second factor is the relatively gentle slope over most of the ice surface which causes the ice velocities to be low. Since the accumulation of snow at these high elevations is small due to the lack of moisture, the small ice velocities are necessary if an equilibrium is to exist.

Further experiments were done varying the value of A in the northern and southern hemisphere ice sheets to .6 $yr^{-1}bar^{-3}$ and 2.1 $yr^{-1}bar^{-3}$. These experiments were originally initialized as before with the equilibrium ice sheet when A was equal to .15 $yr^{-1}bar^{-3}$. However, when A was changed to .6 $yr^{-1}bar^{-3}$ or 2.1 $yr^{-1}bar^{-3}$ the ice velocities of the southern hemisphere ice sheet in the region where it begins to slope toward the northern edge became high enough to cause the ice sheet to go numerically unstable. In order to further investigate the sensitivity of the ice sheets to
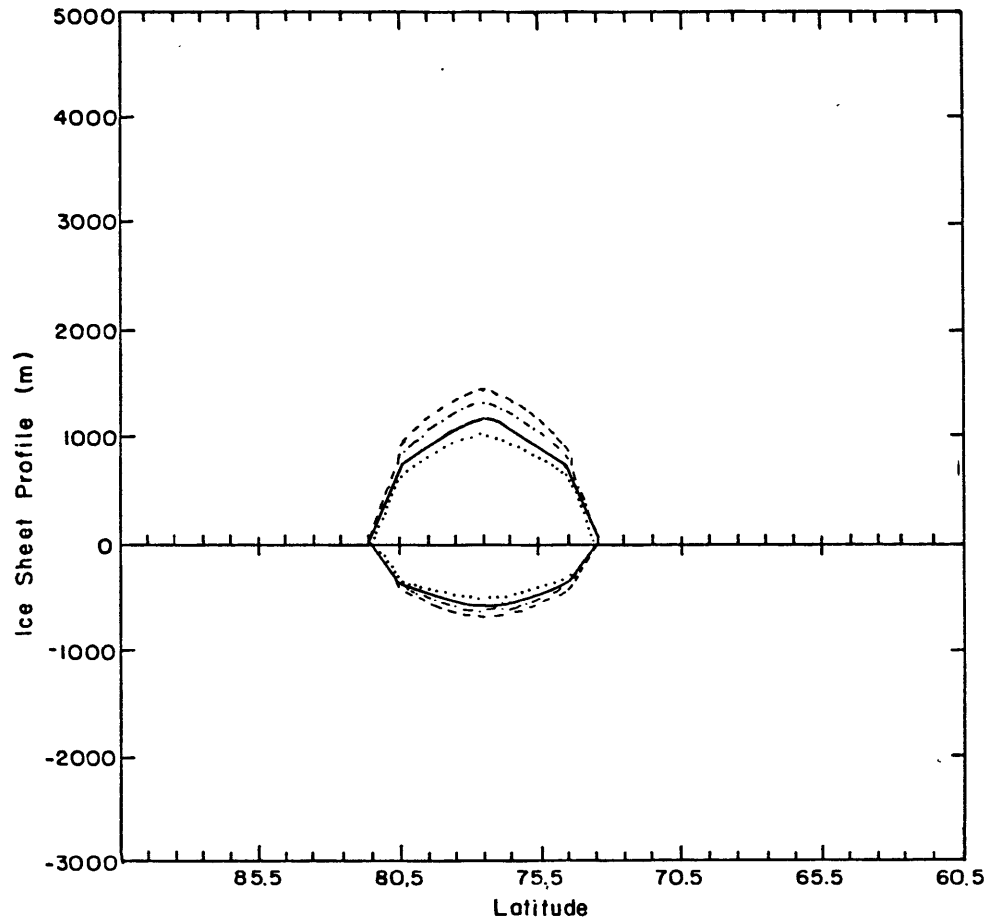
Figure 4.9 Response of the northern hemisphere ice sheet
from 2/3 of its equilibrium size when A = .15
$yr^{-1}bar^{-3}$ (solid line) at the end of 10000 years
when A is changed to .3 $yr^{-1}bar^{-3}$ (dashed line),
.6 $yr^{-1}bar^{-3}$ (dot dashed line), and 2.1
$yr^{-1}bar^{-3}$ (dotted line).
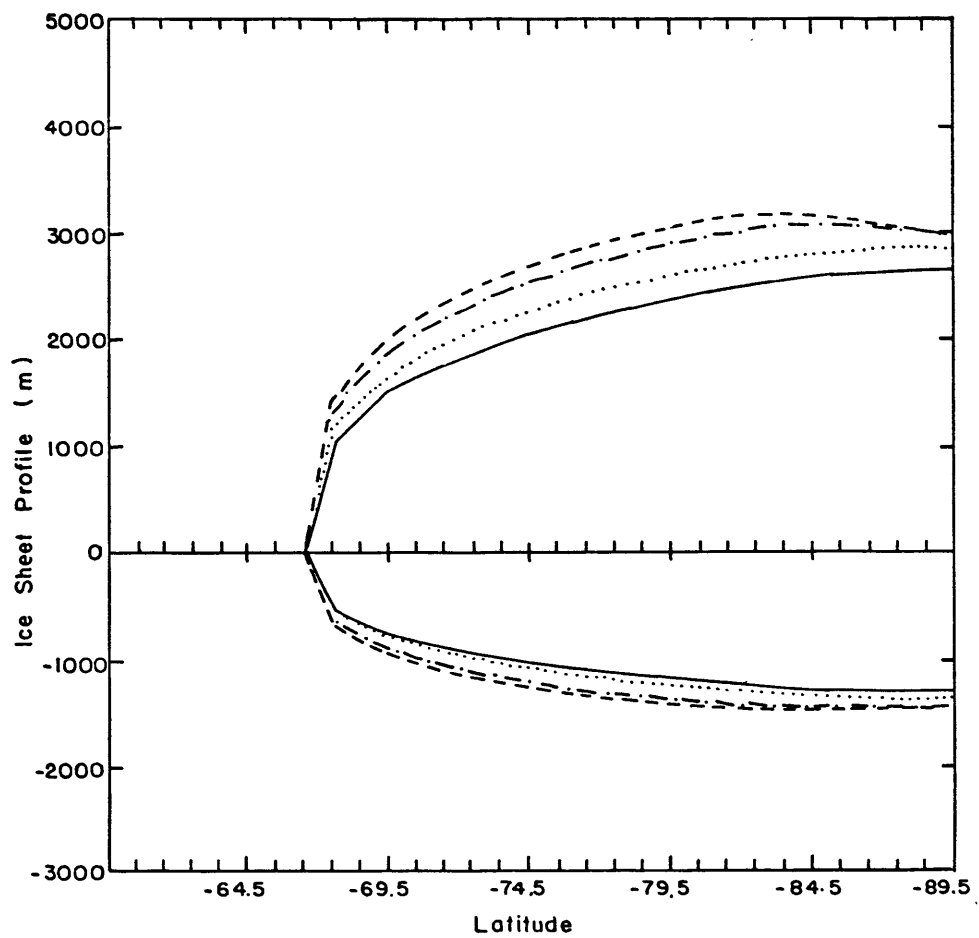
Figure 4.10 Same as for Figure 4.9 for the southern
hemisphere ice sheet.

the value of A the experiments were repeated with the
initial ice sheet reduced to 2/3 of its equilibrium size.
The results of these experiments are shown in Figures 4.9
and 4.10 for the northern and southern hemispheres
respectively.

In the northern hemisphere the ice sheet begins to grow
when A is set equal to .3 $yr^{-1}bar^{-3}$ and .6 $yr^{-1}bar^{-3}$,
although at distinctly different rates. At the end of 10000
years the ice sheet has grown almost 300 m when A is set
equal to .3 $yr^{-1}bar^{-3}$, and only about 150 m when A is set
equal to .6 $yr^{-1}bar^{-3}$. These results suggest that the ice
sheet will not melt away as was suggested as a possibility
in the previous ice sheet experiment, but will establish an
equilibrium profile that is distinct depending on the value
of A. However, when A was set equal to 2.1 $yr^{-1}bar^{-3}$ the ice
sheet profile continued to shrink and at the end of 10000
years the maximum elevation had reduced by about 200 m. It
seems possible that in this case the ice may be flowing fast
enough to further reduce the ice sheet elevation until it is
completely under ablation, at which point the ice sheet
will melt away completely.

In the southern hemisphere the ice sheet grows from the
initial conditions for all the values of A that were tried.
When A is equal to .3 $yr^{-1}bar^{-3}$ and .6 $yr^{-1}bar^{-3}$ the ice
sheet is still growing rapidly, although at different rates,
at the end of 10000 years. However, when A is 2.1 $yr^{-1}bar^{-3}$
the ice sheet has just about reached its new equilibrium

profile with an ice elevation at the south pole of 2800 m compared to 4000 m when A was .15 $yr^{-1}bar^{-3}$.

These results indicate the large impact the value of A can have on size and possibly on the existence of the continental ice sheets, however, they do not point to a particularly "good" value to use. Since the value of A can not be determined in this model due to the lack of information about the temperature of the bulk of the ice, it must be chosen. The value used for most of the experiments described here, .15 $yr^{-1}bar^{-3}$, was chosen because of its similarity with values measured over Greenland and Antartica (Budd, 1969) and with values used in the majority of the modeling studies (Birchfield et.al., 1981; Mahaffy, 1976).

V. Applications of Models to Possible Variations in Climate
   Conditions on Ice Age Time Scales

The stated purpose of this thesis is to investigate the response of the sea ice and continental ice to some of the specified and parameterized variables external to the climate system, such as incident solar radiation, or external to the cryospheric system but part of the climate system, such as air temperature, and the bedrock depression time constant and sea level variations in the case of continental ice. In this chapter the response of the cryosphere to these variables which can vary over ice age time scales is examined and possible explanations are discussed.

A. Sea Ice

1. Insolation Variations

Milankovitch suggested in 1941 that variations in the distribution of solar radiation on the earth caused by changes in the earth's orbital geometry would cause large climatic variations. These climate variations should be reflected in the seasonal variation of sea ice and thus in teh energy exchange between the atmosphere and the ice/ocean surface. In order to examine the response of sea ice to such variations in the solar insolation experiments are performed in which the insolation regimes at -10k (a period of higher northern hemisphere summer insolation), -24k (a period of lower northern hemisphere summer insolation), and the

present are specifed. Figure 5.1 shows the response of the
seasonal cycle of sea ice at 72.5N and 67.5S to those
changes in insolation. The figure indicates that sea ice
thickness does not vary appreciably with variations in
insolation, though there is a slight difference in the
period of time ice free conditions exist. This variation in
the period of ice free ocean ranges from zero to one extra
week in the northern hemisphere, too two to three less weeks
in the southern hemisphere at -10k and -24k compared to the
present. In addition, in the northern hemisphere, the period
of ice free conditions is shifted to begin and end one week
earlier at -10k than at -24k and the present. These
variations, or lack of variations, are due to the way in
which the solar insolation changes from one regime to the
next.

The lack of variations in the sea ice thickness is due
to the fact that the period during which the maximum sea ice
thickness is determined is a time of low solar radiation.
Any insolation variations that occur during this period are
consequently very small so that solar radiation, and
therefore sea ice thickness, doesn't vary much during this
period.

The changes in the period of open ocean and the shift
in the period of ice free conditions for the -10k insolation
regime are a consequence of changes in the amplitude and
seasonal cycle of insolation between the different regimes.
At 72.5N the maximum incoming solar radiation at the sea ice
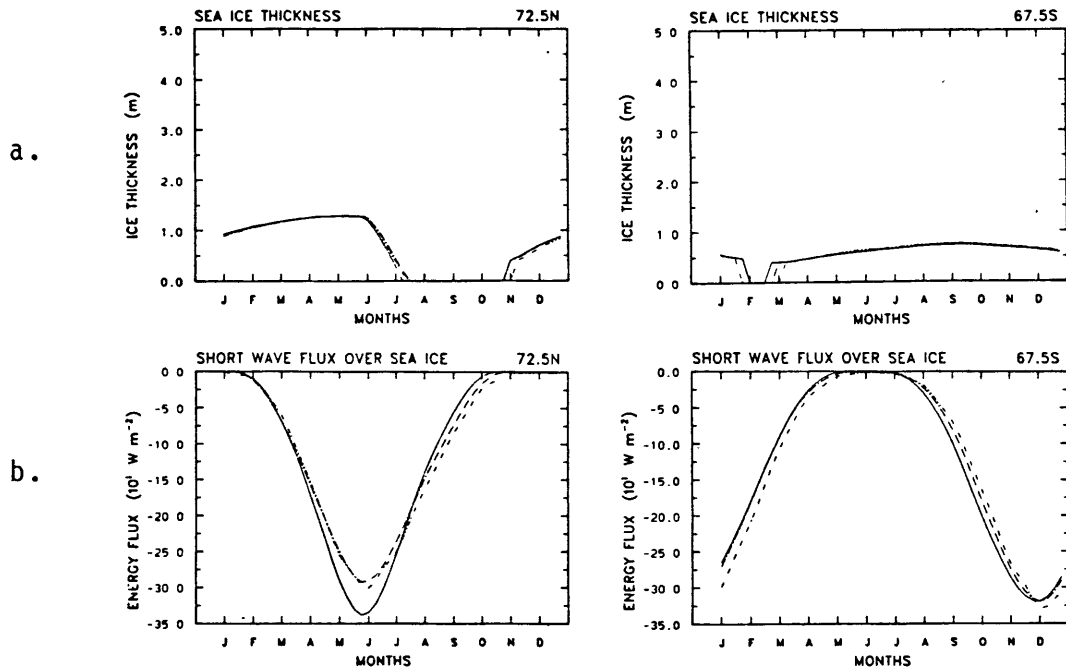
Figure 5.1. a) Seasonal cycle of sea ice thickness at 72.5N and 67.5S for insolation at -10k (solid line), -24k (single dot dashed line), and the present (double dot dashed line). b) Seasonal cycle of solar radiation available at the ice surface at the correspondings times.

surface is 339 W m^{-2} at -10k, at the present it is 301 W m^{-2}, and at -24k it is only 293 W m^{-2}. The higher maximum insolation at -10k has very little effect on the period of time open ocean conditions exist, ice free conditions exist for 15 time steps (about 4 months) at both -10k and at the present; however, the maximum at -10k comes about one week earlier and drops off rather quickly compared to the insolation at the present or at -24k. As a result the period of ice free conditions at 72.5N occurs earlier for the insolation regime at -10k than for the other regimes.

At 67.5S the difference between the three insolation regimes is not as great, with the maximum insolation over sea ice at -10k, -24k, and the present being 319 W m^{-2}, 320W m^{-2}, and 329 W m^{-2} respectively. The higher insolation at the present causes ice free conditions to exist for 6 time steps (about 1.5 months) while at -10k and -24k ice free conditions are reduced to 3 and 4 time steps respectively.

Table 5.1 Annual Mean Components of the Heat Balance Equation Weighted Over Ice and Ocean in W m^{-2} at 72.5N and 67.5S at -24k, -10k, and 0k.

Latitude	Time	F_{ir}	F_{sw}	F_{lh}	F_{sh}	F_{lw}	Net
72.5N	-10k	271	-39	1	-3	-228	1
	0k	272	-41	1	-3	-228	2
	-24k	270	-37	1	-3	-228	3
67.5S	-10k	276	-37	12	-12	-230	8
	0k	276	-41	13	-10	-230	8
	-24k	276	-37	12	-12	-230	9

Note: F_{sw} is the absorbed short wave flux. It will be indicated this way unless otherwise noted.

Insolation variations induced by orbital geometry changes seem to have a rather small effect on the seasonal cycle of sea ice. The only real changes occur in the period of time that the leads are expanded. The question is how much does this change affect the energy exchange with the atmosphere? Table 5.1 shows the annual average of the equilibrium seasonal cycle of each of the components of the heat balance equation and the net flux between the atmosphere and the ice/ocean surface at 72.5N and 67.5S. At 72.5N the table shows that the maximum annual average incoming solar radiation occurs for the present insolation regime rather than -10k for which the highest insolation values occur. This is due to the fact that the insolation in the -10k regime is lower than for the present for a period approximately from August through January, and that the period of open ocean is approximately the same for the two regimes. The outgoing long wave radiation shows the largest variations in response to the changes in insolation; however, these changes only partially offset the changes in solar radiation causing the annual net flux to vary between the different regimes and are 1 W m^{-2}, 2 W m^{-2}, and 3 W m^{-2} at -10k, the present, and -24k respectively.

The significance of these variations is difficult to evaluate; however, one measure might be to consider how much ice could be formed by such an energy loss. The volumetric heat of fusion of ice used here is 3.0139 x 10^8 J m^{-3}. Energy losses of 1 W m^{-2}, 2 W m^{-2}, and 3 W m^{-2} over the

period of a year would therefore correspond to ice of .1 m, .2 m, and .3 m thick, producing a variation of .2 m of ice between the different insolation regimes. This variation seems relatively small compared to the 1.25 m range in thickness that sea ice goes through in a year.

At 67.5S the variation in the annual net flux between the different insolation regimes is even smaller than in the northern hemisphere with values of 8 W m^{-2}, 8 W m^{-2}, and 9 W m^{-2} for the regimes at -10k, the present, and -24k. It may be surprising that the annual net flux at -10k and at the present are the same given that the present insolation regime has the highest mean annual short wave flux at 67.5S. However, the higher insolation regime results in a longer period of ice free conditions to which the turbulent fluxes as well as the outgoing long wave flux respond, offsetting the higher solar radiation.

Overall the variations in sea ice and the corresponding energy exchanges between the atmosphere and the ice/ocean surface caused by varying insolation alone seem small. In reality insolation variations affect sea ice both directly and indirectly through accompanying variations in air temperature. These indirect effects would be included if the sea ice model were coupled to a climate model; however, they have been ignored here. In the following section the response of the sea ice to possible changes in the mean and amplitude of the seasonal cycle of air temperature that may be induced by insolation variations are examined.

2. Air Temperature Variations

Variations in insolation will induce changes in the surface air temperature. The magnitude and seasonal distribution of the temperature changes will eventually be determined by a coupled climate model; however, here the possible changes will be estimated and specified in model experiments.

The results of Suarez and Held's (1979) climate model indicated that the change in northern hemispheric mean air temperatures varied between +1.5K and -1K from present conditions. Their model did not include an ice sheet, and thus the variations over the past 150k were out of phase with the geologic record by about 5k or 6k years. However, their results are indicative of what the air temperature variations might be.

The CLIMAP Project Members (1981) showed in their reconstructions of last glacial maximum that the largest variations in sea surface temperature occurred north of 30N, and that the largest change was as much as 14K in the North Atlantic during the summer. In general their results showed a drop in sea surface temperatures ranging from 2K to 10K with most of the larger changes occurring in the North Atlantic again during the summer. The decrease in sea surface temperature in the southern hemisphere was less dramatic ranging from 2K to 5K; while in the tropics and subtropics the variation ranged from a decrease to a rise of

4K.

These results indicate, assuming that a similar variation in mean air temperature would occur, that the 1K variation in mean hemispheric air temperature in the results of Suarez and Held (1979) is mostly due to high latitude variations that are of greater amplitude than the hemispheric mean, and that the change is mostly consentrated in the summer season in the northern hemisphere. Therefore, there are changes in the mean and amplitude of the seasonal cycle of air temperature. In the following sections the response of the sea ice at both 72.5N and 67.5S to variations in the air temperature that are of the order of magnitude that seem to have occurred between glacial and interglacial periods is examined.

a. Variation in the Mean of the Air Temperature

In order to examine the response of sea ice and the seasonal cycle of energy exchange between the atmosphere and ice/ocean surface to changes in mean air temperature possibly induced by insolation variations a series of experiments were performed in which the mean of the seasonal cycle of air temperature was varied over a range of +5K to -5K from the present. Figure 5.2 shows how the seasonal cycle of sea ice responds to such changes in air temperature at 72.5N and 67.5S. At 72.5N for present conditions the sea ice exhibits a maximum thickness of 1.28 m and a period of ice free conditions of 15 time steps (about 4 months).

Increasing the mean air temperature by 1K, 3K, and 5K has the effect of decreasing the maximum ice thickness to 1.22 m, 1.10 m, and .97 m respectively and increasing the period of ice free conditions to 18, 23, and 27 time steps (about 4.9, 6.3, and 7.3 months) respectively. Decreasing the mean air temperature by similar amounts increases the maximum ice thickness to 1.35 m, 1.47 m, and 2.54 m respectively and reduces the period of ice free conditions to 12, 0, and 0 time steps (about 3.3, 0, and 0 months) respectively.

The sea ice at 67.5S responds in a similar manner. The maximum sea ice thickness for present conditions is .76 m and there are 6 time steps (about 1.6 months) of ice free conditions. An increase in air temperature of 1K, 3K, and 5K reduces the maximum ice thickness to .72 m, .65 m, and .56 m respectively and increases the period of ice free conditions to 10, 17, and 21 time steps (about 2.7, 4.6, and 5.7 months) respectively. When the air temperature is decreased by 1K the maximum ice thickness remains nearly the same at .75 m, but the period of ice free conditions is eliminated. As the temperature is decreased further, 3K and 5K, the maximum ice thickness is increased to .86 and .96 m.

While changes in the sea ice thickness are important especially when ice is thin, changes in the period of ice free conditions have major consequences on the energy exchange between the atmosphere and the ice/ocean surface. As was discussed earlier sea ice can be very effective at
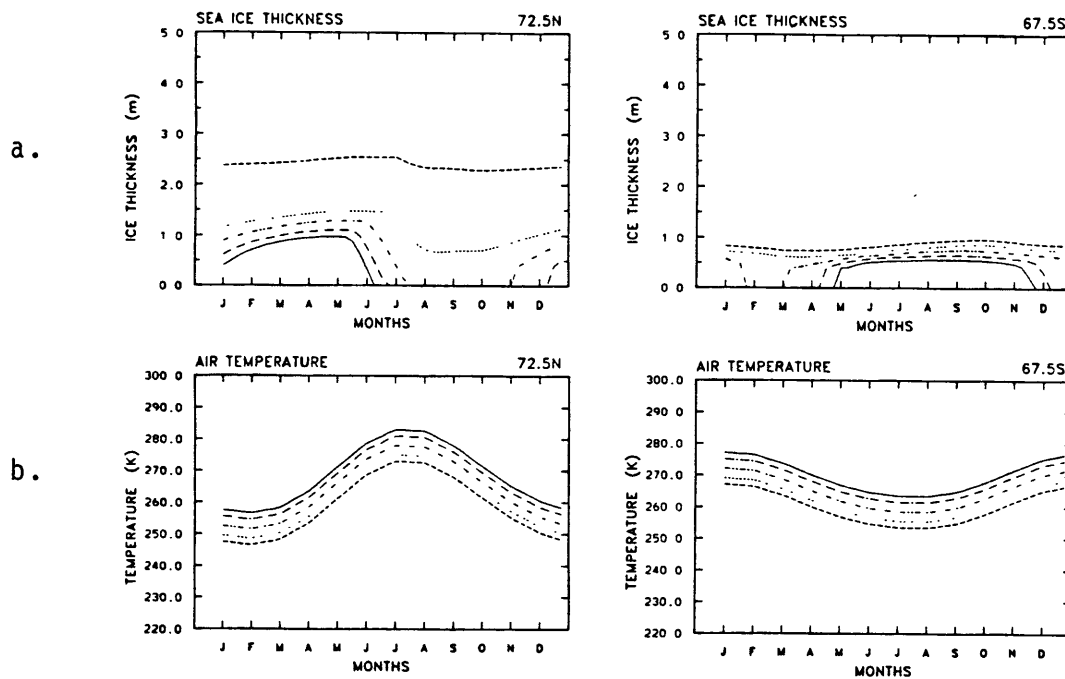
Figure 5.2 a) Seasonal cycle of sea ice thickness for
changes in the mean air temperature of +5K
(solid line), +3K (single dot dashed line), OK
(double dot dashed line), -3K (dotted line), and
-5K (dashed line). b) Seasonal cycle of air
temperature for the corresponding changes in its
mean.

Table 5.2.a Temperatures of Atmosphere, Ice, and Ocean
at the Atmosphere-Ice/Ocean Interface in
Early November at 72.5N

Change in Mean Air Temperature	0.0 K	-3.0 K
Air Temperature	260.2 K	257.2 K
Snow/Ice Interface Temperature	-	252.6 K
Ocean Temperature	271.4 K	271.2 K
Fraction of Open Water	1.00	.01

Table 5.2.b Energy Exchanges Between Atmosphere and
Ice/Ocean in Early November at 72.5N in W m^{-2}

Change in Mean Air Temperature	0 K		-3 K	
	ice	ocean	ice	ocean
Short Wave	-	-1.96	-2.53	-1.96
Albedo	-	.10	.84	.10
Latent Heat	-	8.53	-.81	9.32
Sensible Heat	-	16.61	-6.84	20.81
Long Wave from Surface	-	308.	231.	307.
Long Wave from Atmosphere	-208.	-208.	-196.	-196.
Sum of Fluxes weighted by fraction of open ocean	123.		26.	

insulating the ocean from the atmosphere. An example of this can be seen by comparing the energy exchanges between the ocean and atmosphere at 72.5N for the present temperature cycle and when the mean temperature is dropped 3K. Table 5.2 shows the individual fluxes at the ice-atmosphere and ocean-atmosphere interface in early November, when the ocean is still ice free for present conditions and completely ice covered for the decreased temperature conditions.

The net effect is that the presence of ice .9 m thick cuts the net flux from the ocean to the atmosphere by almost a factor of five, from 123 W m^{-2} to 26 W m^{-2}. When coupled to a climate model this would create a positive feedback

Table 5.3.a. Seasonal Cycle of Net Flux in W m^{-2}
Weighted Over Ice and Ocean at 72.5N for
Variations in Mean Air Temperature.

Month	+5K	+3K	+1K	0K	-1K	-3K	-5K
Jan	131	81	36	33	30	23	18
Feb	40	30	25	25	23	21	17
Mar	20	19	18	18	18	17	14
Apr	10	10	10	10	11	11	9
May	-8	1	2	3	2	4	3
Jun	-130	-78	-48	-35	-26	-11	-3
Jul	-221	-196	-154	-121	-86	-55	-27
Aug	-140	-130	-129	-126	-115	-44	-11
Sep	-31	-24	-24	-22	-23	0	7
Oct	62	66	65	66	64	26	15
Nov	117	119	116	117	85	27	18
Dec	141	142	83	56	40	26	19
Avg	-1	3	0	2	2	4	7
Range	362	338	271	243	199	82	45

Table 5.3.b Seasonal Cycle of Net Flux in W m^{-2}
Weighted Over Ice and Ocean at 67.5S for
Variations in Mean Air Temperature.

Month	+5K	+3K	+1K	0K	-1K	-3K	-5K
Jan	-154	-172	-123	-47	-18	-2	1
Feb	-37	-52	-67	-72	-23	2	4
Mar	92	80	69	61	19	9	11
Apr	173	165	90	33	17	16	17
May	145	71	31	28	22	21	22
Jun	29	25	25	25	24	23	24
Jul	19	20	21	22	23	23	24
Aug	16	18	20	21	23	23	24
Sep	13	15	17	18	20	21	22
Oct	6	9	12	13	15	16	18
Nov	-14	1	4	5	7	9	11
Dec	-183	-96	-15	-5	-1	1	5
Avg	9	7	7	8	11	14	15
Range	355	338	214	133	47	26	23

Note: Seasonal cycle is comprised of monthly averages.

which would cool the air further and in turn allow the formation of more ice. In addition the latent heat flux is dereased from an upward value on the order of 10 W m^{-2} to an upward flux on the order of 1 W m^{-2} effectively cutting off the moisture exchange.

While this effect seems large it is very short lived in that only the time steps during which the transition occurs are affected. Tables 5.3.a and 5.3.b show the seasonal cycle (monthly averages), the annual average and range of the net energy exchange between the atmosphere and the ice/ocean surface at 72.5N and 67.5S for changes in the mean annual air temperature of +5K, +3K, +1K, 0K, -1K, -3K, and -5K.

The table indicates that at 72.5N in October and November, the period covered by the result in Table 5.2, the the net energy flux to the atmosphere is decreased by 40 W m^{-2} and 90 W m^{-2} respectively for a reduction in mean air temperature of 3K from present conditions. However, the annual average net flux is actually increased from 2 W m^{-2} to 4 W m^{-2}, and when the mean air temperature is decreased by 5K the annual net flux is increased further to 7 W m^{-2}.

Table 5.4 shows the annual averaged components of the balance equation for each of the energy fluxes. This table indicates that the increase in the annual net flux is caused by a large decrease in absorbed solar radiation of 14 W m^{-2} between the case where air temperature is dropped by three degrees and the present, compared to a decrease of 8 W m^{-2} in the net long wave radiation (the term of major importance

Table 5.4 Annual Mean Components of the Heat Balance
         Equation Weighted Over Ice and Ocean in W m^{-2}
         at 72.5N and 67.5S for Variations in the
         Annual Mean Air Temperature

Latitude	T	F_{ir}	F_{sw}	F_{lh}	F_{sh}	F_{lw}	Net
72.5N	+5K	300	-52	2	0	-252	-1
	+3K	291	-48	2	0	-242	3
	+1K	277	-44	1	-2	-232	0
	0K	272	-41	1	-3	-228	2
	-1K	265	-37	1	-4	-223	2
	-3K	251	-27	0	-6	-215	4
	-5K	242	-23	0	-7	-206	7
67.5S	+5K	301	-64	26	1	-254	9
	+3K	291	-57	21	-3	-244	7
	+1K	281	-48	16	-7	-235	7
	0K	276	-41	13	-10	-230	8
	-1K	271	-31	10	-14	-225	11
	-3K	263	-26	8	-15	-217	14
	-5K	255	-24	7	-14	-208	15

in Table 5.2). Both of these fluxes decrease with reduced
mean air temperature. The absorbed solar radiation decreases
because as the period of open ocean decreases the albedo
over the year increases thus decreasing the percentage of
the incident solar radiation that is absorbed. The net long
wave radiation decreases because as ice becomes dominant in
the zone over the year the surface temperature drops thus
decreasing the outgoing infrared radiation. Over the year
the outgoing infrared radiation is larger than the incoming
long wave radiation from the atmosphere so the net long wave
radiation is reduced. However, the reduction in absorbed
solar radiation is dominant so the annual net flux toward
the atmosphere increases as the mean air temperature

decreases.

The same situation occurs in the southern hemisphere at 67.5S. Table 5.3.b shows that as mean air temperature is reduced 3K the net flux toward the atmosphere in March and April, the transition period between ice free to ice covered conditions as the mean air temperature is dropped, decreases by 52 W m^{-2} and 17 W m^{-2} respectively, while the mean annual net flux increases from 8 W m^{-2} to 14 W m^{-2}. Table TAB4 shows again that this result is due mainly to a decrease in absorbed solar radiation of 15 W m^{-2} which is partially offset by the decrease in the upward turbulent flux of 10 W m^{-2}.

When the mean air temperature is initially raised (1K increase in temperature) the response of the annual net flux is to decrease from 2 W m^{-2} to 0 W m^{-2} at 72.5N and from 8 W m^{-2} to 7 W m^{-2} at 67.5S. This decrease in the upward flux is due to an increase in the amount of absorbed solar radiation resulting from an increase in the period of ice free conditions.

When the temperature is raised further, by 3K and 5K, the rate of increase in the amount of absorbed solar radiation slows because the periods of ice free conditions extend into times of low values of solar radiation. Therefore, the large change in surface albedo from ice covered to ice free conditions gives a relatively small additional effect. This can be seen in Table TAB4 which indicates that for a rise in mean air temperature of 3K the

absorbed short wave energy is increased 7 W m^{-2} and 16 W m^{-2} at 72.5N and 67.5S respectively, and for a rise of 5K the absorbed short wave energy is increased an additional 4 W m^{-2} and 7 W m^{-2} respectively.

The decreasing influence of the changing absorbed solar radiation as mean air temperature rises combined with the increases in the net long wave flux and upward turbulent fluxes (Table 5.4) causes the annual net upward flux to increase at both 72.5N and 67.5S. The exception to this is at 72.5N when the air temperature is raised 5K. Table 5.3.a shows that the decrease in the annual net flux in this experiment is caused by large differences in the net flux in May, August, and September compared to those fluxes in the experiment in which the air temperature is increased only 3K.

The decrease in the net upward flux in May is caused by the constraint that the temperature of the ice surface can not exceed the freezing point. In May when the temperature is increased 3K both the air and surface temperatures are rising maintaining a relatively constant gradient; however, when the temperature is increased 5K the surface temperature attains the freezing point while the air temperature continues to rise, increasing the temperature gradient and thus the flux toward the surface (ie. decreasing the upward flux).

The increased downward flux in August and September, a period of ice free conditions, from the case of a 3K to 5K

rise in air temperature is due to a decrease in the upward net long wave flux. The 2K rise in air temperature from +3K to +5K is translated into only a 1K to 1.5K rise in ocean temperature. Air temperature during this period is higher than ocean temperature so the temperature gradient is increased downward and the net upward longwave flux is reduced from 9 W m^{-2} to 1 W m^{-2} and from 39 W m^{-2} to 32 W m^{-2} in August and September respectively. This effect occurs in the other temperature experiments; however, it is generally overshadowed by the larger variations in the absorbed solar radiation.

Varying the mean of the seasonal cycle of air temperature also affects the range of the seasonal cycle of the net flux between the atmosphere and ice/ocean surface (see Tables 5.3.a and 5.3.b). At 72.5N increasing the mean air temperature 5K increases the seasonal range of the net flux from 243 W m^{-2} to 362 W m^{-2} or by approximately 50%. A comparable decrease in the mean air temperature has the affect of reducing the seasonal range of the net flux to 45 W m^{-2} or to about 20% of the present range. At 67.5S the variation in the seasonal range in the net flux is similar ranging from 355 W m^{-2} to 23 W m^{-2} with the present range being 133 W m^{-2}.

It seems clear that the increased period of ice covered conditions has a major damping effect on the amplitude of the seasonal cycle of the net flux between the atmosphere and ice/ocean surface. Table 5.5 gives the ranges of the

individual fluxes in each of the experiments at 72.5N and 67.5S, and indicates that in general the ranges of all the component fluxes decrease with decreasing mean air temperature. However, the term for which the range changes the most is the absorbed short wave flux, 137 W m^{-2} and 160 W m^{-2} at 72.5N and 67.5S respectively. This again is due to the large change in albedo and therefore absorption of short wave radiation as sea ice becomes more continuous through the year.

Table 5.5 Range of the Components of the Seasonal Cycle of the Heat Balance Equation Weighted Over Ice and Ocean for Variations in the Amplitude of the Seasonal Cycle of Air Temperature at 72.5N and 67.5S in W m^{-2}

Latitude	T	F_{ir}	F_{sw}	F_{lh}	F_{sh}	F_{lw}	Net
72.5N	+5K	113	210	21	40	150	362
	+3K	116	196	19	41	143	338
	+1K	115	188	15	33	137	271
	0K	115	168	14	31	134	243
	-1K	113	137	12	26	131	199
	-3K	113	79	5	13	125	82
	-5K	121	74	6	15	120	45
67.5S	+5K	74	224	74	103	77	355
	+3K	71	223	65	99	73	338
	+1K	67	207	57	93	70	214
	0K	64	158	49	76	68	133
	-1K	63	89	22	32	67	47
	-3K	63	67	15	29	64	26
	-5K	61	64	13	30	61	23

The decrease in the range of turbulent fluxes, latent and sensible heat, is striking despite the fact that it is an order of magnitude smaller than that of the short wave flux. The range of the latent heat flux drops from 21 W m^{-2}

to 6 W m^{-2} and from 74 W m^{-2} to 13 W m^{-2}, and the range of the sensible heat flux drops from 40 W m^{-2} to 15 W m^{-2} and 103 W m^{-2} to 30 W m^{-2} at 72.5N and 67.5S respectively for a change in the mean air temperature from +5K to -5K. The implication this may have on climate could be quite important in that the changes in the turbulent fluxes, especially latent heat, implies changes in the availability of moisture for precipitation and thus snowfall on land areas.

The reason for the dramatic change in the range of the seasonal cycle of the turbulent fluxes is the change in the period of open ocean conditions. When mean air temperature is dropped 5K the ocean essentially becomes ice covered year round with leads remaining at the minimum of the total area except for a couple of months during the summer when they increase to 4% at 72.5N. Under these conditions the ice surface is colder than the air with the possible exception during the summer months when slight melting occurs. As a result the sensible heat flux averaged over the year is directed toward the surface with a magnitude of 7 W m^{-2} and a range of only 15 W m^{-2}.

The cold temperatures significantly reduce the specific humidity in the air and in the air at the ice surface so the latent heat flux is also small averaging 0 W m^{-2} over the year with a range of 6 W m^{-2}.

When the mean air temperature is increased the area of the leads and the period they remain open increases. This

exposes a warm moisture source to the atmosphere. The
temperature gradient between the air and the surface is
therefore reduced, decreasing the sensible heat flux to the
surface and possibly reversing its direction. However, the
warm water now produces a large gradient in the specific
humidity between the air and the air at the surface causing
the mean annual latent heat flux to increase. The range of
the seasonal cycle also increases because there is more
contrast in the extent of exposure of the warm ocean between
the winter and summer months. It seems probable that if air
temperature were increased to the point where no ice would
exist the latent heat flux over the year would remain high,
but the seasonal range would stabilize or decrease due to
the lack of seasonal contrast in ocean exposure.

b. Variation in the Amplitude of the Air Temperature

In addition to changes in the mean annual air
temperature, insolation variations also seem to cause
changes in the amplitude of the seasonal cycle. In order to
examine the extent to which sea ice responds to such a
change a series of experiments were performed in which the
amplitude of the seasonal cycle of air temperature was
varied. Figure 5.3 shows the response of sea ice thickness
at 72.5N and 67.5S when that amplitude is reduced and
increased by 20% and 30%. In general it seems that the
maximum thickness of ice is affected to a small extent by
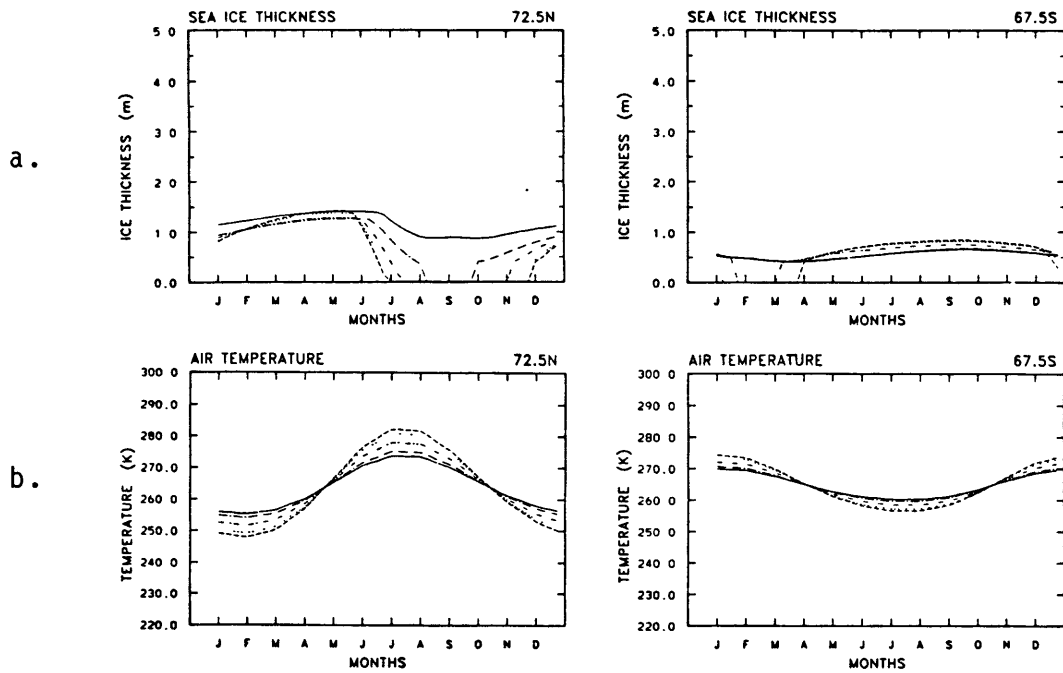varying the amplitude; however, the period of ice free

Figure 5.3 a) Seasonal cycle of sea ice thickness for
changes in the amplitude of the seasonal cycle
of air temperature of -30% (solid line), -20%
(single dot dashed line), 0% (double dot dashed
line), +20% (dotted line), and +30% (dashed
line). b) Seasonal cycle of air temperature for
the corresponding changes in its amplitude.

conditions changes dramatically.

At 72.5N the maximum ice thickness ranges from 1.27 m
and 1.28 m when the amplitude is decreased 20% and 0% to
1.41 m and 1.42 m when the amplitude is decreased and
increased 30%. This seemingly odd sequence of maximum ice
thickness can be explained by looking at how the variation
in amplitude of temperature affects how close the maximum
air temperature is to the freezing point. When the amplitude
is reduced by 30% the air temperature in the summer exceeds
the freezing point by only about 2.5K. As a result there is
little surface melt and leads only partially open during the
summer leaving a relatively large amount of sea ice on which
to build as temperatures drop with the approach of winter.
This results in larger maximum sea ice thickness. When the
amplitude is increased by 30% the situation is the same as
the lower amplitude cases when new ice is formed at the end
of the summer; however, the extremely low winter
temperatures enhances the sea ice growth rate compared to
the present amplitude case causing thicker ice to be formed
by the end of the winter. This thick ice melts away through
the expansion of leads in the summer which is due to the
extremely high summer temperatures.

At 67.5S the high maximum ice thickness only occurs
when the amplitude of the seasonal cycle of air temperature
is increased and ranges from .66 m and .67 m when the
amplitude is decreased 30% and 20% to .85 m when it is
increased 30%. The maximum ice thickness remains low once

year round ice coverage is attained because relatively warm
winter temperatures surpress ice growth and high values of
vertical oceanic heat flux, 12 W m^{-2}, promote further melt.
The ice layer is not completely melted away by this process
because snow at the surface, which does not melt away
because it never reaches the melting point, is converted
into "white ice". "White ice" is formed from snow at the sea
ice surface which is depressed below sea level and then
infiltrated with sea water which freezes and becomes part of
the ice layer (see chapter II.C.2.e).

These changes in sea ice thickness are very small
compared to the effect that changing the amplitude of the
seasonal cycle of air temperature has on the period of open
ocean. The period of open ocean varies from 0 to 20 time
steps (about 0 to 5.4 months) and from 0 to 12 time steps
(about 0 to 3.3 months) at 72.5N and 67.5S respectively for
a decrease to an increase of 30% in the amplitude of air
temperature.

The impact these changes have on the net energy flux
between the atmosphere and the ice/ocean surface is similar
to that when the annual mean air temperature was varied (see
Table 5.6). As the period of time ice free conditions exist
decreases the amount of absorbed solar radiation decreases
dramatically, from 45 W m^{-2} to 26 W m^{-2} and 49 W m^{-2} to 30 W
m^{-2} at 72.5N and 67.5S respectively. This drop in absorbed
solar radiation is most strongly reflected in the annual net
budget when conditions change from short periods of

Table 5.6 Annual Mean Components of the Heat Balance Equation Weighted Over Ice and Ocean in W m^{-2} for Variations in the Amplitude of the Seasonal Cycle of Air Temperature at 72.5N and 67.5S

Latitude	T amp	F_{ir}	F_{sw}	F_{lh}	F_{sh}	F_{lw}	Net
72.5N	-30%	260	-26	0	-7	-225	2
	-20%	265	-34	0	-5	-226	1
	-10%	269	-38	1	-4	-227	1
	0%	272	-41	1	-3	-22ዩ	2
	+10%	275	-42	1	-2	-229	3
	+20%	278	-44	1	-1	-230	5
	+30%	280	-45	1	0	-231	5
67.5S	-30%	275	-30	10	-15	-229	11
	-20%	275	-33	11	-14	-230	10
	-10%	275	-37	12	-12	-230	9
	0%	276	-41	13	-10	-230	8
	+10%	277	-44	14	-9	-230	8
	+20%	277	-47	15	-7	-231	9
	+30%	278	-49	17	-4	-231	11

completely open ocean to moderate or slight expansion of the lead area during the summer.

At 72.5N the number of time steps of ice free conditions drops from 7 to 0 as the reduction in the amplitude of temperature is increased from 20% to 30%. The effect on the absorbed short wave radiation is to reduce it by 8 W m^{-2}. This is partially offset by a reduction in the net upward long wave radiative flux and an increase in the downward turbulent fluxes, but the annual net upward flux increases from 1 W m^{-2} to 2 W m^{-2}.

At 67.5S the transition between a short period of ice free conditions to moderate expansion of the leads in the summer occurs when the amplitude of the air temperature is decreased only 10%. The absorbed solar radiation is reduced

by 4 W m^{-2} in this case and when the amplitude is reduced by 20% and 30% the absorbed solar radiation is reduced an additional 4 W m^{-2} and 3 W m^{-2} respectively (a total of 8 W m^{-2} and 11 W m^{-2} for the 20% and 30% reductions in the amplitude). Again these are partially offset by decreases in the net upward longwave flux and increases in the downward turbulent flux, but the annual net upward flux increases from 8 W m^{-2} to 9W m^{-2}, 10 W m^{-2}, and 11 W m^{-2} for a 10%, 20%, and 30% reduction in the amplitude of the seasonal cycle of air temperature.

When the amplitude of the seasonal cycle of air temperature and thus the period of open ocean is increased the net flux to the atmosphere also increases. At 72.5N all of the fluxes seem to adjust to the new forcing. When the amplitude is increased 30% the net long wave radiative flux increases 5 W m^{-2}, the incoming short wave flux increases 4 W m^{-2}, and the turbulent fluxes increase from a downward flux of 2 W m^{-2} to an upward flux of 1 W m^{-2} for a total of 3 W m^{-2}. The net effect is an increase of 3 W m^{-2} from 2 W m^{-2} to 5 W m^{-2} in the net upward energy flux. In essence the changes in the radiative fluxes offset each other and the increase in the upward turbulent fluxes, produced by longer exposures of the warm ocean to the atmosphere, cause this increase in the annual net energy flux from the ocean to the atmosphere.

At 67.5S the role played by the turbulent fluxes in increasing the annual net upward energy flux when the

amplitude of the seasonal cycle of air temperature is
increased is even more evident. The net long wave flux is
increased 1 W m^{-2} and the absorbed short wave flux is
increased 8 W m^{-2} for a 30% increase in the amplitude. If
these were the only components of the energy budget the
annual upward flux would be decreased by 7 W m^{-2}; however,
this flux is increased about 2 W m^{-2}. The large increase in
the upward flux is due to the change in the turbulent
fluxes. Latent heat flux is increased from 13 W m^{-2} to 17 W
m^{-2} and the sensible heat flux is decreased from a downward
flux of 10 W m^{-2} to a downward flux of 4 W m^{-2} for a total
gain of 10 W m^{-2}. This change in the turbulent fluxes is due
to two factors. First, as in the northern hemisphere, the
increased exposure of the warm ocean to the atmosphere
decreases the downward temperature gradient and increases
the upward moisture gradient which forces the turbulent
fluxes. Second, the high wind speeds in the southern
hemisphere enhance the effect of the gradient changes
increasing the upward turbulent exchange.

In addition to the changes in the annual net energy
flux between the atmosphere and ocean there are large
changes in the amplitude of the seasonal cycle of these
fluxes when the amplitude of the seasonal cycle of air
temperature is varied (see Table 5.7). At 72.5N a variation
in the amplitude of the seasonal cycle of air temperature
from -30% to +30% changes the range of the seasonal cycle of
energy exchange between the atmosphere and ice/ocean surface

from 70 W m^{-2} to 400 W m^{-2}. At 67.5S a similar change in the temperature cycle produces a change in the range of the net flux between the atmosphere and ice/ocean surface from 39 W m^{-2} to 452 W m^{-2}.

Table 5.7 Range of the Components of the Seasonal Cycle of the Heat Balance Equation Weighted Over Ice and Ocean for Variations in the Amplitude of the Seasonal Cycle of Air Temperature at 72.5N and 67.5S in W m^{-2} +

Latitude	T amp	T_a	F_{ir}	F_{sw}	F_{lh}	F_{sh}	F_{lw}	Net
72.5N	-30%	18.4	95	75	5	15	97	70
	-20%	21.1	99	106	6	19	109	153
	-10%	23.7	107	137	11	25	121	243
	0K	26.4	115	168	14	31	134	243
	+10%	29.0	121	172	17	36	146	334
	+20%	31.6	127	188	18	40	159	375
	+30%	34.2	132	187	21	47	172	400
67.5S	-30%	9.6	49	83	19	31	49	39
	-20%	10.9	54	99	25	39	56	53
	-10%	12.3	59	123	32	49	62	97
	0K	13.6	64	158	49	76	68	133
	+10%	14.9	69	174	55	89	75	288
	+20%	16.4	75	189	61	102	82	364
	+30%	17.7	80	207	73	119	88	452

+ T_a in this table is the range of the seasonal cycle of air temperature in K.

It seems clear, as in the case where the mean air temperature was varied, that ice coverage has a major damping affect on the seasonal range of all of the components of the heat budget with the absorbed solar radiation being the most affected. However, the varying amplitude of the seasonal cycle of air temperature affects the variability of all the terms in the energy balance.

An example of the extent to which a variation in the

net flux between the atmosphere and ice/ocean surface can be changed by varying the amplitude of the cycle of air temperature can be seen by comparing the cases where mean air temperature is dropped 1K and where the amplitude of the seasonal cycle of air temperature is decreased 30% at 67.5S. In both of these cases the largest extent the leads attain is 38% and the annual average net flux to the atmosphere is approximately 11 W m^{-2}. However, when the mean air temperature is decreased the seasonal range of the net flux is 47 W m^{-2} compared to 39 W m^{-2} when the amplitude of the seasonal cycle of air temperature is decreased 30%. Therefore, in this case a 30% decrease in amplitude of the seasonal cycle of air temperature produced approximately a 17% decrease in the seasonal variability in the net flux from a case in which sea ice extent and mean annual net flux were similar.

c. Variation in the Mean and Amplitude of Air Temperature

In the preceeding two sections experiments in which either the mean or the amplitude of the seasonal cycle of air temperature was varied. However, in the process of climatic change these features of air temperature would vary simultaneously. In this section experiments in which the mean and amplitude of the seasonal cycle of air temperature are varied together are described.

Figure 5.4 shows the response of the seasonal cycle of sea ice thickness for a combination of changing the
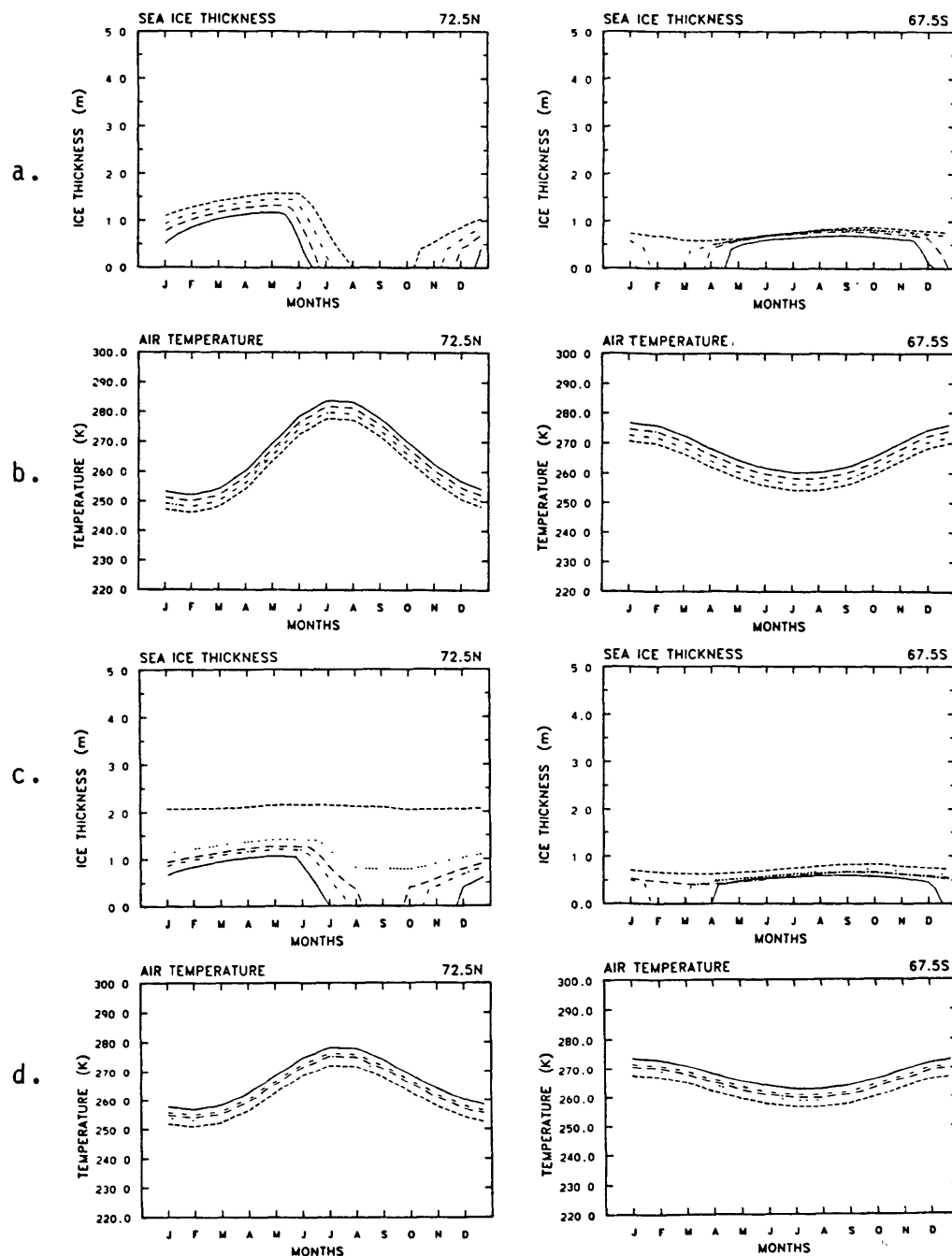
Figure 5.4 a) Seasonal cycle of sea ice thickness for a 20%
increase in the amplitude of the seasonal cycle of air
temperature and a change in the mean of +3K (solid
line), +1K (single dot dashed line), 0K (double dot
dashed line), -1K (dotted line), and -3K (dashed line).
b) Seasonal cycle of air temperature corresponding to
changes in a. c) Same as for a with a 20% decrease in
the amplitude of air temperature. d) Seasonal cycle of
air temperature corresponding to changes in c.

Table 5.8 Maximum Ice Thickness in m and Period of Ice
Free Conditions for Variations in the Mean and
Amplitude of the Seasonal Cycle of Air Temperature

Latitude	T amp	T	Max Ice Thickness	Ice Free TS
72.5N	-20%	+3K	1.06	20
	-20%	+1K	1.20	12
	-20%	0K	1.27	7
	-20%	-1K	1.41	0
	-20%	-3K	2.15	0
	0%	+3K	1.10	23
	0%	+1K	1.22	18
	0%	0K	1.28	15
	0%	-1K	1.35	12
	0%	-3K	1.47	0
	+20%	+3K	1.16	25
	+20%	+1K	1.31	21
	+20%	0K	1.37	19
	+20%	-1K	1.44	17
	+20%	-3K	1.57	10
67.5S	-20%	+3K	.60	15
	-20%	+1K	.67	6
	-20%	0K	.67	0
	-20%	-1K	.73	0
	-20%	-3K	.83	0
	0%	+3K	.65	17
	0%	+1K	.73	10
	0%	0K	.76	6
	0%	-1K	.75	0
	0%	-3K	.86	0
	+20%	+3K	.70	18
	+20%	+1K	.79	13
	+20%	0K	.82	10
	+20%	-1K	.84	6
	+20%	-3K	.88	0

amplitude of the seasonal cycle of air temperature plus and minus 20% and changing the mean air temperature plus and minus 1K and 3K. The results at both 72.5N and 67.5S are a hybrid of those when the air temperature mean and the amplitude of its seasonal cycle are varied individually. The way in which these two effects combined can be seen in Table 5.8 where the maximum ice thickness and the period of ice free conditions is given for each of these experiments.

When the amplitude of the seasonal cycle of air temperature is increased 20% at 72.5N the maximum ice thickness increases from 1.28 m to 1.37 m and the period of ice free ocean increases from 15 to 19 time steps (from about 4.1 to 5.2 months). If the mean air temperature is then raised 1K and 3K the maximum ice thickness decreases from 1.37 m to 1.31 m and 1.16 m and the period of ice free conditions increases to 21 and 25 time steps (about 5.7 and 6.8 months) respectively. The increase in maximum ice thickness when the amplitude of the seasonal cycle of air temperature is increased is caused by an increase in the ice growth rate due to the winter temperatures which are lower by a maximum of 2.6K than in the base case. The increase in the mean air temperature of 1K begins to compensate for the lower winter temperatures and the increase in the mean by 3K over compensates for it decreasing the maximum ice thickness below that of the base case. The period of ice free conditions is increased by both changes in the air temperature. The increase in the amplitude of the seasonal

cycle of air temperatures causes a maximum increase of 2.6K in the summer air temperatures which increases the period of ice free conditions. A rise in the mean air temperature adds to this effect.

If the mean air temperature is reduced 1K and 3K once the amplitude has been increased the maximum ice thickness increases from 1.37 m to 1.44 m and 1.57 m and the period of ice free conditions drops from 19 to 17 and 10 time steps (from about 5.2 to 4.6 and 2.7 months) respectively. Both of these effects are due to the increase in the period of time the air temperatures are below the freezing point.

When the amplitude of the seasonal cycle of air temperature is decreased 20% at 72.5N the maximum ice thickness decreases only .01 m from 1.28 m to 1.27 m, but the period of ice free conditions drops from 15 to 7 time steps (from about 4.1 to 1.9 months). As was discussed earlier, changes in the amplitude of the seasonal cycle of air temperature affect ice thickness to a very limited extent but greatly affect the period of ice free conditions. In this case the period of ice free ocean is cut in half because the maximum summer air temperature is decreased 2.6K, thus decreasing the period of time the air temperature is above the freezing point.

If the mean air temperature is raised 1K and 3K after first decreasing the amplitude of the air temperature the maximum ice thickness decreases more dramatically from 1.27 m to 1.20 m and 1.06 m and the period of ice free conditions

increases from 7 to 12 and 20 time steps (from about 1.9 to 3.3 and 5.4 months) respectively.

When the mean air temperature is decreased 1K and 3K the maximum ice thickness increases from 1.27 m to 1.41 m and 2.15 m respectively, and the period of ice free conditions is eliminated. The combined effect of decreasing the amplitude and the mean temperature 1K and 3K is to decrease the summer air temperatures to the point where they barely exceed the freezing point, in the case of a 1K decrease, or they don't reach the freezing point at all, in the case of a 3K decrease. This strongly reduces summer melt and thus eliminates the period of ice free conditions. Once this occurs, further decreases in air temperature cause the sea ice to grow thicker and increase the maximum ice thickness.

In the southern hemisphere at 67.5S the situation is somewhat different because, for the base case, the period of ice free conditions is much shorter and the amplitude of the seasonal cycle is about half that at 72.5N. This causes the summer air temperature to exceed the freezing point in only about half the experiments and then at most by 4.6K compared to 11.4K at 72.5N. Despite these differences the response of the maximum sea ice thickness to combined variations in the mean and amplitude of the seasonal cycle of air temperature is similar to, although smaller than, in the northern hemisphere. When the amplitude is increased 20% the ice thickness increases from .76 m to .82 m and the period of

ice free conditions increases from 6 to 10 time steps (from about 1.6 to 2.7 months). When the temperature mean is then raised 1K and 3K the maximum ice thickness decreases to .79 m and .70 m and the period of ice free conditions increases to 13 and 18 time steps (about 3.5 and 4.9 months) respectively. When the mean air temperature is dropped 1K and 3K the maximum ice thickness increases to .84 m and .88 m respectively while the period of open ocean drops to 6 and 0 time steps (about 1.6 and 0 months) respectively.

When the amplitude of the seasonal cycle of air temperature is decreased 20% at 67.5S the maximum ice thickness decreases from .76 m to .67 m and the period of ice free conditions drops from 6 to 0 time steps. The decrease in the ice thickness is caused by a reduction in the ice growth due to warmer winter temperatures. This is not compensated for by a decrease in summer ice melt as at 72.5N because there is little melt for either the base case or the reduced amplitude case since the maximum air temperature is so low; therefore, maximum ice thickness decreases.

If the mean air temperature is then raised 1K the maximum ice thickness does not change, but the period of open ocean increases from 0 to 6 time steps (from about 0 to 1.6 months). If the mean air temperature is raised further to 3K over the base case the maximum ice thickness decreases to .60 m and the period of ice free conditions increases to 15 time steps (about 4.1 months). When the mean air

temperature is reduced by 1K and 3K after the amplitude has been reduced the ocean remains ice covered and the ice thickness increases from .67 m to .73 m and .83 m respectively.

Overall the effects of changing the mean and amplitude of the seasonal cycle of air temperature on the sea ice thickness and the period of ice free ocean seems additive if periods of ice free conditions exist. The results indicate that the maximum ice thickness is more strongly controlled by the variations in the mean of the air temperature; however, that is because amplitude variations do not have a large effect in that aspect of sea ice. In cases where the amplitude does effect ice thickness the magnitude of the effect is modified by changes caused by variations in the mean air temperature. The period of ice free conditions seem to be equally modified by variations in the mean and amplitude of air temperature.

When periods of ice free conditions are eliminated the situation becomes somewhat different. If the transition is from ice free to ice covered conditions, the tendency is for the energy deficit that would have gone into freezing over the leads further to be used to form ice that is thicker than would be predicted if the changes caused by the individual variations in air temperature were simply added.

When starting from ice covered conditions the variations in the maximum ice thickness can be approximated by adding the variations resulting from changing the mean

and amplitude of the seasonal cycle of air temperature
individually. However, the period of ice free ocean can not
be approximated in the same way. This may be due to the fact
that the freezing point provides a threshold which may not
be reached by the individual changes in air temperature, but
is exceeded when these temperature variations are combined.
In cases where mean air temperatures are raised the period
of ice free conditions tends to follow that of the mean air
temperature change modified slightly by the change caused by
the variation in amplitude, but it is not an additive
modification. When mean air temperatures are dropped the
tendency is to reduce the ice free period or to go to
completely ice covered conditions.

Changes in the sea ice thickness and the period of open
ocean resulting from variations in the mean and amplitude of
the seasonal cycle of air temperature also cause variations
in the annual net flux between the atmosphere and the
ice/ocean surface. Table 5.9 shows the annual net flux for
each of the experiments in which the mean and amplitude of
the seasonal cycle of air temperature is varied.

Overall the variation in the net flux for the double
variations in air temperature have the same sense as for the
individual variations in air temperature. When temperature
is raised by 1K after either an increase or decrease in the
amplitude of the seasonal cycle of air temperature at 72.5N
the net upward flux drops due to the increase in the
absorbed solar radiation at the surface. When the mean air

Table 5.9 Annual Mean Net Flux Between the Atmosphere
         and Ice/Ocean Surface at 72.5N and 67.5S in W m^{-2}
         for Variations in the Mean and Amplitude of the
         Seasonal Cycle of Air Temperature

Latitude	T	-20%	0%	+20%
72.5N	+3K	2	3	4
	+1K	0	0	1
	0K	1	2	5
	-1K	3	2	5
	-3K	4	4	3
67.5S	+3K	6	7	11
	+1K	8	7	7
	0K	10	8	9
	-1K	12	11	9
	-3K	14	14	13

temperature is increased further the increase in the
absorbed solar radiation is more than compensated for by an
increase in the upward net long wave radiative flux and the
turbulent fluxes. The increases in these fluxes are the
result of the greater exposure of the warm ocean to the
atmosphere. The same situation occurs at 67.5S when the
amplitude of the air temperature is increased 20%; however,
when the amplitude is decreased 20% the increase in the
absorbed solar radiation still dominates when the mean air
temperature is raised 3K so the net flux continues to
decrease.

The initial response at both latitudes when the mean
air temperature is dropped is to increase the net upward
flux. This is due to a decrease in absorbed solar radiation
which results from the higher albedo of more extensive ice
cover. As the air temperature is reduced further the net

flux continues to increase in the cases where the amplitude
of the cycle of temperature is either unchanged, or reduced
20% at both latitudes, or increased 20% at 67.5S. When the
amplitude is increased at 72.5N the net flux drops when the
mean air temperature is decreased 3K. In this case the
increase in the period of ice coverage from 17 to 10 time
steps causes a decrease in the net upward long wave flux and
an increase in the downward turbulent fluxes which overcome
the decrease in the absorbed short wave flux, and therefore,
the net flux decreases. There are two possible reasons that
this does not occur in the other cases. In some cases
completely ice covered conditions had been attained for a
smaller drop in air temperature. Decreasing the air
temperature further affects the long wave and turbulent
fluxes to a small extent; however, the large change
associated with a transition from ice free to ice covered
conditions has already occurred. In other cases, where the
transition from ice free to ice covered conditions occurs
for a drop in mean air temperature of 3K, the change in the
absorbed short wave radiation is so great that accompanying
variations in the long wave radiation and the turbulent
exchanges are not large enough to compensate for it.

d. Implications of Air Temperature Variations on Climate

The results presented in the above sections show that
sea ice thickness and the accompanying energy exchange
between the atmosphere and ice/ocean surface are much more

responsive to variations in air temperature than to
insolation variations. This does not mean that insolation
variations do not affect sea ice, but that alone they are
not large enough to have a significant effect . In reality,
insolation variations would have a more direct affect on air
temperature, and possibly on other atmospheric variables,
and through them affect sea ice thickness and the energy
exchange between the atmosphere and ocean.

The experiments described above examined the response
of sea ice to possible variations in air temperature that
may be caused by insolation variations. The results indicate
that variations in ice thickness and the period of ice free
conditions change in an approximately linear way with
variations in the mean air temperature and the amplitude of
its seasonal cycle. However, the variation in both the
seasonal cycle and the annual net flux between the
atmosphere and the ice/ocean surface is not simply related
to the air temperature variations. The major cause for the
complex behavior of the net flux is the change in the
absorbed solar radiation which is caused by the change in
the albedo of the surface with the transition between ice
covered and ice free conditions. This large change is
partially compensated for by variations in the net long wave
radiation and the turbulent fluxes when the period of ice
free conditions is short and the transitions occur during
the period of high incident solar radiation. However, once
the period of ice free conditions extends into times of low

incident solar radiation, or ice covered conditions prevail, the variations in the longwave and turbulent fluxes begin to dominate the changes in the net flux between the atmosphere and ice/ocean surface with changes in air temperature.

A point that should be noted is that at both 72.5N and 67.5S the net flux toward the atmosphere in general increases from the base case for both positive and negative variations in air temperature. This is a result of the choice of latitudes which have moderately long periods of open ocean in the base case. Reducing the period of open ocean decreases absorbed solar radiations and thus increases the net upward flux. Increasing the period of open ocean initially increases absorbed solar radiation and thus reduces the net flux, but ultimately upward turbulent fluxes dominate and the upward net flux is increased. At other latitudes where ice covered or ice free conditions dominate the response to air temperature variations will be altered.

While the net energy exchange between the atmosphere and the ice/ocean surface varies in a complex way with air temperature, the latent heat flux generally increases as the period of open ocean increases, putting a great deal of moisture into the atmosphere. While much of this moisture will be precipitated back into the oceans some of it will be transported over land surfaces. This excess moisture will then be available for snowfall that could feed the ice sheets of an ice age.

The amount of moisture transported onto land areas

would be determined in a climate model from the specific humidity of the air, the horizontal wind speed, and the appropriate area of the land-sea boundary. In this study the specific humidity is determined only from the air temperature which is specified, therefore, the effect of variations in the latent heat flux on the specific humidity and thus on the moisture transport onto land area can not be determined directly. However, an examination of the relative magnitudes of the effect can be made.

It must first be assumed that the excess water put into the atmosphere by the latent heat flux is redeposited in the ocean and that this exchange is the only one of importance over a zonally averaged ocean. It is then possible to estimate the specific humidity of the air from the latent heat flux from the surface and the deposition rate for moisture in the air. This value of specific humidity can then be multiplied by the horizontal winds and the area of the ocean-land boundary to determine the moisture flux onto the land. However, the depostion rate is known only to about a factor of 3, and the wind velocity is known only to a factor of 10, therefore, the horizontal moisture flux may be in error by as much as a factor of 30. In addition, the magnitude of the variations in the wind field between ice free and ice covered conditions is not known; however, the change in the thermal contrast between land and sea when the ocean changes from ice covered to ice free conditions would have a large effect on the atmospheric circulation

systems and thus on the wind field.

Because of all the uncertainties in determining the wind velocity and deposition rates these will be assumed to be constants which do not change between glacial and interglacial regimes. As a result the latent heat flux from the ice/ocean surface can be directly related to the moisture flux across the land-ocean boundary, and thus the relative change in the moisture flux onto land areas can be determined from the ratio of the latent heat flux from the ice/ocean surface for some climatic regime and the base case.

An example of how the moisture flux can change can be seen in the case when the mean air temperature and thus the period of open ocean is varied. In the base case at 72.5N the net latent heat flux to the atmosphere is 1.1 W m^{-2}. When air temperature is increased 1K, 3K, and 5K (increases in the period of open ocean of 3, 8, and 12 time steps) the latent heat flux increases to 1.2, 2.1, and 2.2 W m^{-2} for an increase of 9%, 90%, and 100% respectively. When the air temperature is decreased by 1K, 3K, and 5K (decreases in the period of open ocean of 4, 15, and 15 time steps) the latent heat flux decreases to .7, 0, and .2 W m^{-2} for a decrease of 36%, 100%, and 82% respectively.

Similar, although smaller changes occur when the period of open ocean is changed through variations in the amplitude of the seasonal cycle of air temperature. When the amplitude is increased at 72.5N by 10%, 20%, and 30% the latent heat

flux is increased 27%, 27%, and 18% respectively; while a decrease in the amplitude of the same magnitude produces a decrease in the moisture flux of 36%, 64%, and 109% respectively.

These seem to be very large changes in moisture flux onto land areas, and could prove significant in the formation of ice sheets. However, a coupling of the physical systems will allow an in depth analysis of the magnitude of this effect and its importance in the initialization and growth of ice sheets.

B. Continental Ice

1. Insolation and Net Budget Variations in the Northern Hemisphere

There have been many studies examining the response of continental ice sheets to variations in solar radiation (Weertman, 1976; Birchfield et.al., 1981; Pollard, 1978, 1982a, 1982b, 1982c; Oerlemans, 1980). In all of these studies simple parameterizations of the net accumulation (net budget) at the surface were used.

The first was that used by Weertman (1976) in which an equilibrium snowfall line, the firn line, was defined as a function of latitude, then any surface above this line experienced a constant net accumulation of snow and any surface below the line experienced a constant net ablation. The net budget was made responsive to insolation variations by varying the elevation of the firn line with half year insolation variations at a specified latitude. The results indicated that much of the glacial-interglacial cycles could be explained by insolation variations; however, the magnitude of the effect proved very sensitive to the ratio of the rates of net accumulation and ablation.

Birchfield et.al. (1981) modified the parameterization used by Weertman by making the accumulation and ablation rates a decreasing linear function of the elevation of the ice sheet which approximated the saturation mixing ratio dependence on elevation in the standard atmosphere, and thus included the "desert-elevation" effect.

The most recent parameterization of the net budget was developed by Oerlemans and Bienfait (1980) and was adapted by Pollard (1982a,b,c). The final form of this parameterization is similar to that used by Birchfield et.al. (1981) and by Budd and Smith (1981) in that it relies on the definition of an equilibrium line as a function of latitude about which the net budget varies quadratically, and whose elevation can be changed in response to insolation variations at a specified latitude. However, the derivation of this parameterization was based on the results of a calculation of an energy balance of the surface layer of an ice sheet. Until now the net budget parameterizations have been derived empirically providing no method by which the mechanisms involved in snow accumulation and melt could be examined. The derivation of this parameterization makes an attempt to consider some of the physical processes involved in melting at the ice sheet surface and thus the opportunity to examine the quality of the net budget parameterization.

Oerlemans and Bienfait first developed a snow/ice melt model which considered the energy balance of a snow/ice layer through the daily cycle over the year at various latitudes. The energy balance equation took the form:

$$C * \partial T/\partial t = (1 - a) * Q - \tau \sigma T^4 - HF$$

where C is the heat capacity of the layer, T is its temperature, a is the effective albedo dependent on surface albedo, cloud fraction, and solar zenith angle, Q is the incoming solar radiation at the top of the atmosphere, τ is

the effective transmissivity of the atmosphere for long wave
radiation originating at the surface, and HF is the
turbulent energy flux from the ice surface to the
atmosphere.

Oerlemans and Bienfait admit that the representation of
the energy balance is rather crude; however, while short and
long wave radiative terms are rather standard forms used in
simple models their representation of the turbulent exchange
is very simple. In essence, the turbulent exchange is set
equal to a constant times the difference between the air and
surface temperatures if the surface is warmer, otherwise the
turbulent flux is set to zero. This means that energy
exchange only occurs during unstable conditions, neglecting
any exchange from the atmosphere to the surface when
downward temperature gradients occur and the turbulent
exchange is induced by winds. In addition, the air
temperature is defined as the air temperature at sea level,
set to the freezing point, and adjusted to the elevation of
the ice sheet by a lapse rate. Oerlemans and Bienfait
justify using the freezing point by suggesting that "a more
flexible treatment of $T_a(0)$ seems possible only if the
boundary-layer properties, including horizontal advection of
heat, are computed" and that adding such properties would
make the model more cumbersome and the computations too
costly. However, this neglects the fact that the air
temperatures do become much colder in the winter months and
that air temperature is a strong function of latitude.

Using the energy balance equation Oerlemans and
Bienfait compute the energy balance throught the year and
sum the amount of melt from each daily cycle, and obtain as
a function of latitude and elevation the total melt in a
year. Through an analysis of these results they found that
the elevation dependence of melt for various insolation
regimes was conserved with respect to the 1 m yr^{-1} melt
isoline, and that this dependence was quadratic in the
difference between the elevation of interest and that of the
1 m yr^{-1} isoline. They also found that variations in the
elevation of the 1 m yr^{-1} isoline were closely related to a
function of the ratio of the annual mean solar radiation at
some time to the present.

With the melt field determined it was now left to
determine the total mass balance field by including
precipitation. This was done by neglecting variation of
precipitation with height and simply adding a constant to
the melt field, and setting an upper limit on the mass
balance on the order of .5 m yr^{-1}. In addition, the
moderately complex variation in the elevation of the 1 m
yr^{-1} isoline with latitude was eliminated by setting the
slope of that line to a constant.

There are a number of flaws in the development of this
parameterization. First, the energy balance is computed at
all latitudes assuming an ice covered high albedo surface.
Besides the fact that this is an erroneous assumption for
present conditions, it causes the amount of solar radiation

absorbed at the surface to be severely reduced and thus limits snow melt. A second problem is that the "net" long wave radiation as defined in their energy balance equation is always toward the atmosphere; however, during the summer, while the surface is held at the freezing point, the net long wave flux can reverse direction enhancing surface melt. Another problem is the choice of a constant precipitation rate in the total mass balance. Besides the fact that this disregards the difference between snowfall and rain in the growth of ice sheets and the variation in their relative amounts with latitude, it also disregards the fact that moisture and thus precipiatation decreases with elevation which results in the highest elevation of an ice sheet having a reduced net accumulation.

These are a few of the major problems with the Oerlemans and Bienfait net budget parameterization (the equilibrium line parameterization); however, it has been used in many studies of the response of ice sheets to insolation variations with very interesting results. In the remainder of this section a comparison will first be made between the response of the present ice sheet model and that used by Pollard (1982a,b,c) to variations in the net budget as defined by the equilibrium line parameterization and solar insolation variations. Then those results will be compared with the response of the present ice sheet model to variations in the energy balance net budget parameterization as described in chapter II.

An experiment using the equilibrium line parameterization was performed in order to examine the correspondence between the present ice sheet model and that employed by Pollard (1982a). Figure 5.5 shows the results of this experiment indicating the variation of the ice sheet cross sectional area over the past 240k years for the present continental ice sheet model and that used by Pollard, when bedrock was added, in response to variations in the summer half year insolation at 55N. In the present model the flow parameter, A, was equal to 2.1 $yr^{-1}bar^{-3}$ (the value used by Pollard), and the bedrock depression time constant was set to 3000 years for this experiment.

The results are very encouraging with all of the relative maxima and minima in cross sectional ice area in Pollard's results being reproduced by the present model. However, Pollard's result shows a much greater range in ice area with maxima that are as much as a factor of two larger than for the present model. This discrepancy may be due to the difference in the way in which bedrock depression is parameterized, the only major difference between the two models.
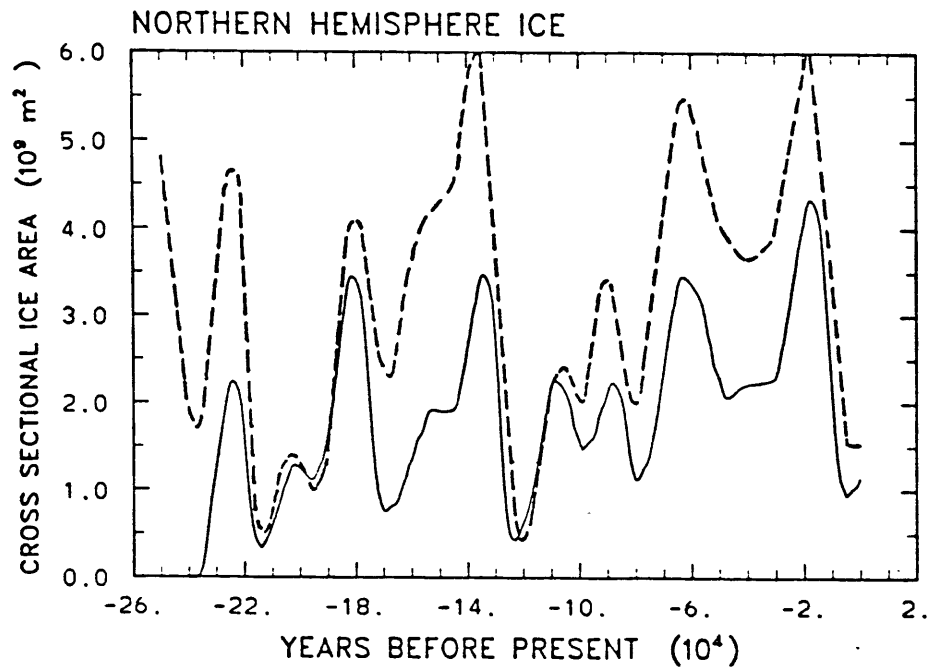
Figure 5.5 Northern hemisphere cross sectional ice area from
-240k to the present using the equilibrium line
net budget parameterization for the present ice
sheet model (solid line) with A equal 2.1
$yr^{-1}bar^{-3}$ and the bedrock depression time constant
equal to 3000 yr and Pollard's (1982a) results
(dashed line).

Pollard's bedrock response incorporates an elastic deformation of the lithosphere and a deeper viscous flow of the asthensophere. This description has the effect of allowing the bedock to respond quickly, with a small time constant, to small scale changes and much more slowly to larger scale variations. In the present ice sheet model the bedrock depression is described by a simple exponential local response equation with only one time constant, so the bedrock response is determined by the local ice thickness regardless of the horizontal scale. This difference in the parameterization of the bedrock depression can to a certain extent be thought of as a difference in the bedrock depression time constant and, as will be seen later, this can cause large changes in the maximum cross sectional ice area.

Overall, it seems that the present ice sheet model responds in a similar way to Pollard's model to insolation induced variations in the equilibrium line net budget.

In order to examine the response of the present ice sheet model to insolation induced variations in the energy balance net budget it is necessary to devise a parameterization which links air temperature variations to insolation variations. The response of air temperature to insolation variations will eventually be determined by a coupled climate model; however, in the interest of examining the response of the ice sheet to variations of as few variables as possible a simple linear parameterization will

be used.

The form of the parameterization is:

$$\Delta T_a = ((Q * (1 - \alpha_p)) - (Q_b * (1 - \alpha_{pb}))) / B$$

where Q is the insolation at the top of the atmosphere, α_p is the planetary albedo, T_a is the surface air temperature, B is the sensitivity parameter of air temperature to absorbed insolation variations, and the subscript b indicates the present. This equation states that the change in surface air temperature is proportional, through the sensitivity parameter, to the change in the absorbed solar radiation from the present.

The value of B is uncertain. Results from a study by Warren and Schneider (1979) indicate that for a global equilibrium response of outgoing infrared radiation to a change in surface air temperature the value of B is about 2 W $m^{-2}K^{-1}$. However, in this study the air temperature is not permitted to come to equilibrium with changes in the net radiation, therefore, a larger value of B would seem more appropriate.

It should be noted that this is a very crude parameterization of the response of air temperature to variations in net radiation. In fact, Schneider and Thompson (1981) refined the sensitivity parameter to include the albedo-temperature feedback. This causes some variation in the value of B; however, given the uncertainty of its value in the present problem, this additional affect will be neglected. Eventually when the ice sheet is coupled to a

climate model the response of the air temperature to variations in the net radiation will be able to be evaluated with more confidence.

Experiments have been performed in which the model was initialized with the ice sheet profile at -48k in the equilibrium line experiment and integrated for 58k years with values of B ranging from 4 to 12 W $m^{-2}K^{-1}$, and the flow parameter A, set to .15 $yr^{-1}bar^{-3}$.

The results, shown in Figure 5.6, indicate that the ice sheet is very sensitive to the value of B. When B is set to 4 W $m^{-2}K^{-1}$ the ice sheet grows from its initial size, and comes to an approximate equilibrium which seems independent of insolation and temperature variations. The growth over the first 20k years is due to the large decrease in summer air temperatures resulting from a large increase in surface albedo between present ice free and ice age summers, which decreases summer ablation at the ice surface. Surface albation at the ice sheet surface remains low because the air temperatures are so low, due to the lapse rate and the higher elevation of the surface, that insolation changes do not increase them enough to warm the surface to the freezing point. As a result the ice sheet maintains itself with a balance of snowfall at its surface, and ablation at its edges. The same seems to be true when B is equal to 6 and 8 W $m^{-2}K^{-1}$, although the equilibrium size is smaller.
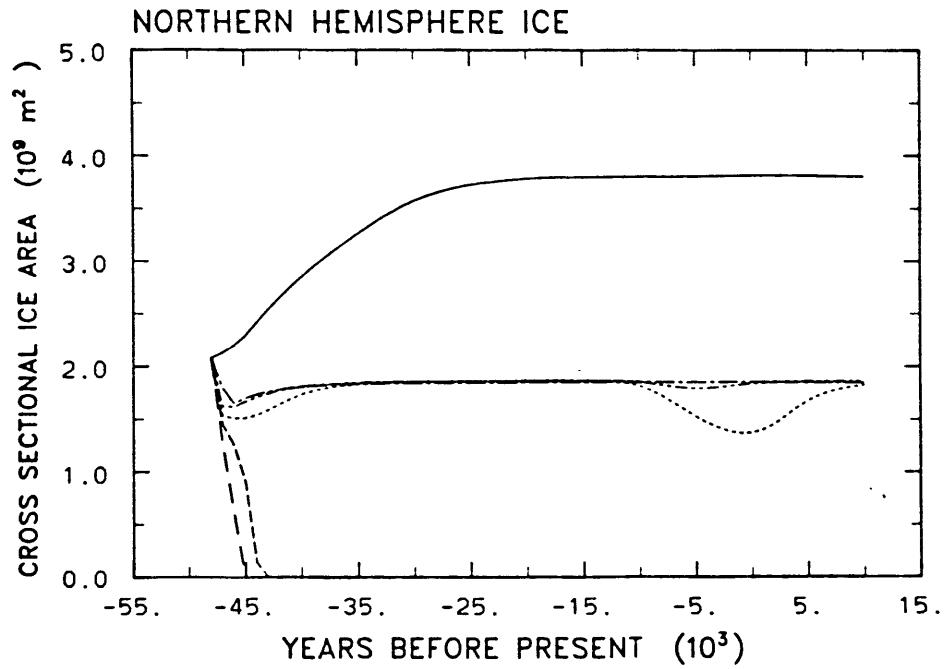
NORTHERN HEMISPHERE ICE

Figure 5.6 Northern hemisphere cross sectional ice area from
-48k to +10k computed from the energy balance net
budget parameterization for A equal to .15
$yr^{-1}bar^{-3}$ and B set to 4 (solid line), 6 (single
dot dashed line), 8 (double dot dashed line), 9
(dotted line), 10 (short dashed line), and 12
(long dashed line) W $m^{-2}K^{-1}$.

The situation begins to change when B is equal to 9 W $m^{-2}K^{-1}$. In this case the ice reaches the same maximum size as when B was set to 6 W $m^{-2}K^{-1}$ and 8 W $m^{-2}K^{-1}$; however, when the summer insolation begins to increase at about -11k ablation becomes large enough to decrease the ice sheet size appreciably.

When B is equal to 10 and 12 W $m^{-2}K^{-1}$ the ice sheet melts away completely within a few thousand years. In these cases the air temperatures are so insensitive to insolation variations, due to the large values of B, that the computed net budget is very similar to present day conditions. As a result ablation increases as the ice sheet shrinks until it melts away completely.

Aside from the sensitivity to the value of B the results shown in Figure 5.6 show a striking lack of variation in the cross sectional ice area over time compared to that when the equilibrium line net budget parameterization was used. There seem to be a number of factors contributing to this. An examination of the energy balance and net budget at latitude zones just to the north and south of the ice edge, 67.5N and 62.5N for the case where B is equal to 8 W $m^{-2}K^{-1}$ indicates what some of the factors are which limit ice sheet growth and melt.

The limit on the growth of the ice sheet occurs because of the nature of the energy balance at 62.5N. At that latitude the air temperatures are so high, reaching a maximum of 289.6K at -10k and 287.4K at -18k that the snow

and ice, including the 3 m of ice that is the average
thickness of the ice sheet in the 5 degree latitude zone, is
completely melted away. This places a tremendous ablation
rate just south of the ice sheet which is about a factor of
three larger than the positive net budget computed at 67.5N
(the computed net budget is $.33 \times 10^{-8}$ m s^{-1} and -1.05×10^{-8} m
s^{-1} at 67.5N and 62.5N respectively). The ablation rates for
the intermediate latitudes are determined by interpolating
between these two values, placing high ablation rates over
the southern edge of the ice sheet thus restricting ice
growth.

The only case in which the high ablation at 62.5N is
overcome is when B is set to 4 W m^{-2}K^{-1} (see Figure 5.7). In
this case air temperatures drop much more severely at 67.5N
when insolation drops. The decreases in air temperature
inhibit ablation at the ice surface and increases the
percentage of the precipitation that falls as snow. This
causes the ice sheet to grow larger, thus increasing its
flow rate to the south. When B is set to 4 W m^{-2}K^{-1} the
increased flow rate becomes enough to overcome the ablation
caused by the warmer air temperatures at 62.5N, which are
also reduced. The ice accumulating at 62.5N increases the
surface albedo during the summer and slowly increases the
surface elevation which has the effect of reducing both the
amount of absorbed solar radiation and surface air
temperature, surpressing the ablation rate further. However,
once the southern extent of the ice sheet extends past 62.5N

to 59.5N its growth rate is again severly restricted by the high ablation rates computed at 57.5N, but this obstacle is more difficult to overcome because the air temperatures are higher there than at 62.5N.

The ice melt over the northern hemisphere ice sheet is also restricted in these experiments. The reason is that the absorbed solar radiation variations cause the air temperatues to decrease even if the incident solar radiation increases over regions where the ice exists at the time of interest, but not at the present. An example of how this might occur can be seen in the case of the insolation variations at 67.5N where the ice sheet elevation is 1947 m at -10k. The incident insolation at the top of the atmosphere at that time in July is 459 W m^{-2} compared to 433 W m^{-2} at the present. This is an increase of 26 W m^{-2} which would translate into an increase of 3.3K in air temperature from 273.7K for the present at that elevation and would seem to enhance melting. However, the computed planetary albedo at -10k over the ice is .59, while that at 0k over an ice free surface is .41. The effect these albedos have on the absorbed solar radiation is to reduce it from the values at the top of the atmosphere to 188 W m^{-2} and 255 W m^{-2} at -10k and 0k respectively. This is a reduction in air temperature of 8.4k to 265.3K if B is 8 W m^{-2}. The effect is even larger if B is 4 W m^{-2} with a reduction of 16.8K to 256.9K. The reduction in air temperature restricts the melting of the southern half of the ice sheet.

-14k   -6k
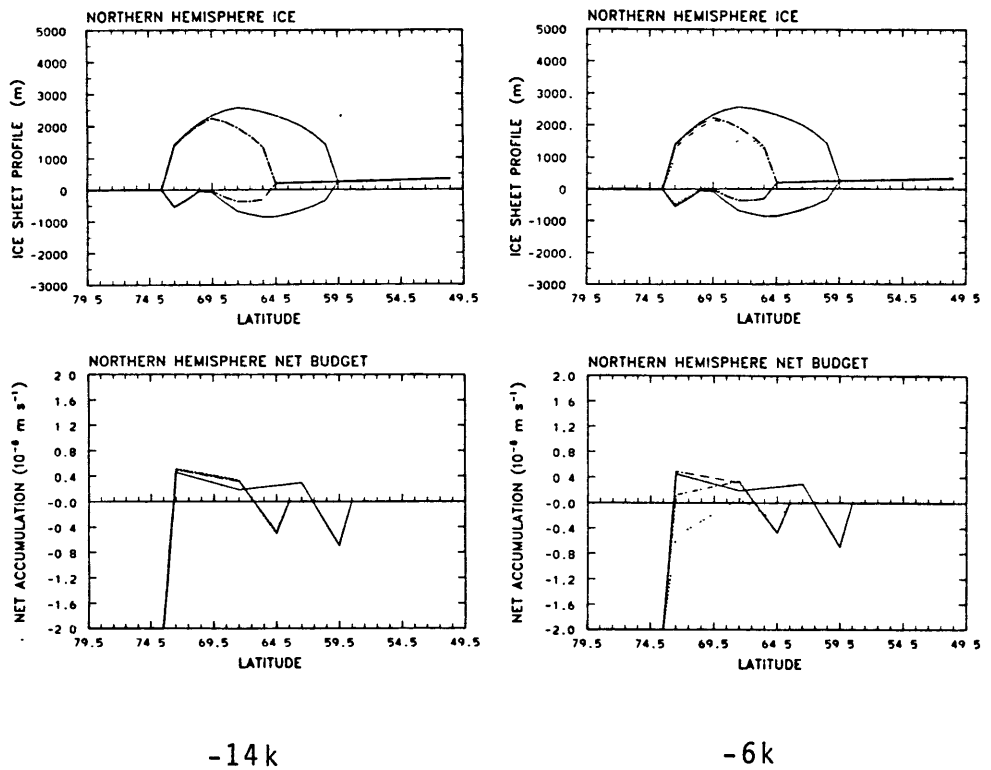
Figure 5.7 Northern hemisphere ice sheet profiles and
           corresponding net budgets at -14k and -6k, when
           the bedrock time constant is 3000 yrs. and A is
           .15 yr^{-1}bar^{-3} and B is 4 (solid line), 6 (single
           dot dashed line), 8 (double dot dashed line), and
           9 (dotted line) W m^{-2}K^{-1}

Figure 5.7 shows that at -6k the ice sheet is reduced

from its maximum size at -14k when B is equal to 8 W $m^{-2}K^{-1}$

and 9 W $m^{-2}K^{-1}$, and that this change occurs over the

northern half of the ice sheet. The reason for this change

in the ice sheet is that an increase in short wave radiation

between -14k and -6k during the summer causes the air

temperatures to be increased. This results in reduced

accumulation rates which cause a drop in the elevation of

the ice sheet through ice flow, and thereby an increase in

the air temperatures. This causes a further reduction in

accumulation and an increase albation rates. This effect

becomes most pronounced for B equal to 9 W $m^{-2}K^{-1}$ where the

ice sheet comes under almost complete ablation. In this case

air temperature is less sensitive to insolation changes, so

instead of absorbed solar radiation causing a decrease in

the air temperature of 9K and 5K at -14k and -6k when B is

equal to 8 W $m^{-2}K^{-1}$, for example, the air temperature is

reduced 8K and 4K at -14k and -6k respectively for B equal

to 9 W $m^{-2}K^{-1}$. Therefore, the temperatures are warmer and if

close to the freezing point cause higher ablation rates.

Once the surface elevation is reduced through ablation the

air temperature and thus ablation increase further

eventually putting the northern edge of the ice sheet in to

an ablation zone. The reason this effect is larger over the

northern half of the ice sheet is possibly because the

snowfall rates as determined in this model are greatly

affected by the variations in air temperature in that

region; and the net budget between 67.5N and 62.5N is determined by interpolating between a moderate and slightly changing positive volume and a large negative value, which results in a net budget for the region which varys very little, therefore changing the ice sheet very little. Since much of the change in the shape of the ice sheet shown in Figure 5.7 is due to the method by which the net budget was computed the results should be viewed with caution.

Overall, there are two major effects which reduce the variation in the cross sectional ice area with time as compared to that produced when the equilibrium net budget is used. The first is the restriction on the growth of the ice sheet resulting from the high ablation rates computed just south of the ice sheet, and second, is the restriction on melt caused by the contrast in surface albedo between ice sheet and ice free conditions. The net budget resulting from these resrictions is in great contrast to that computed over the ice sheet with the equilbrium line parameterization.

Figure 5.8 shows how the net budget for the equilibrium line and energy balance calculations differ for the same ice sheet. The equililbrium line calculation shows a positive net budget over about 75% of the ice sheet compared to about 50% for the energy balance calculation. In addition, the magnitude of the positive net budget in the equilibrium line case is about a third larger than that in the energy balance case. This is due in part to the incorporation of the "desert-elevation" effect (the exponential decrease of water

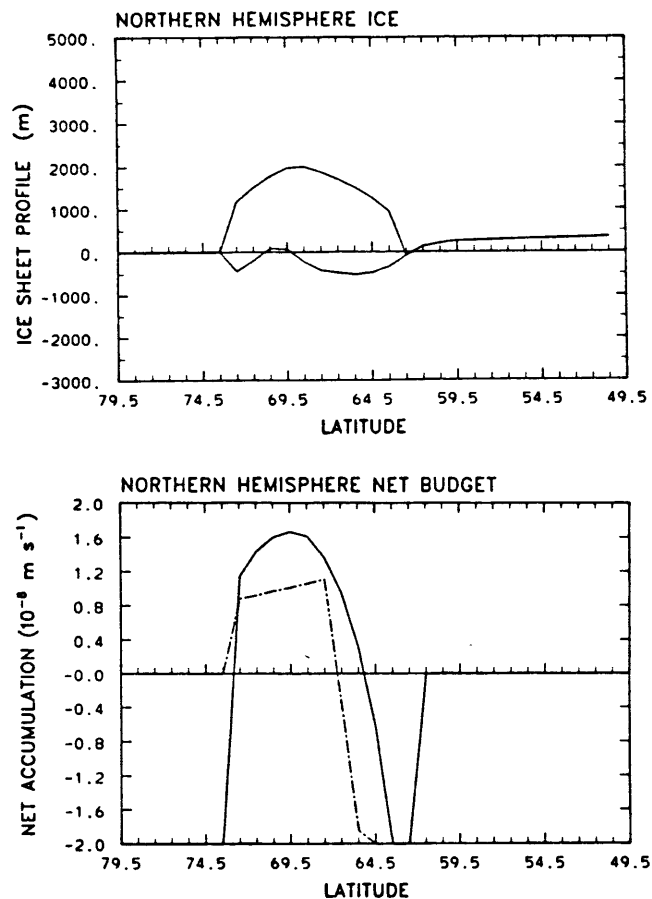NORTHERN HEMISPHERE ICE

NORTHERN HEMISPHERE NET BUDGET

Figure 5.8 Cross section of northern hemisphere initial ice
sheet at -48k and the corresponding net budget as
computed by the equilibrium line net budget
parameterization (solid line) and the energy
balance net budget parameterization (single dot
dashed line).

available for snow with an increase in elevation) in the snowfall parameterization used in the present model.

However, the net net ablation zone in the energy balance computation is larger, and more importantly, the magnitude of the ablation is much larger than for the equilibrium line calculation ($-.63 \times 10^{-7}$ m s^{-1} and $-.5 \times 10^{-8}$ m s^{-1} for the energy balance calculation compared to $-.22 \times 10^{-7}$ and $.95 \times 10^{-8}$ for the equilibrium line calculation at 63.5N and 66.5N respectively). As a result the ice sheet grows much larger using the equilibrium line calculation, while it shrinks back to its "equilibrium" latitudinal extent in a few thousand years using the energy balance calculation.

The reason for the extreme ablation over the southern edge, as stated earlier, is the interpolation from the moderate positive net budget at 67.5N and the large negative net budget at 62.5N. In order to determine if removing the large negative ablation at the southern edge of the ice would allow the ice sheet to extend farther south during an ice age, an experiment was done in which the net budget was reset to zero in any latitude zone in which there was no ice. The interpolation across the southern edge was then between a positive net budget and zero. While this modification changed the shape of the ice sheet, it did not allow the ice sheet to extend farther south because the ice sheet was to small for its flow rate to be sufficient to extend it.

The method used here of computing the net budget at

completely decoupled latitudes, especially at the ice edge, leaves out a number of physical processes which may account for the difficulty in producing ice sheet variations. Some of these processes include the cooling of the air above the ice and the increase in the temperature gradient across the edge of the ice sheet which acts to influence the path of storm tracks and thus the accumulation rates on the ice sheet, the horizontal transport of energy between the various latitude zones, and the katabatic winds which come down off an ice sheet affecting both the turbulent fluxes and air temperatures. In order to determine if including these processes, even in a highly parameterized form, has an effect on the growth and melt rates of the ice sheet it is necessary to couple the ice sheet model to a climate model. This will also make it possible to improve the parameterization of air temperature response to insolation variations.

2. Flow Parameters and Time Varying Insolation

In chapter IV.B.3 the response of an equilibrium ice sheet to variations in the flow parameter, A, with no external forcing was discussed. The results indicated that the value of A has a large impact on the size and possibly on the existence of continental ice sheets through its direct effect on the flow rate of the ice. In this section the responses over time of a non equilibrium northern hemisphere ice sheet under the influence of insolation and

air temperature changes similar to those discussed in the
last section (with B equal to 8 W m^{-2}K^{-1}) to various values
of A, ranging from the base value chosen in chapter IV of
.15 yr^{-1}bar^{-3} to the value used by Pollard of 2.1 yr^{-1}bar^{-3}
will be discussed.

Figure 5.9 shows the variation of the cross sectional
area of continental ice from -48k to +10k for A equal to
.15, .3, .45, .6 and 2.1 yr^{-1}bar^{-3}. The response of the ice
sheet to the various values of A is similar to its response
to the various values of B, with the cross sectional ice
area decreasing as A is increasing until the ice melts away
completely in a few thousand years for A equal to 2.1
yr^{-1}bar^{-3}.

When A is relatively low, as for the base value of .15
yr^{-1}bar^{-3} the flow rate is low and the ice cross sectional
area show little variations over time. However, when A is
increased the ice velocity is also increased, causing more
ice to move from the center of the ice sheet and a net
accumulation zone, to its edges and a net ablation zone.
This causes a lowering of the overall elevation of the ice
sheet with the larger values of A producing the most
decrease in the maximum elevation. The air temperatures are
warmer, closer to the freezing point, at the lower
elevations so the ice sheet becomes more sensitive to
temperature changes induced by insolation variations. When A
is equal to .3 yr^{-1}bar^{-3} the effect is rather
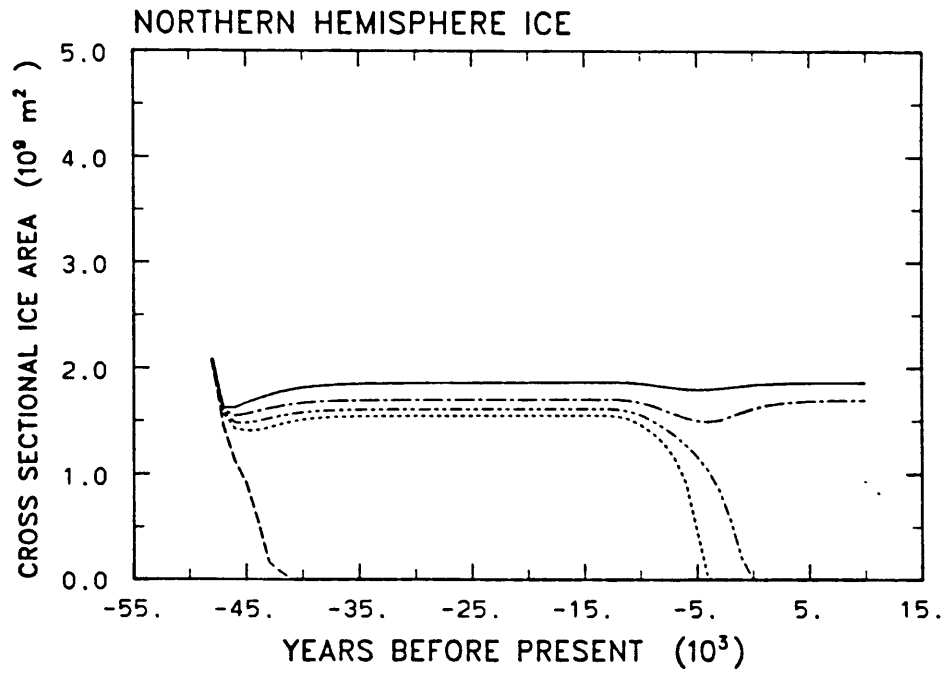small with a small dip in the cross sectional ice

Figure 5.9 Northern hemisphere cross sectional ice areas
from -48k to +10k computed from the energy
balance net budget parameterizaiton for B equal
to 8 W m^{-2} and A equal to .15 (solid line), .3
(single dot dashed line), .45 (double dot dashed
line), .6 (dotted line), and 2.1 (dashed line)
yr^{-1}bar^{-3}.

area when insolation increases; however, when A is increased to .45 $yr^{-1}bar^{-3}$ and .6 $yr^{-1}bar^{-3}$ the higher insolation at around -10k causes the air temperature to rise and thus increases the ablation to the point where ice melts away completely at 0k and -4k respectively. In the case where A is increased to 2.1 $yr^{-1}bar^{-3}$ the flow rate is so rapid that the ice sheet essentially flows away until the drop in elevation puts the ice sheet entirely into the ablation zone. The ice sheet is then melted away in a few thousand years.

Figure 5.10 shows the shape of the ice sheet and its net budget at -14k and -6k, which are times of relative extremes in its size, for A equal to .15 $yr^{-1}bar^{-3}$, .3 $yr^{-1}bar^{-3}$, and .45 $yr^{-1}bar^{-3}$. The ice sheet profiles at -14k are very similar in both shape and net budget. The only real difference is in the central elevation which decreases for increasing A, reflecting the effect of higher ice velocities on elevation. This change in elevation causes the net budget to change putting both the northern and southern edges of the ice sheet into melting ablation zones when A is .3 $yr^{-1}bar^{-3}$, and putting the entire ice sheet into an ablation zone when A is .45 $yr^{-1}bar^{-3}$ fortelling its eventual complete demise.
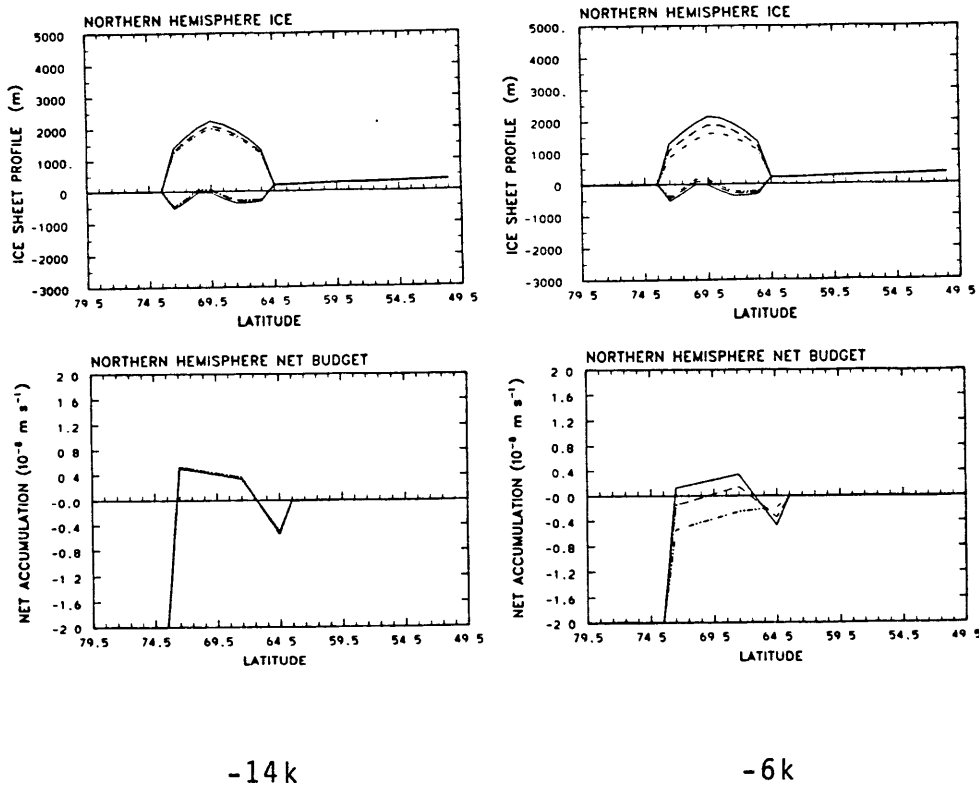
Figure 5.10 Northern hemisphere ice sheet profiles and corresponding net budgets at -14k and -6k when B is 8 W $m^{-2}K^{-1}$ and A is .15 (solid line), .3 (single dot dashed line), and .45 (double dot dashed line) $yr^{-1}bar^{-3}$.

These results indicate the need for more information concerning an appropriate value of A to be used in this type of simple ice sheet model. In addition, it can be argued that the use of a constant value is inappropriate because A is dependent on temperature which can vary within the ice in both the vertical and horizontal. It would be desirable to be able to determine A as a function of latitude and elevation, but in this model such a calculation is impossible because the thermodynamics have been neglected, and to include them would require an extension of the dimension of the model to include vertical resolution. However, more complex continental ice sheet models exist which can not be used for long term ice age studies, but can be used to study the variation of the computed values of A with latitude. Such studies may lead to a parameterization of A as a function of latitude which can be incorporated into the simpler models which are more applicable for the longer term ice age studies.

3. Bedrock Depression Time Constant

Another parameter that must be chosen in this model, but whose value is not well known is the time constant of the bedrock depression under the ice load. It has been recognized by many (Birchfield et.al., 1981; Budd and Smith, 1981; Budd, 1981; Pollard, 1982a) that the time lagged response of the bedrock, and thus the surface elevation, to an ice load is important in producing slow build ups of ice

and rapid deglaciations similar to those recorded in the geologic record. The mechanism by which the slow build up of the ice and rapid deglaciations occur is as follows. An ice sheet might begin to grow as the result of a decrease in solar radiation. While it is growing much of the ice sheet is in a net accumulation zone; however, as the ice sheet approaches its maximum size and its growth rate slows, the depression of the bedrock becomes greater causing more of the large ice sheet to drop to lower elevations and thus into a region of net ablation. If this occurs when insolation changes increase ablation rates the two processes will enhance each other thus bringing about a rapid end to the ice age. If no bedrock depression occurs an ice sheet would grow large, but the increases air temperature at the high elevations due to insolation or other variations would not be enough to terminate the ice age. On the other hand if the bedrock responds immediately, the lower surface elevations and thus the higher air temperatures would greatly inhibit the growth of the ice sheet.

Figure 5.11 shows how the response of the present ice sheet model forced with the equilibrium line net budget parameterization over the last -240k years changes for various bedrock depression time constants ranging from 3000 years to 30000 years. When the time constant is increased from 3000 to 5000 years there are only minor changes in the amplitudes of some of the smaller peaks. The largest of
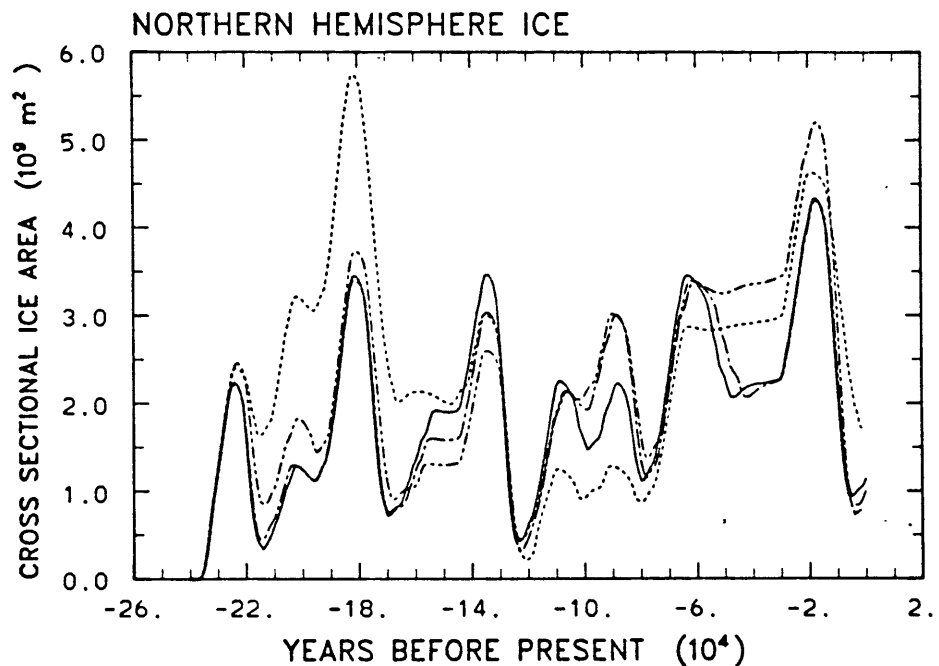
NORTHERN HEMISPHERE ICE

Figure 5.11 Northern hemisphere cross sectional ice area
from -240k to the present using the equilibrium
line net budget parameterization, A equal to 2.1
$yr^{-1}bar^{-3}$ and the bedrock depression time
constant set to 3000 (solid line), 5000 (single
dot dashed line), 10000 (double dot dashed line),
and 30000 (dotted line) years.

these changes occurs at about -130k and -90k. When the time constant is increased to 10000 years the differences become more apparent with amplitude variations in the time series occurring in more of the major peaks including those at -180k and -18k, and in some of the transition periods such as from -60k to -30k. During this latter period the minimum in cross sectional ice area is all but eliminated. However, it is when the time constant is increased to 30000 years that the changes become the most dramatic. In this case the amplitude of the variation in ice sheet size appears to be enhanced; however, this seems to occur on the broader 100k year range rather than on the time scale on the shorter variations. Over the period from about -220k to -150k the cross sectional ice sheet area for a time constant of 30000 years is on the order of a factor of two larger than for the smaller time constants. This may result from the slower sinking of the bedrock in response to the ice load, keeping surface elevations high, thus reducing ablation and allowing the ice sheet to approach a large equilibrium size. Once the ice sheet does decay the depression caused by its large size keeps elevation low, putting most of the ice sheet into regions of net ablation. This results in a much smaller ice sheet over the period from about -120k to -80k than occurred when smaller values of the bedrock time constant were used. The ice sheet then begins to grow again resulting in a cross sectional ice area which is generally larger over the period from -70k to the present than that when the time constant

was set to 3000 or 5000 years.

The changes in the response of the ice sheet to the various bedrock depression time constants suggests a possible reason for the differences in the time series of ice sheet cross sectional area obtained by Pollard and by the present model discussed in section B.1.. However, a direct comparison is difficult because of the different type of parameterization of the bedrock depression. In Pollard's model the bedrock depression time constant was scale dependent so that smaller scale variations in ice were responded to by the bedrock more quickly than for larger scale variations. In the present model all variaitons were responded to on the same time scale.

The choice of the appropriate value of the time constant is also difficult. Birchfield et.al. (1981) suggests that an appropriate value would be 3000 years based on evidence from the Cananda ice sheet and the Fennoscandian ice sheet which indicate values of 2650 years and 4400 years respectively. This was the basis for the choice of the time constant for the base case in this model. More recent studies have suggested that scale dependent time constants such as Pollard's (1982a) are more appropriate given what is known about the structure of the lithosphere and asthenosphere . Pollard's parameterization suggest a time constant ranging from about 1000 to 3000 years for the length scales of his ice sheets. However, results presented at the International Symposium on Milankovitch and Climate

(Peltier and Hyde, 1982) suggest that in addition to a
characteristic time constant for each length scale, each
length scale has multiple time constants. This has been
neglected in previous studies, but may be important in ice
sheet variations.

At the present time it is not certain what the
mathematical description of the bedrock depression should
take, or all the time scales that may arise from a correct
description; however, it is the subject of a major
controversy which will eventually be resolved with more
discussion and research.

4. Affect of Sea Level Variations on Antarctica

Budd (1981) has presented a hypothesis in which he
suggests that major changes in the Antarctic ice sheet are a
response to large sea level variations caused by the growth
and decay of the northern hemisphere ice sheets. There are
several pieces of evidence which he cites in support of this
hypothesis.

The first is the fact that the Antarctic ablation zone
is very small, and is almost exclusively located on the
coast where calving ablation occurs. In addition, southern
hemisphere radiation levels have generally been lower than
at the present, therefore, any insolation changes would only
serve to reduce the small amount of melting ablation
further, affecting the ice sheet very little. This is
supported by some experiments done with the present model

which indicated that air temperatures were so cold that even increases in solar radiation did little to increase the melting ablation on the Antarctic ice sheet. The only effect seemed to be a slight change in the shape of the ice sheet caused by the snowfall rate's dependence on temperature; however, the overall size and latitudinal extent remained unchanged.

The second piece of evidence is based on the discrepancy between derived sea level records which suggest three substancial drops in sea level over the past 120k, and ocean sediment data which show only the most recent sea level drop at about -20k. Budd suggests that the sea level record reflects the waxing and waning of the northern hemisphere ice sheets whose ice volume makes up about 75% of the sea level variatons, and the δO^{18} record, derived from ocean sediments reflects variations in the volume of the Antarctic ice sheet whose O^{18} depletion is about three times that of the northern hemisphere ice sheets. Budd proposes the following hypothesis on how the Antarctic ice volume varies in response to sea level variations. When sea level drops, as a result of northern hemisphere ice sheet growth, the Antarctic ice sheet begins a slow build up which continues through the time of maximum northern hemisphere ice extent. However, for a rapid decay of the Antarctic ice sheet to occur when sea level rises the bedrock needs to be depressed. By the end of northern hemisphere ice expansion the Antarctic ice has not depressed the bedrock sufficiently

for a retreat to occur. Therefore, the Antarctic ice sheet growth simply slows during that period, and then it grows further during the next drop in sea level. Then with the consequent demise of the northern hemisphere ice sheets and the rise in sea level, the Antarctic ice sheet begins to decay rapidly in the coastal regions because the bedrock has now had sufficient time to be depressed.

The present ice sheet model was used to make a first attempt at testing this hypotheses by moving the position of the calving line in response to the sea level variations given in Budd (1981) over the past 120k years. The first step in this experiment was to determine how much more land would be exposed, ie. how far north to move the calving line for a maximum drop in sea level which has been estimated to be about 105 m at -20k. A map of the isobaths (line of constant depth) obtained from the National Geographic Atlas of the World (1981) indicated that the Antarctic continent drops off very rapidly to its continental shelf at about 1000 m below sea level, the deepest continental shelf in the world. This means that a drop in sea level will uncover only a small area of land on which new ice can accumulate, and thus the position of the calving line will be moved only a short distance northward. Measurements taken from the National Geographic maps indicate that the furthest the calving line can justifiably be moved northward for a 105 m drop in sea level is about .5 degrees of latitude or about 55 km.

The restriction of .5 degrees of latitude on the variation of the calving line with sea level changes poses a problem because the resolution of the present ice sheet model is only 1 degree of latitude. However, it was felt that it may be possible to perform experiments with exaggerated amplitudes of the northward movement of the calving line with sea level variations, and then to extrapolate the magnitude of the effect on the ice volume of the Antarctic ice sheet back to a situation where the amplitude was only .5 degrees of latitude.

Figure 5.12 shows the response of the southern hemisphere ice volume to variations in the position of the calving line with amplitudes of 1, 2, 3, and 4 degrees of latitude. The choice of amplitude of the variations in the position of the calving line has a large impact on the amplitude of the variations of ice volume. The magnitude of the change in ice volume when the ampliutde is four degrees is about $.22 \times 10^{17}$ m^3, but the response of the ice volume to a one degree amplitude is so small that an extrapolation would lead to the conclusion that smaller variations in the position of the calving line would produce neglegible changes in the Antarctic ice volume. However, even if this were not the case the large variations in ice volume essentially follow the variations in sea level with a phase lag of about 5000 years, and not the response predicted by Budd (1981).
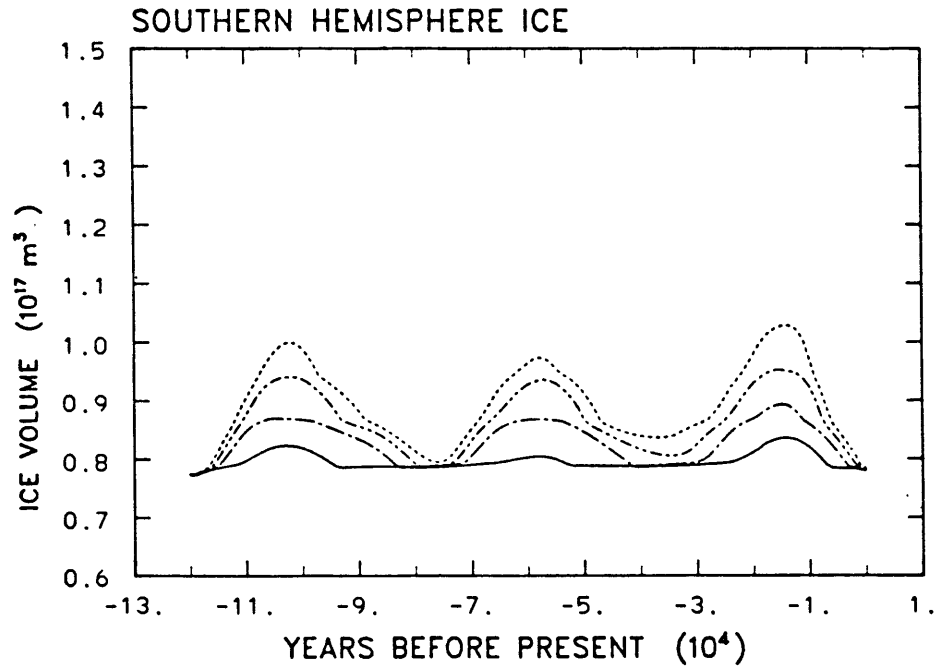
Figure 5.12 Southern hemisphere ice volume changes from
           -120k to the present in response to sea level
           variations which are represented by latitudinal
           variations in the position of the calving line
           with amplitudes of 1 (solid line), 2 (single dot
           dashed line), 3 (double dot dashed line), and 4
           (dotted line) degrees of latitude.

There are two reasons why the results from these
experiments did not agree with Budd's hypothesis. Budd
suggested that rapid decay at the edge of the ice sheet
would occur when the bedrock was sufficiently depressed, and
due to the slow build up of ice at the edge of the ice sheet
when sea level is low, the bedrock would not be sufficiently
depressed at the end of the decay of the northern hemisphere
ice sheets, and therefore the southern hemisphere ice sheet
would not decay. However, the results of the present model
suggest that when sea level drops the newly available land
area would become covered with ice, not slowly due to snow
accumulation, but rapidly due to the flow of ice from the
rather large ice sheet to the south. The bedrock, with a
time constant of 3000 years, would then have time to become
sufficiently depressed so that rapid decay, at the edge of
the ice sheet can occur when the sea level begins to rise.

Other possible reasons that the present ice sheet model
results did not support Budd's hypothesis are that the ice
sheet model neglected some of the mechanisms that may be
important in determining the response of the ice sheet to
sea level variations such as the ungrounding of ice which is
sufficiently below sea level, the inclusion of the physics
of ice shelves and sea ice which may slow the flow of
continental ice from the south as sea level drops, and the
inclusion of bedrock topography. In addition, the crude
resolution of the ice sheet model compared to the estimated
magnitude of the variations of the position of the calving

line may also make this model inadequate to examine the problem of the variations in the Antarctic ice sheet in response to sea level changes.

The results presented here are inconclusive, therefore, it seems that Budd's hypothesis should be examined in greater detail possibly with three dimensional ice sheet models with sufficient resolution, and which include the features of the cryosphere and bedrock mentioned above. Such models will be better suited to examine the response of calving ablation to sea level changes, and thus the long term variations in the Antarctic ice sheet.

VI. Summary and Conclusions

The purpose of this study was to approach a better understanding of what physical processes are important in the variations of the cryosphere, the most important physical feature of an ice age, and thus in climate. In previous studies attempts have been made to examine this problem using either ice sheet or coupled ice sheet-climate models; however, despite rather encouraging results they have not adaquately explained the physical processes involved in producing the large scale climate fluctuations. The reason for this is that the models are either too complex to sort out the relative importance of the individual processes, or the parameterizations used to describe these processes incorporate many tunable parameters which if changed could change the model results.

In studying the physical process involved in long term climate variations one of the features of the climate system which has been either completely neglected or included in only a crude manner is that of sea ice. The sea ice models that have been developed were used to study sea ice variations on short time scales, on the order of ten years. However, the importance of sea ice variations on the growth and decay of continental ice sheets and thus on long term changes in climate may be enormous.

In this thesis an attempt has been made to study the sensitivity of the cryospheric components of the climate system, sea ice and contenental ice, to some of the

specified and parameterized atmospheric variables that can vary over the ice age time scales. In order to do this two models were developed, a thermodynamic sea ice model and a dynamic continental ice sheet model. These models were first tested in studies designed to simulate present climate conditions. Then the sensitivity of the models to variations in parameters and variables whose values are either not well known, or the processes they represent are not well understood was examined. Finally, the response of the cryosphere to variations in climatic variables which might occur on ice age time scales was examined.

The thermodynamic sea ice model which was developed includes conduction within ice and snow, penetration of the solar radiation into ice layers, and surface energy balances. The model has been coupled to a simple mixed layer ocean which allows for the initiation of new ice on open ocean and the inclusion of leads. The major difference between this model and those from which it was adapted is that the numerical scheme is implicit, allowing time steps on the order of one week rather than the eight hour time steps required by the explicit numerical schemes. This makes the model more applicable to long term climate studies.

The continental ice sheet model is a two dimensional zonally averaged dynamic model of ice flow with specified topography, time-lagged bedrock depression, calving at the edges of the ocean, and a surface energy balance that determines the net budget of accumulation and ablation at

the surface of the ice.

The major difference between this model and others which have been published is the computation of the net budget through the use of an energy balance equation. In previous studies equilibrium line net budget parameterizations have been used to describe net budget variations with solar insolation variations. However, this type of parameterization lumps all the physical processes involved in the climate of the atmosphere into one term, therefore making it impossible to sort out the relative importance of these processes and thus to discern the physical mechanisms of climate change.

The first experiments that were performed with these models were simulation experiments in which the sea ice and continental ice were forced with present day seasonal and latitudinal distributions of air temperature, solar radiation, and other atmospheric variables to see how well they simulated present conditions.

The sea ice model produced reasonable simulations of sea ice thickness variations. The seasonal cycle of the fluxes between the atmosphere and ice/ocean surface are for the most part well simulated. The exception to this was the turbulent fluxes; however, these fluxes were generally an order of magnitude smaller than the radiative fluxes.

These simulation experiments showed that the dominant processes in sea ice variations in the northern hemisphere are the radiative processes, with the net loss of long wave

radiation from the ocean and the decreasing input of short
wave radiation in the fall contributing to the formation of
sea ice; and the increase in the incoming short wave
radiation in the spring and summer contributing to its
decay. In the southern hemisphere the radiative processes
are also important, especially in contributing to the decay
of sea ice in the spring and summer; however, the turbulent
energy losses dominate the surface energy balance in the
fall, especially over open ocean, and are therefore the
major cause of the formation of new ice.

Attempts to simulate a northern hemisphere ice sheet
for present day zonally averaged atmospheric conditions
indicated that no such ice sheet exists. This is encouraging
since at the present time only small ice sheets exist in the
northern hemisphere, the largest of which is Greenland, and
these are generally the result of regional conditions.

Initialization of an ice sheet proved difficult. Model
results indicated that the initialization of an ice sheet is
dependent, not on slow approach to colder conditions, but
the crossing of a threshold which is the maintenance of snow
through the summer season. This threshold was difficult to
cross requiring a high summer albedo in conjunction with a 3
K drop in mean air temperature. If summer albedo was not
increased, a 10 K drop in mean air temperature proved
insufficient to cross this threshold and initialize an ice
sheet.

It is possible, however, that the zonally averaged

nature of the ice sheet model exaggerates this initialization problem, by smoothing out high altitude plateaus and eliminating regional effects which may aid in preserving snow through the summer. However, the restraining effect of low bare surface albedos would apply to these regional situations as well, and may dominant them.

The southern hemisphere ice sheet seems to have been simulated with moderate success. The extent of the ice sheet is defined by the position of the edge of the continent where calving ablation occurs; however, this is specified in the model based on present conditions so the result is not surprising.

The thickness and the elevation of the present day Antarctic ice sheet were more difficult to simulate. In one case, where the topography was set at sea level, the elevation of the resulting equilibrium ice sheet seemed reasonable reaching to the 3.5 kilometer level; however, the ice thickness was much too large at about 5 kilometers. A simple topography was then added to the simulation by assuming that the ice free topography was equal to a third of the ice thickness. This simulation produced an ice surface elevation of about 4.25 km, somewhat large but reasonable, and a bedrock depression to only about 100 m below sea level, similar to what is thought to exist today.

These results assume that the Antarctic ice sheet is in equilibrium. This is not at all certain, but present estimates indicate that if it is not in equiblibrium the

rate at which it is changing is so small as to make it very difficult to determine.

The next series of experiments performed with the sea ice and continental ice sheet models involved the sensitivity to factors which were internal to the cryospheric system.

The sea ice model proved to be sensitive to the length of the time step when leads were included. This occurred because the sea ice forming in the leads had a much faster growth rate than the thicker ice and that growth rate was extrapolated over the time step, producing relatively thick lead ice. The net result was that the longer the prescribed time step, the thicker the ice became. In reality, this growth rate slows dramatically as the ice gets thicker, thus producing ice which is thiner than the model simulations. This problem was partially overcome by specifying the thickness of the new ice and computing the areal ice coverage the energy deficit produced. This made the results much less sensitive to time step size. However, a more through investigation needs to be done into methods of representing areas of open ocean, and the formation of new sea ice that are applicable to models which utilize longer time steps.

The sensitivity of the sea ice model to variations in the specified the oceanic heat flux was examined. The results indicated that sea ice was much more sensitive to the mean than the amplitude of the seasonal cycle, and that

the variations in the mean oceanic heat flux affected the period of time ice free conditions existed, and thus the net energy exchange between the atmosphere and ocean. However, the seasonal amplitude parameterization used here was very crude, and therefore more work should be done to see how important such a cycle is.

The sensitivity of the continental ice sheet model to time step size was also tested. It was found that most of the ice sheet was insensitive the the size of the time step which ranged from 10 to 50 years, except at the free flow edge of the ice sheet. However, given the accuracy to which the ice sheet thicknesses are known this sensitivity seemed small. In spite of this, the smaller time step size was used because under certain conditions in experiments with the Antarctic ice sheet the model became numerically unstable.

The sensitivity of the ice sheet model to changes in the flow parameter was also tested. It was found that the flow parameter can affect the size of an equilibrium ice sheet to a great extent, and in some cases its existence through the process of lowering surface elevations by rapid ice flow. It would be desirable to be able to compute this parameter; however, lacking this ability a parameterization of its variation with latitude along with better information of its magnitude would be a great help in the modeling of the ice sheet systems. The results produced from a model in which such a parameterization had been incorporated could be viewed with more confidence.

The main purpose of this thesis was to test the sensitivity of the sea ice and ice sheet models to variations in variables external to the cryospheric system, such as solar radiation, air temperature, oceanic heat flux in the case of sea ice, and the bedrock depression time constant and sea level variations in the case of continental ice which may occur on ice age time scales.

The sea ice model has been used in experiments testing its response to variations in insolation and temperature as a first step toward the coupling of sea ice-ice sheet fluctuations. These experiments showed that the thickness and extent of sea ice, while relatively insensitive to insolation changes alone, were quite sensitive to change in air temperature. Variations in the mean annual air temperature affected both the ice thickness and the period of ice free conditions. The changes in the sea ice thickness can be important in regulating the energy exchange between the atmosphere and ocean; however, the changes in the period of ice free conditions have a dramatic effect on that exchange. The immediate response of the net energy exchange between the atmosphere and ice/ocean surface when the period of ice free conditions was increased was to decrease upward flux. This was surprising at first because it was thought that the exposure of a warm surface (ocean) would increase the upward turbulent fluxes. This did occur; however, the decrease in the area weighted surface albedo caused such a great increase in the absorbed solar radiation that the

increased turbulent fluxes were overcome. When the ocean opened further the increase in the absorbed solar radiation was reduced because the solar radiation was low in comparison to summer levels. As a result the increases in the turbulent fluxes became dominant and the net flux toward the atmosphere began to increase.

When the period of open ocean was decreased the amount of absorbed solar radiation was greatly reduced thus the net flux toward the atmosphere increased. However, once the lead area was reduced to its minimum year round the changes in the net flux were small due to small decreases in the upward turbulent fluxes. These variations were too small and occurred too infrequently in these experiments to draw any conclusions concerning how the net flux would vary if temperatures would drop further.

The range of the seasonal cycle of the net flux to the atmosphere was also affected by varying the mean of the air temperature. This resulted from the large contrast between ice covered and ice free conditions which caused large variations in the maximum absorbed solar radiation at the beginning of the summer, and in the maximum upward long wave radiation in the late fall and early winter.

When the amplitude of the seasonal cycle of air temperature was varied only the period of ice free conditions was affected. The energy exchange between the atmosphere and ocean responded to this change in a manner similar to that when the period of open ocean was affected

by the mean of the air temperature. The only other effect of varying the amplitude of the seasonal air temperature variation was that the amplitude of the seasonal cycle of the energy exchange between the atmosphere and ocean amplitude reflected the change in the forcing.

When the mean and the amplitude of the air temperatures were varied together the response of the sea ice indicated that the effects were somewhat additive if periods of ice free conditions existed. Ice thickness was more strongly controlled by variations in the mean of the air temperature, and the period of ice free conditions was modified approximately equally by changes in the mean and amplitude of the seasonal of air temperature.

These results indicate that the variation in sea ice in response to changes in air temperatures which might occur on climate time scales may have important implications for the net budget over land areas and for further variations in air temperature. It has been theorized (Ruddiman and MacIntyre, 1981) that during the build up of the large continental ice sheets the ocean areas were relatively warm, and therefore ice free. The open oceans were then a large moisture source for snowfall which accumulated on land surfaces and formed the ice sheets. These results indicate that if the open ocean increases a small amount the net energy flux lost to the atmosphere will decrease, and the latent heat flux would increase providing more moisture for precipitation. The decrease in the energy flux toward the atmosphere may cause

competing effects. It could aid in keeping the ocean warm
and therefore relatively ice free, and in keeping air
temperatures relatively low and therefore decrease the
period of ice free conditions. Further investigation is
needed to determine if either of those effects would
dominate. Once the ice sheet got large it would have a large
cooling effect on air temperatures which would result in
extending both the period and horizontal extent of ice
covered conditions. The oceans would then be essentially
capped, cutting off the moisture source for snowfall. This
would starve the ice sheets and initiate their decay.

Speculation as to the cause of the initial increase in
ice area is difficult, especially since the sensitivity
studies presented here do not account for feedback onto the
atmospheric variables. The response of the air temperature
and snowfall to changes in the sea ice extent will be better
understood once the sea ice is coupled to a climate model.
However, such a coupling is premature mainly because of the
uncertainties involved in the the inclusion of leads.
Further studies of the sensitivity of the sea ice to the
numerous parameterization and simplifications of the complex
physical processes important in sea ice growth, such as the
lead parameterization and the use of a simple mixed layer
ocean are needed before the results of such a coupled model
could be meaning fully interpreted.

The continental ice sheet model has been used in
experiments testing its response to coupled insolation

temperature variations when using both an equilibrium line
and energy balance net budget parameterization. The results
showed that when using the equilibrium line parameterization
the present ice sheet model is capable of producing the slow
build up of ice from -125k to -18k including a maximum ice
sheet extent at -18k, a large deglaciation from 18k to 6k,
and shorter term variations on the order of 20k and 40k.
However, these cryospheric variations were not seen using
the energy balance net budget calculation in place of the
equilibrium line calculation. This is despite the fact that
the energy balance calculation should more closely
approximate the physical processes involved in determining
the net budget. Thus, either the strategy employed for
calculating net budget using an energy balance approach is
inadequate to model accumulation and ablation in zonally
averaged ice sheet models, or zonally averaged ice sheet
models themselves may be inadequate to translate the
variations calculated from an energy balance net budget and
changing solar radiation into fluctuations on a climatic
time scale.

The energy balance net budget calculation and the
equilibrium line parameterization behave very differently at
the firn line. The variations in the latitudinal position of
the firn line is much greater for the equilibrium line
calculation than for the energy balance calculation in
response to equivalent fluctuations in solar radiation. In
part the discrepancy between the results of the energy

balance and equilibrium line calculations may be related to the method by which air temperature is coupled to insolation variations. In the energy balance strategy latitudinally and seasonally varying planetary albedo is specifically included in calculation of the surface air temperature, while the equilibrium line parameterization albedo is simply accounted for in a constant coefficient.

Overall there are two major effects which reduce the variation in the cross sectional ice area with time as compared to that when the equilibrium line parameterization is used. The first is the restriction on the growth of the ice sheet resulting from the high ablation rates computed just south of the southern edge of the ice sheet; and second, is the restriction on melt caused by the contrast in surface albedo between ice sheet and ice free conditions. The net budget resulting from these restrictions is in great contrast to that computed over the ice sheet with the equilibrium line parameterization.

The reason for the large ablation over the southern edge of the ice sheet is the interpolation from the moderate positive net budget at 67.5N and the large negative net budget at 62.5N which were computed completely imdependently of each other. The method used here of computing the net budget at completely decoupled latititudes, especially at the ice edge, leaves out a number of physical processes which may account for the difficulty in producing ice sheet variations. Some of these processes include the cooling of

the air above the ice and the increase in the temperature
gradient across the edge of the ice sheet which acts to
influence the path of storm tracks and thus the accumulation
rates on the ice sheet, the horizontal transport of energy
between the various latitude zones, and the katabatic winds
which come down off an ice sheet affecting both the
turbulent fluxes and air temperatures. In order to determine
if including these processes, even in a highly parameterized
form, has an effect on the growth and melt rates of the ice
sheet it is necessary to couple the ice sheet model to a
climate model. This will also make it possible to improve
the parameterization of air temperature response to
insolation variations.

There are other aspects of a complete net budget
calculation that are also not accounted for in these models.
One critical feature that is neglected is the contribution
of the oceans and sea ice to snow accumulation over land
surfaces as mentioned earlier. In an isolated ice sheet
model continental ice is decoupled from its moisture source,
namely the ocean. The extent of sea ice controls the
availability of moisture for snowfall. As the sea ice
extends further south during an ice age it caps off the
oceans and thus reduces the available moisture for transport
over land areas. Conversely the retreat of sea ice should
have the opposite effect. Thus coupling sea ice and ice
sheet fluctuations may be important for calculation of a
more realistic net budget.

The sensitivity of the ice sheet model to various bedrock depression time constants was also examined. The results suggested that the amplitude and variation in ice sheet size is strongly dependent on the way in which the bedrock response is prescribed, therefore pointing to the necessity of sorting out the present controversy, and pursuing a more complete understanding of how bedrock responds to ice load.

Preliminary experiments conducted with the continental ice sheet model suggest that the Antarctic ice sheet is relatively insensitive to insolation and air temperature variations. The reason for this is that the air temperatures are so low that variations, even a change on the order of 10 degrees, do very little to change the net budget. However, Budd (1981) has suggested that variations in the Antarctic ice sheet are caused by variations in sea level caused by the growth and decay of the northern hemisphere ice sheets, and that time delays in the depression of bedrock would cause the response to be on the 100000 year time scale rather than the 40000 year time scale of sea level variations.

Experiments were performed with this model in which the position of the calving line was varied in response to the variations in sea level. The results indicated that the time delay in the Antarctic ice sheet suggested by Budd did not occur because rather than a slow build up of ice on newly uncovered land surfaces the ice flowed rather quickly from

the large ice sheet to the south. This would allow time for the bedrock to be depressed by the next rise in sea level and therefore the ice would decay. In this way the Antarctic ice sheet would respond directly to sea level variations rather than bridging periods of high sea level stands. However, due to insufficient resolution in the model and the lack of some of the features of the edge of the Antarctic continent such as ice shelves and topography these results should be viewed with caution.

The major findings of this study are:

1) Insolations varations, produced by changes in the earth's orbital geometry, are not sufficient themselves to cause significant changes in sea ice; however, if insolation variations cause changes in other atmospheric variables such as air temperature the response of the sea ice can be very large.

2) Sea ice has a large insulating effect on the ocean which effects the energy exchange between the atmosphere and ice/ocean surface in a complex way.

3) When the period of open ocean increases slightly the upward net energy exchange between the atmosphere and ice/ocean surface decreases due to increased absorbed solar radiation. This keeps the ocean relatively warm and ice free, while the latent heat flux increases providing more moisture to the atmosphere which may in

turn increase snowfall over land areas.

4) The energy exchange between the atmosphere and the ice/ocean surface is much greater in the southern hemisphere. This is due mainly to the larger turbulent fluxes in the southern hemisphere. Another factor contributing to this is that the winter temperatures in the southern hemisphere are warmer which increase the upward long wave radiative flux. This effect dominates the net flux if the maximum lead area decreases substantially.

5) The initialization of an ice sheet is dependent on the climatic conditions crossing a threshold in which snow can be maintained through the summer season: changes in both air temperature and surface albedo are required to cross this threshold.

6) With the present zonally averaged energy balance net budget parameterization which decouples the energetics of the latitude zones, a northern hemisphere ice sheet once formed varies little in latitudinal extent due to large ablation rates at the southern edge, and a restriction on melt over the ice resulting from the effect of the large differences between present day and ice age albedos in the air temperature-insolation coupling used here.

7) Bedrock time lagged depression is an important factor in producing the 100k cycle in the ice ages with the longer time constants producing larger amplitude

variations in the northern hemisphere ice sheet with more complete deglaciations.

8) The Antarctic ice sheet volume's response to exaggerated sea level variations seems to be of the same frequency as those variations with a 5000 year phase lag; however, when the sea level changes are not exaggerated the magnitude of the response is small.

Appendix 1. List of Symbols

a - net budget in m s^{-1}; constant; subscript for air; effective albedo dependent on surface albedo, cloud fraction, and solar zenith angle; semi-major axis of the earth's orbit

A - continental ice flow parameter in yr^{-1} bar^{-3} set equal to .15 in base case

A_{hs} - snowfall during time step

$A_r(J)$ - area of one degree latitude zone centered on latitude J

b - constant; subscript indicating the present

B - sensitivity parameter of air temperature to absorbed solar insolation changes, in general set to 8 W m^{-2}K^{-1}

c - constant

C - heat capacity of layer

C(J) - length of latitude circle J

C_D - drag coefficient set to .003 in the continental ice sheet model and .00175 in the sea ice model

C_p - specific heat of dry air in J kg^{-1}K^{-1} set to 1.0048 x 10^3

e - water vapor pressure in kg m^{-1}s^{-2}; eccentricity of earth's orbit

e_s - saturation vapor pressure of water vapor, value at triple point is 611 kg $m^{-1}s^{-2}$

E - energy imbalance used for sea ice growth or melt and continental ice melt

EE' - celestial equator

F - internal conductive fluxes in sea ice in W m^{-2}

F_{cond} - conductive flux within ice or snow layer adjacent to surface in W m^{-2}

f_i - body forces

F_{ir} - long wave flux from surface in W m^{-2}

F_l and F_{lh} - latent heat flux in W m^{-2}

F_{lw} - long wave flux from atmosphere in W m^{-2}

F_o - vertical oceanic heat flux in W m^{-2}

F_s and F_{sh} - sensible heat flux in W m^{-2}

F_{st} - energy accumulated from penetrating solar radiation, in W m^{-2}, up to 30% of energy needed to melt all snow and sea ice is allowed to accumulate

F_{sw} - short wave radiation available at ice/snow surface in W m^{-2}

F_{swo} - short wave radiation available at ocean surface in W m^{-2}

F_u - net upward flux exchange between atmosphere and ocean in W m^{-2}

F_y - fraction of precipitation that falls as snow

g - acceleration of gravity set to 9.8 m s^{-2}

H - ice or snow layer thickness in m; half day length or hour angle of sun at sunset

HF - turbulent energy flux from ice surface to atmosphere

h_g - bedrock elevation in m

h_{ge} - equilibrium bedrock elevation in m

h_{go} - ice free equilibrium bedrock elevation in m

h_i - continental ice thickness in m

H_i - total sea ice thickness in m

H_m - ocean mixed layer depth in m

H_s - snow thickness in m

$I_{o\downarrow}$ - long wave radiation from the atmosphere under clear skies in W m^{-2}

k - multiple of 1000 years; reciprocal of e-folding bedrock response time

K - degrees Kelvin

kg - kilograms

k_i - thermal conductivity of snow, set to .309764 J $m^{-1}s^{-1}K^{-1}$

km - kilometers

k_s - thermal conductivity of ice, set to 2.034396 J $m^{-1}s^{-1}K^{-1}$

L_f - latent heat of fusion set to 3.336 x 10^5 J kg^{-1}

L_s - latent heat of sublimation set to 2.834 x 10^6 J kg^{-1}

L_v - latent heat of vaporization set to 2.500 x 10^6 J kg^{-1}

m - meters

n - ice flow parameter set equal to 3; cloud fraction

N - north

NCP - north celestial pole

P - hydrostatic pressure in kg $m^{-1}s^{-2}$; point of perihelion

P_e - percent of solar radiation transmitted through sea ice surface into ice layer, set equal to 17%

P_r - precipitation rate in m s^{-1}

P_s - surface air pressure in kg $m^{-1}s^{-2}$

Q - insolation at the top of the atmosphere in W m^{-2}; "activation energy" for ice flow

q_a - specific humidity of the air

Q_b - present insolation at the top of the atmosphere in W m^{-2}

q_s - specific humidity of air in contact with surface

r - earth-sun distance in m; relative humidity

$\bar{r}$ - mean earth-sun distance in m

R - radius of earth set to 6.3675×10^6 m; gas constant

r_a - ratio of the density of water to compacted snow or ice

R_v - gas constant for water vapor, set to 460.55 J $kg^{-1}K^{-1}$ in the continental ice sheet model and 461.64 J kg^{-1} in sea ice model

S - south; solar constant set to 1360.75 W m^{-2}; sun

t - time in seconds

T - temperature, generally in degrees Kelvin but where noted in degrees Celcius; length of year in seconds from point P in the orbit of the earth back to that point

T_a - surface air temperature in K; seasonal range of air temperature in K

T_f - freezing point, set to 272.9 K in continental ice sheet model and 271.2 K in sea ice model; triple point of water in K

T_o - temperature of ocean layer in K

T_{ocn} - temperature of ice-ocean interface in K

T_s - ice or snow surface temperature in K

TS - time steps

T_{sn} - temperature of snow-ice interface in K

s - seconds; subscript for surface

S_n - snowfall rate in m s^{-1}

u - eastward ice velocity in m s^{-1}; eccentric anomaly

u_o - eccentric anomaly at the time of the vernal equinox

v - northward ice velocity in m s^{-1}

$\tilde{v}$ - vertically averaged longitudinal (northward) ice velocity in m s^{-1}

V - wind speed in m s^{-1}

$(vq)_i$ - volumetric heat of fusion of ice set to 3.0139 x 10^8 J m^{-3}

$(vq)_o$ - volumetric heat of fusion of ocean adjusted for the density difference between ice and ocean water set to 3.3488 x 10^8 J m^{-3}

$(vq)_s$ - volumetric heat of fusion of ice set to 1.0967 x 10^8 J m^{-3}

w - upward ice velocity in m s^{-1}

W - watts

x - longitudinal corrdinate; portion of snow and ice above
    water level in m

y - latitudinal corrdinate

z - vertical coordinate

$\bar{Z}$ - daily mean solar zenith angle

α - albedo

α_0 - albedo of ocean

α_p - planetary albedo

α_{pb} - present planetary albedo

α_s - albedo of sea ice surface

β - weighting parameter in numerical schemes; varies
    between 0 and 1

γ - vernal equinox

δ - solar declination

ϵ - obliquity; emissivity

ε - ratio of molecular weight of water vapor to dry air

$\dot{\varepsilon}$ - effective strain rate in s^{-1}

$\dot{\epsilon}_{ij}$ - component strain rates in s^{-1}

λ - parameter in Generalized Flow Law; geocentric longitude of sun

ν - true anomaly

π - longitude of perihelion

ρ - air density set to 1.225 kg m^{-3}; ice density in continental ice sheet model set to 900 kg m^{-3}

ρ_i - ice density set to 900 kg m^{-3}

ρ_s - snow density set to 330 kg m^{-3}

ρ_w - ocean water density set to 1000 kg m^{-3}

$(\rho c)_i$ - volumetric specific heat of ice set to 1.8837 x 10^6 J $m^{-3}K^{-1}$

$(\rho c)_o$ - volumetric specific heat of ocean adjusted for the difference in density between ocean water and ice set to 2.093 x 10^6 J $m^{-3}K^{-1}$

$(\rho c)_s$ - volumetric specific heat of snow set to 6.9069 x 10^5 J $m^{-3}K^{-1}$

σ - Stefan-Boltzmann constant set to 5.67 x 10^{-8} W $m^{-2}K^{-4}$

τ - effective shear stress in kg $m^{-1}s^{-2}$; effective transmissivity of atmosphere; period of year from perihelion to perihelion

τ_{ij} - shear stresses on a unit volume of ice in kg $m^{-1}s^{-2}$

t'_{ij} - shear stresses on a unit volume of ice with hydrostatic pressure removed in kg m^{-1}s^{-2}

φ - latitude

Appendix 2. The Astronomical Parameters

The astronomical parameters needed to determine the solar declination, δ, the earth-sun distance, r, the mean earth-sun distance, $\bar{r}$, and the half day length, H, at some time, t, are the longitude of perihelion, $\overline{\omega}$, the eccentricity of the earth's orbit, e, the obliquity of the earth's orbit, ϵ, the eccentric anomaly[4], u, the true anomaly[5], ν, the time of perihelion, τ, and the length of the year from some point P on the orbit back to that point, T.

The longitude of perihelion, the eccentricity, and the obliquity are determined through the use of a program obtained from C. Lawson and W. Wiscombe (personal communication) which is based on the work of Berger (1978)

The other variables are determined from the equations discussed below, obtained from Milankovitch (1941) and Danby (1962).

The time of perihelion is determined using the following equation:

$$(2\overline{\omega} * (t - \tau) / T) = u - e \sin u \qquad (A2-1)$$

If t is set equal to zero (the vernal equinox), and the value of u at that time, u_0, is determined then equation A2-1 can be solved.

u_0 can be determined by applying equations A2-2 and A2-3 at the time of the vernal equinox, t=0, and λ=0.

$$\nu = \lambda + \tilde{\eta} - \overline{\eta} \qquad \text{(A2-2)}$$

$$\mathcal{t} * (u/2) = ((1 - e) / (1 + e))^{.5} * \tan (\nu/2) \qquad \text{(A2-3)}$$

where λ is the geocentric longitude of the sun.

The time of perihelion is then given by equation A2-4:

$$\mathcal{t} = T * (e \sin u_0 - u_0) / 2 \qquad \text{(A2-4)}$$

The next step is to determine the eccentric anolmaly, u, for any time, t. This can be done by applying the iterative Newton's method of tangents to equation A2-1, and using the result of equation A2-4.

This result can be used in equation A2-3 to solve for the true anomaly, ν. Then, solving equation A2-2 for the geocentric longitude of the sun, λ, and given the obliquity, ϵ, we can obtain the solar declination, δ, at some time, t, by solving equation A2-5:

$$\sin \delta = \sin \epsilon \sin \lambda \qquad \text{(A2-5)}$$

Using the results from above, the earth-sun distance, r, the mean earth-sun distance, r, and the half-day length, H, can be determined from equations A2-6, A2-7, and A2-8.

$$r = (a * (1 - e^2)) / (1 + e \cos \nu) \qquad \text{(A2-6)}$$

$$\overline{r} = (a^2 * (1 - e^2)^{.5})^{.5} \qquad \text{(A2-7)}$$

$$H = \text{arc cos } (-\tan \varphi \tan \delta) \qquad\qquad (A2\text{-}8)$$

where a is the semimajor axis of the earth's orbit, and φ is
the latitude.

Footnotes

1. A perfectly plastic material is one which does not deform under the influence of a stress below a value characteristic of the material, called the yield stress. Experiments have never shown ice to have a yield stress: even the lowest stresses have produced some deformation. However, it seems that this deformation is small if the stress is less than 1 bar. (Paterson, 1969)

2. The "desert-elevation" effect is the reducing influence that the decrease in air temperature with increasing elevation has on the saturation vapor pressure and thus on the mositure available for snowfall at the ice sheet surface.

3. This ice sheet model is called a two dimensional model to be consistent with the literature. It has a one dimensional grid along the latitudinal axis so ice can flow from one latitude to the next. However, the vertical thickness of the ice is computed using the law of conservation of mass and assuming the ice is incompressible; there is no vertical axis.

4. If a circle is defined in which the major axis of the earth's orbit is the diameter of the circle and a line is drawn perpendicular to the major axis through the position of the earth to intersect this circle, the eccentric anomaly is the angle defined by the semi-major axis that goes through the sun, the center of the earth's orbit, and the intersection of the perpendicular and circle described above.

5. The true anomaly is the angle defined by the positions of perihelion, the sun, and the earth.

References

Adams, W.P. and R.J. Rogerson, 1968: Snowfall and Snowcover at Knob Lake, Central Labrador - Ungave. Eastern Snow Conference, 110-138.

AIDJEX Bulletin no. 32, First Data Report, 1976, Alma Johnson, editor, Seattle, Washington, 71pp.

Allison, I., 1981: Antarctic Sea Ice Growth and Oceanic Heat Flux. Sea Level, Ice and, Climate Change, (Proceedings of the Canberra Symposium, December 1979), IAHS Publ. no. 131, 161-170.

Allison, I. and G. Akerman, 1980:Sea Ice and Ocean Energy Balance Studies at Mawson, Antarctica. Sea Ice Processes and Models, (Proceedings of the Arctic Ice Dynamics Joint Experiment International Commission on Snow and Ice Symposium), University of Washingtion Press, Seattle, 347-359.

Allison, I., C.M. Tivendale, G.J. Akerman, J.M. Tann, and R.H. Wills, 1981: Seasonal Variations in the Surface Energy Exchanges Over Antarctic Sea Ice and Coastal Waters. (manuscript).

Auer, August, 1974: The Rain Versus Snow Threshold Temperatures. Weatherwise, 27, 67.

Berger, Andre L., 1976: Obliquity and Precession for the Last 5,000,000 Years. Astronomy and Astrophysics, 51, 127-135.

Berger, Andre L., 1978: Long-Term Variations of Daily Insolation and Quaternary Climatic Changes, J.Atmos.Sci., 35, 2362-2367.

Birchfield, G.E., Johannes Weertman, and Albert T. Lunde, 1981: A Paleoclimate Model of Northern Hemisphere Ice Sheets. Quaternary Research, 15, 126-142.

Birchfield, G.E., Johannes Weertman, and Albert T. Lunde, 1982: A Model Study of the Role of High Latitude Topography in the Climate Response to Orbital Insolation Anomalies. J.Atmos.Sci., 39,71-78.

Broecker, W.S., and J. van Donk, 1970: Insolation Changes, Ice Volumes, and the δ180 Record in Deep Sea Cores. Reviews of Geophysics and Space Physics, 8, 169-198.

Budd W.F., 1969: The Dynamics of Ice Masses. ANARE
    Scientific Reports, Series A (IV) Glaciology,
    publication no. 108, 216pp.

Budd, W.F., 1981: The Importance of Ice Sheets in Long Term
    Changes of Climate and Sea Level. Sea Level, Ice, and
    Climate Change (Proceedings of the Canberra Symposium,
    December, 1979), IAHS Publ. No. 131, 441-471.

Budd, W.F. and I.N. Smith, 1981: The Growth and Retreat of
    Ice Sheets in Response to Orbital Radiation Changes.
    Sea Level, Ice, and Climatic Change (Proceedings of the
    Canberra Symposium, December, 1979), IAHS Publ. No.
    131, 369-409.

Budyko, M.I., 1969: The Effect of Solar Radiaiton Variations
    on the Climate of the Earth. Tellus, 21, 611-619.

CLIMAP Project Members, 1981: Seasonal Reconstructions of
    the Earth's Surface at the Last Glacial Maximum, A.
    McIntyre, coordination and compilation, R. Cline,
    editor, Lamont-Doherty Geological Observatory of
    Columbia University, Palisades, New York, The
    Geological Society of America, maps, microfiche, and
    text, 18pp.

Danby, J.M.A., 1962: Fundamentals of Celestial Mechanics,
    The Macmillan Company, New York, 348pp.

Dolgushin L.D., S.A. Yevteyev and V.M. Kotliakov, 1962:
    Current Changes in the Antarctic Ice Sheet.
    Commission of Snow and Ice, Symposium of Obergurgl,
    Variations of the Regime of Existing Glaciers, W. Ward,
    editor, International Association of Scientific
    Hydrology, Publication no. 58, 286-294.

Environomental Technical Applications Center, 1971: Northern
    Hemisphere Cloud Cover, Project #6168, Department of
    the Air Force, Washington D.C.

Flint, R. 1971: Glacial and Quaternary Geology, John Wiley
    and sons, Inc., New York, 892pp.

Gates, W.L. and A.B. Nelson, 1973: A New Tabulation of the
    Scripps Topography on a 1^0 Global Grid, Part I. Terrain
    Heights, Defense Advance Research Projects Agency,
    R-1276-ARPA, 133pp.

Ghil, Michael and Herve LeTreut, 1981: A Climate Model with
    Cryodynamics and Geodynamics. J.Geophys.Res., 86,
    5262-5270.

Glen, J.W, 1955: The Creep of Polycrystalline Ice. Proceedings of the Royal Society of London, 288, 519-538.

Giovinetto, M.B., 1964: The Drainage Systems of Antarctica: Accumulation. Antarctic Snow and Ice Studies I, Malcolm Mellor, editor, Antarctic Research Series, vol 2, American Geophysical Union, no. 1197, 127-156.

Gordon, A., 1981: Seasonality of Southern Ocean Sea Ice. J.Geophys.Res., 86, 4193-4197.

Hays, J.D., J. Imbrie, and N. Shackleton, 1976: Variation of the Earth's Orbit: Pacemaker of the Ice Ages. Science, 194, 1121-1132.

Jaegar, L., 1976: Monatskarten des Niederschlags fur die ganze Erde, Berichte des Deutschen Wetterdienstes. Nr. 139, (Band 18). Offenbach a.M. 38pp.

Jenne, R.L., H.L. Crutcher, H. van Loon, and J.J. Taljaard, 1971: Climate of the Upper Air: Southern Hemisphere Volume III Vector Mean Geostrophic Winds, Isogon and Isotach Analysis, Navair 50-1C-57, NCAR TN/STR-58, National Center for Atmospheric Research, Boulder, Colorado, 68pp.

Kallen, E., C. Crafoord and M. Ghil, 1979: Free Oscillations In a Climate Model with Ice Sheet Dynamics. J.Atmos.Sci., 36, 2292-2303.

King, H.G.R., 1969: The Antarctic, Blandford Press, London, 276pp.

Ledley, Tamara Shapiro, 1979: Secular Variation of Solar Zenith Angle: A Factor in Climatic Change?. Summer Fellowship in Scientific Computing, NCAR Technical Note, NCAR/TN-135+Proc, 117-137.

LeTreut, Herve and Michael Ghil, 1981: Orbital Forcing, Climatic Interactions, and Glaciaiton Cycles. (submitted to J.Geophys.Res.).

London, J., 1957: A Study of the Atmospheric Heat Balance. Report Contract AF 19(122)-165, College of Engineering, New York University, Air Force Cambridge Research Center (NTIS PB 115626), 99pp.

Lowe, Paul R., 1977: An Approximating Polynomial for the Computation of Saturation Vapor Pressure. J.Appl. Meteor., 16, 100-103.

Mahaffy, M.W. 1976: A Three-Dimensional Numerical Model of Ice Sheets: Tests on the Barnes Ice Cap, Northwest Territories. J.Geophys. Res., 81, 1059-1066.

Maykut, Gary A., 1978: Energy Exchange Over Young Sea Ice in the Central Arctic. J.Geophys.Res., 83 C7, 3646-3658.

Maykut, Gary A., 1982: Large-Scale Heat Exchange and Ice Production in the Central Arctic. J.Geophys.Res, 87, 7971-7984.

Maykut, Gary A. and Norbert Untersteiner, 1971: Some Results from a Time Dependent Thermodynamic Model of Sea Ice. J.Geophys.Res., 76 #6, 1550-1575.

Milankovitch, Milutin, 1941: Canon of Insolation and the Ice Age Problem, Beograd, Koninglich Serbische Akademie. 484pp. (English translation by the Israel Program for Scientific Translation and published by the U.S. Department of Commerce and the National Science Foundation.).

Monthly Record, Meteorological Observations in Canada, Environomental Canada, Atmospheric Environoment, January through December 1975, Downsview Ontario.

Murakami, T., 1975: Interannual Cloudiness Changes. Monthly Weather Review, 103, 996-1004.

National Geographic Atlas of the World, 5th edition., 1981: National Geographic Society, Washington D.C., 383pp.

Newell, Reginald E., 1974: Changes in the Poleward Energy Flux by the Atmosphere and Ocean as a Possible Cause of Ice Ages., Quaternary Research, 4, 117-127.

Newell, Reginald E., John W. Kidson, Dayton G. Vincent, and George J. Boer, 1972: The General Circulation of the Tropical Atmosphere and Interactions with Extratropical Latitudes, vol I, MIT Press, Cambridge, Massachusetts, 258pp.

Newell, Reginald E., John W. Kidson, Dayton G. Vincent, and George J. Boer, 1974: The General Circulation of the Tropical Atmosphere and Interactions with Extratropical Latitudes, vol II, MIT Press, Cambridge, Massachusetts, 371pp.

Oerlemans, J., 1980: Model Experiments on the 100,000 Year Glacial Cycle. Nature, 287, 430-432.

Oerlemans, J., 1982: A Model of the Antarctic Ice Sheet, Nature, 297, 550-553.

Oerlemans, J. and J.M. Bienfait, 1980: Linking Ice Sheet Evolution to Milankovitch Radiation Variations: A Model Simulation of the Global Ice Volume Record. Proc.Sun and Climate Conference. (CNES, Toulouse), 357-368.

Orvig, S. (editor), 1970: World Survey of Climatology Volume 14: Climates of the Polar Regions, Elsevier Publishing Company, Amsterdam, 370pp.

Parkinson, C., 1978: A Numerical Simulation of the Annual Cycle of Sea Ice in the Arctic and Antarctic., PhD dissertation, Ohio State University and National Center for Atmospheric Research, 191pp.

Parkinson, C. and W. Washington, 1979: A Large Scale Numerical Model of Sea Ice. J.Geophys.Res., 84 Cl, 311-337.

Paterson, W.S.B., 1969: The Physics of Glaciers, Pergamon Press, New York, 250pp.

Peltier, W.R. and W.T. Hyde, 1982: A Model of the Ice Age Cycle. Milankovitch and Climate, Nov 30 - Dec 4, 1982, Lamont Doherty Geological Observatory, Palisades, New York

Pickard, G.L. 1979: Descriptive Physical Oceanography, Pregamon Press, Oxford, 233pp.

Pollard, David, 1978: An Investigation of the Astronomical Theory of the Ice Ages Using a Simple Climate Ice Sheet Model, Nature, 272, 233-235.

Pollard, David, 1982a: A Simple Ice Sheet Model Yields Realistic 100 KYR Glacial Cycles, Nature, 296, 334-338.

Pollard, David, 1982b: A Coupled Climate-Ice Sheet Model Applied to the Quaternary Ice Ages, Climate Research Institute Report No. 37, Oregon State University, 43pp.

Pollard, David, 1982c: Ice-Age Simulations With a Calving Ice-Sheet Model, Climate Research Institute Report No. 39, Oregon State University, 35pp.

Pollard, D., A.P. Ingersoll, and J.G. Lockwood , 1980: Response of a Zonal Climate-Ice Sheet Model to the Orbital Perturbations During the Quaternary Ice Ages. Tellus, 32, 301-319.

Robock, A., 1980: The Seasonal Cycle of Snow Cover, Sea Ice, and Surface, Albedo. Monthly Weather Review, 108, 267-285.

Rubin, M.J. 1962: Atmospheric Advection and the Antarctic Mass and Heat Budget. Antarctic Research, The Matthew Fontain Maury Memorial Symposium, H. Wexler, M.J. Rubin, and J.E. Caskey, Jr., editors, Geophysical Monograph Series, no. 7, American Geophysical Union, 149-159.

Saltzman, Barry, 1977: Global Mass and Energy Requirements for Glacial Oscillations and Their Implications for Mean Ocean Temperature Oscillations. Tellus, 29, 205-212.

Saltzman, Barry, 1978: A Survey of Statistical-Dynamical Models of the Terrestrial Climate. Advances in Geophysics, 20, 183-307.

Schneider, S.H. and S.L. Thompson, 1979: Ice Ages and Orbital Variations: Some Simple Theory and Modeling. Quaternary Research, 12, 188-203.

Schneider, S.H., and S.L. Thompson, 1981: Atmospheric CO_2 and Climate: Importance of the Transient Response. J.Geophys.Res., 86, 3135-3147.

Schutz, C. and W.L. Gates, 1971: Global Climate Data for Surface, 800mb, 400mb: January, R-915-ARPA, RAND, Santa Monica, CA, 182pp.

Schutz, C. and W.L. Gates, 1972: Global Climate Data for Surface, 800mb, 400mb: July, R-1029-ARPA, RAND, Santa Monica, CA, 180pp.

Schutz, C. and W.L. Gates, 1973: Global Climate Data for Surface, 800mb, 400mb: April, R-1317-ARPA, RAND, Santa Monica, CA, 192pp.

Schutz, C. and W.L. Gates, 1974: Global Climate Data for Surface, 800mb, 400mb: October, R-1425-ARPA, RAND, Santa Monica, CA, 192pp.

Sellers, W., 1965: Physical Clima4ology, University of Chicago Press, Chicago and London, 272pp.

Sellers, W., 1969: A Global Climatic Model Based on the Energy Balance of the Earth-Atmosphere System. J.Appl.Meteor., 8, 382-400.

Sellers, W., 1973: A New Global Model. J.Appl.Meteor., 12, 241-254.

Semtner, Albert J. Jr., 1976: A Model for the Thermodynamic Growth of Sea Ice in Numerical Investigations of Climate. J.Phys.Oceanogr., 6, 379-389.

Sergin, V.Ya., 1979: Numerical Modeling of the Glaciers-Ocean-Atmosphere System. J.Geophys.Res., 84, 3191-3204.

Sergin, V.Ya., 1980: Orgin and Mechanism of Large Scale Climatic Oscillations. Science, 209, 1477-1482.

Suarez, M.J. and I.M. Held, 1976: Modeling Climatic Response to Orbital Parameter Variations. Nature, 263, 46-47.

Suarez, M.J. and I.M. Held, 1979: The Sensitivity of an Energy Balance Climate Model to Variations in the Orbital Parameters. J.Geophys.Res., 84, 4825-4836.

Swithinbank, C. and J.H. Zumberge, 1965: The Ice Shelves. Antarctica, T. Hatherton, editor, Frederick A. Pranger Publishers, New York, 199-220.

Thompson, Starley L., 1979: Deveolpment of a Seasonally - Verified Planetary Albedo Parameterization for Zonal Energy Balance Climate Models. Report of the JOC Study Conference on Climate Models: Performance, Intercomparison, and Sensitivity Studies, vol II, W. Lawrence Gates, Editor, GARP Publication Series 22, 1002-1023.

Thomspon, Starley L. and Eric J. Barron, 1981: Comparison of Cretaceous and Present Earth Albedos: Implications for Paleoclimates. J.of Geology, 89, 143-167.

Thorndike, A.S., D.A. Rothrock, G.A. Maykut, and R. Colony, 1975: The Thickness Distribution of Sea Ice. J.Geophys.Res., 80, 4501-4513.

Untersteiner, N., 1961: On the Mass and Heat Budget of Arctic Sea Ice. Arch. Meteor. Geophys. Bioklim., A12, 151-182.

Untersteiner, N., 1964: Calculations of Temperture Regime and Heat Budget of Sea Ice in the Central Arctic, J.Geophys.Res, 69, 4755-4766.

van Loon, H., 1972: Cloudiness and Precipitation in the Southern Hemisphere. Meteor.Monographs, 13, 101-111.

Vowinckel, E. and S. Orvig, 1980: The Climate of the North Polar Basin, World Survey of Climatology, volume 14: Climates of the Polar Regions, S. Orvig editor, Elsievier Publishing Company, Amsterdam, 129-252.

Warren, Stephen G. and Stephen H. Schneider, 1979: Seasonal Simulation as a Test for Uncertainties in the Parameterizations of a Budyko - Sellers Zonal Climate Model. J.Atmos.Sci., 36, 1377-1391

Washington, W., A. Semtner, C. Parkinson, and L. Morrison, 1976: On the Development of a Seasonal Change Sea-Ice Model. J.Phys.Oceanogr., 6, 679-685.

Weeks, Wilford F. and Owen S. Lee, 1958: Observations on the Physical Properties of Sea-Ice at Hopedale, Labrador. Arctic, 11, 135-155.

Weertman, J., 1976: Milankovitch Solar Radiation Variations and Ice Age Ice Sheet Sizes. Nature, 261, 17-20.

Wexler, H. 1961: Ice Budgets for Antarctica and Changes in Sea Level. J.Glaciology, 3, 867-872.

Wollin, G., D.B. Ericson, and W.B. Ryan, 1971: Variations in Magnetic Intensity and Climatic Changes. Nature, 232, 549-551.

Biographical Note

     I was born in Washington D.C. on May 18, 1954 and grew up in Hyattsville and New Carrollton, Maryland where I attended public school.

     I attended the University of Maryland where I was part of the general honors program, and recieved a B.S. degree in astronomy and a citation in general honors for my thesis on the Structure and Evolution of the Jewish Calendar in 1976.

     I got married to Fred David Ledley on June 6, 1976.

     I then attended graduate school at the University of Maryland in the Meteorology Program until 1978. In the summer of 1978 I received a fellowship to the National Center for Atmospheric Research where my serious work on climate began. I came to MIT in the fall of 1978.

     My publications to date are:

Ledley, T.S., 1982: Sensitivities of Crysopheric Models to Insolation and Temperature Variations Through the Use of a Surface Energy Balance Calculation., Proceedings of the International Symposium on Milankovitch and Climate 12/82, (in press).

Ledley, T.S., 1981: Problems of Coupling Ice Sheet and Climate Models., Informal Workshop on Ice Sheet Modeling 24-28 August 1981, Cooperative Institute for Research in Environomental Sciences (CIRES), 9-10.

Ledley, T.S., 1979: Secular Variation of Solar Zenith Angle: A Factor in Climatic Change?, Summer Fellowship in Scientific Computing, NCAR Technical Note, NCAR/TM-135+Proc, 117-137.